



BIOMEDICAL ASPECTS OF MEMBRANE CHEMISTRY

A thesis submitted in part fulfilment of the degree of
Doctor of Philosophy

CORINNE E. A. MCEWAN

Department of Chemistry

Supervised by: Professor H. M. Colquhoun and Professor W. Hayes

Sponsored by: BioInteractions Ltd, Reading

2017

Declaration of Original Authorship

I confirm that the research described in this thesis is my own work and that the use of all materials from other sources has been properly and fully acknowledged.

.....

Corinne E. A. McEwan

Abstract

This thesis is focused on the development of a prototype membrane medical device for the treatment of oedema and lymphoedema via interosmolar fluid removal. These medical disorders disrupt body fluid regulation causing excess fluid to accumulate in the body's tissues resulting in swelling of affected areas and can severely impact quality of life of affected patients.

The device concept was based on a US patent (No. 8,211,053 B2) licensed to BioInteractions Ltd which proposes, but does not exemplify, an implantable medical device based on a semipermeable membrane compartment containing trapped osmotic solutes which can act as a draw solution for the abnormally accumulated fluid in the tissues surrounding the device, allowing the fluid to be drained from the body. Following extensive literature research and consultation with experts in the field (detailed in **Chapter 1**) it became apparent that alongside the oedema fluid, accumulated plasma proteins would also require removal to prevent oedema reforming as a result of protein oncotic pressure. To accommodate this, a design modification was proposed; employing porous membranes to enable to removal of proteins alongside the fluid. This adaptation necessarily affected the draw solution selection limiting the options to high molecular weight species which could be retained by the porous membrane.

Alongside this clinically-oriented project, a secondary project involved the development of thin-film composite membranes using novel coatings based on hydrophilic poly-ylids as well as investigations into a new solvent resistant support membrane.

Chapter 2 focused on investigating the forward osmosis process using a novel combination of porous ultrafiltration membranes and high molecular weight polymer and polyelectrolyte draw solutions. The best-performing draw solution and membrane was found to be 225K sodium polyacrylate and a 50K MWCO polyethersulfone (PES) UF membrane which were then further studied to determine model oedema fluid removal performance, membrane fouling properties, osmotic pressure characteristics and protein transport.

Chapter 3 involved the synthesis and characterisation of novel hydrophilic poly-ylids derived from the interfacial polycondensation of 1,1'-diamino-4,4'-bipyridinium with aromatic di-sulfonyl chlorides and di-isocyanates. These poly-ylids were then used to fabricate thin-film composite nanofiltration membranes, alongside a number of

previously reported acid chloride based poly-ylids for comparison, which were then analysed in terms of their flux and salt rejection properties. Additionally investigations into pH effects, surface morphology and biocompatibility were carried out.

Chapter 4 describes the development of solvent resistant thin-film composite membranes based on poly-ylids synthesised in **Chapter 3**, in combination with a novel polyetherketone support membranes. This system enabled the fabrication of nanofiltration membranes using monomers that were incompatible with a traditional PES membrane support. The membranes were analysed as described in **Chapter 3** and were found to have reasonable flux and salt rejection properties. Additionally, initial biocompatibility testing found that all three PEK TFC poly-ylid membranes were able to reduce protein adhesion relative to an uncoated PEK support membrane.

Chapter 5 details the design, fabrication and testing of two generations of device prototypes using both an *in vitro* and *ex vivo* model, both developed specifically for the project. This chapter provides proof-of-concept for the device, as fluid removal was successfully demonstrated using a second generation prototype tested in an *ex vivo* perfused limb.

Acknowledgements

I would first like to thank my PhD supervisor, Professor Howard Colquhoun for all the support and advice throughout the project. I would also like to thank Professor Hayes for additional input during the project and Dr Alister McNeish for all the help and advice with developing the perfused limb model. Additionally I would like to acknowledge my industrial sponsor BioInteractions Ltd for the opportunity to undertake this PhD, and also my industrial supervisors; Dr Ajay Luthra (Chief Executive Officer), Simon Onis (Chief Scientific Officer) and Dr Alan Rhodes (Chief Technical Officer).

I am also grateful to colleagues who have shared their expertise and time to help progress this project, especially; Amanpreet Kaur (SEM), Krish Kapoor (BCA Assay) and Tahkur Singh Babra (GPC), the CAF Lab technical staff and all members of both the Colquhoun and Hayes groups, past and present.

I would also like to thank my undergraduate project student Ben Plackett for helping with PEK membrane optimisation and producing a brilliant crossflow rig schematic.

Additionally I would like to thank the University of Reading Knowledge Transfer Partnership team for all their support throughout the project, particularly Deborah Edwards and Owen Lloyd.

Most importantly I would like to thank my friends and family who have supported me throughout the highs and lows of this PhD; Kate, my first and best friend in Reading, the craft club ladies (Clare, Priya, Emma and Emily), my chemistry gurl gang from Bath Uni (Lucie, Kat, Gem, Mel and Lottie), and most especially my best girlfriends Barbara, Amy B and Amy C.

I am eternally grateful for my loving and supportive family; my maman cherie and sister Mathilde for being strong and beautiful women and for always wanting the best for me, my stepdad Andrew for always being there for me and for being part of our family, my partner Ben for all the adventures and encouragement and for helping me achieve things I didn't think I was capable of.

Finally I would like to dedicate this PhD to my dad Pete, who didn't get to see me complete it - thank you for always being of proud me.

Acronyms and Abbreviations

AFM	atomic force microscopy
appt. d	apparent doublet
BCA	bicinchoninic acid assay
BSA	bovine serum albumin
<i>c</i>	concentration
CC	counterion condensation
CDT	complex decongestive therapy
C_f	feed concentration
C_p	permeate concentration
DI	deionised
DMF	N,N'-dimethylformamide
DMSO	dimethyl sulfoxide
DSC	differential scanning calorimetry
EAS	electrophilic aromatic substitution
ECF	extracellular fluid
ESEM	environmental scanning electron microscopy
FIB	fibrinogen
FO	forward osmosis
<i>g</i>	acceleration due to gravity
GAGs	glycosaminoglycans
GPC	gel permeation chromatography
<i>h</i>	height
Δh	change in height
ICF	intracellular fluid
<i>i</i>	van't Hoff Factor
IF	interstitial fluid

IPC	intermittent pneumatic compression
IR	infra-red
K_c	capillary filtration coefficient
K-PA	potassium polyacrylate
m	multiplet
M	molarity
MF	microfiltration
MLD	manual lymphatic drainage
MWCO	molecular weight cut-off
MW	molecular weight
n	moles
Na-PA	sodium polyacrylate
NIPAM	N-isopropylacrylamide
NMP	N-methylpyrrolidone
NMR	nuclear magnetic resonance
P	pressure
PA	polyamide
PAEK	polyaryletherketone
PAES	polyarylethersulfone
PBS	phosphate buffered saline
PEG	poly(ethylene glycol)
PEK	polyetherketone
PES	polyethersulfone
PEO	poly(ethylene oxide)
PGs	proteoglycans
pm	picometers
ppm	parts per million
PPS	polyphenylenesulphide

PSF	polysulfone
PSSA	polystyrene sulfonic acid sodium salt
PVP	polyvinylpyrrolidone
R	rejection
<i>R</i>	gas constant
RI	refractive index
RO	reverse osmosis
s	singlet
SEM	scanning electron microscopy
SD	standard deviation
SDS	sodium dodeceyl sulfate
t	triplet
t_1	absolute viscosity of solvent
t_2	absolute viscosity of polymer solution
<i>T</i>	temperature
T_{deg}	degradation temperature
T_g	glass transition
T_m	melting temperature
TEM	transmission electron microscopy
TFC	thin-film composite
TGA	thermal gravimetric analysis
TMC	trimesoyl chloride
UBK	unbuffered Krebs solution
UF	ultrafiltration
UV/Vis	ultraviolet/visible
<i>V</i>	volume

\AA	angstroms
η	viscosity
η_{abs}	absolute viscosity
η_{inh}	inherent viscosity
π	osmotic pressure
ρ	density
σ	retention coefficient

Table of Contents

CHAPTER 1 – Introduction

1.1	Research Motivation	1
1.2	Membrane Technology	3
	1.2.1 <i>Overview and History</i>	3
	1.2.2 <i>Membrane Classification</i>	4
	1.2.3 <i>Membrane Processes</i>	6
	1.2.4 <i>Membrane Fabrication and Characterisation</i>	11
	1.2.4.1 <i>Membrane Fabrication</i>	11
	1.2.4.2 <i>Membrane Characterisation</i>	14
1.3	Forward Osmosis	18
	1.3.1 <i>Overview</i>	18
	1.3.2 <i>FO Membranes</i>	19
	1.3.3 <i>FO Configuration</i>	20
1.4	Membrane Modification	21
	1.4.1 <i>Overview</i>	21
	1.4.2 <i>Interfacial Polymerisation</i>	23
1.5	Oedema	23
	1.5.1 <i>Overview</i>	23
	1.5.2 <i>Fluid Homeostasis</i>	24
	1.5.3 <i>Physiology</i>	30
	1.5.4 <i>Pathophysiology</i>	35
	1.5.5 <i>Clinical Symptoms and Diagnosis</i>	36
	1.5.6 <i>Treatment</i>	38
	1.5.7 <i>Fluid Composition</i>	39
1.6	Project Aims and Objectives	41
1.7	References	42

CHAPTER 2 – Forward Osmosis Processes with Ultrafiltration Membranes

2.1	Abstract	56
2.2	Introduction	56
2.3	Results and Discussion	58
	2.3.1 <i>Initial FO Studies using Ultrafiltration Membranes</i>	58
	2.3.1.1 <i>Cellulose Membranes</i>	60
	2.3.1.2 <i>PES Membranes</i>	61

2.3.2 Ultrafiltration Membrane Fouling Studies	65
2.3.3 PEG Behaviour in Solution	67
2.3.4 Sodium Polyacrylate Behaviour in Solution	68
2.3.5 Polyacrylate Draw Solution Optimisation	78
2.3.5.1 Molecular Weight Variation	78
2.3.5.2 Variation of Draw Solution Concentration	79
2.3.5.3 Changing Counter-ion Identity	80
2.3.6 Ultrafiltration Membrane Osmotic Pressure Studies	81
2.3.7 Reverse Osmosis vs. Ultrafiltration Membranes	86
2.3.8 Protein Studies	96
2.4 Conclusions	101
2.5 Future Work	103
2.6 Experimental	104
2.6.1 Materials	104
2.6.2 Equipment	105
2.6.3 Methods	106
2.6.3.1 Stirred Cell Forward Osmosis Experiments	106
2.6.3.2 Ultrafiltration Membrane Forward Osmosis Studies	107
2.6.3.3 Ultrafiltration Membrane FO Fouling Studies	108
2.6.3.4 Ultrafiltration Membrane FO Osmotic Pressure Studies	108
2.6.3.5 Reverse Osmosis vs. Ultrafiltration	108
2.6.3.6 Protein Studies	109
2.6.3.7 Commercial Ultrafiltration Membranes	110
2.7 References	111
 CHAPTER 3 – Poly-ylid Membranes by Interfacial Polycondensation	
3.1 Abstract	113
3.2 Introduction	113
3.3 Results and Discussion	115
3.3.1 Synthesis of 1,1'-Diamino-4,4'-bipyridinium di-iodide	115
3.3.2 Poly-ylid Synthesis	117
3.3.3. Poly-ylid Characterisation	119
3.3.3.1 Infrared Spectroscopy	119
3.3.3.2 ¹ H Nuclear Magnetic Resonance Spectroscopy	123
3.3.3.3 Inherent Viscosity	125
3.3.3.4 Thermogravimetric analysis	126

3.3.3.5 Differential Scanning Calorimetry	127
3.3.4 <i>Membrane Fabrication</i>	131
3.3.5 <i>Membrane Characterisation</i>	131
3.3.5.1 Membrane Permeability	132
3.3.5.2 Salt Rejection	134
3.3.5.3 pH Effects on Permeability	135
3.3.5.4 Surface Morphology	136
3.3.5.5 Biocompatibility Testing	138
3.4 Conclusions	141
3.5 Future Work	143
3.6 Experimental	143
3.6.1 <i>Materials</i>	143
3.6.2 <i>Equipment</i>	144
3.6.3 <i>Methods</i>	145
3.6.3.1 Synthesis of 1,1'-diamino-4,4'-bipyridinium di-iodide	145
3.6.3.2 Stirred Interfacial Polycondensation	146
3.6.3.3 Thin-film Composite Membrane Fabrication	148
3.6.3.4 Membrane Flux Determination	149
3.6.3.5 Membrane Salt Rejection Determination	149
3.6.3.6 pH Effects on Permeability	150
3.6.3.7 Biocompatibility Testing	150
3.7 References	151

CHAPTER 4 – Membranes based on Polyetherketone (PEK)

4.1 Abstract	153
4.2 Introduction	153
4.3 Results and Discussion	155
4.3.1 <i>PEK TFC Membrane Fabrication</i>	155
4.3.2 <i>Membrane Characterisation</i>	156
4.3.2.1 Membrane Permeability	157
4.3.2.2 Salt Rejection	158
4.3.2.3 pH Effects on Permeability	159
4.3.2.4 Surface Morphology	160
4.3.2.5 Biocompatibility Testing	161
4.3.3 <i>PEK Support Membrane Optimisation</i>	162
4.3.3.1 Backing Paper Exploration	162

4.3.3.2 PEK Crystallisation	164
4.3.3.3 Characterisation of Crystallised PEK Membranes	164
4.3.3.4 Interfacial Polycondensation on a Crystallised PEK Membrane	166
4.4 Conclusions	167
4.5 Future Work	168
4.6 Experimental	168
4.6.1 <i>Materials</i>	168
4.6.2 <i>Equipment</i>	168
4.6.3 <i>Methods</i>	169
4.6.3.1 PEK Thin-film Composite Membrane Fabrication	169
4.6.3.2 Membrane Flux Determination	170
4.6.3.3 Membrane Salt Rejection Determination	170
4.6.3.4 pH Effects on Permeability	170
4.6.3.5 Biocompatibility Testing	170
4.6.3.6 PEK Crystallisation	170
4.6.3.7 PEK Crystallinity Investigation via DSC Analysis	170
4.6.3.8 MWCO Analysis	170
4.7 References	171
CHAPTER 5 – Device Prototype Design, Fabrication and Testing	
5.1 Abstract	172
5.2 Introduction	172
5.3 Results and Discussion	175
5.3.1 <i>Prototype Design</i>	175
5.3.2 <i>Prototype Fabrication</i>	176
5.3.2.1 1 st Generation Prototype	176
5.3.2.2 2 nd Generation Prototype	177
5.3.3 <i>Prototype Testing</i>	179
5.3.3.1 <i>In vitro</i> Testing	179
5.3.3.2 Perfused Limb Model	182
5.4 Conclusions	185
5.5 Future Work	186
5.6 Experimental	186
5.6.1 <i>Materials</i>	186
5.6.2 <i>Equipment</i>	187

5.6.3 <i>Methods</i>	187
5.6.3.1 Prototype Fabrication	187
5.6.3.2 Prototype Testing	188
5.7 References	189

Chapter 1 - Introduction

1.1 Research Motivation

Oedema and lymphoedema are medical conditions which can have a severe impact on quality of life. These disorders cause excess fluid to accumulate in the bodies' tissues - rather than being returned back to the circulatory system, which thus leads to swelling in the affected areas. Current treatments for these conditions are labour- and time-intensive, often requiring high patient compliance to be effective. In this thesis, a new approach is proposed based on an implantable medical device with a semipermeable membrane containing an osmotic driving solution which can remove accumulated fluid in oedema. The main advantage of this approach is that the conditions for fluid removal do not require harsh suction or pumping and therefore may be more compatible with treating these conditions.

The device concept for this novel treatment is based on a US patent licenced to BioInteractions Ltd (**Figure 1.1**)¹ for interosmolar fluid removal which proposes, but does not exemplify, an implantable medical device based on a semipermeable membrane compartment containing trapped osmotic solutes which can act as a draw solution, removing abnormally accumulated fluid in the tissues surrounding the medical device, allowing them to be drained from the body via a tube in communication with an external reservoir.

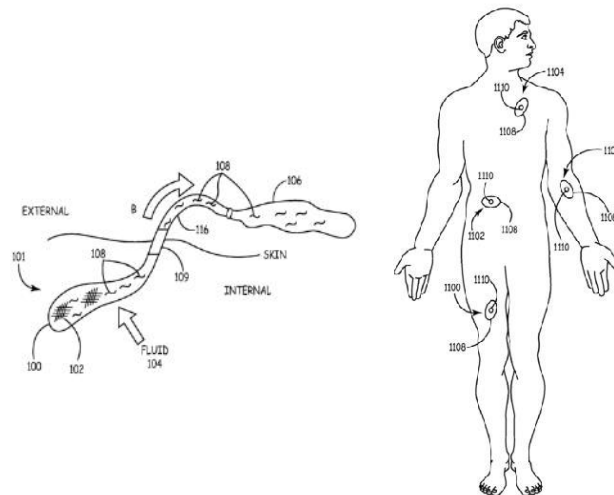


Figure 1.1: Schematic from US Patent 8,211,053,B2 showing sketches of possible device design and configuration and potential implantation sites. Note that this patent simply introduces a concept. No actual device or process was reported in the patent.

The aims of this project were principally to provide proof of concept to support this proposed device design. In order to achieve this several objectives had to be met: investigation into the forward osmosis process itself, analysis of potential membranes and draw solutions, development of bench top model systems and device prototypes, exploration of device design and finally the development of an *ex vivo* porcine limb oedema model for prototype device testing.

Additionally in this thesis, research on membrane modification via interfacial polymerisation coating techniques has led to the development of two new classes of poly-ylid membrane coatings for the fabrication of thin-film composite nanofiltration (NF) membranes (**Figure 1.2**). Analysis of these membranes showed them to have good flux and salt rejection properties. Furthermore some of these new coatings were combined with novel PEK support membranes to create solvent resistant nanofiltration membranes which were demonstrated to have reasonable flux and rejection properties. Studies were carried out to investigate these novel NF membranes' biocompatibility, examining the adsorption of different proteins.

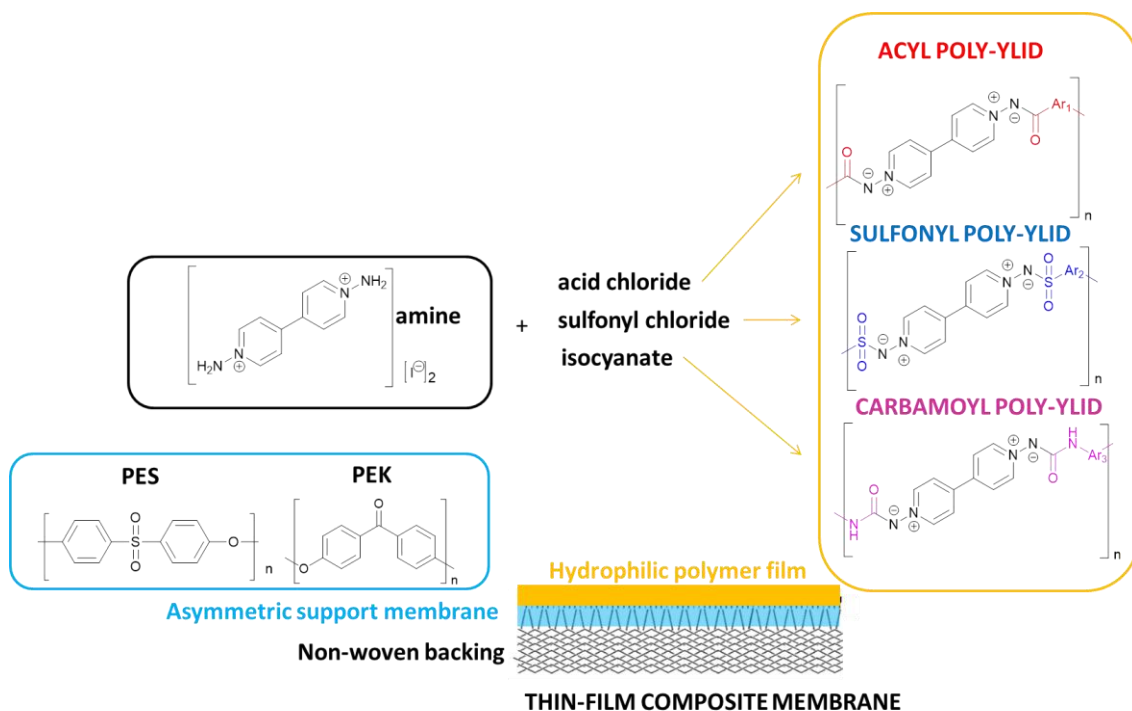


Figure 1.2: Schematic depicting the fabrication of novel thin-film composite membranes using two different asymmetric support membrane; PES and PEK and a new class of poly-ylid coatings based on the polymerisation of 1,1'-diamino-4,4'-bipyridylium di-iodide with various acid chloride, sulfonyl chloride and isocyanate monomers to give the corresponding amide, sulfonamide and urea poly-ylids.

1.2 Membrane Technology

1.2.1 Overview and History

Membranes can be described as semi-permeable interfaces separating two phases, only allowing certain components to permeate through.² Whilst there are both synthetic and biological membranes this review will focus on the former.

Early investigations into membrane science in the 18th century involved experiments with animal intestines and bladders³ and led to the discovery of the phenomenon which drives the permeation of water through a semipermeable membrane from an area of high water concentration to an area of lower water concentration, a process known as *osmosis*. The first semisynthetic membranes were developed a century later.⁴ These 'collodion' (nitrocellulose) membranes became commercially available in the 1930's⁵ and soon this technology was applied to other polymers.

The next significant breakthrough came in the 1960's with the development of the first high flux anisotropic reverse osmosis membrane. Loeb and Sourirajan are widely credited with making reverse osmosis a practical process for industrial use.^{2,6,7} With their development of an anisotropic cellulose acetate membrane (also known as a Loeb-Sourirajan membrane)⁸ they were able to make the possibility of desalination by reverse osmosis an economically viable process.

Michaels at Amicon realised the potential of the asymmetric RO Loeb-Sourirajan membrane and applied this technology to create asymmetric ultrafiltration membranes with a skin layer containing pores in the 10-200 Å range.⁹ These UF membranes exhibited high retention of macromolecules including proteins and synthetic water-soluble polymers whilst demonstrating excellent hydraulic permeability.¹⁰ Michaels and his co-workers were able to produce asymmetric cellulose acetate UF membranes along with other polymers such as polysulfones (PSF), aromatic polyamides (PA) and polyacrylonitrile.¹¹ These types of membranes are now also used as supports in composite reverse osmosis membranes.

Another key breakthrough in membrane science was the development of the interfacial polymerization (IP) technique which led to the creation of the first non-cellulosic membrane with comparable flux and salt rejection.¹² This type of polymerization was initially reported by Morgan in 1965.¹³ However, it was not until it was further developed by Cadotte at FilmTec Corporation that its potential for RO membrane production was fully realised.¹⁴ Interfacial polymerisation, involving the spontaneous growth of a semi-permeable polyamide membrane on the surface of a supporting UF membrane, is currently the most widely used method to manufacture high performance thin-film

composite reverse osmosis and nanofiltration membranes.⁶ The significance of these membranes is that the two layers (skin layer and microporous substrate layer) of the anisotropic membrane are prepared separately allowing for individual optimization before combination to form the asymmetric membrane.^{6,7} This allows for a great deal of customisation, and a wide variety of these thin-film composite (TFC) membranes have since been developed.¹⁵

In order to develop a high-performing membrane, there are several factors which need to be considered. These include the *selectivity*, defined as the rate at which different species permeate relative to each other, the *permeability* which is the absolute rate at which a permeate traverses a membrane and the *flux* which is the amount of permeate that is transported through the membrane per unit membrane area per unit time.^{16,17} Other practical aspects to consider include; reproducibility, mechanical stability, resistance to fouling, resistance to chemicals and temperature stability¹⁸.

1.2.2 Membrane Classification

Membranes can be classified in a variety of ways. Many membrane classifications stem from the membrane materials and structure. When considering synthetic membranes the first key distinction is whether they are based on organic¹⁹ or inorganic materials (such as oxides, ceramic and metals).²⁰ This review will focus on synthetic polymeric materials which have many advantages including low cost, ease of manufacture and ability to create a wide range of pore sizes.¹²

An alternative membrane classification system is based on the composition and structure of the membrane cross section (**Figure 1.3**). There are two broad classes; *isotropic* (symmetric) which have a uniform composition and structure throughout the membrane cross-section and *anisotropic* (asymmetric) which can be homogenous in chemical composition but not structure (phase separation or Loeb-Sourirajan membranes). The latter may also be chemically and structurally heterogeneous (thin film composite).²¹ Isotropic membranes can further be classified into either microporous or dense/non-porous membranes.

Anisotropic membranes made of two or more materials are also known as composite membranes. A classic example of this membrane type is the thin-film composite membrane as prepared by the interfacial polymerisation technique. As mentioned above these types of membranes have a significant advantage in that the layers can be prepared separately. Composite membranes can also have a biocompatible coating applied to the skin layer for use in medical devices, i.e. dialysis membranes.²² A major

disadvantage of many types of membrane is their susceptibility to fouling which leads to a rapid decline in permeate flux: strategies to reduce this often include surface modifications or coatings to reduce fouling.²³

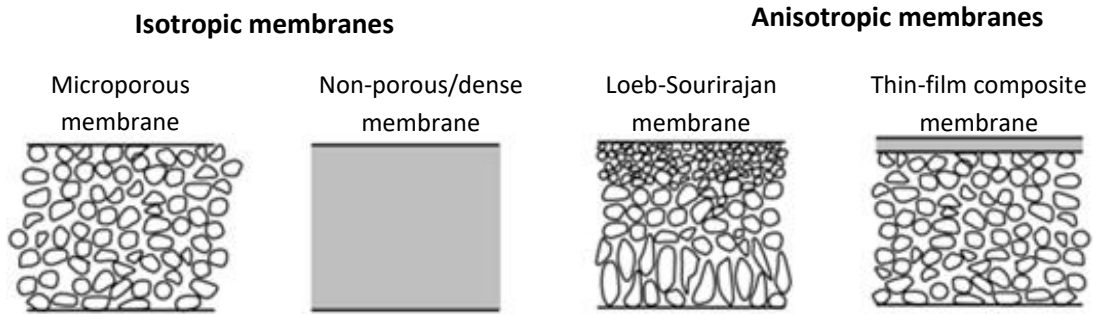


Figure 1.3: Schematic diagrams of cross sections of isotropic vs. anisotropic membranes.²

Another way of distinguishing between membrane types is in terms of the method by which they are prepared: the most common technique being phase-separation, although other methods include interfacial reaction, track etching, extrusion and stretching.^{6,19} Membranes can also be classified by the shape of the membrane module into which they are configured. There are two main geometries; *flat* including flat sheet, disc, spirally wound and plate & frame, and *cylindrical* which comprise tubular and capillary/hollow fibre modules.⁶ Finally, membranes are frequently described by the process in which they are used, e.g. reverse osmosis membranes, nanofiltration membranes, ultrafiltration membranes or microfiltration membranes.

Figure 1.4 summarises the classification of synthetic polymer membranes.

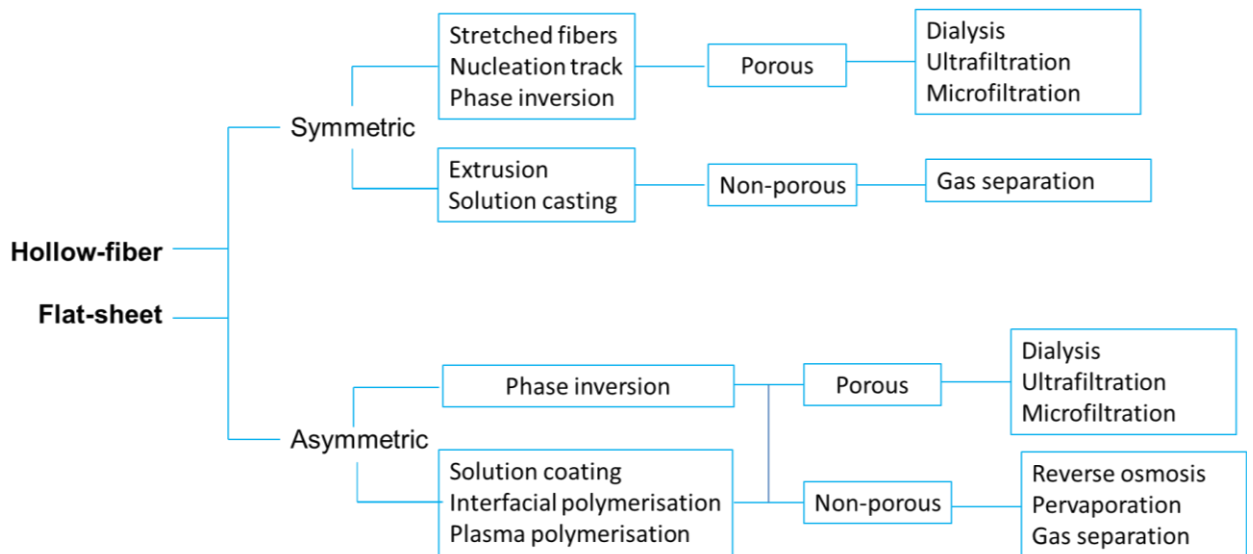


Figure 1.4: Classification of synthetic polymer membranes, adapted from reference.¹⁸

1.2.3 Membrane Processes

Membrane filtration involves the flow of fluid from a bulk (feed) solution, often comprising a single phase containing dissolved species, through a semipermeable membrane to give a purified permeate (**Figure 1.5**). Membrane separations can be driven by either a concentration, electrical or pressure gradient.²

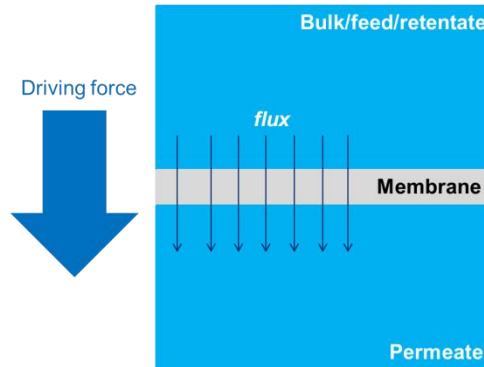


Figure 1.5: Membrane filtration process, adapted from reference.²⁴

Membrane filtration processes rely on the ability of membranes to control the rate of permeation of different chemical species resulting in the separation of a mixture of components.² There are two main mechanisms of membrane permeation; *solution-diffusion* and *porous flow* (**Figure 1.6**). In the solution-diffusion model; separation is achieved by differences in the solubility of components within the membrane itself and the rate at which the material diffuses through the membrane.²⁵ This model is commonly used to describe transport through dense or non-porous membranes. For membranes which contain pores an alternative model is used known as the porous or pore flow model. Separation in this case is based on size-exclusion and is related to the pore size.

The porous flow model can be broken down into several sub-models such as; finely porous, preferential sorption-capillary flow, and surface force-pore flow models.²⁶ In reality the actual mechanisms of mass transport of selected components through a membrane is much more complex and can often be a combination of both models.²⁷

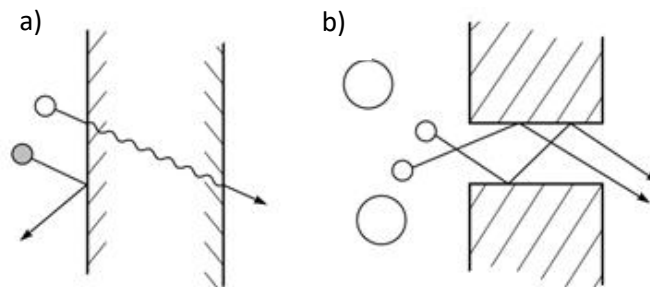


Figure 1.6: Molecular transport through membranes can occur either via a) *solution diffusion* - separation results from differences in the solubility and mobility of the permeates in the membrane materials or b) *porous flow* – separation by molecular filtration, adapted from reference.²⁸

Another key consideration when discussing membranes is the *electrical double layer* which is the name given to two parallel levels of charged particles which form on a surface when it is exposed to an electrolyte solution. Polymeric membranes will acquire a characteristic surface charge when in contact with an aqueous solution which will influence the ion distribution at the membrane-solution interface resulting in the formation of this electrical double layer.²⁹ The membrane surface charge will result in the accumulation of an excess of counter-ions adjacent to the membrane-solution interface.³⁰ This surface charge can occur via several mechanisms including: ionisation of membrane surface groups or adsorption of ions, polyelectrolytes and charged macromolecules from solution.³¹ The surface charge can be characterised by measurement of the membrane zeta potential.⁷

Another important principle of membrane chemistry is the *concentration polarisation* effect which can be defined as the phenomenon which occurs when the solute concentration on the membrane surface is higher than the solute concentration in the bulk solution, resulting in a concentration gradient at the membrane/solution interface (**Figure 1.7**).³² This effect arises due to preferential loss of solvent from the solution on the permeate side of the membrane accompanied by an increase in the solvent concentration on the permeate side of the membrane.³³ The presence of this gradient at the interface can dramatically decrease the rate of flux by reducing the permeating component concentration difference across the membrane. Formation of this boundary layer can in some cases be irreversible, resulting in the development of an insoluble *gel layer*.

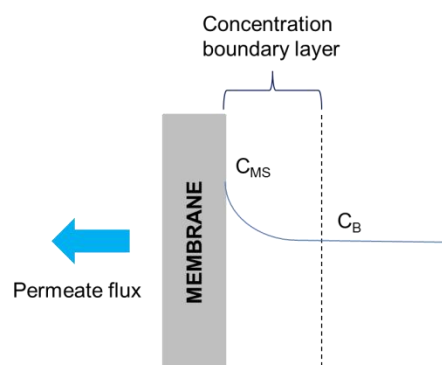


Figure 1.7: Concentration polarisation leading to a build-up of solutes forming a boundary layer where C_B is the bulk solute concentration and C_{MS} is the membrane surface solute concentration, adapted from reference.³⁴

When a semi-permeable membrane is placed between two phases; one comprising pure solvent and the other being a solution, the osmotic pressure generated will result in diffusion of the solvent into the solution phase in order to reach an equilibrium pressure-distribution. However if a pressure gradient (greater than the osmotic pressure) is applied across the membrane i.e. against the direction of the osmotic

pressure gradient, then this tendency is reversed (hence "reverse osmosis") resulting in concentration of the solution and dilution of the solvent.³⁵ When a pressure gradient is imposed to drive filtration this is known as a pressure-driven membrane process.

Pressure-driven membrane processes are well-established in industry and are widely used in applications such as desalination and water treatment,^{21,35,36} the food industry³⁷⁻⁴⁰ and in the biotechnology sector.^{17,40,41} Major advantages of membrane technologies in separation include: i) their comparatively low energy cost (since no phase change is required), ii) the ability to carry out these processes at ambient temperatures (making this process suitable for filtration of temperature-sensitive mixtures – particularly useful in the biotechnology field) and iii) the ease of integration of membrane filtration into other separation processes.^{19,42}

In pressure-driven membrane processes, the flux of the permeate across a membrane is driven by a difference in hydrostatic pressure which is induced between the bulk and the permeate sides of the membrane.²⁴ There are two main methods of carrying out pressure-driven experiments; dead-end filtration and cross-flow filtration. Dead-end filtration involves the bulk solution being forced (i.e. pumped or pressurised) through the membrane in a perpendicular fashion with one stream entering the system (the feed) and one stream leaving the filter (the permeate).²⁴ A major disadvantage of this method is the build-up of retained particles on the surface of the membrane, forming a 'cake layer' which eventually results in reduced filtration rate.⁴³ For this reason dead-end filtration is usually employed in batch processes allowing the membrane to be changed between batches. Most pressure-driven membrane processes are carried out using cross-flow filtration. In this configuration the feed is pumped tangentially across the membrane surface with one stream entering the system (the bulk) and two streams leaving (the permeate and the retentate).⁴⁴ The main advantage of this system is that cross-flow reduces the accumulation of retained particles on the membrane surface decreasing the likelihood of the formation of a 'cake layer' and therefore allowing the membrane to be used for much longer than when dead-end filtration is used.⁴⁵

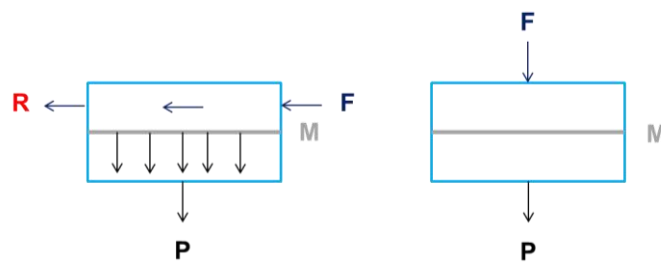


Figure 1.8: Schematic of a) cross-flow and b) dead-end filtration systems. F: feed, M: membrane, P: permeate R: retentate, adapted from reference.¹⁶

Pressure-driven processes have many advantages; the permeate can be obtained extremely pure, the process can be carried out at moderate temperatures so that the energy requirements are reasonably low and finally such processes are suitable for easy scaling up or combination with other processes.⁴⁶

A major disadvantage of pressure-driven membrane processes is their susceptibility to membrane fouling through the accumulation of retained species on the membrane surface or within the membrane matrix resulting in a decrease in membrane permeability.⁴⁷ There are several different types of foulant; *colloidal fouling* from particles such as clay or silica, *organic fouling* from hydrocarbons and proteins, *inorganic fouling* from precipitation and deposition of dissolved salts in scaling (arises due to changes in pH) or oxidation and finally *biofouling* from plant matter such as algae or microbial contamination (biofilm formation).^{23,47,48}

The issue of fouling can be overcome by two main approaches; either pre-treatment of the feed solution to remove contaminants or modification of operating conditions to promote membrane cleaning through backwashing or forward flushing to avoid long-term build-up of deposited matter or by additional chemical/air scouring membrane cleaning procedures.⁴⁷ A common pre-treatment in drinking water production is sterilisation by chlorine. However, this may shorten the membrane usage lifetime since certain membranes (notably those based on aromatic polyamides) are very susceptible to degradation by chlorine.

There are several types of pressure-driven membrane processes; reverse osmosis, nanofiltration, ultrafiltration and microfiltration. Their corresponding membranes can be distinguished by their pore size. These processes can also be divided into *Low-pressure* (microfiltration and ultrafiltration) and *High-pressure* methods (reverse osmosis and nanofiltration) due to the differing operating pressures required.

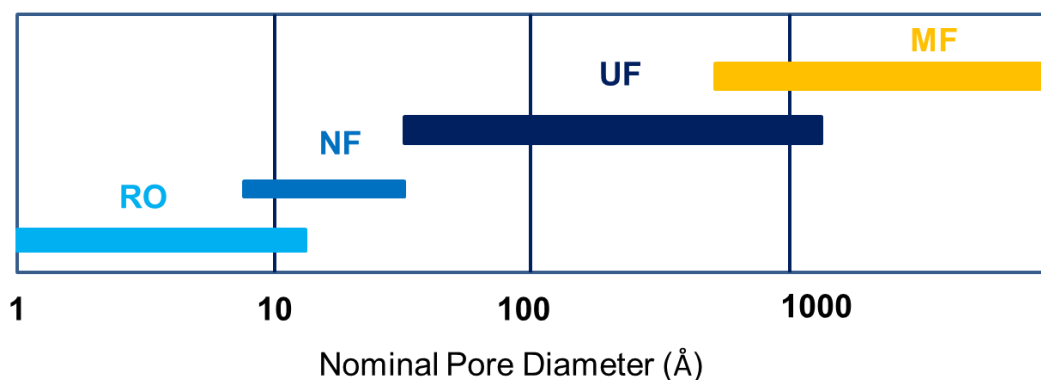


Figure 1.9: Pressure-driven membrane processes and their pore size ranges. Adapted from reference.²¹

Low-Pressure Membrane processes (typically 0.5-2 bar)

Microfiltration

Microfiltration retains and concentrates particles in the “micron” range which typically encompasses suspended particles or colloids with a radius of 0.10 μm to 5 μm (depending on the particular membrane pore size) and can include microorganisms such as bacteria and viruses as well as other particles.⁴⁹ Although both dead-end and cross-flow configurations can be used, the latter configuration is preferred as this avoids the build-up of retained particles on the membrane surface which can reduce the rate of filtration.⁵⁰ Microfiltration is used in many industrial applications, including sterile filtration of pharmaceutical products to produce injectable drug solutions,⁵¹ and in the dairy industry where cross-flow MF is used to remove bacteria from milk.³⁷

Ultrafiltration

Ultrafiltration membranes have a pore diameter in the range 2 - 100 nm.⁵² Over the past two decades UF has been widely used in the food processing industry due to its significant advantages over other separation processes including non-harsh conditions (ambient temperatures, no need for addition of chemicals) and low energy requirements.³⁹ UF is used in the dairy industry to fractionate milk for cheese production and to produce high-calcium milk.³⁸

High-Pressure Membrane Processes (typically 5-100 bar)

Nanofiltration

Nanofiltration is characterised by a membrane pore size range which corresponds to a molecular weight cut-off of approximately 200 – 1000 Da.⁵³ Nanofiltration is used primarily in water treatment either to produce drinking water from ground and surface water or as a pre-treatment for desalination.⁵⁴ A moderately high pressure of 10-40 bar is typically required.⁵⁵

Reverse Osmosis

Currently reverse osmosis is the most widely used desalination technology globally.¹² Unlike the above three membrane types (NF, UF and MF) reverse osmosis membranes are non-porous and instead have a complex ‘web-like’ molecular structure forcing the permeating water through a tortuous pathway between hydrated polymer chains.⁵⁶ Reverse osmosis requires relatively high operating pressures in comparison to the other pressure-driven processes both because of the membrane’s inherently low

permeability and in order to overcome osmotic pressure.⁵⁷ Commercial RO membranes are mainly based on two different types of polymers; cellulose acetate (CA) or aromatic polyamides (PA). However, the former are limited by their susceptibility to microbiological attack and sensitivity to pH, so most industrial applications will preferentially use PA thin film composite RO membranes.⁵⁸ One disadvantage of PA membranes is that they are degraded on prolonged exposure to oxidising agents such as chlorine which is often used as a biocide in water treatment.^{59,60}

1.2.4 Membrane Fabrication and Characterisation

1.2.4.1 Membrane Fabrication

The most commonly used methods in polymer membrane synthesis include phase inversion, interfacial polymerisation, stretching, track-etching and electrospinning.⁷ This review will focus on the first two methods since they were used to fabricate membranes for this project. Phase inversion and interfacial polymerisation are used to produce asymmetric (anisotropic membranes).¹⁸

Phase Inversion

Phase inversion involves the controlled conversion of a homogenous polymer solution from a liquid to a solid state. Although there are several techniques to achieve this, each involves first casting a film of the polymer solution usually onto a non-woven backing paper support (in the case of ultrafiltration membrane fabrication) or directly onto a sheet of glass. Following the film casting the polymer is precipitated which can be done in a variety of ways:^{7,18,61}

- Immersion precipitation
- Thermally induced phase separation
- Evaporation-induced phase separation
- Vapour-induced phase separation

The most common technique – immersion precipitation – involves immersing the polymer film in a non-solvent bath (typically water). Precipitation occurs due to the exchange of solvent (within the polymer solution) and non-solvent which therefore requires these two solvents to be miscible. During this solvent exchange the polymer solution itself is separated into two phases; a solid polymer-rich phase which forms the matrix and a liquid polymer-poor phase which forms the pores.⁶² This process results

in the formation of an asymmetric membrane consisting of a dense skin layer on top of a porous sub layer containing structures such as macrovoids, pores and micropores.⁶³

Membranes created by immersion precipitation have been found to contain key structural elements such as; cellular structures, nodules, bicontinuous structures and macrovoids.⁶⁴ Macrovoids are large conical ‘finger-like cavities’ which can extend throughout the entire thickness of the membrane and are generally unfavourable as they are considered to be structural flaws resulting in mechanical weaknesses in the membrane.^{64,65} **Figure 1.10** shows scanning electron micrographs of two lab-fabricated asymmetric polysulfone membranes and demonstrates the presence of pores and long finger-like macrovoids in **1.10 a)**, as well as the dense surface skin layer in **1.10 b)**.

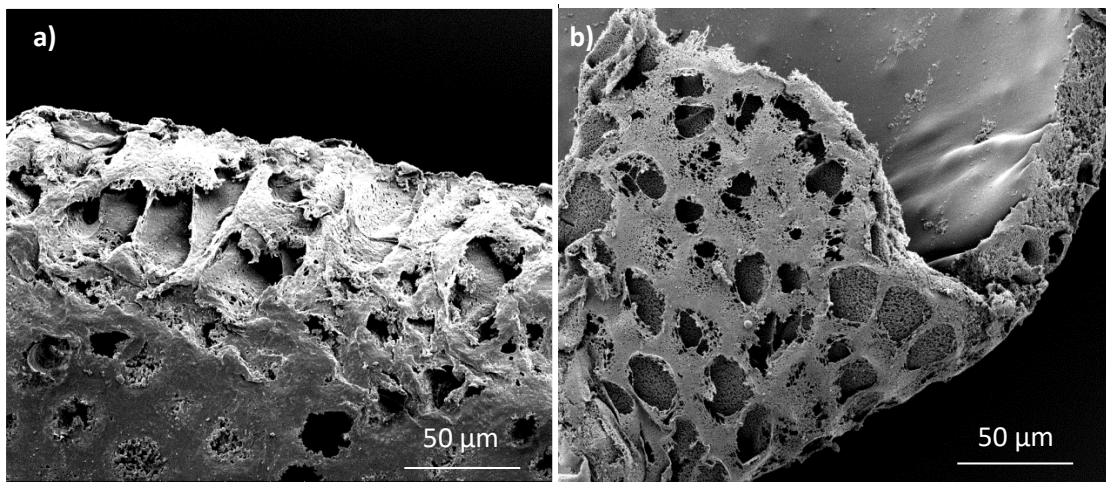


Figure 1.10: a) Scanning electron micrograph of edge and underside of gold-coated asymmetric polysulfone membrane (PSF with 5%wt PEG 600 pore-forming additive) (x1170) b) Scanning electron micrograph of edge and underside of gold coated asymmetric polysulfone membrane (PSF with 5%wt PEG 35,000 pore-forming additive) (x1091) (author images).

The occurrence of these microstructures can be controlled by the precipitation process and is affected by several variables such as the casting solution composition and concentration, the non-solvent used and its temperature as well as by organic and inorganic additives.^{7,62,63} Membranes formed by rapid solvent exchange generally have a highly porous sub-structure, containing macrovoids, with a finely porous, thin skin layer whilst membranes formed by a delayed de-mixing mechanism show a porous, macrovoid-free, substructure with a dense, relatively thick skin layer.^{61,66}

The first phase inversion RO membrane was developed by Loeb and Sourirajan in the late 1950's using cellulose acetate dissolved in a water-miscible solvent which was cast as a thin film on a glass plate before being submerged in a water bath where the polymer precipitated forming a “skinned” asymmetric membrane.⁶²

Interfacial Polymerisation

Interfacial polymerisation is a step-growth polymerisation technique which involves dissolving the monomer reagents in two different insoluble solvents before combining them to produce a polymer at the solvent interface. The classic example of this technique is the 'nylon rope trick', discovered by Morgan *et al.* in 1959, which involves interfacial polymerisation at the interface formed between an aqueous solution of a diamine and a diacid chloride in organic solvent to produce a nylon filament.⁶⁷ Before this discovery, condensation polymerisations usually required high temperatures and reduced pressures to remove low molecular weight by-products such as water, and so drive the reaction forward, thus limiting the substrates that could be used. Morgan's method, however, allowed such chemistry to be carried out at atmospheric conditions using basic laboratory equipment.^{68,69} This novel approach was based on the Schotten-Bauman reaction where an acid chloride is reacted with a compound containing an OH or NH bond to form the corresponding esters and amides. In these reactions the two reactants are dissolved in immiscible solvents so that the reaction occurs at the interface of a heterogeneous liquid system. If a di-acid chloride and a diol or diamine are used, then polymers are generally formed.

This technique is often employed in the fabrication of reverse osmosis (RO) and nanofiltration (NF) membranes by polymerising a thin polymer skin layer on the surface of a microporous polymer support membrane. This support membrane is often an ultrafiltration membrane which itself consists of a woven or non-woven polyester paper coated with a porous polysulfone or polyethersulfone.⁷⁰ These types of anisotropic membrane are also known as thin film composite (TFC) membranes.

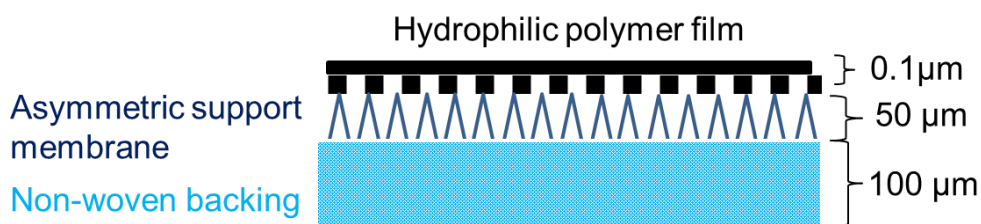


Figure 1.11: Structure of a thin film composite membrane.⁷¹

The thin-film polymer layer is most often derived from the *in situ* interfacial polycondensation of aromatic diamines with aromatic di- and/or tri-acid chlorides to give a porous cross-linked polyamide on the solid support surface. Commonly used diamines have included both aliphatic and aromatic species including triethylamine, piperazine and *meta/para*-phenylene diamine.⁷ The preferred acid chloride monomer is trimesoyl chloride.

A major advantage of the TFC membranes relative to earlier, integral-asymmetric RO membranes is that the two layers can be independently modified and optimised allowing for control of properties such as permeability and selectivity¹⁵.

1.2.4.2 Membrane Characterisation

Membranes can be characterised in a variety of ways which are commonly classified into three main categories; morphology (physical), composition (chemical) and performance based characterisation techniques (i.e. permeation/flux, fouling and filtration properties). In order to truly understand all of a membrane's properties it is necessary to investigate all three aspects of characterisation.

Membrane Morphology

Membrane morphology characterisation techniques can examine either the membrane surface or bulk physical structure (see below). When examining the membrane face or topmost portion responsible for membrane selectivity, electron microscopy and scanning probe microscopy techniques can be used.

In electron microscopy the sample surface is exposed to a beam of electrons within a vacuum. There are two basic techniques; transmission electron microscopy (TEM) and scanning electron microscopy (SEM). In the former a detector will register electrons passing through the sample whilst in SEM, interaction between the electron beam and the sample causes the emission of secondary electrons which are then detected and can be converted into an image. **Figure 1.12** shows a SEM micrograph of a gold-coated polytetrafluoroethylene (PTFE) microfiltration membrane.

In SEM the electron beam is scanned across the surface of the sample and has a resolution limit of 10 nm allowing for the imaging of pores in microfiltration membranes which have a size range of 100-10,000 nm.⁷² Ultrafiltration membranes, however, have a pore size range between 1 nm-30 nm which is much more difficult to resolve.⁷³ In addition the membrane cross section can also be imaged and together with surface images these micrographs can provide information on pore size distribution, surface porosity (number of pores per unit area³⁴) and pore geometry. It is worth noting these micrographs can only provide information on a very limited surface area and therefore are not necessarily representative of the entire membrane surface as highlighted in a review by Tang *et al.*⁷⁴ This review also noted that the sample preparation (metallization via sputter coating) can affect the pore size distribution determination. Similarly cross section preparation either by cutting with a razorblade or through the

freeze fracture method can result in membrane compression and tearing.⁷⁵ An alternative form of SEM known as environmental scanning electron microscopy (ESEM) can allow for sample analysis under less harsh conditions as the specimen chamber is separated from the electron source allowing for a reduced working pressure.⁷⁶

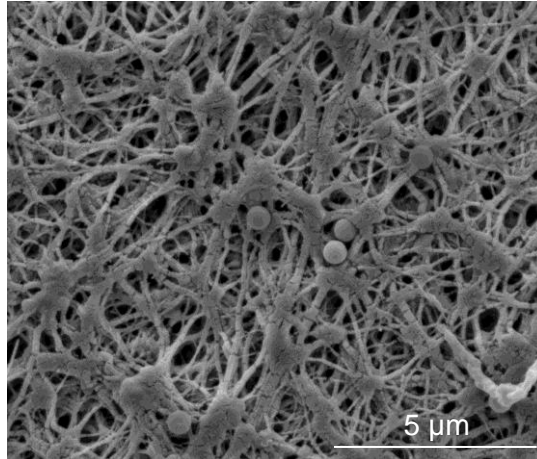


Figure 1.12: Scanning electron micrograph of a gold-coated microfiltration membrane (Omnipore™ - PTFE, pore size 0.1 μm) with retained 0.6 μm latex particles (x 50,000) (author image).

Scanning probe microscopy methods exploit interactions (electromagnetic or mechanical) between the sample surface and a probe mounted on a flexible cantilever to map the surface morphology. Atomic force microscopy (AFM) is perhaps the most well-researched technique and employs a piezo-electric scanner to move the probe relative to the sample whilst measuring mechanical interactions.⁷⁶ A great advantage of the AFM technique is the ability to examine membranes whilst wet, thus simulating conditions under which the membrane will operate, unlike the electron microscopy methods which require a dry sample.⁷⁶ AFM has also been used to determine various membrane surface characteristics including surface roughness, pore density and pore size. However this technique is limited by restrictions on the scanning probe tip size which can affect the scanning depth. Additionally there can be distortion effects which can lead to overestimation of pore size relative to other techniques.⁷⁷⁻⁷⁹

When investigating the bulk properties of a membrane it is important to distinguish between porous and dense membranes. The former type are used for microfiltration and ultrafiltration processes and are identified by the presence of permanent voids or pores which can be classed as either macropores ($r > 50\mu\text{m}$), mesopores ($2\mu\text{m} \leq r \leq 50\mu\text{m}$) and micropores ($r < 2\mu\text{m}$).⁷⁶ These membrane pores can be quantified in various ways and a common term used to describe the pores is the membrane porosity (also known as bulk porosity to distinguish from surface porosity) which is defined as

the volume of the pores divided by the total volume of the membrane (void volume).⁸⁰ Since the pores are not all of the same size and shape they can also be described by other means such as the pore size distribution, average pore radius and pore geometry (i.e. dead or dead-end pores which are not connected to the surface or are only connected at one end, respectively).

To describe the pore size a system has been developed in order to quantify membrane filtration properties whereby macromolecules of known molecular weights are filtered through the membrane and the feed solution is compared with the permeate in order to determine percentage rejections. From this the membrane molecular weight cut-off (MWCO) is assigned – a value which corresponds to the minimum molecular weight of a solute which is 90% rejected. This method is widely accepted and is also used by membrane manufacturers to classify their products. The most common probe macromolecules are dextrans and polyethylene glycols (PEGs) and the feed/permeate solutions are typically analysed using aqueous gel permeation chromatography (GPC) which can separate these polymers based on their size via a filtration through a column containing porous beads. Smaller analytes will enter the pores and take longer to traverse through the column whereas larger polymers will pass through the column rapidly. The polymers are detected after exiting the column and each one will have a unique retention time range which can be used to compare the amount of each polymer within the feed solution and the permeate after filtration through the membrane. An example of this is shown in **Figure 1.13** where **a)** shows the GPC chromatograms of individual PEG solutions whilst **b)** shows the traces produced after filtration of these PEG feed solutions through a commercial 50K MWCO PES UF membrane. In the permeate chromatograms the 100K PEG peak is greatly reduced since the PEG molecular weight is above the membrane MWCO and therefore the sample is retained by the membrane.

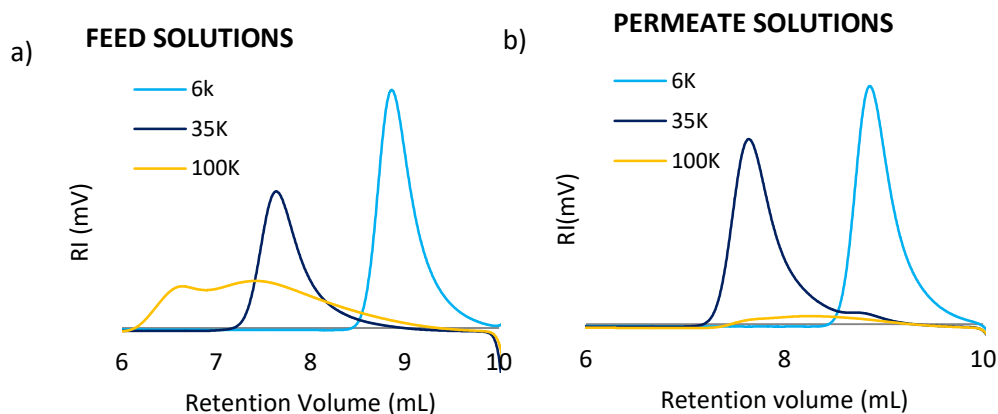


Figure 1.13: Comparison of a) feed and b) permeate GPC traces of individual PEG solutions (0.1% w/v in GPC mobile phase) after filtration with a commercial 50K MWCO PES UF membrane (present project).

Morphology characterisation methods can allow for the investigation of mechanisms which lead to changes in membrane performance or to quantify the effects of modification (i.e. coatings on surface modified membranes) or even to examine the effects of membrane ageing and changes caused by fouling or exposure to chemicals.⁷⁶

Membrane Chemistry

In order to understand the chemistry of membrane materials it is important to fully characterise these materials and to understand their properties before they are incorporated into a membrane. Since this review is focused on synthetic polymer membranes the analysis can involve a wide range of standard polymer characterisation techniques including NMR and IR spectroscopies, viscosity studies, thermal analyses, GPC characterisation. The membrane polymers can also be characterised after incorporation into the membranes themselves. For example, IR spectroscopy can be used to examine the surface chemistry of membranes. In particular IR is useful for examining chemical changes in a membrane surface, e.g. as a result of processes such as chlorination, irradiation or hydrolysis.⁷⁶ It has also been used to examine fouling processes: for example Belfer *et al.* were able to use IR to identify the presence of adsorbed albumin on surface-modified PES UF after first using IR to characterise the pristine functionalised membranes.⁸¹ This group also monitored the removal of preservatives from commercial membranes using IR spectroscopic analysis.

Membrane Performance

In order to fully characterise membranes it is important to understand how they will function when used in separation processes. Key parameters that need to be determined for pressure-driven membrane separation processes are described below.

The first key parameter to be measured is usually the **membrane flux** which relates to the water permeability and is defined as the amount of permeate produced per unit area of membrane surface per unit time. This can be measured by filtering deionised water under standard membrane operating conditions and calculating the average volume per hour of permeate. Standard units of this parameter are L/m²/h.

A second key parameter is the **% rejection** which relates to solute permeability. For dense membranes salt rejection is measured, usually for both mono and divalent salts. The divalent salts will have a larger hydrated radius and higher rejection rates are

expected for them relative to monovalent salts. For porous membranes macromolecule rejection is measured (i.e. dextrans or PEGs) which can then be used to determine the MWCO. The salt rejection can be calculated using **Equation (1)**, where C_p and C_f are the concentrations of the permeate and the feed, respectively:⁸²

$$R = \left(1 - \frac{C_p}{C_f}\right) \times 100\% \quad (1)$$

An ideal membrane will exhibit both high flux and high rejection of the target solute.

1.3 Forward Osmosis

1.3.1 Overview

As described above, osmosis is the movement of water through a semipermeable membrane driven by a difference in osmotic pressure which is generated by differing solute concentration across the membrane. *Forward (direct) osmosis* is the term used to describe a membrane separation process which is driven by a concentration gradient across a semi-permeable membrane via this naturally occurring phenomenon of osmosis.⁸³

Osmotic pressure (Π) can be defined as the minimum pressure that must be applied to the draw solution to prevent the influx of solvent from the feed solution in a system such as the one in the image below where a solution and solvent are separated by a semipermeable membrane.⁸⁴

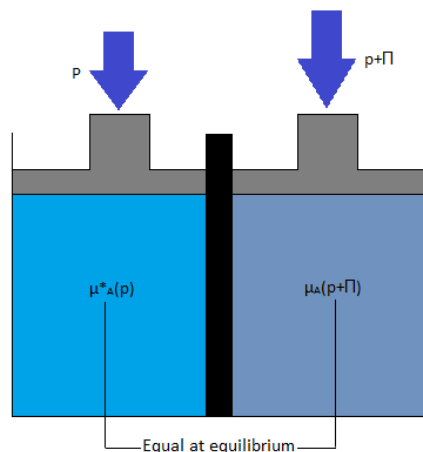


Figure 1.14: Equilibrium involved in calculation of osmotic pressure (Π), adapted from reference.⁸⁴

Figure 1.14 demonstrates the equilibrium involved in the calculation of osmotic pressure Π . This equilibrium exists between pure solvent A at pressure p on the left hand side of the semipermeable membrane (in black) and solvent A as a component of a solution (containing dissolved solutes) at pressure $p+\Pi$ on the right hand side of the

semipermeable membrane.⁸⁴ Osmosis is a *colligative property* meaning it depends only on the number of solute “particles” (i.e. ions or molecules) present in solution, not their identity.

Forward osmosis processes rely on the use of a concentrated "draw" solution which has a higher osmotic pressure than the feed solution therefore allowing it to draw water out of the feed. This results in dilution of the draw solution and concentration of the feed as illustrated in **Figure 1.15**.

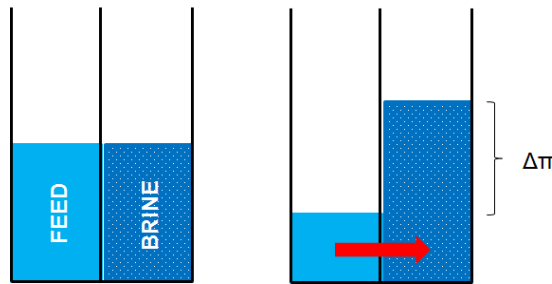


Figure 1.15: The process of forward osmosis relies on the use of a concentrated draw solution to move fluid from the feed into the draw (diluting it) across a semipermeable membrane, adapted from reference.⁸³

Forward osmosis has attracted increasing attention in recent years due to its many advantages over the pressure-driven membrane processes. The major benefit of FO technology is that it operates at no or very low hydraulic pressures since the process is driven by the concentration gradient. The low hydraulic pressure conditions result in reduced operating costs, less irreversible fouling and therefore less need for cleaning.⁸⁵ Overall these advantages make FO processes potentially much cheaper and much more energy efficient to run.

Despite these advantages FO technology has been slow to advance since its initial proposition as an alternative to the energy intensive pressure-driven membrane processes decades ago.^{86,87} This is due in part to the fact that (unlike RO) it is not a route to pure water, and in part to a lack of effective semi-permeable membranes and draw solutions⁸⁸ – the two key components of a FO process.

1.3.2 FO Membranes

Any non-porous, selectively permeable membrane can be used for FO and historically much FO research has been carried out using commercial RO membranes.⁸³ For two decades the only commercially available FO membrane was a cellulose triacetate membrane from Hydration Technology Innovations (HTI, Oregon, USA).⁸⁹ In recent years however there has been more research into membranes specifically designed for FO.⁹⁰ Considerations when designing such membranes include; reduction of the

concentration polarisation effect (described above) which results in decreased flux and inhibiting reverse solute diffusion which decreases the osmotic driving force.^{90,91}

1.3.3 FO System configuration

An ideal draw solution will exhibit the following properties;

- 1) A significantly higher osmotic pressure than the feed solution, to drive high permeate flux,⁹²
- 2) Minimal reverse diffusion, as osmotic draw solutes lost in this way will need replenishing, which increases cost. Moreover accumulation of these solutes in the feed may cause problems with disposal or continued processing of the feed;⁹³
- 3) When FO is used in water purification, a second step will be required to isolate the water from the diluted draw solution (i.e. re-concentration of draw).

This second step would need to be inexpensive, and result in high recovery of draw solution, whilst also generating high purity water, for this process to be economic.^{83,94} This re-concentration step is usually achieved through reverse osmosis or distillation for standard electrolyte draw solutions which are based on aqueous solutions of inorganic compounds such as sodium chloride (highly soluble, nontoxic and easily reconstituted).^{83,94} Other draw solutions have been explored, including thermolytic draw solutes such as ammonium carbonate which decompose into volatile gases on gentle heating.^{95,96}

Although most traditional draw solutions are based on salts or small molecules, some research has also been done into polymeric draw solutions using hydrogels^{97,98} and polyelectrolytes.^{82,98,99} It is proposed that these high molecular weight draw solutions may provide an easier route to draw solution regeneration/water isolation and could avoid issues of draw solution leakage/backflow into the feed. A new class of draw solutions has been explored by Wang *et al.* where thermo-sensitive polymer hydrogels were synthesised and were found to induce high water permeation in osmosis processes whilst also demonstrating high water release rates under a combination of pressure and thermal stimuli allowing for the regeneration of the draw solution.⁹⁷

Chung *et al.* investigated an alternative strategy - polyelectrolyte draw solutions, in this case sodium salts of polyacrylic acid (sodium polyacrylate – NaPA) which is known to be highly water soluble and can therefore create high osmotic pressures whilst being retained by a forward osmosis membrane due to the expanded conformation of the

polyelectrolyte chain resulting from charge-charge repulsions.⁸² In experiments using deionised water feed solutions and forward osmosis membranes the group found that NaPA was able to generate high water flux with insignificant back diffusion. To subsequently separate the water from the polyelectrolyte the group employed a pressure-driven ultrafiltration process although it is reported that increasing the feed concentration reduced the water production and rejection of the polyacrylate which is attributed to concentration polarization and fouling effects. Wang *et al.* also investigated an alternative draw solution strategy this time using novel thermo-sensitive polyelectrolytes based on copolymerised *N*-isopropylacrylamide (NIPAM) the polymer form of which (PNIPAM) can be used to create a thermo-sensitive hydrogel which was combined with different amounts of sodium acrylate.¹⁰⁰

As mentioned above, a major drawback of the pressure-driven membrane processes is their susceptibility to fouling. Membrane fouling in FO has also yet to be fully explored and understood.¹⁰¹ However, for osmotically driven processes fouling is potentially less of an issue as it is usually more reversible than in membrane processes reliant on applied hydraulic pressure. This is due to the rejected solutes forming a far less compacted 'cake layer' in osmotically-driven membrane processes than in pressure-driven membrane processes. It can thus be re-dispersed by simple physical methods such as hydraulic flushing, without the need for harsh chemicals which could degrade the membrane.^{101–103}

1.4 Membrane Modification

1.4.1 Overview

In order to achieve the best possible membrane properties it is sometimes beneficial to either modify the polymers used or to blend them with another polymer or non-polymer additive. This can allow control of the membrane structure, porosity, pore distribution and thickness, as well as other properties which will affect the overall selectivity of the membrane.¹⁰⁴ There are several strategies which can be employed to modify membranes and they can be loosely classed as either bulk or surface modifications. Membrane surface modifications allow for the retention of desirable bulk mechanical properties of the polymer whilst achieving suitable surface properties for the end application¹⁰⁵. Surface modification strategies include; membrane coating, grafting and chemical modification. One of the main applications of membrane surface modification is to decrease membrane fouling and this is often done through increasing the polymer surface hydrophilicity.¹⁰⁶ The following approaches can be used to modify membranes;

Bulk Modification

Additives - where organic (hydrophilic/amphiphilic polymers) or inorganic substances are mixed with the membrane casting solution to give either polymer blend or composite membranes, respectively. In composite membranes the two or more materials have different chemical and/or physical properties allowing them to remain distinct at a macroscopic level.¹⁰⁵

Surface Modification

Coatings - Polymers or small molecules are deposited on the membrane surface where they adhere through non-covalent interactions to form a membrane coating. There are several types of coating techniques; hydrophilic thin layer (physical absorption), coating with a monolayer (Langmuir-Blodgett), deposition from glow discharge plasma and casting of two or more polymer solutions using simultaneous spinning equipment.¹⁰⁵

Grafting - Grafting involves the addition of polymer chains onto the membrane surface where they are bound via covalent interactions. There are two key types; 'grafting-from' where active species on an existing membrane surface initiate the polymerisation of monomers from the surface (graft polymerisation) and 'grafting-to' where polymer chains with reactive side groups are covalently coupled to the membrane surface.¹⁰⁷ There are several ways to initiate the polymerisation reaction giving rise to different sub-categories of grafting; chemical, radiation, plasma photochemical or enzymatic induced grafting.¹⁰⁸ It is also possible to graft either one monomer or a mixture of two or more.

Chemical modification - This involves treating the membrane with chemical species which will introduce new functionality on the membrane surface. Reactions which have been applied to membrane functionalisation include; sulfonation, chloromethylation, aminomethylation and lithiation.¹⁰⁵ Sulfonation of membrane polymers can be achieved by either *post-sulfonation* of the final polymer or through copolymerisation with sulfonated monomer (*pre-sulfonation*).¹⁰⁹ Both strategies involve electrophilic aromatic substitution (EAS) reactions to introduce the sulfonic acid groups. Poly(arylsulfones) which include PSF and PES are widely used membrane materials due to their relatively low cost but, as mentioned above, the hydrophobic nature of these polymers makes them highly susceptible to fouling. Sulfonation offers a route to increased membrane surface hydrophilicity therefore decreased fouling tendency.

1.4.2 Interfacial Polymerisation

Interfacial polymerisation is an alternative form of membrane modification which not only modifies the membrane surface but also alters the membrane application. As outlined in *Section 1.2.1* and *Section 1.2.4*, interfacial polymerisation involves the spontaneous growth of a semi-permeable polyamide membrane on the surface of a supporting ultrafiltration membrane effectively converting the UF membrane into a reverse osmosis membrane or nanofiltration membrane. The porous support is coated with an ultra-thin yet dense polyamide film allowing this composite membrane to now reject much smaller solutes such as hydrated ions. **Figure 1.16** illustrates the two step process involved in coating an ultrafiltration membrane to produce an interfacially polymerised thin-film composite membrane. The microporous support membrane is first impregnated with an aqueous solution of the amine. After the membrane is drained, the membrane surface is contacted with an organic solution of a multivalent crosslinking species allowing a polymer film to form on the surface of the membrane.

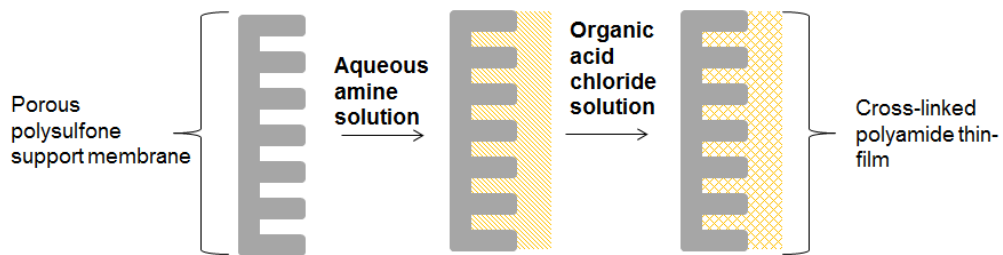


Figure 1.16: Schematic of thin film composite anisotropic membrane fabrication using the interfacial polymerisation technique, adapted from reference.⁶²

1.5 Oedema

1.5.1 Overview

Oedema can be defined as the abnormal accumulation of fluid in the body's tissues or cavities which causes swelling of the affected areas. Oedema can occur within cells (intracellular oedema) but more commonly develops within tissues (extracellular oedema)¹¹⁰ which is the focus of the present literature survey. Intra- and extra-cellular oedema are, however, often not mutually exclusive; the extracellular oedema in the body's tissues results in swelling which will affect blood supply therefore leading to intracellular oedema.¹¹¹

Oedema can be caused by several mechanisms and is usually the symptom of an underlying pathological condition. Consequently classification of oedema is not well defined due to lack of standardised definitions and methods of quantification. Currently there is no cure and only very limited methods of treatment for a condition which can have a severe impact on quality of life.

1.5.2 Fluid Homeostasis

Oedema arises when systems maintaining fluid homeostasis in the body malfunction, causing disruption of normal body fluid distribution, and ultimately resulting in the accumulation of fluid in the affected area. The human body consists of approximately 60% water by weight, or 42 litres for an average 70 kg adult male. The amount is slightly less in females (55%) due to a higher fat content.¹¹¹ The principle of homeostasis requires that total body fluid **volume** and **osmolarity** (osmotic concentration) remain relatively constant. This is achieved by the regulation of two main factors; sodium balance and water balance. Sodium salts are the principal paracellular solutes and the regulation of sodium concentration is related to the circulating fluid volume.¹¹² Proper maintenance of sodium balance ensures that all tissues are sufficiently perfused with fluid.¹¹³ The regulation of water balance is related to the osmolarity of body fluids and is essential in maintaining normal cell volume.¹¹⁴

The overall volume and osmolarity of the body fluids is regulated by a complex system involving the brain, the central nervous system and hormones which are responsible for controlling water and salt excretion by the kidneys in response to detected volume and osmolarity.^{115,116}

The distribution of the fluid throughout the body is also important in maintaining optimal physiological conditions. The body fluid is divided between two compartments; the *intracellular* (ICF) and *extracellular* (ECF) spaces as illustrated by the diagram below (**Figure 1.17**). The intracellular fluid is the larger compartment and consists of the liquid component within cells, otherwise known as the cytosol. The extracellular fluid can be further split into two major components; intravascular **blood plasma** in the blood vessels (~25%) and the extravascular **interstitial fluid** in the tissue spaces (~75%).¹¹⁷ There are also additional minor compartments within the ECF including **lymph fluid** and **transcellular fluid**.¹¹¹

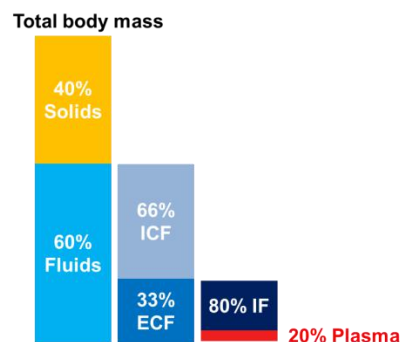


Figure 1.17: Body fluid distribution in an average lean adult male, ICF – intracellular fluid, ECF – extracellular fluid, IF – interstitial fluid, adapted from reference.¹¹⁸

The different compositions of these fluids are essential in maintaining normal physiological conditions and are maintained by the physiological barriers (e.g. cell membranes, blood vessel walls) separating them. However, all body fluids will have approximately the same osmolarity, which is essential in preventing net movement of water in or out of the cells, which would result in cell shrinkage or swelling.¹¹⁹

There are three key extracellular body fluids which are relevant to extracellular oedema formation. These include the two major ECF components; blood plasma and interstitial fluid along with the lymph fluid (a lesser component of the ECF). These fluids are able to exchange through a specialised *microvascular exchange system* (see below), so that changes in the volume and composition of one fluid will impact on the volume and composition of the others. It is important to note that the interstitial fluid can also exchange with the ICF compartment within the cells. The ability for exchange between all these fluids is paramount to their function; the blood transports substances such as nutrients, metabolites and oxygen to the cells in the tissues whilst simultaneously removing cellular waste. The exchange of these substances between the blood plasma in the capillaries and the intracellular fluid within the cells occurs via an intermediate fluid – the interstitial fluid bathing the tissue cells. The majority of the interstitial fluid is returned to the circulation via the lymphatic system.

Compositions of Body Fluids

The blood plasma and the interstitial fluid, being the two major components of the ECF compartment, can be exchanged across the selectively permeable blood capillary wall which separates them. These two fluids have similar compositions, although due to the selective barrier dividing them there is one major difference – the protein content. The diffusion of blood plasma proteins into the interstitium is severely restricted by their large molecular size relative to the capillary pores (see **Table 1.2**). However there are other routes by which proteins can traverse the membrane and enter the tissues; specialised vesicles can transport proteins out of the capillary and into the tissues, or the action of neurotransmitters such as histamine and serotonin can increase capillary permeability.^{120–122} Despite this, in normal tissues the rate of protein extravasation is relatively low and the concentration of protein in the blood plasma is usually 2 to 3 times greater than in the interstitial fluid.¹²³ It is important to note, however, that the total protein content in the 12 L of interstitial fluid is greater than in the plasma but because the volume of IF is four times that of the plasma (3 L) the average protein concentration of the IF is approximately 3 g/dL, i.e. 40% of that in plasma.¹²⁴

Other plasma components are able to traverse the capillary much more freely through various mechanisms discussed below. These include: hormones, gases (carbon dioxide and oxygen) and nutrients such as fatty acids, amino acids and glucose.¹²⁵ The blood also contains 'non plasma' components; white and red blood cells (leukocytes and erythrocytes) and platelets (thrombocytes)¹²⁶ which are also not able to readily permeate through the capillary walls, again due to their large size.

The interstitial fluid is also able to exchange with the intracellular fluid within the tissue cells themselves. The barrier separating these two fluids is the cell membrane which has many mechanisms for transporting components in and out of the cell as required, resulting in a significant difference in the compositions of these two fluids. The major difference between the ICF and the tissue fluid is in salt composition. Unlike the extracellular fluids the ICF is high in K^+ and low in Na^+/Cl^- which differs significantly from the high Na^+/Cl^- and low K^+ levels found in both the tissue fluid and blood plasma. The intracellular fluid also has a higher amount of protein than both the plasma and the interstitial fluid (see **Table 1.1**).

Table 1.1: Body fluid compositions, adapted from reference.¹²⁷

	Plasma (mOsm/L H₂O)	Interstitial Fluid (mOsm/L H₂O)	Intracellular Fluid (mOsm/L H₂O)
Na⁺	142	139	14
K⁺	4.2	4.0	140
Mg²⁺	1.3	1.2	0
Cl⁻	108	108	4
HCO₃⁻	24	28.3	10
HPO₄⁻, H₂PO₄⁻	2	2	11
SO₄⁻	0.5	0.5	1
Phosphocreatine			45
Carnosine			14
Amino acids	2	2	8
Creatine	0.2	0.2	9
Lactate	1.2	1.2	1.5
Adenosine triphosphate			5
Hexose monophosphate			3.7
Glucose	5.6	5.6	
Protein	1.2	0.2	4
Urea	4	4	4
Others	4.8	3.9	10
Total mOsm/L	301.8	281.0	281.0
Total osmotic pressure at 37°C (mm Hg)	5443	5423	5423

Finally the interstitial fluid can be converted into lymph fluid. Unlike the above exchanges between the blood plasma/interstitial fluid or the interstitial fluid/intracellular fluid, the conversion of interstitial fluid into lymph fluid is a one-way process. This is due to the structure of the initial lymphatics which consist of overlapping endothelial cells forming a valve and preventing back-flow of fluid and solutes which, once within the lymphatic vasculature, from then on is referred to as lymph fluid.¹²⁸ The fluid collected is generally thought to have a similar composition to the interstitial fluid¹¹¹ but it has been well-documented that the lymph fluid is modified by passage through the lymph node. This results in changes in protein concentration which are thought to be involved in establishing the equilibrium of Starling's forces (see *Section 1.5.3*).¹²⁹ Few studies have analysed the composition of lymph fluid, but analysis of ovine samples has shown that lymph contains a wide variety of proteins, not all of which are derived from plasma, suggesting lymph fluid is more than just an ultrafiltrate of plasma.¹³⁰ As with plasma, however, the major protein was found to be albumin.

Lymph fluid also contains other components which can include; cytokines (signalling proteins) extracellular matrix constituents, proteases, intracellular proteins, plasma proteins, erythrocytes and lymphocytes.¹³⁰⁻¹³³

Barriers in Fluid Homeostasis

The blood plasma in the capillary is separated from the interstitial fluid in the tissue spaces by the capillary wall which consists of a single layer of endothelial cells, less than 2µm thick, supported on the basement membrane which is part of the surrounding *extracellular matrix* (see below) and is secreted by the endothelial cells themselves.¹²⁵ The basement membrane prevents the passage of macromolecules from within the blood into the extracellular space.¹³⁴ The diameter of the blood capillary forces blood cells to pass in single file.¹³⁵ There are three types of capillaries with differing permeabilities according to their function; **continuous capillaries**, **fenestrated capillaries** and **sinusoid (discontinuous) capillaries**, see **Figure 1.19**. All three types have leaky junctions between the endothelial cells creating small pores known as intracellular junctions (clefts) which allow the diffusion of water, ions and small hydrophilic molecules, such as urea and glucose, into the interstitium - a process known as the paracellular pathway.¹³⁶ These clefts represent 1/1000 of the capillary surface area and have a radius of 6-7 nm, which is slightly smaller than the diameter of albumin.¹²⁴ Clearly the molecular size of plasma components will affect their ability to pass through the intracellular junctions. The relative permeabilities of a range of substrates are given in **Table 1.2**.

Table 1.2: Relative permeability of skeletal muscle capillary pore to molecules of different sizes.^{124,137}

Substance	Molecular Mass (Da)	Relative Permeability
Water	18	1.00
NaCl	58.5	0.96
Glucose	180	0.6
Albumin	69,000	0.001

Water is also transported through specialised water-selective protein channels called *aquaporins*,¹³⁸ whereas lipid-soluble substances such as dissolved oxygen and carbon dioxide can passively diffuse through the endothelium cells themselves – this is known as the transcellular route.¹³⁷ All three capillary types also have specialised vesicles that can transport various substances across the capillary wall.¹³⁹

Continuous capillaries are found almost everywhere in the body, particularly in muscle, connective tissue and neural tissue.¹⁴⁰ Fenestrated capillaries have large pores (*fenestrae*) with diameters of between 500 and 600 Å¹²⁵ which allow larger volumes of fluid to be exchanged between the plasma and the interstitium, this type of capillary is found in the kidney and the intestine.¹³⁵ Sinusoidal capillaries are found in bone marrow, liver and spleen and have large gaps which allow blood cells through, as these types of tissues are involved in blood processing.¹⁴¹ The rate of fluid exchange is highest in the sinusoidal capillaries, followed by fenestrated then continuous capillaries. However, net rate of diffusion of substances will be dependent on the concentration gradient across the capillary wall.

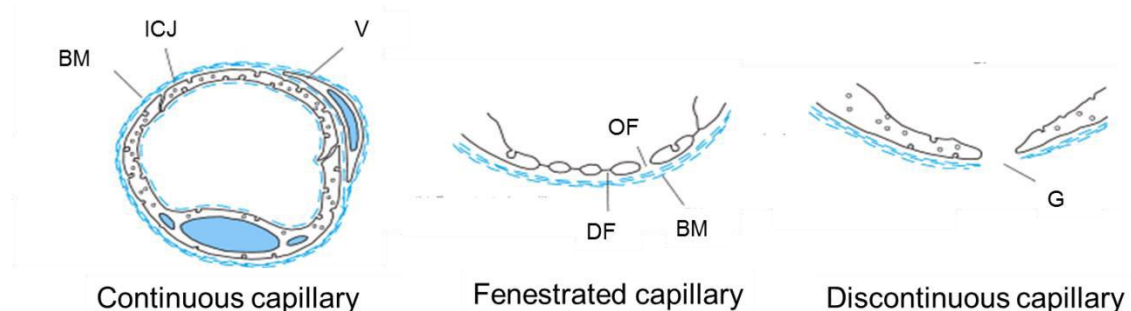


Figure 1.19: Cross-sections of different capillary types, BM- basement membrane, ICJ – intercellular junction, V – vesicles, OF –open fenestrae, DF – diaphragmed fenestrae, G – gap, adapted from reference.¹²⁵

As discussed above, the interstitial fluid and intracellular fluid have significantly different salt concentrations maintained by the barrier which separates them - the cell membrane. The cell membrane has many mechanisms in place to transport different substances in and out of the cell. These include active carrier systems (e.g. the Na-K

pump) which can transport specific substances through the cell membrane as illustrated in **Figure 1.20**.¹⁴² Other substances such as water can move freely between the intracellular compartment and the interstitial fluid due to the high hydraulic permeability of the cell membrane. If the osmotic concentration of either the interstitial fluid or ICF changes, water can traverse the semipermeable cell membrane until equilibrium is attained.¹⁴³ The cell membrane is also known to be permeable to solutes which contribute to the osmotic concentration of the interstitial fluid.¹⁴⁴ Thus, it is clear that the osmolarity and volume of the IF will affect cell volume and osmolarity which is significant since changes in cell volume can impair cell function.¹⁴⁵ A decrease in IF osmolarity will result in net movement of water into the cells increasing cell volume/decreasing the cell osmolarity. An increase in IF osmolarity will cause water to move out of the cell decreasing the cell volume and increasing the cell osmolarity.¹⁴⁶ The volume of the ECF (plasma and IF) is primarily determined by the total body sodium content as well as by the total body water content.¹⁴⁷

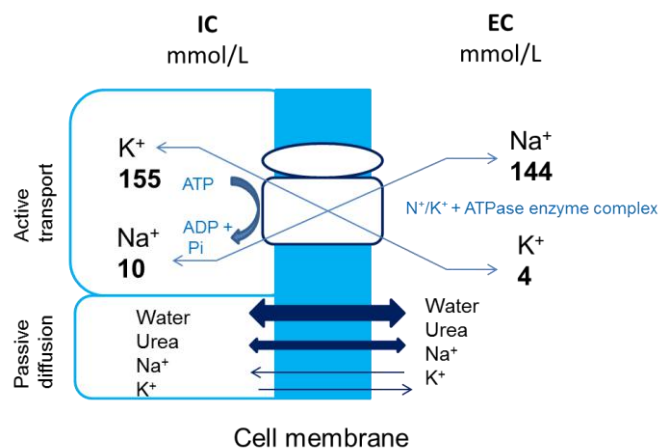


Figure 1.20: Active and passive transport across a plasma cell membrane, adapted from reference.¹⁴²

Gibbs-Donnan Effect

The presence of barriers separating fluids, such as the capillary wall or cell membrane, gives rise to the so-called Gibbs-Donnan effect.¹⁴⁸ The Gibbs-Donnan effect is a phenomenon responsible for the behaviour of charged particles near the surface of a semi-permeable membrane resulting in the uneven distribution of the particles on both sides of the membrane, usually due to the presence of a charged substance on one side of the membrane which cannot traverse it.¹⁴⁹ The ions which can traverse the membrane will redistribute in order to preserve electro-neutrality.

This effect exists across the capillary wall, between the blood plasma and interstitial fluids as well as across the cell membrane separating the interstitial fluid and the cytosol.¹⁵⁰ In the case of the capillary wall, the low permeability to plasma proteins

results in an ionic concentration difference between the plasma and the IF. This is caused by the highly negatively charged proteins attracting positively charged ions, whilst repelling negatively charged ions to give uneven distributions of ions across the capillary membrane despite it being freely permeable to the ions.¹⁵⁰ With cell membranes, the effect is similar; negatively charged cytoplasmic proteins will have an effect on the distribution of ions across the membranes causing positively charged IF ions to enter the cell, whilst repelling negatively charged ions.¹⁵¹ Although overall electro-neutrality will be maintained, the high intracellular osmolarity should cause an influx of water into the cell which would disrupt the Gibbs-Donnan equilibrium, causing more ions to diffuse eventually resulting in cell swelling (cellular oedema).¹⁵⁰ This undesirable effect is mitigated by the action of the Na-K pump which removes sodium ions from the cell to balance the Gibbs-Donnan effect by restricting sodium to the ECF; intracellular chloride ions are forced out of the cell cytoplasm, the overall effect of which is to decrease the osmotic burden.^{150,151}

1.5.3 Physiology

As discussed above, the total body fluid is normally divided between the intracellular and extracellular spaces. These fluids can exchange through the *microvascular fluid exchange system* (**Figure 1.21** below) which is involved in the regulation of blood flow in individual organs as well as the transport of nutrients to the tissue cells and the removal of cellular waste products.¹²⁶

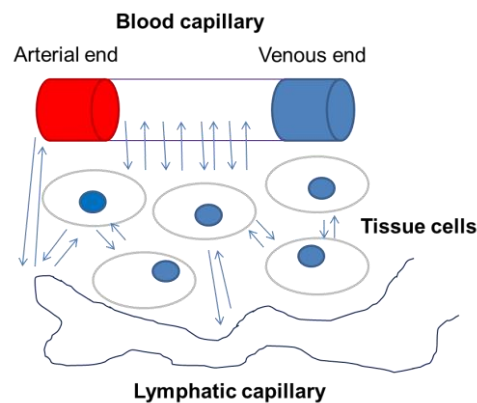


Figure 1.21: Microvascular fluid exchange system, adapted from reference.¹²⁴

The microvascular fluid exchange system consists of three ECF components; blood plasma in the capillaries, interstitial fluid bathing the tissue cells and lymph fluid in the lymphatic vessels.¹⁵² The exchange process involves; capillary filtration (fluid moving into the interstitium) to give interstitial fluid which can exchange with intracellular fluid within the tissue cells before returning to the circulation either through capillary absorption or via the lymphatic system.

The Interstitium

The interstitium occupying the space between the vascular and lymphatic systems has a complex structure and although the composition can vary between tissues, the basic components of all connective tissue are similar. These include the tissue cells which are supported on a skeleton of insoluble fibres, surrounded by a soluble polymer gel and the interstitial fluid containing solutes and plasma proteins (See **Figure 1.22**).^{124,153} The fibres and the polymer gel together are known collectively as the extracellular matrix (ECM). As noted above, the *basement membrane* is also considered to be part of the ECM.^{154,155}

The ECM fibrils form a meshwork consisting of polyamides such as elastin and collagen which is the most abundant protein in animal tissue.^{155–157} The soluble polymer component of the ECM, otherwise known as 'ground substance', is a hydrophilic amorphous gel phase occupying the space between the cells and the fibres.¹⁵⁸ The ground substance is made up of:

1. *Glycosaminoglycans* (GAGs) - repeating disaccharide units forming unbranched polysaccharide chains. The majority of the GAGs are highly negatively charged, causing the chains to repel each other due to the presence of sulfate and carboxylate groups and therefore bind cations such as Na^+ and trap water molecules in the interstitial fluid to form hydrogels.^{155,159} Hyaluronan (hyaluronic acid) is an exception in that it does not contain sulfate groups and is therefore less negatively charged than the other GAGs, allowing it to form infinite meshworks in dilute solution.^{155,158} Within connective tissues, GAGs do not appear as free polymers and are found in the form of proteoglycans.¹⁶⁰
2. *Proteoglycans* (PGs) formed from GAGs covalently bonded to a protein to give a highly cross-linked gel.^{154,161}
3. *Multiadhesive glycoproteins* responsible for linking components of the ECM and the cells.¹⁵⁵

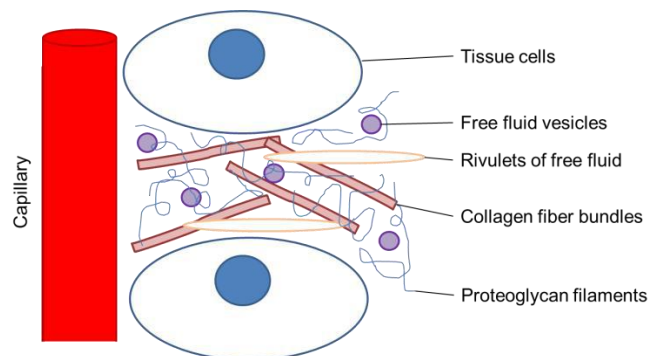


Figure 1.22: Interstitium structure, adapted from reference.¹²⁴

A major role of the ECM component of the interstitium is the regulation of the interstitial fluid volume which it achieves through the specialised physical and biochemical properties of its components.¹⁶² The proteoglycans are known to immobilise water molecules, resisting flow through the interstitium and therefore affecting hydraulic conductivity.¹⁶⁰ The polysaccharides can also 'relax' the concentration gradient and therefore reduce the osmotic pressure of the tissue causing water to be drawn in.¹⁶³

The fibrous component of the ECM also has a role. The entangled structure of the fibres results in the formation of pores approximately 200-250 Å in diameter.¹⁶⁴ Macromolecules such as extravasated plasma proteins, present in the interstitial fluid, can only reside in regions of the interstitium unoccupied by the structural components of the ECM and consequently these macromolecules will only occupy a fraction of the interstitial fluid volume. The larger proteins will remain in the solution phase, as the gel phase prevents bulk flow of fluid through the interstitium.¹⁶⁵ This phenomenon is known as interstitial exclusion.¹⁶² Solute exclusion will vary with hydration state. In states of increased hydration, the effective pore radii of the gel phase will increase to give a larger volume for the fluid to be distributed in and in dehydration the reverse is true.¹⁶⁴ Hence, the tissue water content is important as it defines the tissue volume and controls the space available for molecular transport processes.¹⁶³

The significance of solute exclusion is related to an oedema-preventing mechanism. As fluid accumulates in the interstitium, the accessible volume will increase thus reducing the tissue oncotic pressure making capillary filtration less favourable and protecting against oedema formation.¹⁶⁴ This effect is often referred to as '*wash-down of interstitial protein concentration*' and can withstand an increase in capillary pressure corresponding to 7 mm Hg.¹¹¹ There are another two safety factors which normally prevent oedema formation. These include; 1) *low tissue compliance* when the interstitial fluid pressure is in the negative pressure range corresponding to 3 mm Hg and 2) the *ability of lymph-flow to increase 10-50 fold* to accommodate large fluctuations in fluid corresponding to 7mm Hg.^{110,111} Overall, this results in a total safety factor of 17mm Hg, theoretically allowing the capillary pressure to rise by this amount before oedema will occur.

Although the fluid in the interstitium is usually found trapped within the ECM to form a gel there are still small rivulets and vesicles of "free" fluid not associated with proteoglycan molecules and therefore able to flow freely. This free fluid accounts for less than 1% in normal tissues, but in oedema, the pockets of free fluid will expand to give large volumes of freely flowing oedema fluid.¹²⁴

The extracellular matrix has many complex functions and, as well as regulation of water content of tissues, it is particularly important for the maintenance of shape and protection of the organs of the circulatory, nervous and digestive systems.^{159,166}

The Lymphatic System

As discussed previously, the major function of the lymphatic system is the removal of excess interstitial fluid from the tissues and returning this fluid along with extravasated plasma proteins and other large molecules to the circulation. This means the lymphatic system has a key role in control of; interstitial fluid protein concentration, volume and pressure. In normal conditions these three factors are balanced in steady state levels; leaked proteins cause the interstitial fluid oncotic pressure to rise, causing increased capillary filtration resulting in increased interstitial fluid volume and pressure, the latter of which will increase the rate of lymph flow.¹²⁴

The lymphatic system originates in the interstitial tissues with the initial lymphatics (lymphatic capillaries) which merge to give collecting lymphatics which will go on to give way to lymph nodes, trunks and ducts which return the lymph to the circulation.¹⁶⁷

Figure 1.23 shows a cross-section of skin showing the relative positions of both the lymphatic and blood capillaries in the dermis. The thoracic duct is the final branch of the lymphatic system and is connected to the subclavian and jugular veins near their junctions in the neck allowing the lymph fluid to be returned to the circulation.¹⁶⁸

Lymph formation is a passive process involving a hydraulic pressure gradient developing between the hydrated tissue and the lumen of the lymph vessel causing the endothelial cell valves in the initial lymphatics to be pulled open, trapping fluid and solutes.¹²⁸ Unlike the circulatory system the lymphatic system has no central pump, although the main lymphatic vessels contain valves to prevent lymph backflow.¹⁶⁹

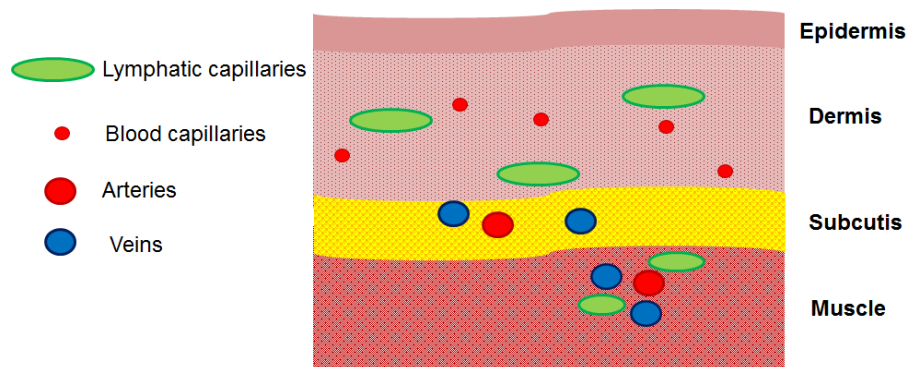


Figure 1.23: Cross-section of skin showing relative positions of lymphatic capillaries and blood capillaries in dermis made up of connective tissue consisting of cells and the ECM, adapted from reference.¹⁷⁰

Microvascular Exchange

Fluid exchange between the blood plasma in capillary and the interstitial fluid in the tissue spaces is controlled by the opposing forces of hydrostatic pressure and oncotic (colloid osmotic) pressure also known as *Starling Forces*, see **Figure 1.24**.¹⁷¹ Hydrostatic pressure is generated by the heart pumping blood through the arteries so that in the arterial end of the capillary the blood plasma fluid is forced out into the interstitial space (*filtration*).

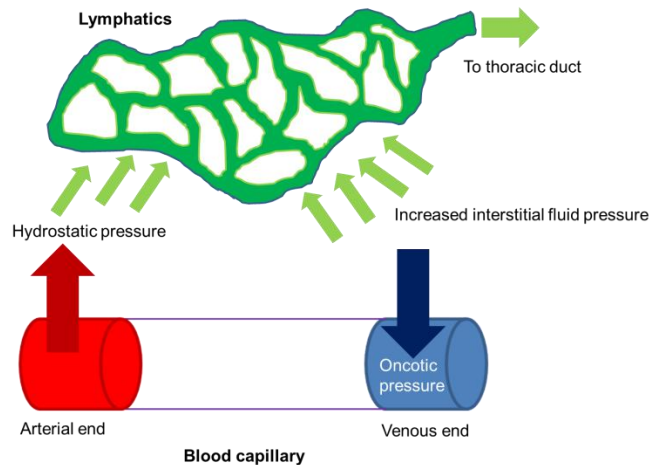


Figure 1.24: Microvascular fluid exchange system, adapted from reference.¹⁷²

The blood plasma proteins are mostly retained within the capillary as they are too large to traverse the pores in the capillary wall. These proteins will generate the oncotic pressure at the venous end of the capillary causing the interstitial fluid to be drawn back into the capillary (*adsorption*).¹⁷³ Filtration is usually greater than adsorption resulting in more fluid moving out of the capillary than is returned, and therefore the lymphatic system has a role in the removal of interstitial fluid from the tissue spaces and returning it to the circulatory system.¹³⁵ Since some proteins will still leak out of the capillary and cannot be reabsorbed into the capillary the lymphatic system has a key role in returning these proteins to the circulation, thereby maintaining the oncotic pressure of the blood.¹⁷⁴ There are three major types of blood plasma protein; albumin, globulin and fibrinogen.¹⁷⁵ Albumin (68 kDa) accounts for 50% of the plasma protein present in healthy individuals and it is this high concentration combined with its high negative charge which results in albumin generating approximately 70% of the plasma oncotic pressure.¹⁷⁶

The forces which determine fluid movement through the capillary membrane can be described by the **Equation (2)**;

$$\text{Flow per unit area} = Kc[(P_c - P_{if}) - \sigma(\Pi_c - \Pi_{if})] \quad (2)$$

Where K_c is the capillary filtration coefficient, P is the hydrostatic pressure for the capillary and interstitial fluid whereas Π is the oncotic pressure again for the capillary and interstitial fluid.¹⁴⁸ The symbol σ represents a retention coefficient which quantifies the ratio of the oncotic pressure exerted by a given concentration of protein to the theoretical oncotic pressure expected for a capillary wall which did not allow proteins to leak through.^{173,148} This is required as Π_c is affected by the permeability of the capillary since in reality the capillary wall is not a perfect semipermeable membrane and the plasma proteins are able to leak into the interstitium.¹⁷³ According to Guyton *et al.* normal values for these pressures are; P_c 17-25mm Hg, P_{if} -3mm Hg, Π_c 28mm Hg (19mm from dissolved proteins and 9mm from the Gibbs-Donnan effect) and Π_{if} 8mm Hg.¹²⁴

A positive value for the flow per unit area indicates that capillary *filtration* is favoured and a negative value is obtained when capillary *absorption* is favoured.

1.5.4 Pathophysiology

There are two types of mechanisms which can lead to the development of extracellular (interstitial) oedema;

1. Non-Inflammatory

- a) *Disruption of the capillary dynamics* resulting in abnormal leakage of plasma fluid into the interstitium. This can be caused by excessive capillary filtration due to increased hydrostatic pressure (hydrostatic oedema) or decreased oncotic pressure preventing reabsorption of fluid back into the capillary, or a combination of both effects.¹⁷⁷
- b) *Lymphatic obstruction* resulting in failure of lymphatic system to return fluid from the interstitial space back into the blood. This gives rise to a specific form of oedema known as lymphoedema.^{111,178}

2. Inflammatory

- a) *Stimulation of the inflammatory immune response* resulting in histamine release which will increase the permeability of the capillary (permeability oedema) allowing plasma proteins to diffuse into the interstitium.¹⁷⁹⁻¹⁸¹

Causes of non-inflammatory oedema include renal disorders, cirrhosis, congestive heart failure, nephrotic syndrome and chronic venous insufficiency.^{177,182} When caused by right-sided heart failure or other systemic disease the oedema will be symmetrical and will develop from the ankles upwards.¹⁸³ Unilateral oedema will

usually result from a local cause such as deep vein thrombosis, venous insufficiency or lymphedema.^{183,184}

Inflammatory oedema is caused by physical damage to the tissue from sprains, freezing injuries and thermal damage.^{161,180}

1.5.5 Clinical Symptoms And Diagnosis

Initially it can be difficult to distinguish between chronic peripheral oedema and lymphoedema. The differential diagnosis of swollen limbs includes systemic and local causes. The former comprising of heart failure, renal disorders, hypoalbuminemia whereas the latter includes primary and secondary lymphoedema, venous disorders, bacterial infections and complications following surgery.^{185,186} A thorough medical history is required along with a physical examination of the affected area. This information is usually enough to make a diagnosis, but in some cases if the cause is not known lymphoscintigraphy may be used to image the lymphatic system and check for abnormalities. This technique involves an intradermal injection of radiolabelled colloid into the affected area followed by imaging using a gamma camera to trace the lymphatic transport of the radiotracer.¹⁸⁷ Other techniques which can be used to image the lymphatic system include magnetic resonance imaging (MRI), computed tomography (CT) and ultrasound examination.^{185,187,188}

Chronic Oedema

Chronic oedema is a broad term used to describe oedema not caused by lymphatic obstruction/defects lasting 3 months or more which is not relieved by elevation or bed rest.¹⁸⁹ There are a mixture of causes and ultimately the lymphatic system will be impacted by the condition if it is not treated.¹⁹⁰ Oedema is often not clinically apparent until at least 2.5-3 L of fluid has accumulated in the interstitium.¹⁹¹ Clinically there are two types of oedema; pitting and non-pitting oedema, over time pitting oedema can develop into non-pitting oedema as the subcutaneous tissue becomes fibrotic.^{192,193}

Pitting oedema can be differentiated from non-pitting oedema with a simple test which involves the physician pressing the affected area with their thumb for a set time then seeing whether a 'pit' is formed. In pitting oedema the resistance to tissue fluid displacement is lowered by the accumulation of fluid in the interstitium resulting in dilution of the interstitial gel compartment to produce pockets of water which are easily displaced by the application of pressure therefore forming a pit.¹⁹⁴ The duration that the pit lasts can also be used to assign the oedema a number in the 'Pitting Oedema Scale' which gives some idea of the severity of the oedema.¹⁹⁵

Pitting oedema is often caused by systemic diseases such as heart failure and kidney and liver disorders which result in decreased serum protein, increased systematic venous pressure.^{184,196} Other causes of pitting oedema include venous insufficiency and deep vein thrombosis (DVT).^{182,197} The accumulated oedema fluid is of low viscosity and is protein poor.¹⁸⁴ Non-pitting oedema occurs in advanced lymphoedema. Initially the lymphoedematous swelling shows pitting, but with time the tissue becomes fibrotic to give non-pitting oedema.¹⁹²

Lymphoedema

Lymphoedema can be classed as primary or secondary. Primary lymphoedema encompasses genetic abnormalities and syndromes and can be further subdivided into categories based on the age of the patient when the symptoms began to develop.¹⁸⁸ Congenital lymphoedema can be detected at birth or within the first two years of life, lymphoedema praecox usually develops during puberty although can occur into the early 30's, and the final type - lymphoedema tarda is detectable after 35 years.¹⁹⁸ Secondary or acquired lymphoedema develops as a consequence of disruption or obstruction of the lymphatics and has many causes. These include; traumatic lymphoedema in response to direct injury to the lymphatic system, post-infection lymphoedema often as a result of recurrent cellulitis infections or infection by a parasitic worm (filariasis) and finally cancer and cancer treatments.¹⁸⁷ In the western world most diagnosed forms of lymphoedema are malignancy-related, but it is thought that non-cancer forms of the condition are likely to be more prevalent but poorly recognised and underdiagnosed.¹⁹⁹ In developing countries the most common cause is infection by filariasis which is in fact the most common cause worldwide with an estimated 120 million people currently infected and nearly 947 million people at risk in 54 countries.²⁰⁰ The clinical classification of lymphoedematous swelling is defined by the stages of lymphoedema outline by the International Society of Lymphology:²⁰¹

Stage 0 Latent or subclinical condition where swelling is not evident despite impaired lymph transport. Can exist months or years before overt oedema occurs (stages I–III).

Stage I Early accumulation of fluid relatively high in protein content (e.g. in comparison with “venous” oedema) that subsides with limb elevation. Pitting may occur.

Stage II Pitting may or may not occur as tissue fibrosis develops. Limb elevation alone rarely reduces tissue swelling.

Stage III Lymphostatic elephantiasis - pitting is absent. Trophic skin changes, fat deposits, and warty overgrowths often develop. (Adapted from references^{188,201})

Oedema can also be classified by its localisation; *generalized oedema* – involving multiple organs as well as peripheral (subcutaneous) oedema and *organ-specific oedema* – i.e. cerebral, pulmonary and peritoneum (ascites).¹⁴⁷ The present research project will focus on the treatment of peripheral oedema, i.e. subcutaneous oedema in the limbs.

Accumulation of excess interstitial fluid increases the diffusion distance for oxygen and other nutrients to reach the cells as well impeding the removal of toxic cellular waste products. In severe cases this disturbance in blood supply to the tissues is known as *ischemia* and can result in cell damage and death.^{202,203}

1.5.6 Treatment

Current treatments for oedema/lymphoedema are very limited, and at present there is no satisfactory resolution for either condition. Since oedema is often the sign of an underlying medical condition, initial strategies generally aim to treat and manage the primary cause. Other approaches involve restricting dietary sodium to reduce water retention, weight loss for obese patients and in certain cases, such as hydrostatic oedemas caused by congestive heart failure or venous disorders such as chronic venous insufficiency, the use of diuretics to promote fluid excretion through kidneys.^{184,204} Diuretics will have little effect on lymphedematous oedema as pathogenesis of this condition relies on elevated tissue oncotic pressure from accumulated macromolecules (mainly proteins) and not excess water retention.²⁰⁵

Lymphoedema treatment can be divided into conservative (non-operative) and operative approaches, although underpinning both methods is a meticulous skin care regime along with careful exercise and compression.²⁰¹ The main approach is Complex Decongestive Therapy (CDT) which should be performed by a certified therapist and involves a combination of: lymphatic-specific massage known as manual lymphatic drainage (MLD), compression in the form of multilayer bandaging and specially designed compression garments along with the above mentioned exercise and skin care regimes.^{205–207} After an intensive CDT course in a clinical setting, the treatment is adapted to include self-management at home.²⁰⁸ The use of additional compressive devices alongside the CDT may also be appropriate – intermittent pneumatic compression (IPC) therapy in particular is considered a safe and effective addition which has the advantage of being designed for use at home.²⁰⁹ If properly executed this approach can have very good results, but it is very time- and labour intensive, requiring specially trained personnel, personalised treatment plans and high patient compliance to ensure effectiveness.

Benzo-pyrones have been investigated as potential drugs for lymphoedema treatments as they act by reducing vascular permeability, thereby reducing fluid accumulation in tissues.²¹⁰ It has also been suggested that they may increase macrophage activity leading to proteolysis in the interstitium and therefore reducing the tissue oncotic pressure.²¹¹ A recent review of benzo-pyrones as treatment for lymphoedema was unable to draw conclusions about the effectiveness of the drugs from the available clinical research and additionally there are concerns regarding side-effects affecting liver function.²¹⁰

In extreme cases, or for patients who have not responded to standard treatments, surgical procedures may be used to reduce limb volume by removing excessive tissues (debulking procedures) or to bypass lymphatic defects.²⁰⁶ Other indicators for surgery include recurrent infections, impaired movement or for cosmetic purposes.^{206,209}

Future approaches in lymphoedema treatment include molecular strategies, and much research has focused on the identification of molecular targets.²¹² One such approach is uses gene therapy particularly for therapeutic lymphangiogenesis where growth factors can be used to stimulate lymphatic vessel growth.^{213,214}

1.5.7 Fluid Composition

Studies investigating the composition of these fluids are limited by difficulties in isolating the interstitial fluid in both normal and oedematous tissues. Although many techniques exist for this purpose they all have their inherent weaknesses, meaning there is no universally accepted method of interstitial fluid collection.^{129,165} Techniques for direct sampling include the wick technique²¹⁵ and suction blister techniques.²¹⁶ Many studies also use lymph fluid since it is more accessible and, as discussed above, the initial lymph fluid is thought to be representative of the interstitial fluid. Microdialysis is another widely used technique for indirect sampling of fluid from the interstitium. This minimally invasive technique allows for continuous sampling of small (endogenous and exogenous) water soluble molecules within the interstitial fluid.²¹⁷ The technique involves the insertion of a dialysis catheter (probe) into the tissue of interest using a guide cannula.²¹⁸ The probe consists of a shaft with a semipermeable hollow fibre membrane tip and mimics the structure of a blood capillary.²¹⁹ The probe has an inlet and outlet tube and is continuously perfused with a solution with an ionic composition similar to that of the surrounding tissue fluid (perfusate).²¹⁸ Water soluble molecules within the tissues can passively diffuse through the pores of the membrane and leaves the probe as a dialysate where it can be analysed. Providing there is a suitable assay,

virtually any water-soluble molecule in the interstitium can be sampled.²¹⁸ Commercial polyethersulfone microdialysis probes are available with a MWCO of 6,000-100,000 Da.²¹⁷ This technique has been used to investigate the role of histamine in oedema formation after thermal injury.¹²¹

Normal interstitial fluid protein levels have been quoted as 0.6-3.49 g/dL derived from normal leg lymph (including plasma protein, cytokine and cellular content)²²⁰ and 2.06 g/dL estimated from average protein content of plasma in 20 subjects.²²¹

In the past it was thought that the composition of the accumulated oedema fluid would vary with the mechanism of oedema formation. Non-inflammatory oedema from enhanced capillary filtration (increased hydrostatic pressure) or decreased reabsorption (decreased plasma protein) was thought to result in the accumulation of a protein-poor fluid known as a *transudate*.²²² In contrast, inflammatory oedema mechanisms result in increased capillary permeability, therefore allowing plasma proteins to leak into the interstitium to give a protein rich fluid known as *exudate*.²²² In lymphoedema it is thought that insufficient interstitial fluid drainage results in the accumulation of the extravasated proteins resulting in a protein rich fluid.¹⁹⁸

Early studies into primary lymphoedema fluid composition corroborated this theory. Taylor *et al.* analysed the protein content of fluid obtained from 38 patients with primary lymphoedema and found an average protein content of 2.8 g/dL although the range was from 1-5.5 g/dL.²²³

More recent studies have found the protein content of lymphoedema fluid to be the same or even lower in comparison to fluid extracted from an unaffected limb. These studies have often focused on secondary or obstructive lymphoedema. Olszewski *et al.* found that the lymph protein content in patients with postoperative and inflammatory lymphoedema was similar to that found in the controls although cytokine levels were found to be different with significantly higher levels found in those suffering from lymphoedema.²²⁴ In another study Olszewski *et al.* reported that the peripheral 'tissue fluid-lymph' of 15 patients suffering from filarial lymphoedema had a total protein content of 2.37 g/dL with a lymph: serum protein ratio of 0.48, whereas controls exhibited a total protein content of 2.39 g/dL.²²⁵ Bates *et al.* found reduced colloid osmotic pressures in post-mastectomy arm lymphoedema fluid in comparison to the normal arm, which again goes against the theory of a high protein concentration.²²⁶

There are many theories to explain these findings. One proposal is that, particularly in the early stages of lymphoedema, the interstitial and lymphatic spaces can expand and

accumulate the excess fluid, causing the protein concentration to remain within normal limits as it is diluted by the accumulated fluid.²²⁴ Other theories include: reduced capillary permeability to plasma proteins, proteolysis within the interstitium, and increased capillary filtration rate which decreases the transendothelial transfer of protein.^{226,227}

Other components which have been investigated include lipoproteins, which are present in the interstitium due to their role in peripheral cell cholesterol metabolism,^{165,228} and immune cells (i.e. lymphocytes) to investigate inflammatory processes and susceptibility to infections.²²⁹

1.6 Project Aims and Objectives

The core aim of the project was to develop and test a prototype membrane medical device for interosmolar fluid removal to treat oedema and related conditions. The major objective was to obtain proof-of-concept. Though the device concept was described by a patent, no supporting evidence or data had yet been produced and so all aspects of the device and process required fundamental investigation. To achieve this, the following project aims were proposed:

1. thorough background research into the conditions of oedema and lymphoedema as well as membrane technology, including both literature research and consultation with clinicians and researchers in the field;
2. practical laboratory work including investigation into the process of forward osmosis (in particular, using UF membranes and specifically to transport model oedema fluid and proteins), membranes and membrane modifications and potential draw solutions;
3. the development of a prototype design and fabrication process, assisted by key findings from this laboratory work and background research;
4. the development of both an in vitro and ex vivo model in order to test the prototype devices;
5. prototype testing to attain proof-of-concept.

Alongside the above clinically-oriented project, a secondary project was proposed involving an investigation into thin-film composite membrane fabrication, to explore new thin film coatings made from novel poly-ylids and a new solvent resistant support membrane.

1.7 References

1. C. B. Herbert and M. N. Blaine, US Pat. 8211 053 B2 (2012), to Equilibrate, LLC.
2. R. W. Baker, *Membrane Technology and Applications*, John Wiley & Sons, Ltd, Chichester, UK, 2004, pp. 1–14.
3. K. W. Boddeker, *J. Membr. Sci.*, 1995, **100**, 65–68.
4. R. E. Kesting, *Synthetic Polymeric Membranes A Structural Perspective*, Wiley-Interscience, Irvine, California, 2nd edn., 1985.
5. S. Atkinson, *Filtr. Sep.*, 1992, **36**, 28.
6. K. C. Khulbe, C. Y. Feng, and T. Matsuura, in *Synthetic Polymeric Membranes Characterisation by Atomic Force Microscopy*, Springer-Verlag, Berlin, 2008, pp. 5–14.
7. B. S. Lalia, V. Kochkodan, R. Hashaikeh, and N. Hilal, *Desalination*, 2013, **326**, 77–95.
8. S. Loeb, in *Synthetic Membranes - Volume 1 - Desalination (ACS Symposium series)*, Washington, D. C., 1980, pp. 1–9.
9. A. S. Michaels, US Pat. 3 615 024 (1971) to Amicon Corporation.
10. A. S. Michaels, *Pure Appl. Chem.*, 1976, **46**, 193–204.
11. R. W. Baker, *Membrane Technology and Applications*, John Wiley & Sons, Ltd, Chichester, UK, 2004, pp. 237–272.
12. K. P. Lee, T. C. Arnot, and D. Mattia, *J. Membr. Sci.*, 2011, **370**, 1–22.
13. W. J. Lau and A. F. Ismail, in *2nd International Conference on Environmental Engineering and Applications International Proceedings of Chemical, Biological and Environmental Engineering*, IACSIT Press, Singapore, 2011, vol. 17, pp. 173–177.
14. J. E. Cadotte, US Patent 4,277,344, (1981) to FilmTec Corporation.
15. W. J. Lau, A. F. Ismail, N. Misdan, and M. A. Kassim, *Desalination*, 2012, **287**, 190–199.

16. W. J. Koros, Y. H. Ma, and T. Shimidzu, *Pure Appl. Chem.*, 1996, **68**, 1479–1489.
17. R. van Reis and A. Zydney, *J. Membr. Sci.*, 2007, **297**, 16–50.
18. I. Pinnau and B. D. Freeman, in *ACS Symposium Series No. 744*, 1999, vol. 744, p. 1.
19. M. Ulbricht, *Polymer*, 2006, **47**, 2217–2262.
20. R. Mallada and M. Menendez, Eds., in *Membrane Science and Technology Series. Volume 13*, Elsevier, Amsterdam, 2008, pp. 1–460.
21. A. Sagle and B. Freeman, *Fundamentals of Membranes for Water Treatment*, University of Texas, Austin, 2004.
22. R. Rautenbach and R. Albrecht, in *Membrane Processes*, John Wiley & Sons, Ltd, Aarau, Switzerland, 1989, pp. 18–47.
23. W. Guo, H.-H. Ngo, and J. Li, *Bioresour. Technol.*, 2012, **122**, 27–34.
24. S. P. Beier, in *Pressure Driven Membrane Processes*, Bookboon, London, 2nd edn., 2007, pp. 4–22.
25. J. G. Wijmans and R. W. Baker, *J. Membr. Sci.*, 1995, **107**, 1–21.
26. M. E. Williams, *A Review of Reverse Osmosis Theory*, EET Corporation and Williams Engineering Services Company Inc, Tennessee, 2003.
27. R. Rautenbach and R. Albrecht, in *Membrane Processes*, John Wiley & Sons, Ltd, Aarau, Switzerland, 1989, pp. 48–74.
28. R. W. Baker, *Membrane Technology and Applications*, John Wiley & Sons, Ltd, Chichester, UK, 2004, pp. 15–84.
29. A. E. Childress and M. Elimelech, *J. Membr. Sci.*, 1996, **119**, 253–268.
30. K. J. Kim, A. G. Fane, M. Nystrom, A. Pihlajamaki, W. R. Bowen, and H. Mukhtar, *J. Membr. Sci.*, 1996, **116**, 149–159.
31. M. Elimelech, W. H. Chen, and J. J. Waypa, *Desalination*, 1994, **95**, 269–286.
32. K. Toyomoto and A. Higuchi, *Membrane Science and Technology*, eds. Y. Osada and T. Nakagawa, Marcel Dekker, Inc, New York, US, 1992, pp. 289–331.

33. R. W. Baker, *Membrane Technology and Applications*, John Wiley and Sons, Ltd, Chichester, UK, 2004.
34. M. Cheryan, *Ultrafiltration and Microfiltration Handbook*, Techomic Publishing Company, Inc., Basel, 2nd edn., 1998.
35. S. Jain and S. K. Gupta, *J. Membr. Sci.*, 2004, **232**, 45–61.
36. J. G. Jacangelo, R. R. Trussell, and M. Watson, *Desalination*, 1997, **9164**, 119–127.
37. G. Daufin, J. Escudier, H. Carrere, S. Berot, L. Fillaudeau, and M. Decloux, *Food Bioprod. Process.*, 2001, **79**, 89–102.
38. B. Butchermaker, *Filtr. Sep.*, 2004, 32–33.
39. A. W. Mohammad, C. Y. Ng, Y. P. Lim, and G. H. Ng, *Food Bioprocess Technol.*, 2012, **5**, 1143–1156.
40. R. van Reis and A. Zydney, *Curr. Opin. Biotechnol.*, 2001, **12**, 208–11.
41. C. Charcosset, *Biotechnol. Adv.*, 2006, **24**, 482–92.
42. A. A. Merdaw, A. O. Sharif, and G. A. W. Derwish, *Chem. Eng. J.*, 2011, **168**, 215–228.
43. R. R. Bhave, in *Fermentation and Biochemical Engineering Handbook*, eds. H. C. Vogel and C. L. Todaro, Noyes Publication, Westwood, New Jersey, 2nd edn., 1997, pp. 271–322.
44. M. C. Porter, in *Handbook of Industrial Membrane Technology*, ed. M. C. Porter, Noyes Publications, New Jersey, USA, 1990, pp. 61–134.
45. G. Russotti and K. E. Goklen, in *Membrane Separations in Biotechnology*, ed. W. K. Wang, Marcel Dekker, Basel, Switzerland, 2nd edn., 2001, pp. 85–188.
46. B. Van der Bruggen, L. Lejon, and C. Vandecasteele, *Environ. Sci. Technol.*, 2003, **37**, 3733–8.
47. W. Gao, H. Liang, J. Ma, M. Han, Z. Chen, Z. Han, and G. Li, *Desalination*, 2011, **272**, 1–8.
48. J. S. Baker and L. Y. Dudley, *Desalination*, 1998, **118**, 81–89.

49. J. A. L. Santos, M. Mateus, and J. A. S. Cabral, in *Chromatographic and Membrane Processes in Biotechnology*, ed. C. A. Costa, Kluwer Academic Publishers, Dordrecht, 1991, pp. 177–205.
50. W. S. Winston Ho and K. K. Sirkar, Eds., in *Membrane Handbook*, Chapman and Hall, London, UK, 1992, pp. 455–571.
51. R. W. Baker, in *Membrane Technology and Applications*, John Wiley & Sons, Ltd, Chichester, UK, 2004, pp. 275–300.
52. K. C. Khulbe, C. Y. Feng, and T. Matsuura, *Synthetic Polymeric Membranes Characterisation by Atomic Force Microscopy*, Springer-Verlag Berlin Heidelberg, Ottawa, 2008, pp. 101–139.
53. H. Yacubowicz and J. Yacubowicz, *Filtr. Sep.*, 2005, **42**, 16–21.
54. N. Hilal, H. Al-Zoubi, N. A. Darwish, A. W. Mohammad, and M. Abu Arabi, *Desalination*, 2004, **170**, 281–308.
55. T. Thorsen and H. Flogstag, in *Nanofiltration in Drinking Water Treatment*, Techneau, Trondheim, 2006, pp. 3–7.
56. L. F. Greenlee, D. F. Lawler, B. D. Freeman, B. Marrot, and P. Moulin, *Water Res.*, 2009, **43**, 2317–48.
57. D. Li and H. Wang, *J. Mater. Chem.*, 2010, **20**, 4551.
58. H. B. Park, B. D. Freeman, Z. Zhang, M. Sankir, and J. E. Mcgrath, *Angew. Chemie, Int. Ed.*, 2008, **47**, 6019–6024.
59. G.-D. Kang, C.-J. Gao, W.-D. Chen, X.-M. Jie, Y.-M. Cao, and Q. Yuan, *J. Membr. Sci.*, 2007, **300**, 165–171.
60. I. C. Tessaro, J. B. a. da Silva, and K. Wada, *Desalination*, 2005, **181**, 275–282.
61. I. M. Wienk, R. M. Boom, M. A. M. Beerlage, A. M. W. Bulte, C. A. Smolders, and H. Strathmann, *J. Membr. Sci.*, 1996, **113**, 361–371.
62. R. W. Baker, *Membrane Technology and Applications*, John Wiley & Sons, Ltd, Chichester, UK, 2004, pp. 89–155.
63. A. Rahimpour and S. S. Madaeni, *J. Membr. Sci.*, 2007, **305**, 299–312.
64. P. Witte van de, P. J. Dijkstra, J. W. A. Berg van den, and J. Feijen, *J. Membr.*

- Sci.*, 1996, **117**, 1–31.
65. J. F. Blanco, J. Sublet, Q. T. Nguyen, and P. Schaetzel, *J. Membr. Sci.*, 2006, **283**, 27–37.
 66. R. M. Boom, I. M. Wienk, T. Van Den Boomgaard, and C. A. Smolders, *J. Membr. Sci.*, 1992, **73**, 277–292.
 67. P. W. Morgan and S. L. Kwolek, *J. Chem. Educ.*, 1959, **36**, 182.
 68. E. L. Wittbecker and P. W. Morgan, *J. Polym. Sci.*, 1959, **XL**, 521–529.
 69. P. W. Morgan and S. L. Kwolek, *J. Polym. Sci.*, 1959, **XL**, 299–327.
 70. J. E. Tomaschke, in *Encyclopedia of Separation Science, Vol. III, Membrane Preparation*, Academic Press Inc, 2000, pp. 3319–3331.
 71. H. M. Colquhoun, D. Chappell, A. L. Lewis, D. F. Lewis, G. T. Finlan, and P. J. Williams, *J. Mater. Chem.*, 2010, **20**, 4629.
 72. M. Mulder, in *Basic Principles of Membrane Technology*, Kluwer Academic Publishers, Dordrecht, 2000, pp. 157–208.
 73. M. Cheryan, in *Ultrafiltration and Microfiltration Handbook*, Techomic Publishing Company, Inc., Basel, 2nd edn., 1998, pp. 71–107.
 74. K. L. Tung, K. S. Chang, T. T. Wu, N. J. Lin, K. R. Lee, and J. Y. Lai, *Curr. Opin. Chem. Eng.*, 2014, **4**, 121–127.
 75. A. E. Childress, J. A. Brant, P. Rempala, D. W. Phipps, and P. Kwan, *Evaluation of Membrane Characterization Methods*, Water Research Foundation, Denver, 2012.
 76. R. Bernstein, Y. Kaufman, and V. Freger, in *Encyclopedia of Membrane Science and Technology*, eds. E. M. V. Hoek and V. V. Tarabara, John Wiley & Sons, Inc, 2013, pp. 1–41.
 77. N. A. Ochoa, P. Prádanos, L. Palacio, C. Pagliero, J. Marchese, and A. Hernández, *J. Membr. Sci.*, 2001, **187**, 227–237.
 78. S. Singh, K. C. Khulbe, T. Matsuura, and P. Ramamurthy, *J. Membr. Sci.*, 1998, **142**, 111–127.
 79. R. Tamime, Y. Wyart, L. Siozade, I. Baudin, C. Deumie, K. Glucina, and P.

- Moulin, *Membranes (Basel)*., 2011, **1**, 91–97.
80. K. Smolders and A. C. M. Franken, *Desalination*, 1989, **72**, 249–262.
 81. S. Belfer, R. Fainchtein, Y. Purinson, and O. Kedem, *J. Membr. Sci.*, 2000, **172**, 113–124.
 82. Q. Ge, J. Su, G. L. Amy, and T.-S. Chung, *Water Res.*, 2012, **46**, 1318–26.
 83. T. Cath, A. Childress, and M. Elimelech, *J. Membr. Sci.*, 2006, **281**, 70–87.
 84. P. Atkins and J. de Paula, in *Atkins' Physical Chemistry*, Oxford University Press, Oxford, 7th edn., 2006, pp. 160–186.
 85. S. Zhao, L. Zou, C. Y. Tang, and D. Mulcahy, *J. Membr. Sci.*, 2012, **396**, 1–21.
 86. A. Davis and E. Kravath, *Desalination*, 1975, **16**, 151–155.
 87. J. O. Kessler and C. D. Moody, *Desalination*, 1976, **8**, 297–306.
 88. T.-S. Chung, S. Zhang, K. Y. Wang, J. Su, and M. M. Ling, *Desalination*, 2012, **287**, 78–81.
 89. J. Ren and J. R. McCutcheon, *Desalination*, 2013, **343**, 187–193.
 90. I. Alsvik and M.-B. Hägg, *Polymers (Basel)*., 2013, **5**, 303–327.
 91. Forward Osmosis: Current Status and Perspectives, R. Wang and L. Setiawan, *J. Memb. Sci Virtual Special Issue*, 2012.
 92. S. K. Yen, F. Mehnas Haja N., M. Su, K. Y. Wang, and T.-S. Chung, *J. Membr. Sci.*, 2010, **364**, 242–252.
 93. N. T. Hancock and T. Y. Cath, *Environ. Sci. Technol.*, 2009, **43**, 6769–75.
 94. A. Achilli, T. Y. Cath, and A. E. Childress, *J. Membr. Sci.*, 2010, **364**, 233–241.
 95. G. W. Batchelder, W. Ave, and S. Monica, US Pat. 3 171 799 (1965).
 96. J. R. McCutcheon, R. L. McGinnis, and M. Elimelech, *Desalination*, 2005, **174**, 1–11.
 97. D. Li, X. Zhang, J. Yao, G. P. Simon, and H. Wang, *Chem. Commun.*, 2011, **47**, 1710–1712.
 98. R. Ou, Y. Wang, H. Wang, and T. Xu, *Desalination*, 2013, **318**, 48–55.

99. Q. Ge, P. Wang, C. Wan, and T.-S. Chung, *Environ. Sci. Technol.*, 2012, **46**, 6236–43.
100. D. Li, X. Zhang, G. P. Simon, and H. Wang, *Water Res.*, 2013, **47**, 209–215.
101. B. Mi and M. Elimelech, *J. Membr. Sci.*, 2010, **348**, 337–345.
102. B. Mi and M. Elimelech, *J. Membr. Sci.*, 2008, **320**, 292–302.
103. S. Lee, C. Boo, M. Elimelech, and S. Hong, *J. Membr. Sci.*, 2010, **365**, 34–39.
104. K. C. Khulbe, C. Feng, and T. Matsuura, *J. Appl. Polym. Sci.*, 2009, **115**, 855–895.
105. N. Nady, M. C. R. Franssen, H. Zuilhof, M. S. M. Eldin, R. Boom, and K. Schroën, *Desalination*, 2011, **275**, 1–9.
106. D. Rana and T. Matsuura, *Chem. Rev.*, 2010, **110**, 2448–71.
107. Z. Xu, L. Wan, and X. Huang, in *Surface Engineering of Polymer Membranes*, Springer, Berlin, 2009, pp. 80–149.
108. A. Bhattacharya and B. N. Misra, *Prog. Polym. Sci.*, 2004, **29**, 767–814.
109. F. Kucera and J. Jancar, *Polym. Eng. Sci.*, 1998, **3**, 783–792.
110. J. Scallan, V. H. Huxley, and R. J. Korthuis, *Capillary Fluid Exchange: Regulation, Functions and Pathology*, Morgan and Claypool Life Sciences, San Rafael, 2010.
111. A. C. Guyton and J. E. Hall, *Guyton and Hall Textbook of Medical Physiology*, Saunders Elsevier, Philadelphia, 12th edn., 2011, pp. 283–301.
112. J. D. Loudon, *Anaesth. Intensive Care Med.*, 2009, **10**, 279–285.
113. A. Ballinger, in *Essentials of Kumar and Clark's Clinical Medicine*, eds. P. Kumar and M. Clark, Elsevier, London, Uk, 5th edn., 2011, pp. 323–353.
114. T. A. Brown, in *Rapid Review Physiology*, ed. E. F. Goljan, Elsevier Mosby, Philadelphia, 2nd edn., 2012, pp. 241–246.
115. B. Andersson, *Ann. Rev. Physiol.*, 1977, **39**, 185–200.
116. J. C. Atherton, *Anaesth. Intensive Care Med.*, 2006, **7**, 227–233.

117. S. Cho and J. E. Atwood, *Am. J. Med.*, 2002, **113**, 580–586.
118. G. J. Tortora and B. H. Derrickson, *Principles of Anatomy and Physiology*, John Wiley & Sons, Ltd, New York, 13th edn., 2012.
119. W. F. Boron and E. L. Boulpap, in *Medical Physiology*, Saunders Elsevier, Philadelphia, 2nd edn., 2009, pp. 106–146.
120. H. F. Dvorak, L. F. Brown, M. Detmar, and A. M. Dvorak, *Am. J. Pathol.*, 1995, **146**, 1029–1039.
121. A. Papp, M. Härmä, R. Harvima, T. Lahtinen, A. Uusaro, and E. Alhava, *Burns*, 2005, **31**, 476–81.
122. G. Majno and G. E. Palade, *J. Biophys. Biochem. Cytol.*, 1961, **11**, 571–605.
123. J. Hankins, *J. Infus. Nurs.*, 2006, **29**, 260–265.
124. A. C. Guyton and J. E. Hall, *Guyton and Hall Textbook of Medical Physiology*, Saunders Elsevier, Philadelphia, 12th edn., 2011, pp. 155–282.
125. D. N. Granger, in *Essential Medical Physiology*, eds. L. R. Johnson and J. H. Byrne, Academic Press Inc, San Diego, California, 3rd Revise., 2003, pp. 235–244.
126. A. S. Popel and P. C. Johnson, *Annu. Rev. Fluid Mech.*, 2005, **37**, 43–69.
127. A. C. Guyton and J. E. Hall, *Guyton and Hall Textbook of Medical Physiology*, Saunders Elsevier, Philadelphia, 12th edn., 2001, p. 288.
128. J. Scallan, V. H. Huxley, and R. J. Korthuis, *Capillary Fluid Exchange: Regulation, Functions and Pathology*, Morgan and Claypool Life Sciences, San Rafael, 2010.
129. H. Wiig and M. Swartz, *Physiol. Rev.*, 2012, **92**, 1005–60.
130. L. V Leak, L. Liotta, H. Krutzsch, M. Jones, V. Fusaro, S. J. Ross, Y. Zhao, E. F. Petricoin, and V. Fusaroa, *Proteomics*, 2004, **4**, 753–65.
131. Z. Meng and T. D. Veenstra, *Proteomics. Clin. Appl.*, 2007, **1**, 747–57.
132. M. Dzieciatkowska, M. V Wohlaer, E. E. Moore, S. Damle, J. Campsen, M. Kelher, C. Silliman, A. Banerjee, and K. C. Hansen, *Shock*, 2012, **35**, 331–338.

133. W. L. Olszewski, J. Pazdur, E. Kubasiewicz, M. Zaleska, C. J. Cooke, and N. E. Miller, *Arthritis Rheum.*, 2001, **44**, 541–549.
134. M. J. Karnovsky, *J. Cell Biol.*, 1967, **35**, 213–36.
135. D. U. Silverthorn, W. C. Ober, C. W. Garrison, A. C. Silverthorn, and B. R. Johnson, in *Human Physiology*, Pearson Education, San Francisco, 4th edn., 2007, pp. 500–524.
136. J. Naish, P. Revest, and D. Syndercombe Court, in *Medical Sciences*, Elsevier, London, 1st edn., 2009.
137. J. R. Pappenheimer, *Physiol. Rev.*, 1953, **33**, 387–423.
138. R. W. Schrier, Y. C. Chen, and M. A. Cadnapaphornchai, *Neuroscience*, 2004, **129**, 897–904.
139. A. S. Lossinsky and R. R. Shivers, *Histol. Histopathol.*, 2004, **19**, 535–64.
140. M. J. Karnovsky, *J. Gen. Physiol.*, 1968, **52**, 64–95.
141. M. Pavelka and J. Roth, *Functional Ultrastructure - An Atlas of Tissue Biology and Pathology*, Springer, Vienna, 2005.
142. S. Stiller, E. Bonnie-schorn, A. Grassmann, H. Mann, and I. Uhlenbusch-ko, *Semin. Dial.*, 2001, **14**, 337–347.
143. D. U. Silverthorn, W. C. Ober, C. W. Garrison, A. C. Silverthorn, and B. R. Johnson, in *Human Physiology*, Pearson Education, San Francisco, 4th edn., 2007, pp. 129–169.
144. A. Leaf, *Ann. N. Y. Acad. Sci.*, 1959, **72**, 396–404.
145. F. Lang, G. L. Busch, M. Ritter, H. Vo, S. Waldegger, and E. Gulbins, *Physiol. Rev.*, 1998, **78**, 247–306.
146. B. M. Koeppe and B. A. Stanton, in *Renal Physiology*, Elsevier, 5th edn., 2013, pp. 5–18.
147. S. Gonem, in *Diagnosis in Acute Medicine*, Radcliffe Publishing Ltd, Abingdon, UK, 1998, pp. 45–48.
148. J. Waterhouse, M. Sawdon, and E. Kirkman, *Anaesth. Intensive Care Med.*, 2013, **14**, 72–78.

149. B. R. Waterhouse and A. D. Farmery, *Anaesth. Intensive Care Med.*, 2012, **13**, 573–580.
150. M. K. Nguyen and I. Kurtz, *J. Appl. Physiol.*, 2006, **100**, 1293–1300.
151. S. Kurbel, *J. Theor. Biol.*, 2008, **252**, 769–72.
152. S. L. Xie, R. K. Reed, B. D. Bowen, and J. L. Bert, *Microvasc. Res.*, 1995, **49**, 141–163.
153. K. Aukland and G. Nicolaysen, *Physiol. Rev.*, 1981, **61**, 556–643.
154. J. A. Davies, in *Encyclopedia of Life Sciences*, Nature Publishing Group, Edinburgh, 2001, pp. 1–7.
155. G. M. Cooper, in *The Cell: A Molecular Approach*, ed. G. Cooper, Sinauer Associates, Sunderland, MA, 2nd edn., 2000.
156. B. Alberts, A. Johnson, and J. Lewis, in *Molecular Biology of the Cell*, Garland Science, New York, 4th edn., 2002, vol. i.
157. M. L. Tanzer, *J. Orthop. Sci.*, 2006, **11**, 326–31.
158. J. E. Scott, *J. Anat.*, 1995, **187**, 259–69.
159. J. E. Scott, *FSAEB J.*, 1992, **6**, 2639–2645.
160. W. D. Comper and T. C. Laurent, *Physiol. Rev.*, 1978, **58**, 255–315.
161. R. K. Reed and K. Rubin, *Cardiovasc. Res.*, 2010, **87**, 211–7.
162. H. Wiig, C. Gyenge, P. O. Iversen, D. Gullberg, and O. Tenstad, *Microcirculation*, 2008, **15**, 283–96.
163. W. D. Comper and O. Zamparo, *Biochem. J.*, 1990, **269**, 561–4.
164. J. Scallan, V. Huxley, and R. J. Korthuis, *Capillary Fluid Exchange: Regulation, Functions and Pathology*, Morgan and Claypool Life Sciences, San Rafael, 2010.
165. J. Lundberg, M. Rudling, and B. Angelin, *J. Lipid Res.*, 1987, **28**, 225–237.
166. J. E. Scott, *Pathol. Biol.*, 2001, **8114**, 284–289.
167. M. A. Swartz, *Adv. Drug Deliv. Rev.*, 2001, **50**, 3–20.

168. W. F. Hamilton and P. Dow, Eds., in *Handbook of Physiology*, American Physiological Society, Baltimore, Maryland, 1963.
169. D. Negrini and A. Moriondo, *J. Physiol.*, 2011, **589**, 2927–34.
170. K. Alitalo, T. Tammela, and T. V Petrova, *Nature*, 2005, **438**, 946–53.
171. A. E. Taylor, *Circ. Res.*, 1981, **49**, 557–575.
172. V. Kumar, A. K. Abbas, and J. C. Aster, *Robbins Basic Pathology*, Saunders Elsevier, Philadelphia, 9th edn., 2012.
173. J. R. Levick, *Exp. Physiol.*, 1991, **76**, 825–857.
174. O. Stucker, C. Pons-Himbert, and E. Laemmel, *Phlebology*, 2008, **15**, 31–36.
175. A. C. Guyton and J. E. Hall, *Guyton and Hall Textbook of Medical Physiology*, Saunders Elsevier, Philadelphia, 12th edn., 2011, pp. 831–836.
176. T. W. Evans, *Aliment. Pharmacol. Ther.*, 2002, **16**, 6–11.
177. R. Gordillo, J. Kumar, and R. P. Woroniecki, in *Nutrition and Health: Fluid and Electrolytes in Pediatrics*, eds. L. G. Feld and F. J. Kaskel, Humana Press, Totowa, NJ, 2010, pp. 47–66.
178. P. S. Mortimer and J. R. Levick, *Clin. Med.*, 2004, **4**, 448–53.
179. G. Majno, G. E. Palade, and G. I. Schoefl, *J. Biophys. Biochem. Cytol.*, 1961, **11**, 607–26.
180. B. V. Reed, *Phys. Ther.*, 1988, **68**, 491–5.
181. B. Y. Geraldine, C. C. Michel, and M. E. Phillips, *J. Physiol.*, 1988, **395**, 99–114.
182. R. T. Eberhardt and J. D. Raffetto, *Circulation*, 2005, **111**, 2398–409.
183. L. Goldman and A. I. Schafer, in *Goldman's Cecil Medicine*, Elsevier Saunders, 24th edn., 2012.
184. J. W. Ely, J. A. Osheroff, M. L. Chambliss, and M. H. Ebell, *J. Am. Board Fam. Med.*, 2006, **19**, 148–60.
185. A. Tiwari, K.-S. Cheng, M. Button, F. Myint, and G. Hamilton, *Arch. Surg.*, 2003, **138**, 152–61.

186. S. J. Simonian, C. L. Morgan, L. L. Tretbar, and B. Blondeau, in *Lymphedema Diagnosis and Treatment*, eds. L. L. Tretbar, C. L. Morgan, S. J. Simonian, and B. Blondeau, Springer-Verlag, London, 2008, pp. 12–21.
187. A. Szuba and S. G. Rockson, *Vasc. Med.*, 1998, **3**, 145–156.
188. A. G. Warren, H. Brorson, L. J. Borud, and S. A. Slavin, *Ann. Plast. Surg.*, 2007, **59**, 464–72.
189. C. J. Moffatt, P. J. Franks, D. C. Doherty, A. F. Williams, C. Badger, E. Jeffs, N. Bosanquet, and P. S. Mortimer, *Q. J. Med.*, 2003, **96**, 731–738.
190. British Lymphoedema Society, in *What is meant by lymphoedema and chronic oedema? The Five Guide*, pp. 1–23.
191. H. G. Rennke and B. M. Denker, in *Renal Pathophysiology: The Essentials*, Lippincott Williams & Wilkins, Philadelphia, 2nd edn., 2007.
192. K. Kerchner, A. Fleischer, and G. Yosipovitch, *J. Am. Acad. Dermatol.*, 2008, **59**, 324–31.
193. O. T. A. Lyons and B. Modarai, *Surg.*, 2013, **31**, 218–223.
194. D. O. Bates, J. R. Levick, and P. S. Mortimer, *Lymphology*, 1994, **27**, 159–172.
195. S. B. O'Sullivan and T. J. Schmitz, in *Physical rehabilitation: assessment and treatment*, F. A. Davies Company, Philadelphia, 5th edn., 2007, p. 659.
196. S. J. Fruth, in *Fundamentals of Physical Therapy Examination: Patient Interview and Tests & Measures*, Jones and Bartlett Publishers, Inc, Burlington, 2013, pp. 115–118.
197. E. J. Topham and P. S. Mortimer, *Clin. Med.*, 2002, **2**, 28–31.
198. S. G. Rockson, *Am. J. Med.*, 2001, **110**, 288–295.
199. P. S. Mortimer, in *Oxford Textbook of Medicine*, Oxford University Press, Oxford, 5th edn., 2012, pp. 3093–3092.
200. WHO, in *Lymphatic Filariasis WHO Factsheet No. 102*, 2016, <http://www.who.int/mediacentre/factsheets/fs102/en>.
201. International Society of Lymphology, in *Lymphology*, 2009, vol. 42, pp. 51–60.

202. G. A. Rosenberg, *Prog. Cardiovasc. Dis.*, 1999, **42**, 209–16.
203. T. G. Walker, *Tech. Vasc. Interv. Radiol.*, 2009, **12**, 117–29.
204. J. G. O'Brien, S. A. Chennubhotla, and R. V Chennubhotla, *Am. Fam. Physician*, 2005, **71**, 2111–2117.
205. S. G. Rockson, *J. Am. Coll. Cardiol.*, 2008, **52**, 799–806.
206. P. S. Mortimer, *Br. Med. J.*, 2000, **320**, 1527–1529.
207. S. R. Cohen, D. K. Payne, and R. S. Tunkel, *Cancer Suppl.*, 2001, **92**, 980–987.
208. H. N. Mayrovitz, *Lymphat. Res. Biol.*, 2009, **7**, 101–8.
209. C. J. Chang and J. N. Cormier, *Semin. Oncol. Nurs.*, 2013, **29**, 28–40.
210. C. M. A. Badger, N. J. Preston, K. Seers, and P. S. Mortimer, *Cochrane Libr.*, 2009, 1–42.
211. J. A. Petrek, P. I. Pressman, and R. A. Smith, *CA-Cancer J. Clin.*, 2000, **50**, 292-307–11.
212. A. An and S. G. Rockson, *Lymphat. Res. Biol.*, 2004, **2**, 173–81.
213. Y. Saito, H. Nakagami, Y. Kaneda, and R. Morishita, *Biomed Res. Int.*, 2013, **2013**, 804675.
214. M. E. Baldwin, S. A. Stacker, and M. G. Achen, *Bioessays*, 2002, **24**, 1030–40.
215. H. O. Fadnes and K. Aukland, *Microvasc. Res.*, 1977, **25**, 11–25.
216. U. Kiistala, *J. Invest. Dermatol.*, 1967, **50**, 129–138.
217. G. F. Clough, *AAPS J.*, 2005, **7**, E686-92.
218. M. Müller, *Br. Med. J.*, 2002, **324**, 588–591.
219. S. Klaus, M. Heringlake, and L. Bahlmann, *Crit. Care*, 2004, **8**, 363–8.
220. W. L. Olszewski, *Lymphat. Res. Biol.*, 2003, **1**, 11–28.
221. N. Fogh-Andersen, B. M. Altura, B. T. Altura, and O. Siggaard-Andersen, *Clin. Chem.*, 1995, **41**, 1522–5.
222. V. Kumar, A. K. Abbas, N. Fausto, and J. C. Aster, in *Robbins and Cotran*

Pathologic Basis of Disease, Saunders Elsevier, Philadelphia, 7th edn., 2009.

223. G. W. Taylor, J. B. Kinmonth, and W. G. Dangerfield, *Br. Med. J.*, 1958, **1**, 1159–60.
224. W. L. Olszewski, *Lymphat. Res. Biol.*, 2003, **1**, 235–243.
225. W. L. Olszewski, S. Jamal, B. Lukomska, G. Manokaran, S. Pani, V. Kumaraswami, U. Kubicka, B. Lukomska, F. M. Tripathi, E. Swoboda, F. Meisel-Mikolajczyk, E. Stelmach and M. Zaleska, *Lymphology*, 1992, **25**, 166–171.
226. D. O. Bates, J. R. Levick, and P. S. Mortimer, *J. Physiol.*, 1994, **477**, 355–63.
227. A. W. B. Stanton and P. S. Mortimer, *Exp. Physiol.*, 1999, **84**, 405–419.
228. M. N. Nanjee, C. J. Cooke, J. S. Wong, R. L. Hamilton, W. L. Olszewski, and N. E. Miller, *J. Lipid Res.*, 2001, **42**, 639–648.
229. W. Olszewski, A. Engeset, I. Romaniuk, G. I., and A. Ziolkowska, *Lymphology*, 1990, **23**, 23–33.

Chapter 2 – Forward Osmosis Processes with Ultrafiltration Membranes

2.1 Abstract

Forward osmosis (FO) processes employing a novel combination of porous ultrafiltration membranes and high molecular weight draw solutions are described in this Chapter. This strategy was used to investigate the possibility of transporting macromolecules, especially proteins along with the water during the forward osmosis process. This represents an attempt to solve a key issue in oedema treatment; the presence of excess proteins in the interstitium which generate high oncotic pressures causing further water accumulation. Investigations compared polymer and polyelectrolyte solutions to determine the best-performing draw solution. This was found to be a polyelectrolyte: 225K sodium polyacrylate. This draw solution was investigated in a variety of studies exploring performance with a model oedema solution consisting of a physiological salt solution containing 2% high molecular weight polymer to model the protein content as established by the combination of a literature survey and consultations with clinicians and researchers in the field. The chosen physiological salt solution was Krebs solution and the protein model was a synthetic polymer, 100K polyethylene oxide (PEO). Following studies employing this model solution it was found that PEO exhibited unwanted complexation behaviour with the sodium polyacrylate which led to further studies in order to understand both PEO and sodium polyacrylate behaviour in solution. After employing the PEO based model oedema solution to optimise the novel FO system (UF membrane with high molecular weight polymer draws) real proteins were substituted for the model PEO's. Finally studies into membrane fouling, system osmotic pressure characteristics and protein transport were carried out.

2.2 Introduction

Forward osmosis is the naturally occurring phenomenon which takes place when a semi-permeable membrane is placed between a pure solvent and a solution containing dissolved solutes; the solvent (usually water) moves from an area of high water potential to an area of low water potential in the mixture across the semipermeable membrane (See **Figure 2.1**). Forward osmosis has been the focus of significant research in recent years for water purification applications in the hope that it may provide a low energy alternative to currently used high pressure water purification processes¹⁻³.

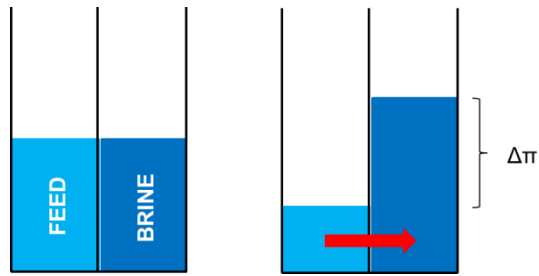


Figure 2.1: The process of forward osmosis relies on the use of a concentrated draw solution to move fluid from the feed into the draw (diluting it) across a semi-permeable membrane, adapted from reference.²

Forward osmosis is driven by an osmotic pressure gradient created by a concentrated draw solution which requires much less energy. A major limitation of this process is that it is not a route to pure water and an additional draw re-concentration/water isolation step is required. The use of forward osmosis in order to move physiological fluids has received less attention, indeed to this author's knowledge this application of forward osmosis has not previously been investigated.

The overall aim of this project was to create an implantable medical device which can be used remove excess accumulated fluid in the limbs of patients suffering from conditions such as oedema and lymphoedema. The device concept was based on a US Patent licensed to Biointeractions Ltd which describes an implantable medical device for interosmolar fluid removal.⁴ The theory proposed that a device based on an implantable semipermeable membrane containing trapped osmotic solutes could be used to remove excess accumulated fluid in tissues surrounding the device allowing them to be removed from the body via a tube connected to an external reservoir.

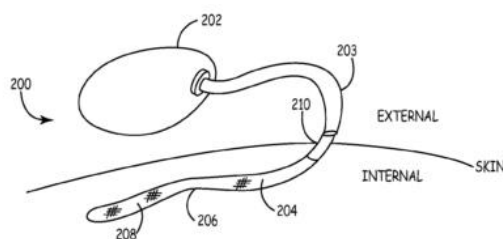


Figure 2.2: Image from US Patent No. US 8,211,053 B2 showing a sketch of potential device configuration; internally implanted portion consisting of a membrane with trapped osmotic solutes connected to an external reservoir for fluid collection.

Although the patent details only the removal of water, after a comprehensive literature review and consultation with clinicians and researchers in the field⁵⁻⁷ it became apparent that removal of the fluid alone would not solve the issue as proteins left in the interstitium would generate an osmotic pressure gradient capable of drawing more fluid into the tissue. The device design was thus adapted to probe the use of porous

ultrafiltration membranes for forward osmosis in order to remove proteins along with the solution.

The use of porous membranes presented a new challenge in draw solution selection as it was essential to use a high molecular weight draw to prevent backflow/leakage through the membrane. For this reason polymeric draw solutions in combination with porous ultrafiltration membranes were chosen as a test system for investigation.

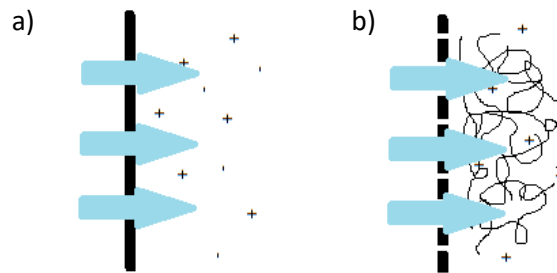


Figure 2.3: a) Traditional FO system using non-porous dense membrane and salt based draw solution vs. b) novel FO system employing porous UF membrane with high molecular weight polymer draw solution.

Furthermore two types of high molecular weight draw solutions were investigated; neutral but strongly hydrophilic polymers and polyelectrolytes - a type of polymer with positive or negative charges on its repeat units. In water polyelectrolytes can dissociate to give a charged poly-ion surrounded by a cloud of small, mobile counter-ions.⁸ It was proposed that the counter-ions present in polyelectrolytes could help produce the high osmotic pressures required to drive the forward osmosis process, as they hugely increase the concentration of solute particles compared to a neutral polymer of similar molecular weight.

2.3 Results and Discussion

2.3.1 Initial FO Studies using Ultrafiltration Membranes

Initial forward osmosis experiments were carried out to investigate potential draw solutions using deionised water feed solutions as a control. These experiments involved evaluating different polymer and polyelectrolyte draw solutions of varying concentrations to determine which could produce the highest flow rates. It was decided that 5% w/v solutions would be the standard but for some of the higher molecular weight polymers the percentage was reduced to decrease the viscosity and allow for more effective stirring. In total seven different draw solutions were investigated. Four **polymer** draw solutions consisting of; three polyethylene glycol PEG/ (poly(ethylene oxide)PEO draws of different molecular weights (5% w/v 35K

PEG, 5% w/v 100K PEO and 1% w/v 1 million PEO), thus allowing for the investigation into the effect of increasing molecular weight on membrane flux. The fourth polymer draw was 5% w/v 160K polyvinylpyrrolidone (PVP), another water soluble polymer. Three **polyelectrolyte** draw solutions were also investigated; 5% w/v 1 million MW polystyrene sulfonic acid sodium salt (PSSA) and two different sodium polyacrylate salts (NaPA) 5% w/v 225K MW NaPA and 6 million MW NaPA.

Experiments were carried out using a modified stirred-cell system usually employed for pressure driven ultrafiltration experiments. The stirred cell was adapted for use in forward osmosis experiments by connecting it to a reservoir containing the feed solution via a tube and placing the membrane face down in the membrane holder, with the draw solution within the stirred cell (see **Figure 2.4**).

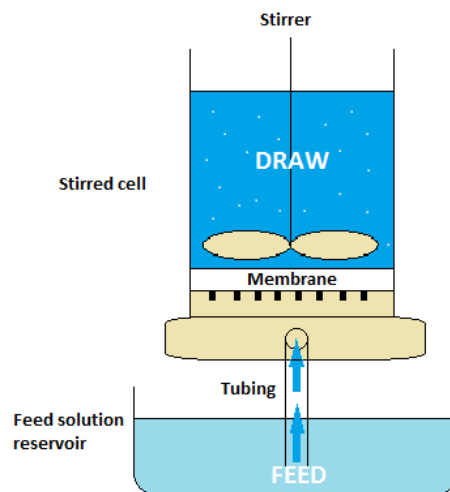


Figure 2.4: Schematic showing stirred cell modified for forward osmosis studies.

The membrane was also varied to investigate the effect of the membrane material and molecular weight cut off (MWCO) - a property related to pore size. Five commercially available ultrafiltration membranes with different MWCO were investigated, two regenerated cellulose (10K and 100K MWCO) and three polyethersulfone (PES) membranes (30K, 50K and 100K MWCO).

General observations from these forward osmosis experiments include that;

1) The polyelectrolytes as a rule generated higher flow rates than the neutral polymers. This corresponds with the fact that polyelectrolytes have free ions associated with each polymeric repeat unit, vastly increasing the number of osmolytes in solution in comparison with a neutral polymer of the same molecular weight without the associated ions.^{9,10}

2) For uncharged polymeric draw solutions, the average flow rate decreased with increasing molecular weight of the draw solution, and the 1% w/v 1 million MW PEO draw solution was unable to generate flow in any experiments with either type of membrane.

3) For polyelectrolytes, the viscosity of the higher molecular weight materials (6 million), even at reduced concentrations, made these solutions unsuitable candidates for draw solutions. This was due to the fact that, in spite of their high flow rates, these solutions could not be measured, poured or stirred efficiently.

4) The PES membranes were more robust and less prone to fouling than the cellulose membranes which often showed a tendency to block after the first hour, giving zero flow after the first measurement (denoted by * after average flow rate). This is unexpected as the more hydrophilic cellulose membranes are normally considered less prone to fouling than the hydrophobic PES.

5) As the membrane MWCO increased, the average flow rates generally decreased.

The trends within each set of data for a particular membrane (i.e. 10K cellulose) are discussed allowing comparison between draw solutions of varying types, molecular weights and concentrations. Additionally trends between the membrane data sets are also explored to assess the effects of membrane materials and MWCO.

2.3.1.1 Cellulose Membranes

Forward osmosis measurements with the **10K cellulose** membrane demonstrated that, for the polymeric PEG/PEO draw solution series, the average flow rate decreased with increasing molecular weight (see **Table 2.1**). This may be attributed to the increasing viscosity which decreases stirring efficiency and reduces membrane wetting therefore creating a less efficient interface between the draw solution and membrane surface. Indeed, it was observed that the 1% w/v 1 million MW PEO was unable to generate flux in any experiment. The 5% w/v 160K PVP had a similar average flow rate to the 5% w/v 100K PEO solution (5 mL/h and 3 mL/h respectively, consistent with their similar molecular weights and the fact that they are both neutral polymers rather than polyelectrolytes. The highest average flow rate was produced by the 1% w/v solution of 6 million MW sodium polyacrylate. The 5% w/v 225K NaPA experiment appeared to experience membrane fouling after only one hour i.e. zero flux after the first hour, symbolised by the * following the average flux.

For the **100K cellulose** membrane two experiments resulted in fouling; 5% w/v 100K MW PEO and 5% w/v 225K NaPA, with zero flow after the first hour (denoted by *, see **Table 2.1** below). The 35K PEG was not a high enough MW to be retained by the membrane therefore resulting in leakage of the draw solution into the feed. As for the 10K cellulose membrane, the highest flow rate for the 100K cellulose membrane was achieved with the 1% w/v solution of 6 million MW NaPA although the 5% w/v 1 million MW PSSA experiment generated a reasonably high average flow rate of 7.1 mL/h. However when this result is compared with the PSSA flow rates across all the membranes it appears to be in contrast with the average fluxes generated in other experiments which tended to be less than 4 mL/h.

Table 2.1: Results from initial forward osmosis experiments with 10K and 100K cellulose membranes.

	Draw solution	Average Deionised Water Flow (mL/h)	
		10K cellulose	100K cellulose
Polymer	5% 35K MW PEG	10	-
	5% 100K MW PEO	3	1.4*
	1% 1 million MW PEO	0	0
	5% 160K MW PVP	5	2.5
Polyelectrolyte	5% 1 million MW PSSA	3.4	7.1
	5% 225K NaPA	1.4*	1.4*
	1% 6 million MW NaPA	20	25

A general observation for the regenerated cellulose membranes was that in three of the 13 experiments the membrane appeared to foul, with flux observed for the first hour but for the following hours zero flux was detected (denoted by * after the average flux). In these cases approximately 10mL of the feed was absorbed into the draw during the first hour after which the flux fell to zero. Two of the latter experiments were with the same draw solution; 5% w/v 225K MW NaPA suggesting some interaction between the draw and the membrane although the higher molecular weight version of the same polymer (1% w/v 6 million MW NaPA) did not exhibit the same issues. This problem was not observed with the PES membranes.

2.3.1.2 PES Membranes

For the **30K PES** membrane, as for the other two PES membranes (**Table 2.2**), there were no experiments with zero flow after the first hour suggesting these membranes are less susceptible to fouling than the cellulose membranes. The two lower MW PEG/PEO draw solutions (35K and 100K) had similar average flow rates and, as in all

experiments, the 1 million MW PEO had zero flow. The 5% w/v 225K NaPA generated an average flow rate of 24mL/h, comparable to the 30mL/h flux generated by the much more viscous and less practical 1% w/v 6 million MW NaPA. Following which, for the subsequent experiments, it was decided that as the 6 million MW NaPA was not practical to use and as the 225K NaPA could conceivably generate a similar result, the 6 million MW draw solution could be omitted from further PES studies.

The **50K PES** membrane when used in conjunction with the lower MW PEG/PEO draw solutions gave similar average flow rates to the 30K PES membrane whilst the 1 million MW PEO again gave zero flow. The 5% w/v 225K NaPA again resulted in a high average flow rate of 26 mL/h, far surpassing the flow rates generated by the other draw solutions in this data set. As discussed previously this is attributed to the high osmotic pressure generated by polyelectrolytes, as a result of the associated counter-ions, relative to neutral polymers.

For the **100K PES** membrane the average flow rate generated by the 5% w/v 225K NaPA was lower than with the lower MWCO PES membranes (30K and 50K MWCO), but this was in agreement with an observed general trend of average flow rate decreasing with increasing membrane MWCO, as discussed in *Section 2.3.2* and it was still the highest flow rate for this data set. As with the other membrane data sets, the 35K PEG and 100K PEO gave similar flow rates.

Table 2.2: Results from initial forward osmosis experiments with 30K, 50K and 100K PES membrane.

Draw solution		Average Deionised Water Flow (mL/h)		
		30K PES	50K PES	100K PES
Polymer	5% 35K PEG	2.3	3.7	3.6
	5% 100K PEO	2.4	5	3
	1% 1 million MW PEO	0	0	0
	5% 160K MW PVP	5	3.6	2.3
Polyelectrolyte	5% 1 million MW PSSA	4	2.6	2.3
	5% 225K MW NaPA	24	26	10.4
	1% 6 million MW NaPA	30	-	-

As mentioned previously none of the PES experiments demonstrated fouling behaviour that resulted in the discontinuation of flux.

When comparing results between membrane data sets it is possible to observe some additional trends which result from membrane material and MWCO effects. For example a simple plot of draw molecular weight vs. average flux (mL/h), see **Figure 2.5**, clearly demonstrates that overall the PES membranes had generally higher fluxes, particularly since they were compatible with the 5% w/v 225K NaPA which appeared to foul both the cellulose membranes.

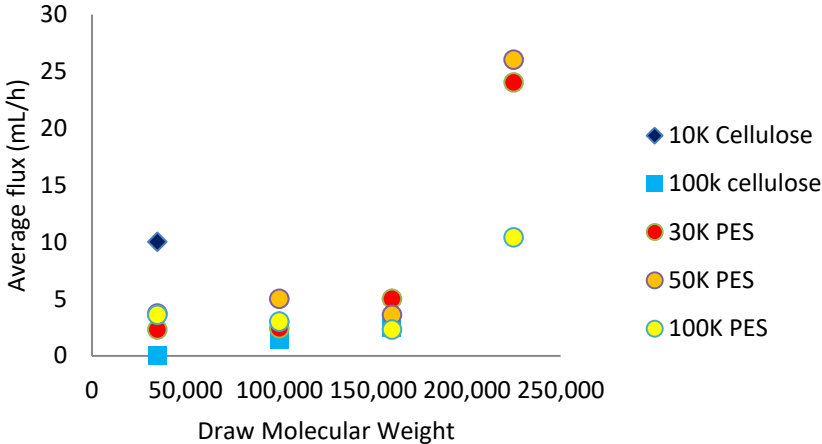


Figure 2.5: Graph showing average flux (mL/h) vs. draw molecular weight for different membrane types 10K and 100K cellulose in comparison with 30K, 50K and 100K PES.

Figure 2.5 also demonstrates that the higher MWCO membranes produce lower membrane fluxes, with both 100K membranes exhibiting much lower fluxes generally than their respective lower MWCO equivalents. This can be shown more clearly by comparing an example of a polymer draw (PVP) and a polyelectrolyte draw (NaPA) of roughly similar molecular weights – 160K and 225K NaPA as shown in **Figure 2.6**. When comparing data from both cellulose membranes with results obtained using the PES membranes both membrane types exhibit a similar general trend; as the membrane MWCO increases the average flow rate decreases regardless of the nature of the draw solution.

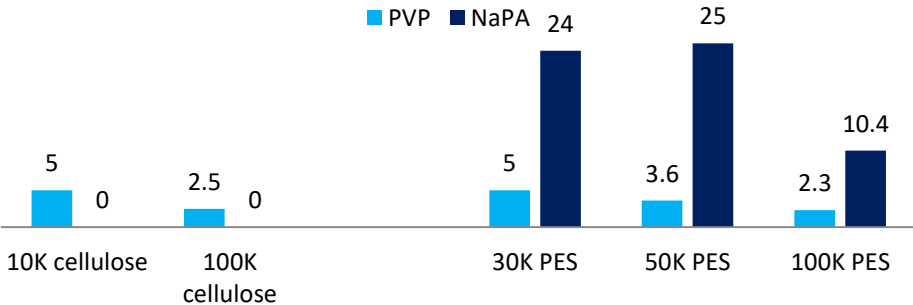


Figure 2.6: Average deionised water flow rate (mL/h) for 5% 160K PVP and 5% 225K NaPA draw solutions for different MWCO cellulose and PES membranes.

Figure 2.6 highlights the large difference between fluxes produced by similar molecular weight polymer and polyelectrolyte draws with the ionic polymer producing a fivefold increase in flux from 5 mL/h to 24 mL/h when using a 30K PES membrane.

After comparing the different membrane materials and MWCO it was evident that a lower MWCO was favourable due to the higher fluxes when compared with higher MWCO membranes regardless of the material. Additionally from these initial studies it is clear the regenerated cellulose membranes are prone to fouling when used for forward osmosis with polymeric draw solutions, thus rendering them unsuitable for application in this project. Having identified the optimal membrane material and MWCO the final component to be optimised was the draw solution.

A general observation, when comparing the different types of draw solutions investigated, was that the polyelectrolytes generate highest fluxes. Whilst the best performing draw was the 6 million MW NaPA the high viscosity of these solutions made them an impractical choice. The 1 million MW PEO failed to produce any flux in any experiment. Plotting the average fluxes for the remaining polymers and polyelectrolytes when used in conjunction with the optimal membrane; 50K MWCO PES UF membrane as decided previously it is clear that the only possible choice capable of generating the high fluxes required is the 5% w/v 225K NaPA (**Figure 2.7**).

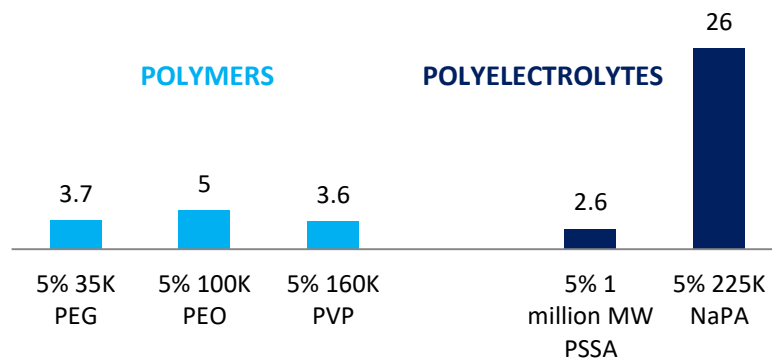


Figure 2.7: Average deionised water flow rate (mL/h) for polymers and polyelectrolytes using a 50K MWCO PES UF membrane.

After identifying the best draw solution (5% w/v 225K NaPA) and the best-performing membrane material (PES) the next step was to carry out studies using the ‘model oedema solution’ which as explained above consists of an (unbuffered) Krebs (UBK) solution with 2% w/v 100K PEO to simulate the protein content. A lower MWCO membrane was initially studied due to the observed decrease in average flow rates with increasing MWCO. In preliminary model oedema fluid experiments with 30K PES membranes **zero flow** was observed. It was proposed that the 100K PEO modelling

the protein was fouling the membranes, blocking the pores and preventing feed permeation. To investigate this, a series of fouling studies with higher MWCO membranes (50K and 100K) were carried out using PEGs and PEO's of different molecular weights.

2.3.2 Ultrafiltration Membrane Fouling Studies

In order to investigate potential membrane fouling by the 100K PEO in the original model oedema solution (Krebs buffer with 2% w/v 100K PEO), forward osmosis experiments were carried out using the same membrane and draw (50K MWCO PES UF membrane and 5% w/v 225K NaPA) with feed solutions containing different MW PEGs/PEOs. The volume of the feed solution was measured hourly and this was plotted against time in order to determine the average flux (mL/h). **Figure 2.8** shows that the feed volume decreased with time as fluid from the feed moved into the draw. However, it also demonstrates that, as the molecular weight of the PEG/PEO increases, the feed flow rate decreases resulting in a levelling out of the feed solution volume with time. There is a significant drop in the flow rate for the higher MW PEGs/PEOs (35K and 100K) when compared with the 6K PEG and the unbuffered Krebs alone. This effect is proposed to be due to membrane fouling caused by higher MW PEGs blocking the membrane pores.

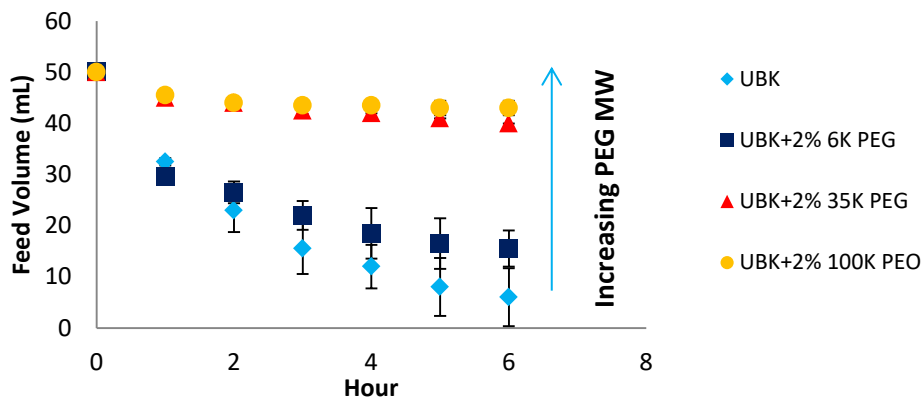


Figure 2.8: Forward osmosis membrane fouling study results showing feed volume decrease vs. time, testing a 50K PES UF membrane with a 5% w/v 225K NaPA draw solution using different feed solutions; unbuffered Krebs solution(UBK) and UBK containing increasing molecular weight PEGs (6K, 35K and 100K), an average of 2 experiments run in parallel.

This theory appears to be in good agreement with the limitations imposed by the MWCO of the membrane which, at 50K, would easily allow the UBK and 6K PEG through whereas the 35K PEG is approaching the MWCO and would be expected to have limited permeability. Furthermore it was observed in *Section 2.3.1* that the 50K PES membrane was capable of retaining the 35K PEG when it was explored as a

draw solution suggesting this polymer cannot freely traverse through the 50K PES membrane. Evidently the 100K PEO is well above the 50K MWCO limit of the membrane and zero permeation would be expected. The effect of PEG/PEO molecular weights on membrane flux is most clearly illustrated in **Figure 2.9** which shows how the average hourly flow rate is decreasing with increasing PEG/PEO molecular weight.

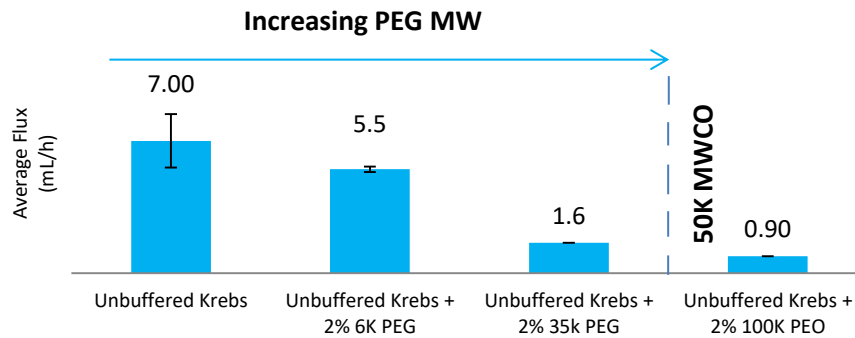


Figure 2.9: Forward osmosis membrane fouling study results showing average membrane flux (mL/h, determined from data in **Figure 2.8**) for different draw solutions, testing 50K PES Membrane with 5%225K NaPA draw using different feed solutions; unbuffered Krebs solution (UBK) and UBK containing increasing molecular weight PEGs, (6K, 35K and 100K).

To further investigate the effects of PEG MW on fouling, the same PEG/PEO feed solutions were tested with a 100K PES membrane to determine whether a larger pore size would result in less fouling and therefore a reduction in the associated decrease in flow rate. As before, plotting the feed volume against time shows a similar result; the flow rate decreases as the PEG MW increases resulting in a levelling out effect in the feed volume associated with reduced/halted flux. However, it is worth noting that there is no sudden drop in flow rate for the higher MW PEG/PEO (35K and 100K) as observed with the 50K PES UF membrane where the two higher MW PEG/PEO data sets diverge from the UBK/UBK +2% 6K PEG data sets.

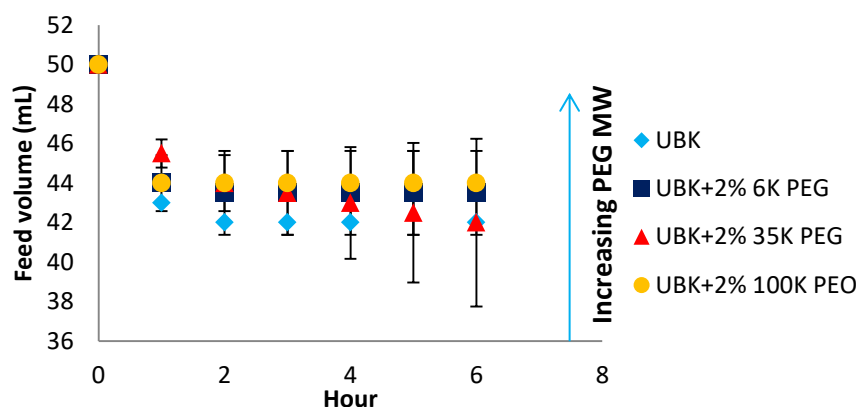


Figure 2.10: Forward osmosis membrane fouling study results showing feed volume decrease vs. time, testing a 100K PES UF membrane with a 5% w/v 225K NaPA draw solution using different feed solutions; unbuffered Krebs solution(UBK) and UBK containing increasing molecular weight PEGs (6K, 35K and 100K), an average of 2 experiments run in parallel.

Furthermore when the overall average hourly flow rate is considered there is little difference between the solutions' flow rates as illustrated in **Figure 2.11**. There is a slight decrease across the series, but this is far less significant than with the 50K PES suggesting that fouling alone may not causing the limited flow rates in this case.

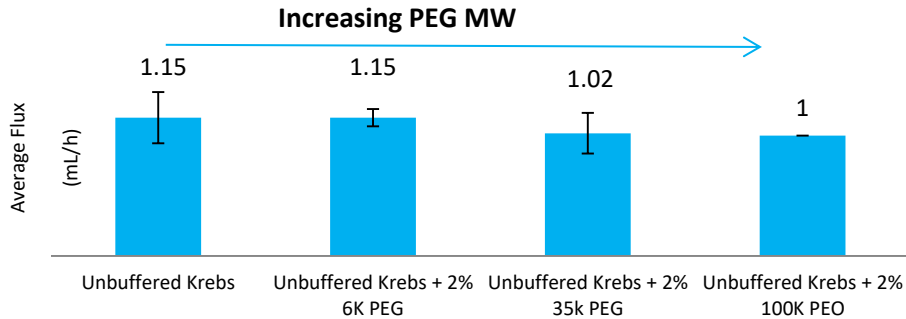


Figure 2.11: Forward osmosis membrane fouling study results showing average membrane flux (mL/h, determined from data in **Figure 2.10**) for different draw solutions, testing 100K PES Membrane with 5%225K NaPA draw using different feed solutions; unbuffered Krebs solution (UBK) and UBK containing increasing molecular weight PEGs, (6K, 35K and 100K).

In order to understand other potential limiting factors for the 100K MWCO membrane comparison between both membranes is required. When comparing results for the 50K PES membrane and 100K PES membrane it can be observed that the flow rate is generally lower for the higher MWCO membrane with the UBK flow rate being on average 7mL/h for the 50K membrane dropping to 1.15mL/h for the 100K membrane.

2.3.3 PEG Behaviour in Solution

Following system configuration determination and model solution testing in *Sections 2.3.1* and *2.3.2* other aspects of the system were then examined. The following two sections describe the solution behaviour of both the draw and feed solutions and how the draw solution is affected when diluted by the feed as a result of forward osmosis.

In order to examine PEG/PEO behaviour in solution, inherent viscosity measurements were obtained to ensure there were no changes in secondary structure with increasing PEG/PEO molecular weight. Changes in polymer structure may increase the risk of fouling for example if the polymer were to become more globular in shape it may be more likely to block the membrane pores. Changes in polymer structure can affect the inherent viscosity of the polymer in solution, leading a sudden change in viscosity which can be detected by measuring the viscosity of different molecular weight solutions of the same polymer (at the same concentration). From the viscosity measurements in deionised water the linear relationship observed for the increasing polymer MW demonstrates there is no change in structure as the molecular weight

increases thereby eliminating this possibility (**Figure 2.12**). Additional measurements were carried out for PEG/PEO in the Krebs solution used in the model oedema studies confirming that the salts do not affect the inherent viscosity of the polymers and therefore also suggesting there are no structural effects.

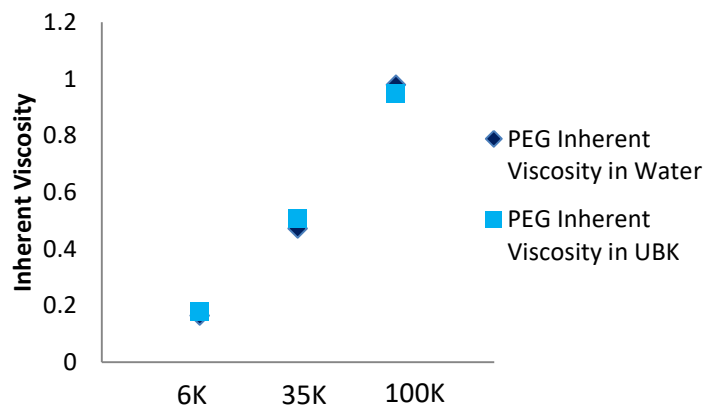


Figure 2.12: Inherent viscosity of solutions of 6K, 35K and 100K PEG (0.1% w/v) in deionised water and unbuffered Krebs solution (UBK) at 25°C.

2.3.4 Sodium Polyacrylate Behaviour in Solution

In addition to understanding the feed solution behaviour, understanding the draw solution and how it is affected by dilution with the feed is essential to the end application of the system as an implantable membrane device for the treatment of oedema. The use of polyelectrolytes as draw solutions has yet to be fully explored and never have they been studied in FO applications with porous membranes.

A *polyelectrolyte* is a type of polymer with ionisable groups which can dissociate in solution to give positive or (in this case) negative charges on its repeat units. Polyelectrolytes in aqueous solution will dissociate to give a charged poly-ion surrounded by a cloud of small, mobile counter-ions.⁸ Well-known naturally occurring polyelectrolytes include proteins and nucleic acids, illustrating the fundamental importance of such molecules. However despite much scientific interest and study they remain one of the least understood systems in macromolecular science.^{11,12} When compared to neutral polymers, the complexity of polyelectrolytes arises from a combination of long range coulombic interactions, excluded volume effects and solvent induced interactions.^{11,13} Electrostatic interactions between charged groups of the polyelectrolyte result in unusual solution behaviour which can affect their bulk properties such as turbidity, viscosity and light scattering behaviour. In turn these properties are themselves affected by multiple factors such as the solvent suitability in terms of solvating the polymer backbone and the salt concentration.¹⁰

In spite of these challenges in studying polyelectrolytes it is their osmotic properties which make them a desirable as potential draw solutions for forward osmosis. When dissolved in salt free or low salt solutions the osmotic pressure of polyelectrolytes exceeds the osmotic pressure of neutral polymers of equivalent concentrations by several orders of magnitude.^{9,10} However, there are key differences between the osmotic behaviour of salt-containing and salt-free polyelectrolyte solutions and both types of solutions exhibit concentration-dependent osmotic effects. This present discussion will focus on salt-containing polyelectrolyte solutions which are more relevant to the project.

In solutions of polyelectrolytes the osmotic pressure is dominated by the counter-ions but only when they are below the counter-ion condensation (CC) threshold and are therefore essentially free in solution.¹¹ Above the CC threshold the counter-ions in solution become localised around the polyelectrolyte chain and a certain fraction of ions condenses onto the polyelectrolyte chain until the charge density of the macroion is reduced below a critical point known as the counter-ion condensation point.^{14,15} This phenomenon occurs as a result of electrostatic interactions between polyelectrolyte chains and counter-ions in solution. Counter-ion condensation is associated with a loss of entropy in the system which is balanced by the electrostatic attraction between the ions and the polyelectrolyte chain.¹⁰

The concentration of the polyelectrolyte solution will influence the likelihood of this phenomenon occurring. In dilute solutions the loss of entropy associated with counter-ion condensation will be significantly higher than for concentrated polyelectrolyte solutions where the entropic penalty will decrease, making counter-ion condensation more favourable.¹⁰ Additionally, for dilute polyelectrolyte-salt solutions, the osmotic pressure scales linearly with the polymer concentration and is independent of the chain degree of polymerisation.⁹ Counter-ion condensation processes will affect both the osmotic pressure and the electrical conductivity of the solution.¹¹

Sodium polyacrylate is an example of a polyelectrolyte and is produced by a reaction between poly(acrylic acid) and a base such as sodium hydroxide to afford an anion polyelectrolyte.

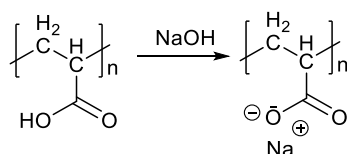


Figure 2.13: Poly(acrylic acid) neutralisation with sodium hydroxide to afford sodium polyacrylate anionic polyelectrolyte.

Polyacrylic acid is soluble in water and in solution adopts the shape of a coiled chain but increasing the pH by neutralisation with sodium hydroxide will cause a change in the polymer conformation and the coil will be transformed into a highly extended chain.¹⁶ This occurs as each negative charge is paired with a sodium cation making the polyelectrolyte electrically neutral. The counter-ions are electrostatically attracted to the carboxylate group through long-ranged Coulomb interactions and will be retained either within the polymer coil or surrounding it within a counter-ion cloud.¹⁷ However when the polyelectrolyte is in solution there will also be an osmotic effect on the ions which will favour their dissociation into the bulk solution where the ion concentration will be lower in order to equilibrate the system. Further dilution of the polyelectrolyte results in an increase in osmotic pressure causing more ions to move from the polymer coil into solution which changes the overall net charge on the polymer from neutral to negatively charged. The unshielded negative charges repel each other which causes the chain to expand from its typical Gaussian coil dimensions.¹⁸ Complete ionisation of the carboxylic acid groups does not occur as, when ionisation increases to high levels, it becomes less favourable for further charges to be created due to the close proximity between the carboxylate groups along the polymer back bone.¹⁹

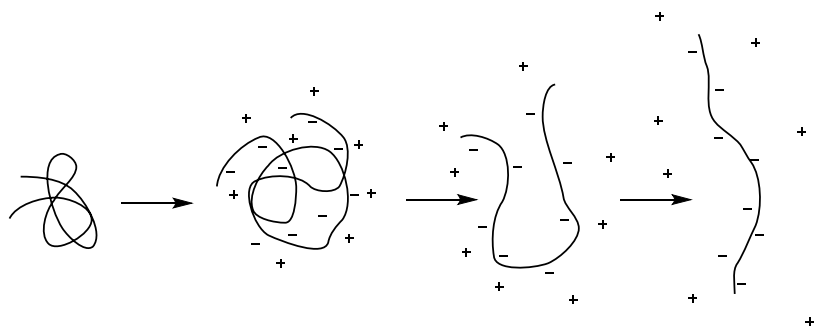


Figure 2.14: Polyelectrolyte coil expansion as a result of counter-ion diffusion away from polymer backbone ‘un-shielding’ negatively charged moieties on chain which will repel each other causing the chain to expand away from its typical Gaussian coil dimensions.¹⁹

It is well documented that polyelectrolytes can interact with a variety of salts and metal cations in solution in a different ways. It has also been shown that the valency of the counter-ions can affect polyelectrolyte behaviour. Simple monovalent cations have generalised electrostatic interactions with the polyelectrolyte whereas multivalent cations are known to form specific interactions with the carboxylate anion of sodium polyacrylate. For example ionised carboxylic acid groups such as those found in polyacrylate salts have been shown to have a high tendency to interact with calcium ions.^{16,20,21} For multivalent ions such as Ca^{2+} these interactions result in two well documented effects; (1) precipitation behaviour and (2) changes in chain confirmation

(reduced coil dimensions).¹⁶ Precipitation occurs when salt binding capacity is exceeded (however, binding to calcium ions can be inhibited in the presence of carbonate anions which allow for the formation of soluble macroscopic CaCO_3) and it has been shown that Ca^{2+} can produce polyelectrolyte coil shrinking.²¹

Additionally, molecular modelling has shown that the polyelectrolyte chain structure is affected by ion density near the chain.²² As discussed above, at high ionic densities ions can 'condense' (counter-ion condensation) onto the chain causing the chain to contract due to charge screening effects. The presence of counter-ions reduces repulsive forces between charged monomer units making up the polyelectrolyte allowing them to move closer together and thus resulting in chain contraction.

Pochard *et al.* have explored the effects of mono- and divalent cations (K^+ and Na^+ from KNO_3/NaCl and Ca^{2+} and Ba^{2+} from $\text{CaCl}_2/\text{BaCl}_2$ respectively) on sodium polyacrylate.²⁰ They propose that monovalent ions will experience generalised electrostatic interactions with polyelectrolytes whereas divalent ions can form complexes with the polyelectrolytes. They also found that complexation effects were not disrupted by electrostatic interactions between the polyelectrolyte and 1:1 electrolytes i.e. addition of a monovalent salt such as NaCl did not affect complexation behaviour.

Shao *et al.* exploited interactions between sodium polyacrylate and Ni^{2+} in order to recover nickel from dilute aqueous solutions.²³ They report a complexation-filtration process based on a simple concept wherein polyelectrolytes such as sodium polyacrylate which are known to bind heavy metals to form complexes are explored as a route to metal removal from water using a membrane filtration process.^{24,25} As these polymers have high molecular weights they can be retained by ultrafiltration membranes with a sufficiently lower MWCO to isolate a metal free permeate whilst concentrating the metal in the polyelectrolyte. This metal-polymer mixture is then at low pH 'decomplexed' to recover the nickel, and the polyelectrolyte salt can then be regenerated by increasing the pH. They found that adding sodium chloride reduced the transition metal removal rate and attributed this to an electrical double layer suppression mechanism rather than competitive complexation (which as explained above may be favoured by multivalent rather than monovalent cations).

This literature study provided the precedent, in the present work, for a series of experiments investigating the effects of different salts on solutions of sodium polyacrylate. The purpose of these studies was to investigate whether interactions

between multivalent salts and the polyacrylate draw solution could be producing large ionic aggregates capable of fouling the membrane and obstructing the pores preventing effective filtration. Solutions of the sodium polyacrylate were diluted with sodium chloride and magnesium sulfate solutions of different concentrations. These solutions were then transferred to an ultrafiltration stirred cell containing a 100K MWCO PES membrane and pressurised using nitrogen. The resulting permeate was collected and the conductivity measured and compared with that of the feed solution to determine % salt rejection. The ultrafiltration experiment was also performed with the salt solutions before mixing with the sodium polyacrylate (i.e. 'salt only' solutions) and a further control was to test the permeation from polyacrylate feeds with no added salt (i.e. dilution with just deionised water).

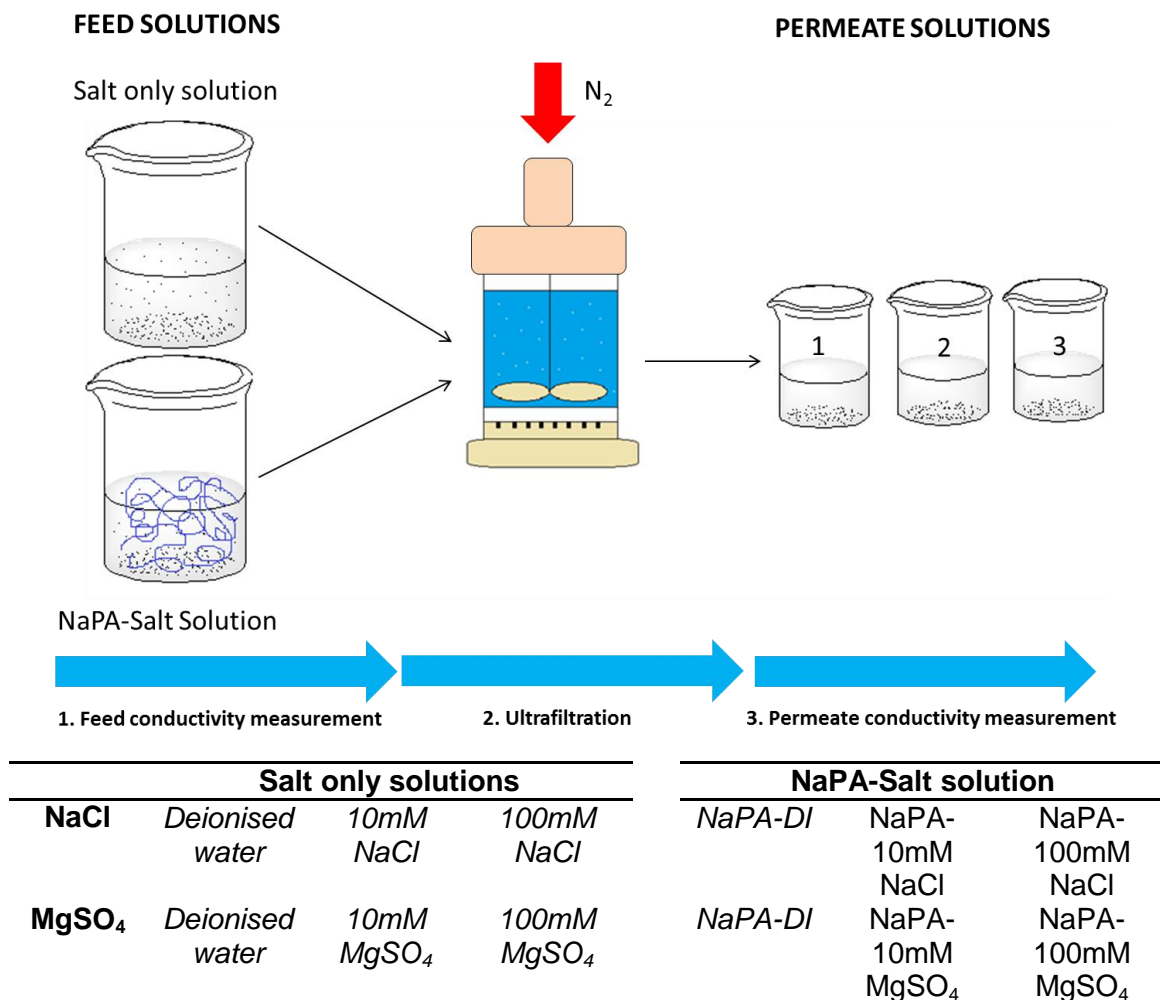


Figure 2.15: NaPA-Salt chelation study schematic showing: 1. Feed solution conductivity measurement 2. Stirred cell ultrafiltration of feed solutions at 1 bar pressure through a 100K MWCO PES UF membrane 3. Permeate solution conductivity measurement – three samples per feed solution to determine average, Table showing compositions of feed solutions; *controls in italics*, NaPA-Salt solutions consist of 5% 225K NaPA (diluted from 20% with either 10 or 100mM salt solutions resulting in final salt concentrations of 8mM and 80mM, respectively).

In both cases (NaCl and MgSO₄) the 'salt only' (i.e. polymer free) solutions exhibited similar conductivities for both feed and permeate confirming that both salts were able to freely permeate through the membrane.

An initial observation from the polyelectrolyte-salt studies is that flux was observed in both the NaCl- and MgSO₄-NaPA solution ultrafiltration experiments. However, in both cases the flux was reduced by a factor of 100 relative to the salt-only solutions such that it took several days to collect enough permeate to measure the conductivity (i.e. from several 100 mL/h to only 1-2 mL/h or even less). It was difficult to compare the NaPA-NaCl and NaPA-MgSO₄ fluxes due to this extended ultrafiltration period so we cannot be sure whether there was an increased risk of membrane fouling in the divalent system relative to the monovalent system. However, direct evidence suggests this may be occurring as it was observed that for the NaPA-MgSO₄ solutions the flux stopped and could only be resumed after membrane cleaning where the feed and draw solutions were removed and the membrane direction was reversed and flushed with deionised water.

In the salt-polyacrylate studies a large difference was observed between the feed and permeate conductivities with the permeate having a significantly lower conductivity than the feed solution: on average the conductivity of the permeate was around 50% less than the conductivity of the feed. Excluding the NaPA-deionised water controls, the conductivity of the permeate was 51% less on average for the two NaPA-NaCl solutions (**Figure 2.16**) and 52% less on average for the two NaPA-MgSO₄ solutions (**Figure 2.17**). However when considering the NaPA-deionised water controls in comparison with the NaPA-salt solutions it is interesting to note that the percentage difference in conductivity decreased with increasing salt concentration. This can be explained since the higher the concentration of salt present in the feed the more salt is likely to be available to permeate through the membrane and therefore the smaller the difference between the conductivities of the feed and permeate solutions. Given that the polyacrylate concentration remains constant whilst the salt concentration is varied and as there are a finite number of carboxylate groups that can interact with counter-ions available in solution any excess of these counter-ions will be free in solution and in theory available to permeate through the membrane.

It is also worth noting that in the NaPA-deionised water controls, the conductivity of the permeate is significantly higher than that of deionised water alone (from the 'salt only' control studies with deionised water) which has an average conductivity of 0.037 mS

cm^{-1} , with the permeate from the two NaPA-DI studies being 2.96 mS cm^{-1} and 2.16 mS cm^{-1} . If we assume the polyacrylate anions are generally too large to traverse the membrane the source of the higher conductivity readings in these experiments suggests that some of the original sodium counter-ions are permeating though. However, if the cations alone were permeating the membrane with no counterbalancing anions a charge imbalance would be created preventing further transport. It is proposed the permeating sodium cations are counterbalanced by hydroxide anions also in solution. The latter are produced by the weakly basic carboxylate groups of the dissolved polyacrylate molecules, abstracting protons from water molecules.

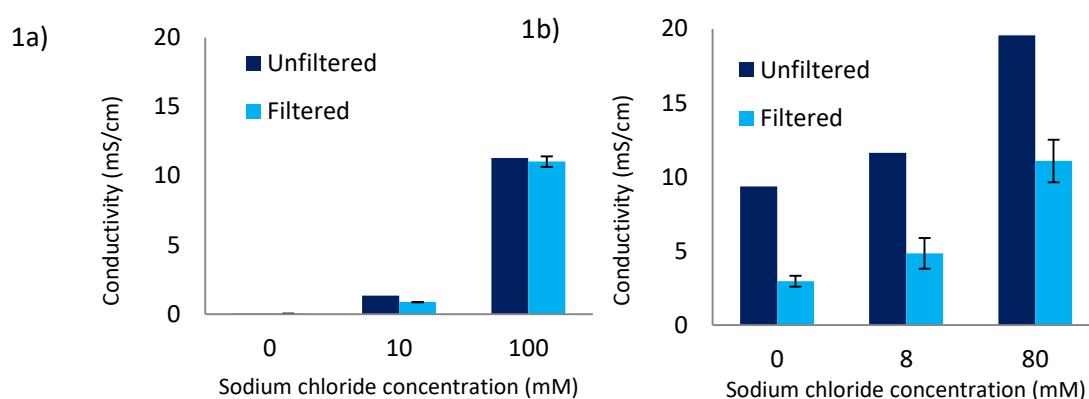


Figure 2.16: Conductivities of 1) NaCl and 2) NaPA-NaCl solutions before and after filtration at 1 bar pressure through a 100K MWCO PES membrane.

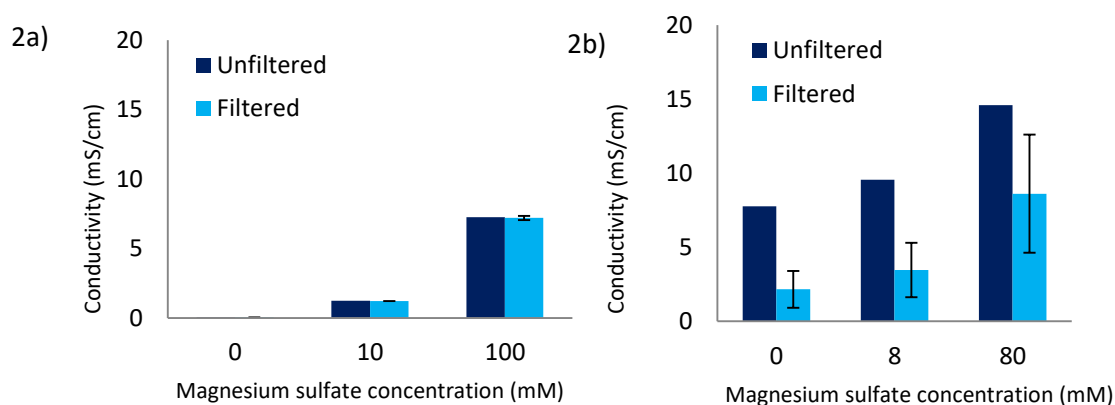


Figure 2.17: Conductivities of 1) MgSO_4 and 2) NaPA- MgSO_4 solutions before and after filtration at 1 bar pressure through a 100K MWCO PES membrane.

From the difference in conductivities between the feed and permeate solution the percentage retention could be calculated i.e. the amount of salt that was retained by the membrane. It was found that increasing the concentration of both the monovalent sodium chloride and divalent salt resulted in a reduced percentage rejection (**Figure 2.18**). However, despite the proposed difference in interactions between the mono and di-valent salts, both types gave similar percentage retentions at each concentration.

The percentage rejection for the 10mM NaPA-NaCl solution was 58% whereas the percentage rejection for the 10mM NaPA MgSO₄ solution was 63%. For the 100mM solutions the percentage rejection for the NaPA-NaCl solution was 43% and for the NaPA-MgSO₄ was 41%. With the difference between the NaCl and MgSO₄ polyelectrolyte solutions being so small; 5% and 2% for the 10 and 100mM respectively, it seems the differing interactions between the mono and divalent salts with the polyelectrolyte may not significantly affect the number of ions 'free in solution' although the general trend is as expected; higher rejections for the divalent salt solutions.

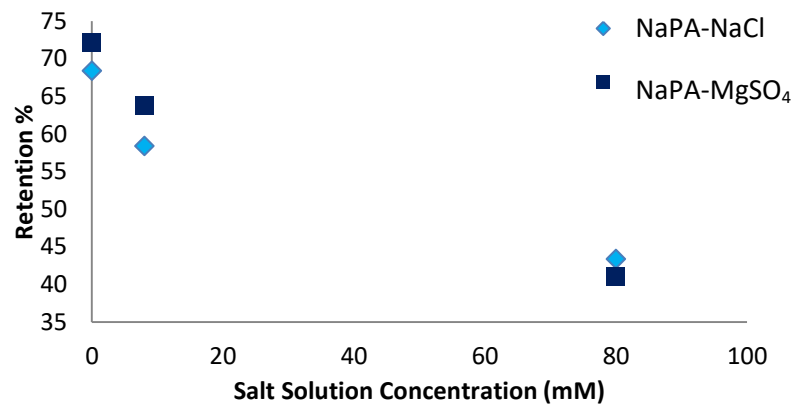


Figure 2.18: Percentage rejection vs. salt concentration of NaPA-salt solutions filtered at 1bar pressure through a 100K MWCO PES membrane.

Upon further consideration of the results from the above experiments it was concluded that the system is more complex than suggested. A proportion of the conductivity measurement for the polyacrylate feed solutions arises from the NaPA itself, which due to its high MW is retained within the stirred cell, this portion will not contribute to the conductivity of the permeate. Thus separating the contribution from the polyacrylate to examine the conductivity contributed by the free ions may clarify the situation. Using a standard curve and plotting conductivity vs. concentration (**Figure 2.19**) it is possible to determine the concentration of unknown salt solutions by measuring their conductivity and if it is assumed that the conductivity of the salt free sodium polyacrylate solutions is equivalent to the contribution from the polyelectrolyte then this can be subtracted from the conductivity of the polyacrylate-salt solutions to isolate the conductivity of the 'free salt'. This can then be used to determine a 'theoretical free salt concentration'.

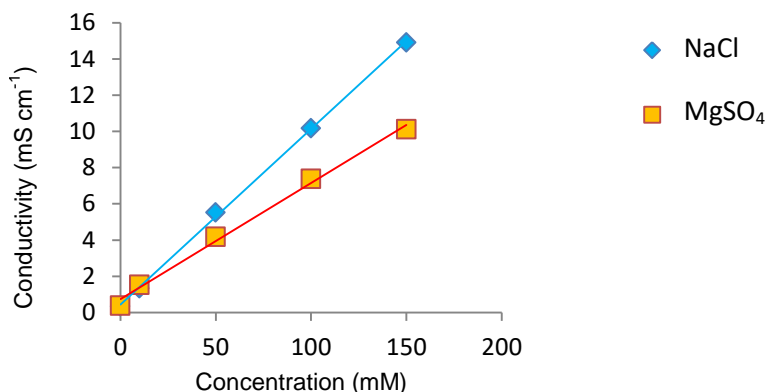


Figure 2.19: Standard curve showing concentration (mM) vs. conductivity (mS cm⁻¹) of different concentration sodium chloride and magnesium sulfate salt solutions.

The theoretical free salt concentration of the feed solution can be calculated to check the accuracy of this method. It was found that the free salt concentration for higher concentration solutions was more accurately calculated than that of the lower concentration solutions (**Table 2.3**).

Table 2.3: Theoretical free salt concentrations of feed solutions.

NaPA-Salt solution	Concentration (mM)	Theoretical free salt concentration (mM)
NaPA-NaCl	10	18.7
NaPA-NaCl	100	100.5
NaPA-MgSO ₄	10	16.49
NaPA-MgSO ₄	100	95.1

Following this the theoretical free salt concentration of the permeate can be compared with that of the feed to determine whether there is in fact a difference in the salt permeation when comparing the mono and divalent species. **Figure 2.20** shows that with this comparison there is more of a difference between the two salts; for both the 10mM and 100mM solutions the theoretical free NaCl present in the feed solution was equivalent to approximately 79% of the feed solution. However, for the MgSO₄ solutions a difference was observed between the two solutions, with the amount of MgSO₄ present in the permeate of the 10mM study being equivalent to 53% of the feed solution and the MgSO₄ present in the feed of the 100mM study being significantly higher at 94%. The difference observed for the divalent salt could be attributed to a complexation effect which in the 100mM study is saturated resulting in a higher percentage of salt permeating through the membrane.

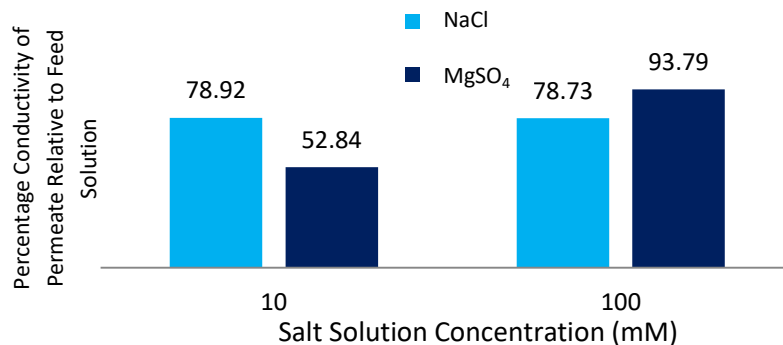


Figure 2.20: Percentage conductivity of permeate concentration relative to feed concentration for both 10mM and 100mM salt-NaPA solutions following subtraction of NaPA contribution.

In order to further probe the effects of counter-ion valency on the structure of the sodium polyacrylate a viscosity study was performed. The absolute viscosity (η_{abs}) of the solutions of the sodium polyacrylate diluted with the same volume but different concentrations of both monovalent sodium chloride and divalent magnesium sulphate solutions was measured (**Figure 2.21**). In each sample the polyacrylate concentration would be the same but the salt concentration was different. Both NaPA-Salt solutions demonstrated a reduction in absolute viscosity with increasing salt concentration. This can be explained by considering the counter-ion effects discussed previously; as the counter-ion concentration increases counter-ion condensation/association with the polyelectrolyte shields the carboxylate group negative charges allowing the polymer to attain a more coiled structure thus reducing the viscosity of the solution. For each different concentration the NaPA-MgSO₄ solutions demonstrated a lower viscosity with respect to the NaPA-NaCl solutions which may be attributed to the better screening ability of divalent ions compared to monovalent ions. If the difference between the two series of solutions is plotted the divide between the mono and divalent solution viscosities decreases with increasing salt concentration.

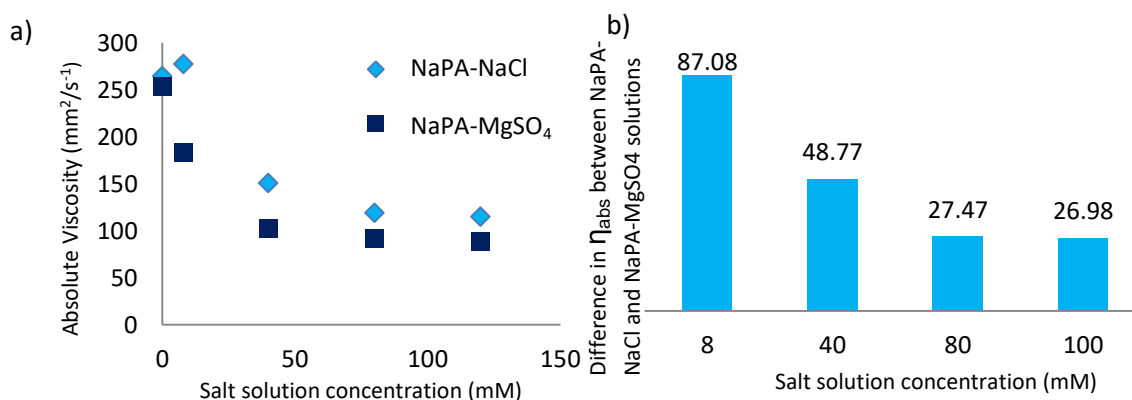


Figure 2.21: a) Absolute viscosities of different solutions of sodium polyacrylate diluted with the same volume of sodium chloride and magnesium sulphate solutions of different concentrations; b) difference between absolute viscosities of NaPA-NaCl and NaPA-MgSO₄ solutions at different salt concentrations.

Overall it is clear that the types of salts present in Krebs solution and therefore present in physiological solutions that would be interacting with the proposed medical device are capable of interacting with the sodium polyacrylate. The different valencies of the counter-ions present in such fluids (**Table 2.4**) may result in different interactions with the polyacrylate and further work is required to investigate possible effects on membrane fouling through possible formation of insoluble complexes – which may be overcome if low MW counter-ions are present i.e. CO_3^{2-} for Ca^{2+} .²¹ Polymer uncoiling effects along with the change in salt concentration produced by an influx of ions will also affect the osmotic pressure of the system. Furthermore it will be necessary to probe the interaction between the sodium polyacrylate and the proteins which will be removed along with the physiological fluid.

Table 2.4: Cations present in Krebs physiological salt solutions

Monovalent	Divalent
Na ⁺	Ca ²⁺
K ⁺	Mg ²⁺

2.3.5 Polyacrylate Draw Solution Optimisation

The following studies were carried out to determine whether variations in the polyacrylate molecular weight, solution concentration and counter-ion could improve the average forward osmosis flux. The flux is influenced by the osmotic pressure of the draw solution so modifications to the draw solution that will change the osmotic pressure properties should have a direct influence on the flux. Osmotic pressure is a colligative property and therefore is dependent on the concentration of solutes and not on their identity.

2.3.5.1 Molecular Weight Variation

From the initial studies it was determined that very high molecular weight polyacrylate solutions (i.e. 6 million MW) despite their high flux generating properties were unsuitable for use in draw solution applications due to their high viscosity. A lower MW sodium polyacrylate 225K was found to produce similarly high fluxes without the limitations imposed by the high viscosity of the higher molecular weight analogues. It has been stated that the osmotic pressure of polyelectrolytes increases linearly with the polyelectrolyte concentration whilst being independent of the chain molecular weight.^{9,10} However, without directly measuring the osmotic pressure it was evident that these different MW solutions produced different fluxes. In addition to the standard 225K NaPA draw solution two other MW draw solutions were investigated in FO

experiments; a 250K NaPA and a 345K NaPA with a deionised water feed and a 50K PES UF membrane. Two experiments were run in tandem to ensure reproducibility. **Figure 2.22** shows that although the three polymers began with similar fluxes, with the feed solution volume decreasing by similar amounts each hour, as the experiment continued the difference between the three draw solutions flux ability increased with the feed volumes diverging more and more as each hour passed. This resulted in the lowest MW 225K NaPA draw ultimately removing the most feed solution – over half at 26.6mL after 6 hours on average. In comparison the 250K NaPA removed 17.5mL on average and the 345K NaPA removed a mere 11.5mL.

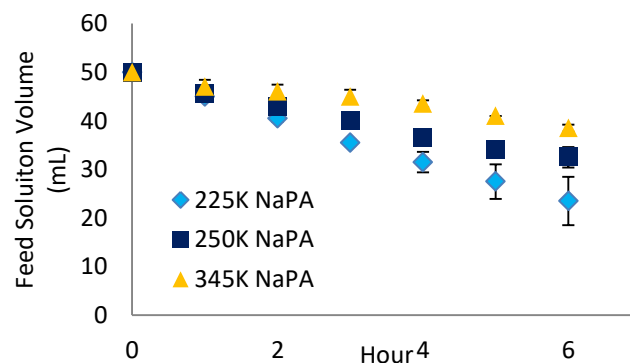


Figure 2.22: Polyacrylate optimisation study, changing molecular weight; 5% 225K NaPA, 250K NaPA and 345K NaPA draw solutions with deionised water feed, 50K PES UF membrane showing feed volume decrease per hour.

Calculating the average flux (mL/h) for each experiment further reveals the difference between the draw solutions. The flux decreases with increasing polyelectrolyte MW; for the 225K NaPA the rate is 4.36 mL/h on average, for the 250K NaPA the rate is 2.92 mL/h and for the 345K NaPA the rate is 1.92mL/h. Although we might expect the three polymers to have similar osmotic pressures this is not the only factor affecting the rate of flux across the membrane. It is possible that the different polyacrylates may have different interactions with the membrane surface resulting in some polymers exhibiting increased fouling behaviour which would affect the flux.¹⁰

2.3.5.2 Variation of Draw Solution Concentration

Changing the draw solution concentration will affect the osmotic pressure as a difference in concentration will create a difference in the number of solute particles in the draw solution. It might therefore be expected that as the concentration increases the flux should also increase, but this is not in fact observed. When comparing 4 different 225K NaPA draw solutions of the following concentrations; 2%, 5%, 7% and

10% with a 50K PES UF membrane and a deionised water feed solution we observe a peak flux when the 5% draw solution is used (**Figure 2.23**).

When increasing the draw solution concentration from a 2% to 5% an increase in flux is observed in both series of experiments. For **Series A** the average flux increases from 3.57 mL/h to 3.86 mL/h whereas for **Series B** the increase is even higher starting at 1.71 mL/h and increasing to 4.86 mL/h. When the draw solution concentration is increased again from 5% to 7% a decrease in flux is observed for both series with the average flux dropping to 2.86 mL/h and 3 mL/h. Interestingly when increasing the draw solution concentration further to 10% the average flux is similar to that achieved with a 7% draw solution in both series (2.8 mL/h). Again this may be attributed to membrane fouling or potentially to issues arising from the increasing viscosity of the draw solutions which can decrease stirring efficiency and therefore reduce membrane wetting resulting in a less efficient interface between the draw solution and membrane surface.

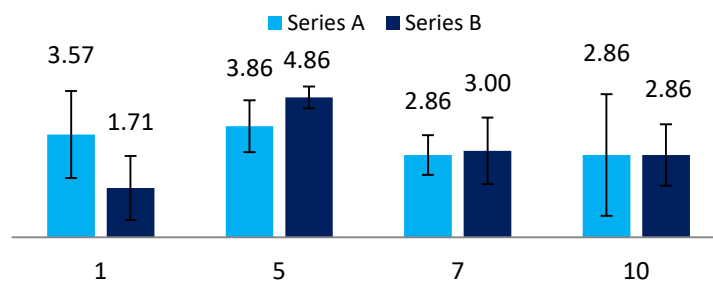


Figure 2.23: Polyacrylate optimisation studies – effect of changing polyacrylate concentration on flux through a 50K PES UF Membrane with a deionised water feed solution, plot shows average flux mL/h for two series of experiments run in tandem (error derived from standard deviation of measured change in fluid volume per hour).

2.3.5.3 Changing Counter-ion Identity

The effect of changing counter-ion identity was examined by comparing both 250K and 345K polyacrylate solutions with either Na⁺ or K⁺ counter-ions. In each case the average flux (mL/h) produced by each solution in a forward osmosis experiment with a 50K MWCO PES UF membrane and a deionised water feed solution was compared. Two series of experiments were run for each of the four possible draw solutions; 250K NaPA, 250K KPa, 345K NaPA and 345K KPa leading to two sets of data. In both series and for both molecular weights (250K and 345K) the potassium polyacrylate generated far higher fluxes than the sodium polyacrylate solutions (**Figure 2.24**). This may be due to difference in the ionic radii of the metals; at 142 pm the ionic radius of the potassium cation is significantly larger than that of the sodium cation 116 pm.²⁶ This difference may result in K⁺ remaining in free solution due its larger size whereas

Na⁺ is more readily condensed onto the polyelectrolyte making it less available to contribute to the osmotic pressure and therefore resulting in reduced membrane flux.

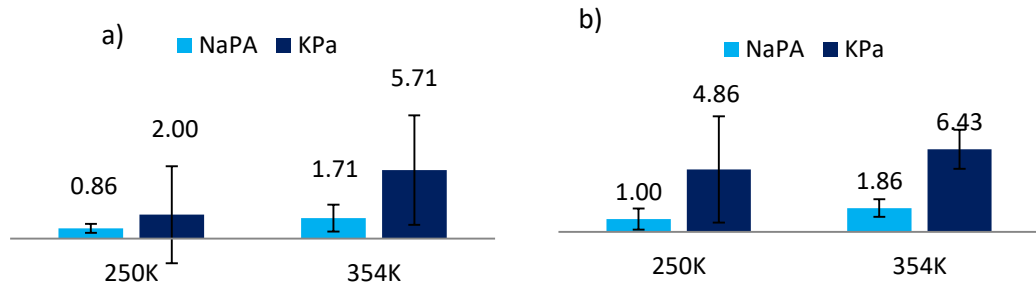


Figure 2.24: Polyacrylate optimisation studies – effect of changing polyacrylate counter-ion on flux through a 50K PES with a deionised water feed solution, plot shows average flux mL/h a) Series 1 and b) Series 2.

2.3.6 Ultrafiltration Membrane Osmotic Pressure Studies

The initial device-design envisaged the use of dense osmosis-type membranes which would be compatible with a wide range of draw solutions including well-studied salt-based ones, but the changing of the design to incorporate UF membranes with their relatively large pores resulted in some limitations for the draw solution. Clearly a larger pore size means simple salts can no longer be effectively contained by the membrane. In order to attain a sufficient molecular weight to prevent back flow of the draw solution into the feed solution, polymeric draw solutions would be required.

A primary concern with polymeric draw solutions is that they may not be able to generate the high osmotic pressure required to drive the forward osmosis process when compared with traditional salt based draw solutions. To investigate this a simple stirred cell-forward osmosis experiment was set up with a saturated salt draw solution on one side of the UF membrane and the optimised polyelectrolyte draw solution (5% 225K NaPA) on the other, allowing observation of the direction of water flow in this system. Interestingly the water moved in the opposite direction to what would conventionally be expected; rather than the water being drawn into the salt solution, which has far higher osmotic pressure, the water moved into the polyelectrolyte draw solution seemingly against the osmotic pressure gradient even for a saturated sodium chloride solution (26%). To investigate this further a series of salt solutions of different concentrations (2%, 5% and 10%) were also tested with the same 50K MWCO PES UF membrane and 225K NaPA draw solution (**Figure 2.25**).

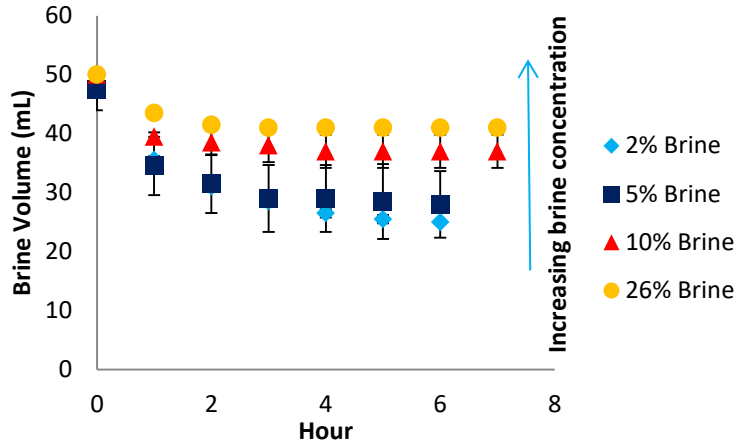


Figure 2.25: Osmotic Pressure study: 50K PES membrane, 5% 225K NaPA draw, average of two repeats run at same time.

In all osmotic pressure experiments using brine vs. 5% sodium polyacrylate with a 50K MWCO PES UF membrane, the water was drawn into the polyelectrolyte draw solution against the osmotic pressure gradient. As the brine concentration (and therefore its osmotic pressure) increased the brine flow rate decreased. It is proposed that the unprecedented movement of water against the osmotic pressure gradient is a result of membrane pore-size effects. Since forward osmosis with salt draw solutions is usually performed with non-porous membranes, the presence of pores in the membrane must be affecting the osmosis process. This was investigated by a simple series of forward osmosis experiments involving the same brine solutions but comparing the 50K PES UF membrane with a non-porous reverse osmosis membrane obtained from a domestic point-of-use reverse osmosis module – See *Section 2.3.7*.

Additionally, studies were carried out to investigate the osmotic pressure properties of brine draw solutions for comparison with the novel polyelectrolyte-UF membrane forward osmosis system. For simple dilute ionic solutions such as sodium chloride solutions it is possible to calculate the theoretical osmotic pressure (π) using the (Morse) **Equation (1)** which is derived from the van't Hoff equation.²⁷

$$\pi = iMRT \quad (1)$$

Where i is the van't Hoff Factor which in the case of sodium chloride will be 2 as NaCl will dissociate into two particles (Na^+ and Cl^-) in solution. M is the molarity, R is the gas constant in units of $\text{L atm K}^{-1} \text{mol}^{-1}$ and T is the temperature in Kelvin.

The molarity is calculated from the % solution using **Equation (2)**.

$$M = \frac{\left(\frac{\text{grams reagent}}{100\text{mL}}\right) * 10}{\text{formula weight}} \quad (2)$$

which can also be simplified to **Equation (3)**:

$$M = n/V \quad (3)$$

Where n is the number of moles and V is the volume in litres. Using equations 1-3 the theoretical osmotic pressure of the brine draw solutions of different concentrations (used in the series of FO osmotic pressure study experiments) can be calculated (See **Table 2.5** and **Figure 2.26**).

Table 2.5: Theoretical osmotic pressures of different % concentration sodium chloride solutions

Percentage NaCl Solution	Molarity (mol/L)	Osmotic Pressure (atm)
2%	0.324	16.7
5%	0.856	41.9
10%	1.711	83.7
26%	4.449	217.0

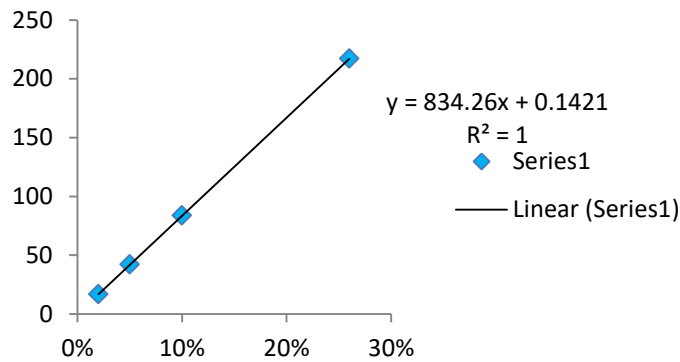


Figure 2.26: Theoretical osmotic pressures (atm) of different percentage concentration sodium chloride solutions (2%, 5%, 10% and 26%).

Following this treatment, from the solution osmotic pressure it is possible to calculate the theoretical Δh or change in fluid height these solutions would produce if placed in one half of a U-tube where the other half contains pure deionised water and both halves are separated by a semi-permeable membrane. If the fluids starting heights are equal, over time the osmotic gradient across the membrane will result in the movement of fluid from the deionised water side into the salt solution side of the U-tube until equilibrium is reached.

Equation (4) relates the osmotic pressure to the solution height (see **Table 2.6**)²⁸ as requires the solution density (ρ in Kg.m^{-3}) and required knowledge of the density of the solution (ρ in Kg.m^{-3}) as well as a constant g which is the acceleration due to gravity (9.8 m.s^{-2}).

$$\pi = \rho gh \quad (4)$$

Table 2.6: Theoretical solution height in m of different concentration salt solutions.

Percentage NaCl Solution	Osmotic Pressure (Pa)	Density (Kg.m ⁻³)	Height (m)
2%	1692128	1012	171
5%	4245518	1034	419
10%	8480903	1070	809
26%	21990000	1197	1875

A custom built U-tube was designed and used to examine the effects of differing salt draw solution concentration on a deionised water feed solution when separated by an RO membrane with the facing/active side towards the feed solution. Since the calculated solution heights are obviously out of range of the U-Tube system the average flux is calculated by hourly measurements of the change in height i.e. the increase in height of the draw combined with the corresponding decrease in height of the feed to give the overall ΔH (cm/h). Additionally a measurement was obtained after 24 hours.

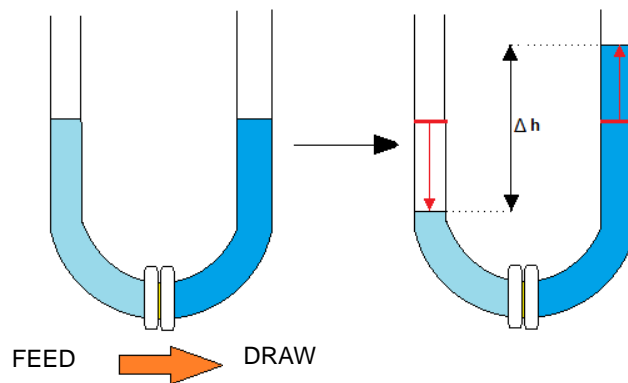


Figure 2.27: Schematic showing average hourly Δh determination using U-tube, orange arrow shows fluid movement.

These initial experiments showed that, as the salt draw solution concentration increased, the flux (cm/h) also increased. From just over 1 cm/h with a 2% salt draw to just over 2 cm/h with a 26% draw (**Figure 2.28**). Measurements at 24 hours could not be obtained as the solution height was beyond range of the U-tube dimensions. These experiments were repeated with a Krebs solution feed replacing the deionised water to examine the effects of the salts in the Krebs solution on the system. The presence of such solutes in the feed solution would affect the osmotic pressure gradient across the membrane, reducing the difference in osmotic pressures of the feed and draw solutions and consequently it was proposed the flux would decrease in the studies on the Krebs solutions. This was observed in the reduction of the flux relative to the deionised water studies. Interestingly the change in hourly flux

(cm/h) between deionised water and Krebs solution was almost the same for all four draw solutions with each experiment showing a decrease in flux of approximately 1 cm/h when the deionised water was replaced by the Krebs solution.

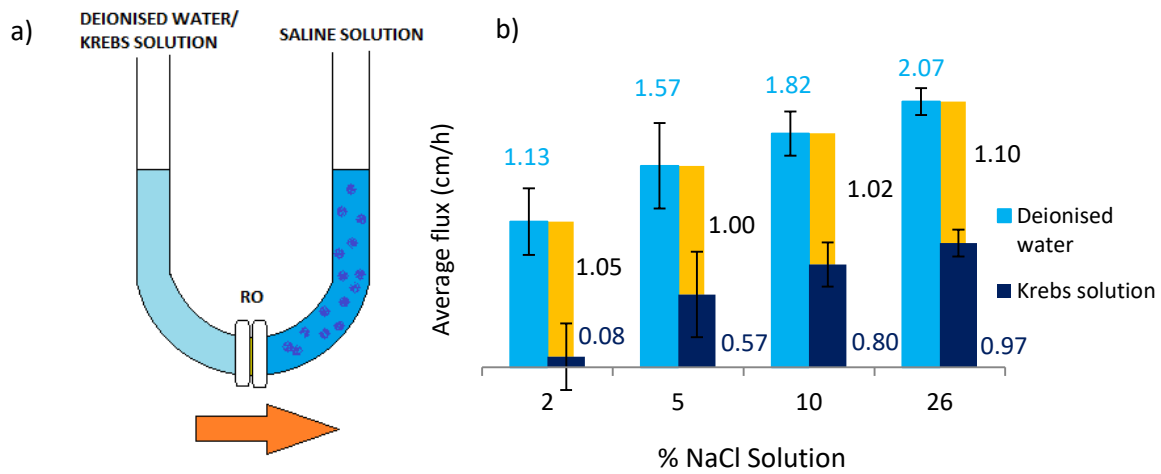


Figure 2.28: a) U-tube schematic demonstrating solution configuration and fluid flow direction b) Average deionised water flux and Krebs solution flux (cm/h) created by sodium chloride draw solutions of different concentrations, determined by U-tube using an RO membrane.

For the studies on Krebs solution, measurements after 24 hours were able to be obtained as the change in fluid height remained in range of the U-tube (**Figure 2.29**). As would be expected, the height increased with increasing saline draw concentration from 3.4 cm using a 2% saline draw solution to 19 cm using a 26% saline draw solution.

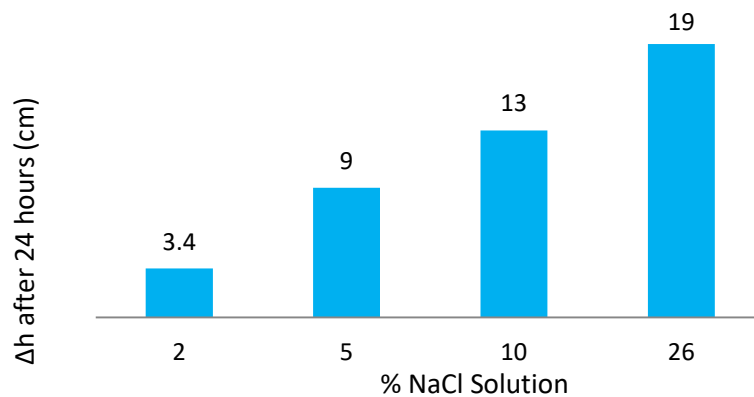


Figure 2.29: Total change in fluid height (Δh , cm) between 0-24 hours Krebs solution feed vs. saline draw solutions of different concentrations.

Table 2.7 compares the measured change in fluid height with the theoretical change in height calculated from the average flux values (**Figure 2.28**). It is interesting to note that, for the majority of the experiments, the measured total change in fluid height after 24hrs values is significantly less than would be expected if the average flux measured

at the start of the experiment was maintained. Exceptions being the lowest concentration draw solution (2% saline) which produced a higher total change in fluid height than predicted by the theoretical calculation. A reduction in flux is often observed as an experiment progresses due to membrane fouling and concentration polarization effects.

Table 2.7: Theoretical vs. actual values for total change in fluid height (Δh , cm) after 24 hours.

Saline Draw Concentration	Average flux (cm/h)	Δh 0-24 hours	
		Theoretical	Actual
2	0.08	2	3.4
5	0.57	13.6	9
10	0.80	19.2	13
26	0.97	23.3	19

Whilst salt-based draw solutions have been traditionally used for FO there have been no previous studies of forward osmosis using ultrafiltration membranes in combination with high molecular weight draw solutions which have more complex solution behaviours. The osmotic properties of sodium polyacrylate and the influence of the membrane type are explored in *Section 2.3.7*.

2.3.7 Reverse Osmosis vs. Ultrafiltration Membranes

In the present study it was proposed that the porous nature of the UF membranes would nullify the osmotic pressure of the brine solutions as the pores allow the salt to freely permeate through in both directions, thus preventing the development of an osmotic pressure gradient across the membrane. Only the larger polyelectrolyte molecules are held by the membrane and therefore can exert an osmotic pressure effect, introducing a gradient across the membrane and hence resulting in fluid flow from the saline solution into the polyacrylate solution. However, if a dense 'non-porous' RO membrane were to be used, the osmotic pressure of the brine solution would be able to create a pressure gradient across the membrane resulting in conventional fluid movement into the brine. To test this proposal, forward osmosis experiments were carried out using the modified stirred cell, comparing an RO membrane with a 50K PES UF membrane using the standard 5% 225K NaPA draw solution, against a variety of brine solutions ranging from 2%-26% (saturated) brine solution. These experiments were also repeated with a 100K PES UF membrane. In each case the membrane face was orientated to be facing the designated feed solution i.e. the UF membrane was placed to be facing the brine solution and the RO membrane was placed to face the polyelectrolyte solution.

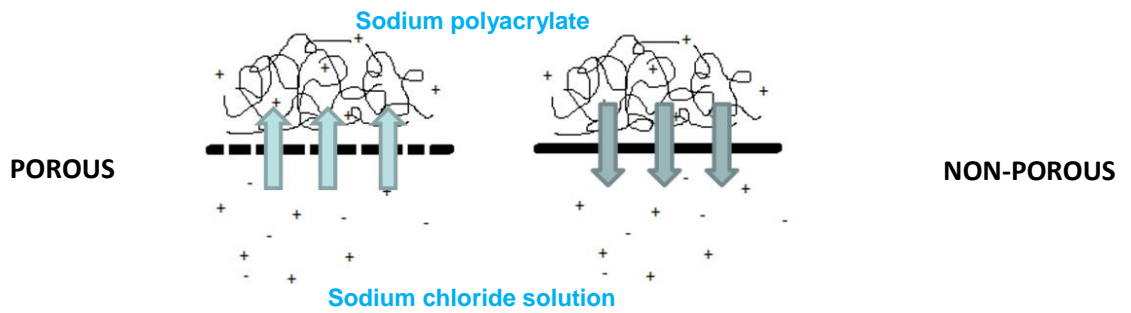


Figure 2.30: Proposed movement of fluid in FO processes using a) porous UF vs. b) non-porous RO membrane with a polyelectrolyte vs. saline draw solution.

For both series of experiments employing either the 50K PES UF membrane or the 100K PES UF membrane the general trend found was that in the UF-FO experiments the fluid moved from the brine into the polyacrylate and for the RO-FO experiments the fluid moved in the opposite direction – from the polyacrylate into the brine. The overall change in feed and draw volume was largest in the UF experiments signifying higher flux rates compared to the RO membrane experiments where little fluid exchange was observed. A final observation was that as the brine concentration increased the flux decreased. This was most clearly seen in the UF-FO experiments for both membranes.

Results from the 50K PES UF membrane experiments are shown in **Figure 2.31**. In the left hand plot the 5% 225K NaPA draw solution volume is increasing with time as it draws fluid from the 5% brine feed solution which consequently decreases in volume with time. A similar result is observed in the right hand side plot where the experiment is repeated with a feed solution of 10% brine. Increasing the concentration of the brine feed solution decreases the flux with average flux for the 5% brine experiment determined to be 1.3 mL/hour whilst doubling the brine concentration to 10% reduces the flux almost by half to 0.8mL/hour.

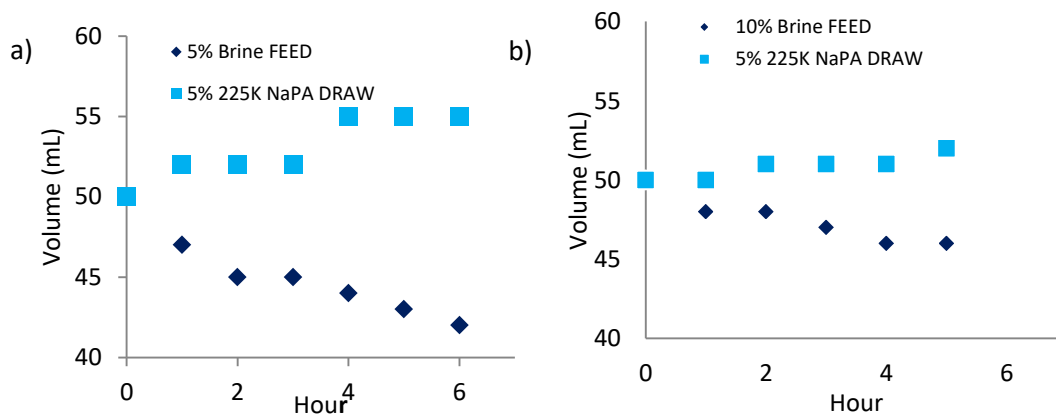


Figure 2.31: Feed and draw solution volume change with time in FO study using a 50K PES UF membrane comparing a) 5% brine vs. 5% 225K NaPA, with b) 10% brine vs. 5% 225K NaPA.

For the UF-FO experiments using a 100K PES UF membrane a similar result was observed; increasing the brine feed concentration reduced the flux as demonstrated in **Figure 2.32** shown below. Increasing the brine feed from 2% to 26% reduced the flux from 2 mL/hour to 0.4 mL/hour.

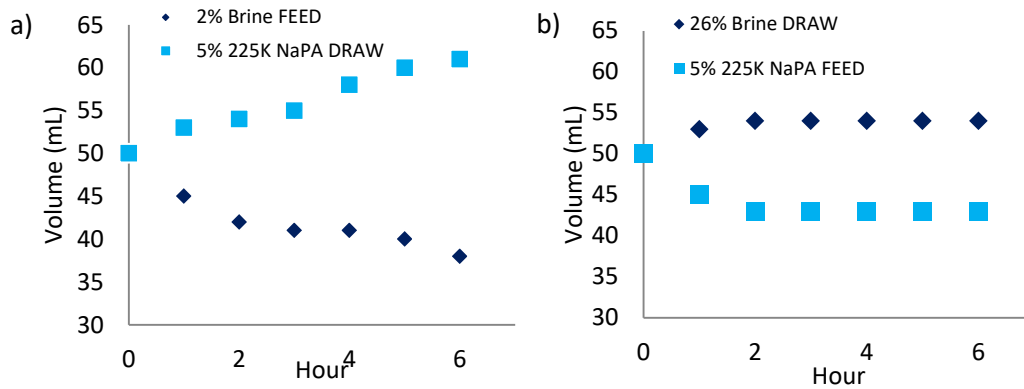


Figure 2.32: Comparison of feed and draw volume change with time in FO study using a 100K PES UF membrane comparing a) 2% brine vs. 5% 225K NaPA, with b) 26% brine vs. 5% 225K NaPA.

Repeating a selection of these studies with a U-tube system allowed for more accurate determination of hourly flux measurements. A series of experiments was performed again comparing a UF membrane (100K PES) with an RO membrane. For each membrane type a U-tube experiment was carried out with one half of the U-tube containing 5% 225K NaPA and the other half containing deionised water or 2%, 5% or 26% saline solution (**Figure 2.33**). Hourly measurements were made to determine the flux (using units of cm/hour) and also the direction of fluid movement. In both series of experiments (UF vs. RO) when the deionised water control was tested against the 5% 225K NaPA the fluid moved from the deionised water into the polyacrylate as would be expected due to the osmotic pressure gradient produced by the sodium polyacrylate. This experiment also produced the highest fluxes for both series of experiments, at 0.88 cm/hour and 2.08 cm/hour for the UF and RO membranes respectively.

For the UF membrane studies, when 26% brine was tested against the polyacrylate no fluid movement in either direction was observed although conductivity measurements discussed below demonstrated that exchange was still occurring across the membrane. For both the 5% and 2% saline experiments the fluid moved in the proposed direction; from the brine into the polyacrylate. For the three experiments in which fluid movement was detected average (DI, 2% and 5%) hourly flux values were calculated and, as would be expected, the flux decreased when deionised water was exchanged for saline from 0.88 cm/hour to 0.2 cm/hour for the 2% brine and 0.46

cm/hour for the 5% brine. It is worth noting that a 5% sodium polyacrylate solution is capable of moving fluid from a brine solution of the same percentage concentration despite its significantly higher osmotic pressure (discussed above) when an ultrafiltration membrane is used to separate the solutions.

For the RO membrane in all three experiments fluid movement was observed. For the three saline experiments (2%, 5% and 26%) fluid movement was from the polyacrylate into the saline solution and the rate increased as the saline concentration was increased – a reversal of the behaviour observed with the UF membrane. The flux increased from 0.2 cm/hour for the 2% solution to 0.36 cm/hour for the 5% solution and 1.32 cm/hour for the 26% solution.

The most significant results are those obtained in the experiments with 5% saline vs. 5% 225K NaPA which support the theory that the membrane type can influence flux direction in forward osmosis processes. In these experiments solutions of the same percentage concentration will behave as either a draw or feed depending on the membrane separating them. The RO membrane enables the saline solution to act as a draw solution whereas the UF membrane enables the polyacrylate solution to act as a draw solution (**Figure 2.33**).

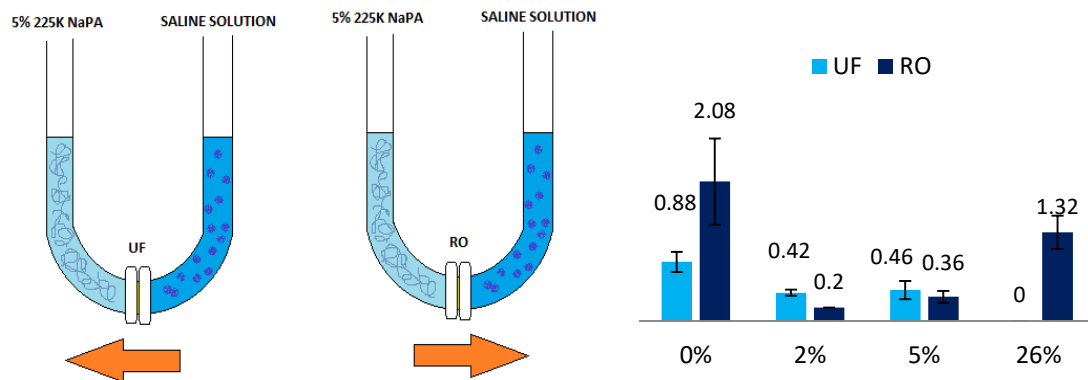


Figure 2.33: a) U-tube schematic demonstrating solution and membrane configuration and proposed fluid flow direction b) Average flux (cm/h) for deionised water, 2% saline, 5% saline and 26% saline vs. 5% 225K NaPA comparing a 100K PES UF membrane with an RO membrane.

As demonstrated in **Figure 2.33**, for the UF membrane when 26% saline was used there was no fluid movement i.e. zero flux, even after 24 hours. This could suggest that the fluids were not exchanging although further investigations demonstrated that this is not the case. Conductivity measurements of the 5% 225K NaPA draw solutions before and after the FO experiments show that there are changes to the fluid compositions. Indeed comparing the conductivity before and after 24 hours of forward osmosis experiments with the different water and salt solutions gives further insight

into the fluid exchange across the membrane. **Figure 2.34** below shows the polyacrylate conductivity before and after the forward osmosis experiments, with the difference between the two readings shown in red when a decrease in conductivity is observed and green when an increase in conductivity is observed.

For the both the UF and the RO membrane FO studies with deionised water result in a decrease in polyacrylate conductivity as would be expected due to the dilution of the polyelectrolyte solution with pure water, reducing the overall concentration. In contrast when saline solutions were used the polyacrylate conductivity increased for both the UF and RO membranes. This observation clearly indicates that there is movement of the sodium chloride ions from the saline solution into the polyacrylate. This is particularly interesting for the UF, 26% saline study which demonstrated no overall fluid movement but exhibited a significant change in conductivity from 10mS cm^{-1} to over 20 mS cm^{-1} (the upper limit of the conductivity meter). The 5% saline UF experiment also increased the polyacrylate conductivity to a point out of range of the conductivity meter (above 20 mS cm^{-1}).

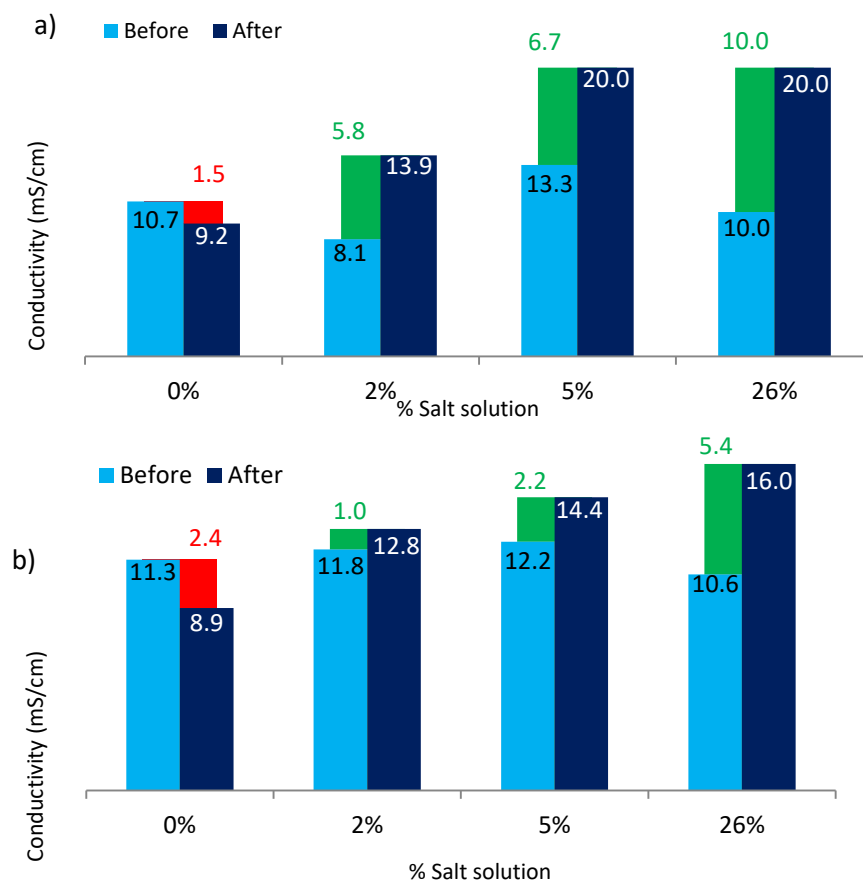


Figure 2.34: Conductivity (mS cm^{-1}) of 5% 225k NaPA before and after U-tube FO experiment with deionised water or 2, 5 or 26% saline solutions comparing a) 100K PES UF membrane and b) RO membrane, red bar shows a decrease in conductivity after the experiment, green bar shows an increase in conductivity.

Additionally, although overall fluid flow in the RO saline studies was from the polyacrylate into the saline there is an increase in conductivity of the polyacrylate. This may be attributed to solution concentration as water is removed whilst the polyelectrolyte is retained. The increase in conductivity in the RO-saline experiments is less than that in the equivalent UF-saline experiments where bulk fluid flow is from the saline into the polyelectrolyte bringing additional ions and therefore increasing the sodium polyacrylate solution conductivity. As would be expected for both the RO and UF studies, as the saline concentration increased the change in conductivity also increased i.e. 5.8 mS cm^{-1} to $>10 \text{ mS cm}^{-1}$ for the UF membrane and 1 mS cm^{-1} to 5.4 mS cm^{-1} for the RO membrane.

For both series, measurements after 24 hours were able to be obtained as the change in fluid height remained in range of the U-tube (with an exception being for the RO-deionised water experiment which produced a change in fluid height out of range of the U-tube).

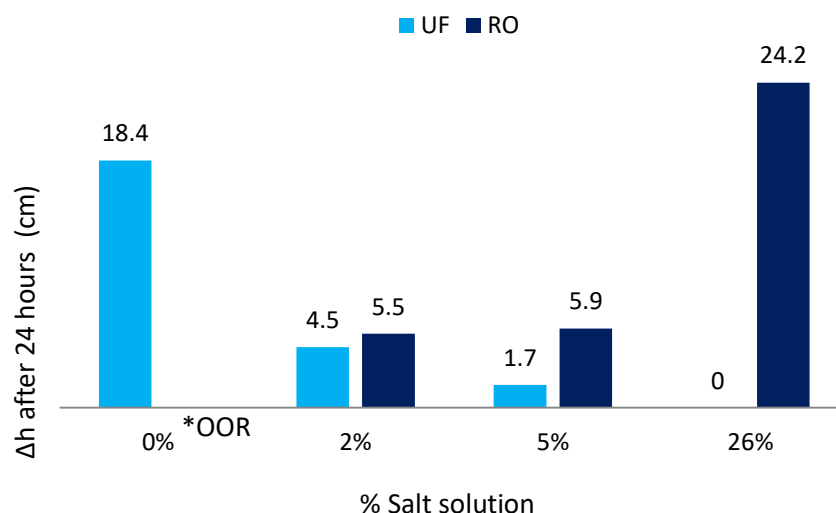


Figure 2.35: Total change in fluid height (Δh , cm) between 0-24 hours for deionised water, 2% saline and 26% saline vs. 5% 225K NaPA comparing a 100K PES UF membrane with an RO membrane *OOR = Out of range.

These values are compared to the theoretical change in height after 24 hours as calculated from the initial average flux (see **Table 2.8**). Again it is interesting to note that the values are less than would be expected if the average flux measured at the start of the experiment was maintained except for the 2% saline in the RO series which in fact has a higher fluid height than predicted by the average flux. A reduction in flux is often observed as an experiment progresses due to membrane fouling and concentration polarization effects.²⁹

Table 2.8: Calculated and measured values for total change in fluid height (Δh , cm) after 24 hours comparing RO and UF membranes with deionised water or 2%, 5% and 26% saline solutions vs. 5% 225K NaPA solution.

Membrane Type	Salt solution	Average flux (cm/h)	Δh 0-24 hours	
			Theoretical	Actual
UF	0	0.88	21.12	18.4
	2	0.42	10.08	4.5
	5	0.46	11.04	1.7
	26	0	0	0
RO	0	2.08	49.92	22
	2	0.2	4.8	5.5
	5	0.36	8.64	5.9
	26	1.32	31.68	24.2

Finally, the absolute viscosity of the sodium polyacrylate solutions was measured both before and after the U-tube-FO study to examine the impact of solution dilution/concentration. Changes in viscosity are associated with changes in the polymer conformation which can be affected by changing concentration and the presence of cations both of which will also affect the osmotic pressure of the system. The structure of polyelectrolytes in solution is determined by the interplay between the strong Coulombic repulsive forces between nearby charged moieties on the chain (favouring chain un-coiling) and the screening of this charge through rearrangement of counter-ions in the surrounding solution (favouring polymer coiling).¹¹ Additionally there are entropy considerations arising from loss of entropy through ion localisation during counter-ion condensation.³⁰ Polyelectrolytes have lower viscosities than neutral polymers at high concentrations as a result of dipolar attraction of condensed counter-ions: this reduces the coil size and therefore lowers the viscosity.^{31,32} Therefore changes in the solution environment which favour counter-ion condensation (i.e. increased salt concentration) should decrease the polyelectrolyte viscosity whilst changes which favour counter-ion diffusion (solution dilution) should increase the polyelectrolyte viscosity. Of course in this study both factors are intertwined since the salt is added in solution form therefore diluting the overall polyelectrolyte concentration. However, simplifying the effects to 1) dilution with water or 2) addition of salt for the purposes of this study allows for the study of processes which are relevant to the future application of the system (the oedema treatment device) whereby the polyacrylate draw solution will be diluted by salt containing physiological fluids.

Figure 2.36 demonstrates the viscosities of the polyelectrolyte solutions before and after 24 hours of forward osmosis in the U-tube experiments comparing the RO and UF membranes using 5% NaPA vs. deionised water, 2% saline, 5% saline and 26%

saline. When considering the experiments using **deionised water** (0%) the bulk movement of the fluid was from the water into the polyacrylate solution for both the UF and RO membrane. While it might be expected that the impact on the viscosity to be similar in both cases we instead observe an increase in viscosity in the UF experiment and a decrease in viscosity in the RO experiment. In both cases the sodium polyacrylate was diluted but to different extents; for the UF membrane the overall fluid height difference after 24 hours was 18.3 cm whereas for the RO membrane the fluid height difference was out of range of the U-tube (**Figure 2.35**). For the UF experiment this is equivalent to the movement of 21.6 mL (calculated from the dimensions of the tube) of fluid from the deionised water into the polyacrylate diluting it by a fifth of its original volume which results in a small increase in viscosity which could be attributed to the dilution increasing the osmotic pressure favouring counter-ion diffusion resulting in polymer uncoiling. Conversely for the RO membrane this viscosity is reduced in the FO study despite this solution being further diluted which in itself is unexpected since the more porous UF membrane should produce higher fluxes when compared to the non-porous RO membrane when using the same draw solution as in this case.

For the **2% saline solution** opposite effects on viscosity were observed for the two different membranes. The UF study showed an increase in polyacrylate viscosity whereas the RO study showed a decrease in viscosity. Although similar fluid height changes were obtained after 24 hours for both the UF and the RO experiment (4.5 cm and 5.5 cm, **Figure 2.35**) the fluid flux direction must be considered. In the UF study fluid moved from the saline into the polyacrylate whilst in the RO study bulk fluid flux was in the reverse direction. In the UF study the polyacrylate is not only diluted but is also flooded with excess cations, a volume of 4.72 mL of the 2% saline solution moved into the sodium polyacrylate. The two factors, dilution and cation concentration increase, will have opposing effects; counter-ions in excess can condense on the polyacrylate favouring polymer coiling whereas dilution favours counter-ion displacement through osmotic effects favouring polymer uncoiling. For the RO membrane a volume of 6.61 mL moved from the polyelectrolyte into the saline solution, concentrating the polyelectrolyte by approximately a twentieth of its original volume.

For the **5% saline solution** opposite effects on polyacrylate viscosity were observed for the two different membranes. In these experiments the bulk fluid movement was in the same direction as observed in the 2% saline experiments (in the UF membrane experiment the fluid moved from the saline solution into the polyacrylate whilst for the

RO membrane the bulk fluid movement was from the polyacrylate into the saline solution) however the effects on the polyacrylate viscosity were reversed. For the RO experiment the polyacrylate viscosity increased slightly which is attributed to concentration of the polyelectrolyte as fluid moves into the saline solution. For the UF experiment a decrease in polyacrylate viscosity was observed. To understand this reversal in trends it is important to consider the changes in fluid volume in comparison to the 2% saline experiment. In the 5% experiment the fluid height changes after 24 hours were significantly different with the UF membrane producing a 1.7 cm change in height (equivalent to 3 mL in volume) whilst the RO membrane produced a 5.9 cm change (equivalent to 10.43 mL in volume). In going from a 2% to 5% saline solution, the saline concentration has more than doubled which, in the UF experiment, results in a smaller volume has moving from the saline into the polyelectrolyte. As discussed above the movement of fluid from the saline into the polyelectrolyte has two opposing effects; 1) increasing counterion concentration favouring polyelectrolyte coiling and therefore decreasing the viscosity and 2) dilution which favours polyelectrolyte uncoiling, increasing the viscosity. Since, compared to the 2% saline experiment, a smaller volume with a higher salt concentration is entering the polyelectrolyte perhaps the counterion condensation effect is stronger than the dilution effect hence the decrease in polyelectrolyte viscosity. For the RO experiment the polyelectrolyte is further concentrated compared to the 2% saline experiment hence an increase in viscosity.

For the **26% saline solution** opposite effects on viscosity were observed for the different membranes however in this case the changes in viscosity are the reverse of what was observed in the 2% saline study (**Figure 2.36**). In this case the UF study showed a decrease in polyacrylate viscosity whereas the RO study showed an increase in viscosity. On this occasion however for the UF membrane zero flux was observed. Nevertheless, from conductivity measurements before and after the UF study it is clear that salt exchange across the membrane has occurred and this is also reflected in the change in viscosity which is hugely reduced in this case. For the RO study fluid (28.59 mL) moved from the polyacrylate into the saline solution (as for the RO study with 2% saline) therefore concentrating the polyacrylate which results in an increased viscosity.

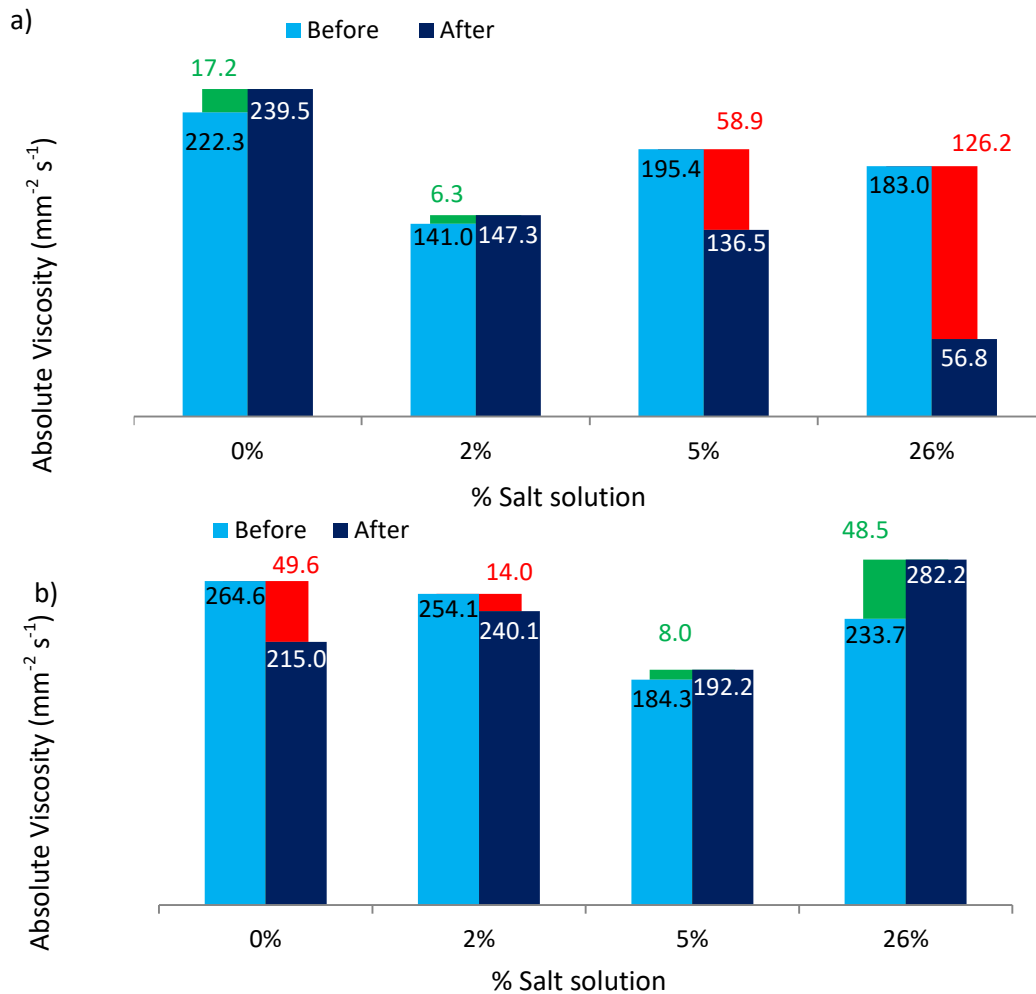


Figure 2.36: Absolute viscosity ($\text{mm}^2 \text{s}^{-1}$, measured at 25°C) of 5% 225k NaPA before and after U-tube FO experiment with deionised water or 2/26% saline solutions comparing a) 100K PES UF membrane and b) RO membrane, red bar shows a decrease in viscosity after the experiment, green bar shows an increase in viscosity.

This section has focused on examining the osmotic properties of a sodium polyacrylate draw solution in comparison to traditional salt-based draw solutions and the effects of the membrane type used. It has been found that by using porous membranes the osmotic effects of the polyacrylate can dominate over the high osmotic pressures of salt-based draw solutions. Since the membrane is permeable to the salt solution but not the polymer, fluid can be transported from a brine solution into a polyelectrolyte solution when using porous membranes. When using non-porous membranes the fluid flows in the reverse direction as would be expected due to the high osmotic pressures of saline solutions. This means that fluid flow direction can be controlled by the choice of membrane. Additionally conductivity measurements before and after 24 hours of forward osmosis have demonstrated that in some experiments where no fluid height change is detected, suggesting zero flux, there are in fact changes in conductivity which signify that salt exchange across the membrane is still occurring. This is further

corroborated by viscosity measurements before and after 24 hours of forward osmosis which also show a change in solution properties even if the volume has remained the same implying no fluid exchange. Additionally these viscosity measurements allow the effects of polymer solution dilution and changing salt concentration to be quantified. Combining all three elements of data; the fluid height and volume changes, the conductivity changes and the viscosity changes enables the effect of changing solution environment on polyelectrolyte structure and therefore its solution behaviour to be identified.

2.3.8 Protein Studies

Due to the complexation and membrane fouling issues which arose from using PEGs to model the proteins it was decided to explore using real proteins to model the oedema fluid in forward osmosis studies. This strategy would also provide information on how the proteins will interact with the membranes and the draw solutions. The first protein investigated was bovine serum albumin (BSA) which has a molecular weight of 69 kDa. The BSA would be expected to have limited permeability through the 50K MWCO PES membrane, so a 100K MWCO PES membrane was used for this initial study. A 2% w/v BSA protein solution in phosphate buffered saline (PBS) was used as a feed solution and the draw was 5% 225K NaPA. Every hour 500 μ L aliquots were taken from the draw solution and the sample volume was replaced by an equivalent volume of the original draw solution. Furthermore a sample was taken the following morning after stirring overnight.

Following this a bicinchoninic acid (BCA) assay was performed in order to determine the protein concentration in the samples. This biochemical assay relies on combining the samples and a series of standards of known concentration with a 'working reagent' (consisting of a combination of two solutions; copper sulfate and BCA) which will undergo a colour change that is dependent on the protein concentration. Specific amino acid residues in the protein (cysteine/Cys, tyrosine/Tyr and tryptophan/Trp) will reduce the copper(II) to copper(I) allowing it to be chelated by two molecules of the acid forming a brightly coloured water soluble complex with a strong linear absorbance at 562nm (**Figure 2.37**).³³ This results in a colour change from green to purple which can be measured by colorimetric techniques using UV-Vis spectroscopy or a microplate photometer. The absorbance of the samples can be used to determine their protein concentration relative to a standard plot of known concentrations. The absorbance of the draw solution was also measured to ensure no interference with the results.

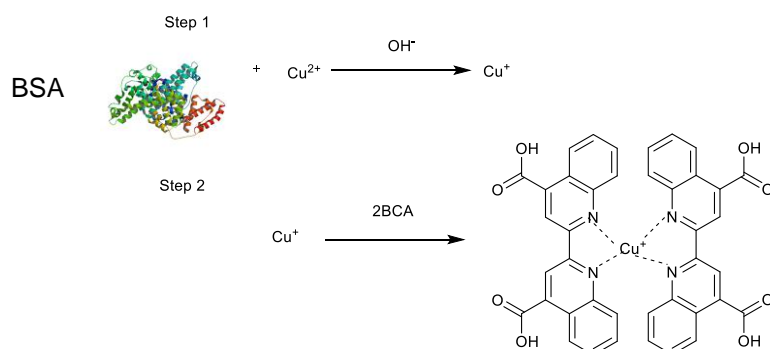


Figure 2.37: BCA Assay schematic; Step 1. Cu^{2+} reduced to Cu^+ by protein (specifically amino acid residues Cys, Tyr or Trp). Step 2. Cu^+ chelated by two BCA molecules to form a complex with an absorbance evident at 562 nm.

Following an initial FO experiment using a 5% 225K NaPA draw solution with a 2% BSA in PBS feed separated by a 100K MWCO PES UF membrane and a UV-Vis spectrometer to measure sample and standard absorbance from the subsequent BCA assay, it was observed that the BSA was able to permeate through the membrane. The samples showed that the protein concentration increased with time (**Figure 2.38**). A calculated concentration of less than zero indicates the sample produced zero absorbance therefore signifying zero protein present. This was the case in the first hour where the calculated concentration is less than zero $\mu\text{g/mL}$ i.e. no protein. In the following hours the calculated protein present increases with time from 18.25 $\mu\text{g/mL}$ to 147.74 $\mu\text{g/mL}$ for hours 2 and 3, respectively. After 24 hours the protein concentration increased to 661.60 $\mu\text{g/mL}$.

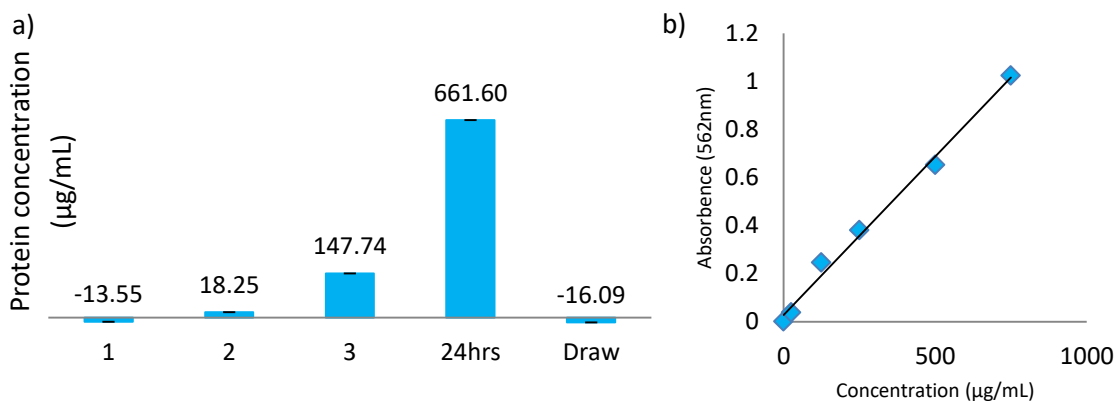


Figure 2.38: Initial FO-Protein experiment using a 100K MWCO PES UF membrane with a 5% 225K NaPA draw solution and 2% BSA in PBS feed solution a) calculated protein concentration ($\mu\text{g/mL}$) in 500 μL samples taken hourly and after 24 hours from the 5% 225K NaPA draw solution b) standard curve used for protein concentration calculation.

Additionally monitoring the feed volume to determine the average hourly flux (2 mL/h) demonstrated the protein did not appear to be noticeably fouling the membrane as

there was no significant decline in flux with time as associated with fouling events (**Figure 2.39**).



Figure 2.39: Initial FO-Protein study - 2% BSA solution feed volume vs. time.

Following these results the study was repeated using a microplate reader for sample analysis following the BCA Assay to provide more accurate results. The experiment was also performed with a 50K MWCO PES UF membrane to determine whether a lower membrane MWCO, associated with a smaller membrane pore size, would result in a reduction in protein permeation.

As expected the 50K MWCO membrane did result in a lower protein concentration detected in the draw solution (**Figure 2.40**). After 3 hours of forward osmosis the protein concentration in the draw solution of the 100K experiment was 250 µg/mL whereas for the 50K experiment the protein concentration was only 60.60 µg/mL. In both studies the protein concentration increased with time. As with the previous experiment, the proteins did not appear to foul the membrane or affect the flux with a similar rate of decline in feed volume measured for both membrane studies.

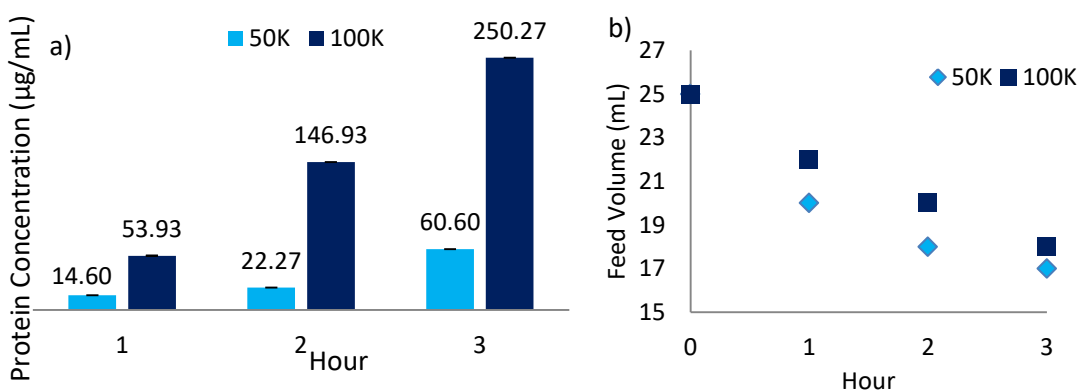


Figure 2.40: Data from protein-FO studies comparing protein permeation through a 50K and 100K MWCO PES UF membrane using a 5% 225K NaPA draw and a 2% BSA in PBS feed solution a) Calculated protein concentration (µg/mL) in 500 µL samples taken hourly from the 5% 225K NaPA draw solution b) feed solution volume (mL) vs. time.

An alternative protein was also studied – fibrinogen with molecular weight of 340 kDa was expected to be too large to permeate through either the 50K or the 100K PES MWCO UF membranes. As shown in **Figure 2.41** in neither case was any protein was detected in the draw solution after 3 hours (i.e. absorbance at 562 nm >0 as observed for the zero protein concentration control). As explained above, calculated negative concentrations from absorbance values which are less than zero signifies zero protein present. As for the albumin studies, the 50K membrane flux did not appear to be affected by the presence of the proteins in the feed solution with the feed solution volume decreasing at a steady rate, however, for the 100K membrane the flux appeared to begin plateauing between hours 2 and 3 (flux = 0 mL/h). This suggests in this particular experiment the high molecular weight protein was in fact beginning to foul the membrane.

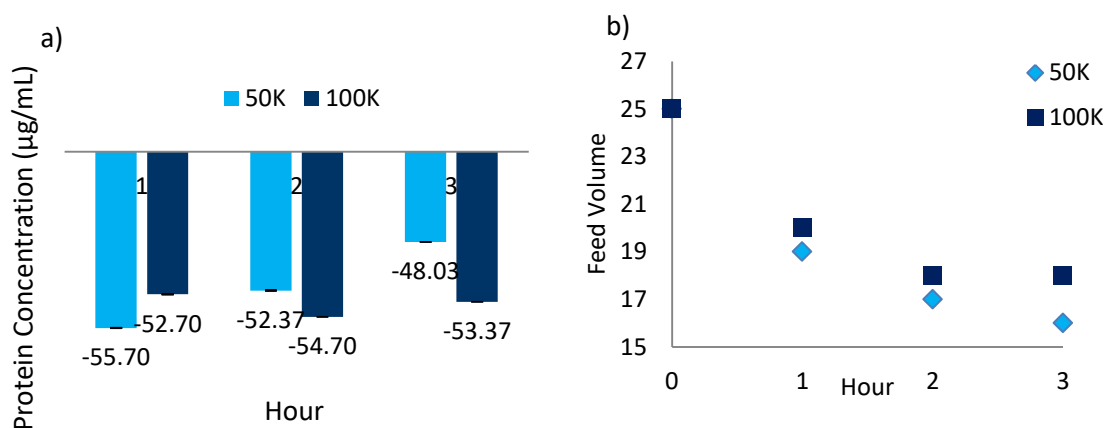


Figure 2.41: Data from protein-FO studies comparing protein permeation through a 50K and 100K MWCO PES UF membrane using a 5% 225K NaPA draw and a 2% fibrinogen in PBS feed solution a) calculated protein concentration (µg/mL) in 500 µL samples taken hourly from the 5% 225K NaPA draw solution b) feed solution volume (mL) vs. time.

Additionally, the membranes used in all four experiments were analysed for protein adhesion. The membranes were rinsed to remove any non-bound proteins and then were heated in a solution of hydroxylated sodium dodecyl sulfate to desorb the attached proteins and release them into solution. Samples of the protein solutions were subsequently analysed using the BCA assay to determine the concentration of adhered protein. Control membranes unexposed to proteins show an absorbance equating to zero protein present. For both membranes adhered fibrinogen was present in higher concentrations than BSA (**Figure 2.42**) which is attributed to differences in absorption mechanisms with fibrinogen having a higher affinity for hydrophobic surfaces^{34,35}. A larger protein surface area increases the risk of adhesion to the membrane surface. Additionally, fibrinogen is much larger than the membrane pores and cannot permeate through further increasing the risk of fouling. Interestingly the

difference between BSA and fibrinogen adhesion is not large, which suggests the fibrinogen does not foul as much as might be expected. This result is supported by the flux data which shows the fibrinogen did not appear to foul the membrane in the first few hours of the experiment. It is also surprising that for both BSA and fibrinogen the 100K membrane appeared to have slightly less protein adhered than the 50K membrane. Again this may be related to the membrane pore size, the larger pores in the 100K membrane may prevent membrane adherence or potentially the larger MWCO may have a lower porosity as discussed above providing a surface which is less compatible with protein adhesion.

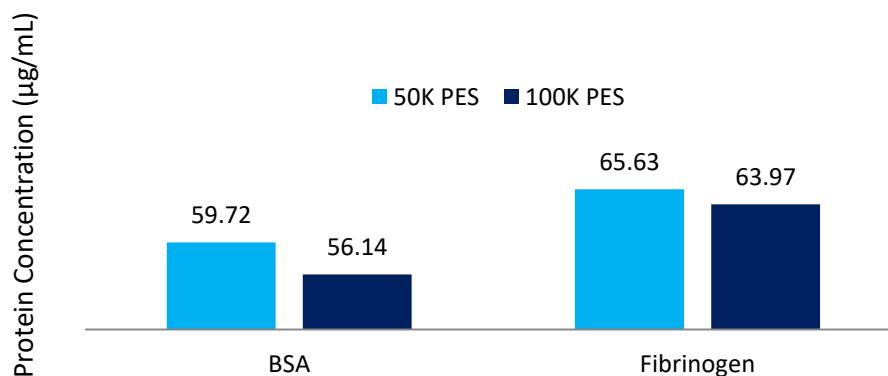


Figure 2.42: Calculated protein concentration ($\mu\text{g}/\text{mm}^2$) adhered to membranes used in FO-protein experiments (membrane sample area 31.67 mm^2).

A third protein was also examined; myoglobin with a MW of 16,951 kDa which was expected to easily permeate through both the 50K and 100K MWCO membrane. As before, an FO experiment was set up with a 2 mg/mL myoglobin in PBS feed solution, a 5% 225K NaPA draw and either a 50K or 100K PES UF membrane (face down in the stirred cell). Hourly samples of the draw solution were taken. Following this the samples were analysed to determine the protein content. Since myoglobin is already deeply coloured (red, wavelength 409 nm) a specific assay was not required to determine the protein concentration in samples taken hourly during the FO experiment. Instead a standard curve was prepared using a stock solution of 1 mg/mL myoglobin in PBS which was diluted to provide a selection of standards of known concentration.

As with the BSA studies the protein concentration in the draw solution increased with time and there was little difference in amount of protein detected for the two different MWCO of membranes which is consistent with the theory that the myoglobin is small enough to easily permeate through both membranes (**Figure 2.43**).

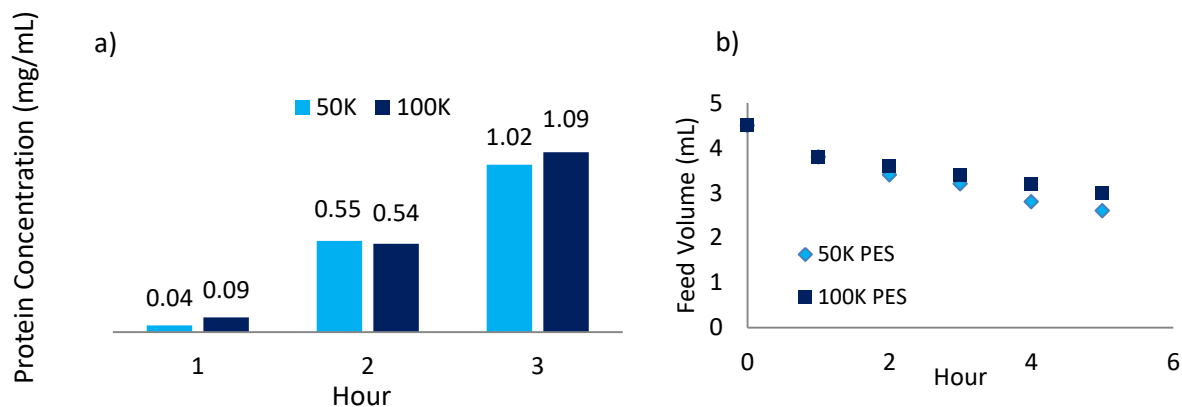


Figure 2.43: : Data from protein-FO studies comparing protein permeation through a 50K and 100K MWCO PES UF membrane using a 5% 225K NaPA draw and a 2% myoglobin in PBS feed solution a) calculated protein concentration (mg/mL) in 500 μ L samples taken hourly from the 5% 225K NaPA draw solution b) feed solution volume (mL) vs. time.

Overall the experiments using real proteins have provided key results to support the fundamental device concept outlined in **Chapter 1** and *Section 2.2*. It has been shown that it is possible to move proteins through a semipermeable porous membrane of an appropriate MWCO using forward osmosis employing high molecular weight polyelectrolyte draw solutions. Additionally these experiments have also shown this process can be carried out for several hours without membrane fouling affecting the flux properties of the system.

2.4 Conclusions

In conclusion, forward osmosis processes with ultrafiltration membranes and high molecular weight polyelectrolyte draw solutions have been investigated, for the first time, as a means of transporting not only water and salts but also macromolecules such as polymers/proteins. It has been shown that this system is capable of transporting proteins of an appropriate size through a UF membrane of corresponding MWCO and that this can occur over several hours without membrane fouling.

Additionally, various different factors involved in this process have been studied to probe their effects on flux and on fouling. In *Section 2.3.1* it has been shown that polyelectrolyte draw solutions outperform neutral polymers when used as draw solutions with UF membranes generating higher fluxes. It was also found that the molecular weight of the draw solution is important due to viscosity effects: higher molecular weight polymers, although capable of generating higher fluxes, are too viscous to work with in practice. When investigating different membrane materials and MWCO it was found that PES performed better (experienced less fouling) than regenerated cellulose in FO experiments and lower MWCO membranes were found give higher fluxes.

In *Section 2.3.2* whilst trying to model physiological proteins using PEG/PEO it was found that the higher molecular weight PEO fouled the membranes but lower molecular weight PEGs did not create the same drop in membrane flux. Investigations into PEG behaviour in solution (*Section 2.3.3*) showed they were not affected by the salts of the Krebs solution used to simulate physiological interstitial fluid.

When investigating sodium polyacrylate behaviour in solution (*Section 2.3.4*) it was found that cations present in physiological salt solutions interact with the polyacrylate affecting the polymer structure which could potentially influence membrane fouling. Additionally the change in structure and salt concentration would alter the osmotic pressure of the system. These complex effects would require further research in the context of the medical device system to fully understand their implications.

Related to polyacrylate behaviour in solution; in *Section 2.3.5* studies were carried out to optimise the polyacrylate draw by investigation the effect on flux when molecular weight, polymer concentration and counter-ion identity were varied found that these three factors could influence the flux of the system. It was found that:

- 1) the average flux decreases with increasing polyelectrolyte molecular weight;
- 2) when comparing four different 225K NaPA draw solutions of the following concentration; 2%, 5%, 7% and 10% with a 50K PES UF membrane and a deionised water feed solution we observe a peak flux when the 5% draw solution is used;
- 3) exchanging sodium for potassium in the polyacrylate salts can also increase the flux by a factor of up to five, presumably as a result of weaker ion-pairing with the polyelectrolyte chain.

When investigating the osmotic properties of the system (*Section 2.3.6*) it was found that polyacrylate draw solutions could generate large enough osmotic pressure gradients to transport fluid from brine solutions (traditionally used as draw solutions in FO with non-porous membranes) into polyacrylate draw solutions. It was proposed this phenomenon may result from the porosity of the membrane preventing the saline from exerting any osmotic effects since it can freely permeate through the membrane whilst the polyelectrolyte is retained on one side. This theory was further examined in *Section 2.3.7* where the osmotic properties of sodium polyacrylic acid was probed using both porous and non-porous membranes. It was confirmed that by using porous

membranes the osmotic effects of the polyacrylate can dominate over the high osmotic pressures of salt based draw solutions since the membrane is permeable to the salt solution but not the polymer. This means that fluid can be transported from a brine solution into a polyelectrolyte solution when using porous membranes whereas when using non-porous membranes the fluid flows in the reverse direction allowing control of fluid flow direction by the choice of membrane used. Additionally further information about the system obtained from conductivity and viscosity measurements before and after 24 hours of forward osmosis demonstrated that in some experiments where no fluid height change is detected, suggesting zero flux, there are in fact changes in conductivity and viscosity which confirm that salt exchange across the membrane is still occurring. Additionally these viscosity and conductivity measurements allow the effects of polymer solution dilution and changing salt concentration to be quantified.

The final experiments in this Chapter, *Section 2.3.8* explored the behaviour of the optimised forward osmosis system (determined in *Sections 2.3.1* and *2.3.2*) with real proteins. It has been found that it is possible to move proteins through a semipermeable porous membrane of an appropriate MWCO using forward osmosis employing high molecular weight polyelectrolyte draw solutions. Additionally these experiments have shown this process can be carried out for several hours without membrane fouling affecting the flux properties of the system

Overall this Chapter provided some fundamental results which were then used to design, develop and fabricate a prototype, membrane-based medical device which was then tested both in an *in vitro* system and in an *ex-vivo* mammalian limb model specifically designed for the project – see **Chapter 5**.

2.5 Future Work

In order to continue the work into forward osmosis processes with ultrafiltration membranes investigated in this chapter, several aspects of this process could be further studied. For example initial work using PEGs to model proteins resulted in membrane fouling causing zero flux. To verify this preliminary work was carried out investigating tagging PEG molecules with a fluorophore in order to identify whether different MW PEGs were able to permeate through the membranes. This approach could also potentially quantify the amount of PEG traversing the membrane. In addition using fluorescently tagged proteins would allow for real-time monitoring and quantification of proteins being transported via forward osmosis, allowing for a clearer understanding of this process. This would also remove the need for the complex assay step simplifying the procedure.

The work carried out in this chapter also identified that, in the context of this project, a better understanding of polyelectrolyte behaviour in solution, particularly with solutions containing mixtures of salts, is required. For example, whilst interactions with NaCl and MgSO₄ were investigated it would also be beneficial to study the interactions between the polyacrylate and mono- and divalent salts from the fourth period such as KCl and CaCl₂ for comparison. Particularly since K⁺ and Ca²⁺ cations are also present in the Krebs solution, which was used as a feed solution to simulate oedema fluid. Additionally, the present work discovered that exchanging potassium ions for sodium ions in the polyelectrolyte salt draw solution significantly altered the flux generated (resulting in a fivefold increase) suggesting such a change may have a major effect on the polyelectrolyte properties. This discovery was only made towards the end of the present project and clearly warrants more extensive investigation.

2.6 Experimental

2.6.1 Materials

All materials were used as supplied unless otherwise stated. The following materials were purchased from Fisher Scientific UK Ltd (Leicestershire, UK); Pierce™ BCA Protein assay kit (containing; Reagent A - bichinchonic acid, Reagent B - 4% (w/v) copper sulfate, 2 mg/mL albumin standard ampules), 96-well flat-bottomed microplates, and micrometre feeler gauges. All membrane disks were obtained from Merk Millipore (Massachusetts, USA). These included; 10 KDa regenerated cellulose UF discs, 30 KDa/50 KDa/100 KDa polyethersulfone UF discs and Ultracel® 100 KDa UF discs. The following polymers were acquired from Poysciences, Inc; 225,000 MW Poly(acrylic acid) sodium salt (20% aqueous solution), 345,000 MW Poly(acrylic acid) (25% aqueous solution) 1,000,000 MW poly(acrylic acid, 1,000,000 MW poly(styrene sulfonic acid) sodium salt. The commercial RO membrane was sourced from a Vontron® Residential Membrane Element (Vontron®, China). All other materials including; bovine serum albumin, calcium chloride, diglyme, dimethylformamide, fibrinogen, glucose, magnesium sulphate, myoglobin from equine skeletal muscle poly(ethylene glycol) - M_n 600, 6,000 and 35,000 , poly(ethylene oxide)- M_v 100,000 and 1,000,000, polysulfone (average M_w 35K by LS, average M_n 16K), 250,000 MW poly(acrylic acid) (35% aqueous solution), 45% 160K M_r poly(vinylpyrrolidone) solution, 6,000K MW poly(acrylic acid) sodium salt, phosphate buffered saline, potassium chloride, potassium phosphate monobasic, sodium azide, sodium chloride, sodium hydrocarbonate and sodium hydroxide were purchased from Sigma Aldrich (Dorset, UK).

2.6.2 Equipment

The following equipment was sourced from Fisher Scientific (Leicestershire, UK); portable conductivity meter, disposable glass test tubes, Eppendorf tubes (0.5, 1.5 and 2 mL), micropipettes (1000 μ L and 200 μ L) and tips. The Amicon® 200 mL and 10 mL stirred cells were obtained from Merck Millipore (Massachusetts, USA). The U-tube was custom built U-Tube using membrane flange and seal from Adams & Chittenden Scientific Glass (CA, USA).

All conductivity measurements were made using a calibrated conductivity meter.

Solution viscosity measurements were carried out using a Schott-Geräte CT-52 auto-viscometer with capillary No.I for the 0.1% (w/v) PEG solutions (stirred overnight to ensure complete dissolution) and capillary No. II (53102, H₂SO₄) for the polyelectrolyte solutions which were 5% (w/v) prior to forward osmosis experiments and of an unknown concentration following FO (see *Section 2.3.7*). In the case of the PEG solutions, the inherent viscosities of the solvents (Krebs solution and deionised water) were also measured. The viscometer was used to measure the absolute viscosity of the samples (mm² s⁻¹) which was then used to calculate the inherent viscosity using **Equation 5** and the absolute viscosity of the appropriate solvent.

$$\eta_{inh} = \left(\frac{\left\{ \ln \frac{t_2}{t_1} \right\}}{c} \right) \quad (5)$$

Where η_{inh} is the inherent viscosity (dL g⁻¹), t_1 and t_2 are the average absolute viscosities (mm² s⁻¹) of the solvent and polymer solution(s) respectively and c is the concentration of the polymer solution (g dL⁻¹). The t values are an average of 5 measurements per sample. In the case of the polyelectrolyte solutions, the absolute viscosities were used as measured.

Absorbance data was collected using either Varian Cary 300 UV-Visible spectrometer or a FLUOstar Omega Microplate Reader. When employing the UV-Vis spectrometer, samples and standards were analysed in quartz cuvettes with a 5.0 mm path length and were baseline corrected with respect to a blank cell with the appropriate solvent. When using the microplate reader, samples and standards were transferred to a clear flat-bottomed 96-well microplate before the absorbance was read at 562 nm. In both cases the samples and standards underwent an assay before the absorbance was read (described in *Section 2.6.3.6*).

2.6.3 Methods

2.6.3.1 Stirred Cell Forward Osmosis Experiments

All stirred cell forward osmosis experiments were carried out using an Amicon® 200 mL stirred cell in which the membrane was placed in the membrane holder facing the feed solution (i.e. active skin layer face down). The cell was then filled with deionised water and pressurised to fill the inlet tube which was then placed in a beaker containing the relevant feed (50 mL) solution (**Figure 2.44**). The deionised water in the stirred cell was then replaced by the draw solution (50 mL) and the draw solution was left to stir for an entire day (6-7 hours). The decrease in volume of the feed solution was measured every hour and in some cases the increase in volume of the draw solution was also monitored. Deionised water was used as a control feed and a model oedema fluid was developed to use in test conditions. To determine the average flux (mL/h) the average of the change in feed volume every hour was calculated.

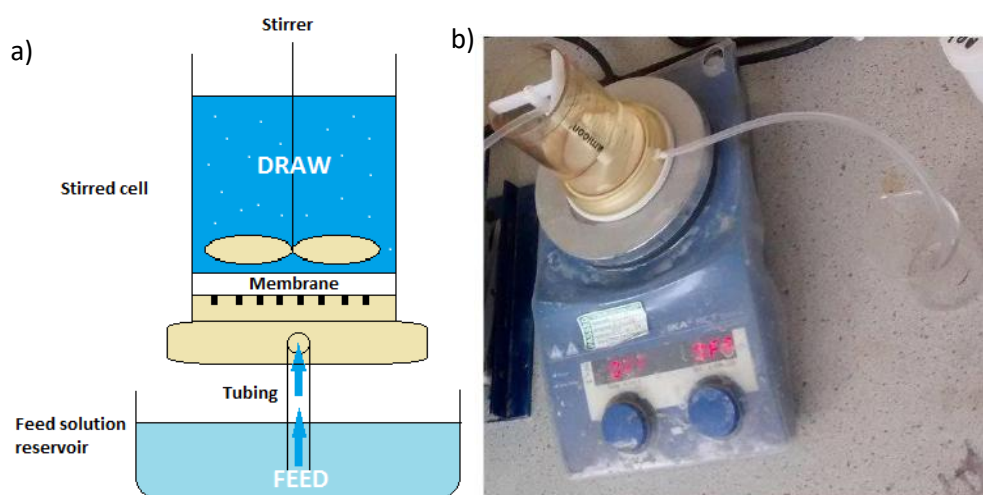


Figure 2.44: a) Schematic showing stirred cell modified for forward osmosis studies and b) experimental set up: stirred cell on stirrer-hotplate connected via silicone tubing to beaker containing feed solution.

Model Oedema Fluid

The model oedema solution was derived from a physiological salt solution (Krebs solution, see below) containing high molecular weight polymers poly(ethylene glycol)/poly(ethylene oxide) (PEG/PEO) to model high molecular weight protein components (i.e. plasma proteins such as serum albumin - MW 67K). For the standard model oedema fluid 100K PEO (2 g/dL) was used although other molecular weight PEGs (6K and 35K) were also used to investigate the effects of MW on membrane

fouling. In later studies the PEO was replaced by proteins; myoglobin at 16,951 KDa, bovine serum albumin (BSA) at 69 KDa and fibrinogen at 340 KDa.

Table 2.9: Krebs Solution composition.³⁶

Component	Concentration (mM)	Mass (g) in 1L
NaCl	118	6.9
KCl	3.4	0.25
CaCl ₂	2.5	1.3 mL
KH ₂ PO ₄	1.2	0.16
MgSO ₄	1.2	0.14
NaHCO ₃	2.5	2.10
Glucose	11.1	2.00

2.6.3.2 Ultrafiltration Membrane Forward Osmosis Studies

Initial studies into forward osmosis processes with ultrafiltration membranes were carried out to investigate potential draw solutions and membrane effects. Seven draw solutions were investigated; four uncharged polymers and three polyelectrolytes (see **Table 2.10**). A control feed solution of deionised water was used during these experiments.

Table 2.10: Draw solutions investigated in preliminary forward osmosis experiments.

		Draw solution
Polymer	1	5% 35K MW PEG
	2	5% 100K MW PEO
	3	1% 1 million MW PEO
	4	5% 160K MW PVP
Poly-electrolyte	5	5% 1 million MW PSSA
	6	5% 225K NaPA
	7	1% 6 million MW NaPA

The membrane was also varied to investigate the effect of the membrane material and molecular weight cut off (MWCO) - a property related to pore size. Five commercially available ultrafiltration membranes with different MWCO were investigated, two regenerated cellulose (10K, 100K) and three polyethersulfone (PES) membranes (30K, 50K and 100K).

2.6.3.3 Ultrafiltration Membrane FO Fouling Studies

Fouling studies involved forward osmosis experiments with feed solutions consisting of Krebs solutions with varying molecular weight PEGs/PEO's all at 2 g/dL to investigate the effects of PEG/PEO MW on fouling. The draw was a 50 mL 5% 225K NaPA solution and the PES membrane MWCO was varied.

2.6.3.4 Ultrafiltration Membrane FO Osmotic Pressure Studies

Osmotic pressure studies involved running forward osmosis experiments with 'feed' solutions of sodium chloride at varying percentages (2%, 5%, 10% and fully saturated – 26%). Again, in combination with a stirred cell, a draw of 50 mL 5% 225K NaPA solution was used and the PES membrane MWCO was varied. For U-tube experiments the draw and feed solution volumes were 100 mL. The change in fluid height was recorded hourly and an additional measurement was made after 24 hours where possible, providing the fluid height did not exceed that of the U-Tube.

2.6.3.5 Reverse Osmosis vs. Ultrafiltration Membranes

Forward osmosis experiments were carried out comparing reverse osmosis membranes with ultrafiltration membranes to investigate the effects of membrane structure on the forward osmosis process. As above for stirred cell experiments, a draw solution 50 mL 5% 225K NaPA was used. The membranes used were a RO membrane obtained from a domestic RO module and a 50K PES UF membrane. For U-Tube experiments the draw and feed solution volumes were 100 mL. The membrane was clamped in the membrane holder and the feed solution was placed in the U-Tube chamber in contact with the membrane surface whilst the draw solution was placed in the remaining U-tube chamber. Both fluid heights were made level and the change in fluid height was recorded hourly and an additional measurement was made after 24 hours where possible (i.e. where fluid height did not surpass U-tube).

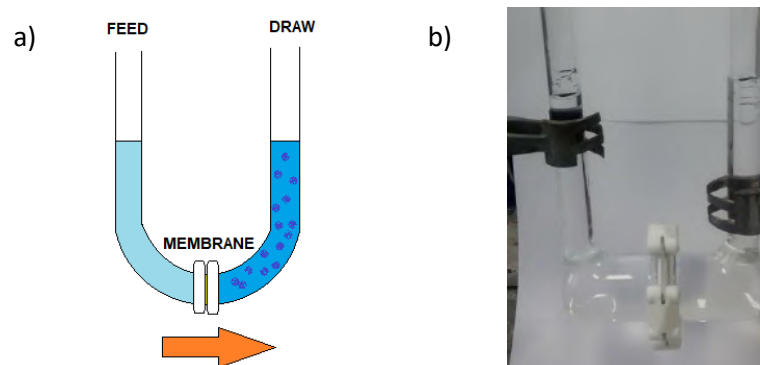


Figure 2.45: a) schematic of U-tube and b) membrane holder and fluid chambers in custom-built U-tube.

2.6.3.6 Protein Studies

Forward osmosis experiments were performed using the modified stirred cell as described previously with 5% 225K NaPA draw solution and either a 50K or 100K membrane face down in the stirred cell with a 2% protein (BSA or fibrinogen) in PBS solution feed (or plasma). Every hour 500 μL aliquots were taken and the sample volume was replaced by an equivalent volume of the draw solution. Furthermore a sample was taken the following morning after stirring overnight.

Following this a bicinchoninic (BCA) Assay was performed in order to determine the protein concentration in the samples. The absorbance of the draw solution was also measured to ensure no interference with the results.

Bicinchoninic Acid Assay

The resulting supernatant was analysed using the BCA assay (bicinchoninic acid assay) to determine the protein concentration present in each sample with respect to a standard curve of BSA solutions of known concentrations. The calculated concentration of the unknown samples was then extrapolated to estimate the protein concentration per unit membrane area.

A standard curve was prepared using a 2 mg/mL stock solution of BSA with dilutions ranging from 2000-25 $\mu\text{g}/\text{mL}$ (**Table 2.11**). The diluent was PBS.

Table 2.11: Preparation of standard BSA solutions for standard curve

Solution No.	Final BSA Concentration ($\mu\text{g}/\text{mL}$)	Volume of Diluent (μL)	Volume and source of BSA (μL)	Final Volume (μL)
A	2000	0	300 (stock)	300
B	1500	125	375 (stock)	325
C	1000	325	325 (stock)	325
D	750	175	175 (vial B dilution)	350
E	500	325	325 (vial C dilution)	325
F	250	325	325 (vial E dilution)	325
G	125	325	325 (vial F dilution)	550
H	25	400	100 (vial G dilution)	500
I	0	400	0	400

The BCA standard working reagent was prepared by combining the BCA reagent (component A) with 4% (w/v) CuSO_4 (component B) in a ratio of 50:1.

Standards and samples were vortexed before 25 μL of each added to a clear, flat-bottomed 96-well microplate in triplicate. Following this 200 μL of the BCA standard

working reagent was added in a randomised pattern to each well containing a sample or standard. The microplate was incubated for 37 °C for 30 minutes before measuring the absorbance at 562nm in a FLUOstar Omega Microplate Reader

For the myoglobin studies due to the proteins inherent colour no assay was required to provide a measurable colour change. Instead a standard curve was prepared using solutions of myoglobin of known concentrations (**Table 2.12**). Standards and samples were vortexed before 25 µL of each added to a clear, flat-bottomed 96-well microplate in triplicate following which; the absorbance was measured at 409 nm in a FLUOstar Omega Microplate Reader.

Table 2.12: Preparation of standard myoglobin solutions for standard curve

Solution No.	Final Myoglobin Concentration (mg/mL)	Volume of Diluent (µL)	Volume and source of Myoglobin (µL)	Final Volume (µL)
A	1	0	500 (stock)	300
B	0.5	250	250 (vial A dilution)	500
C	0.2	400	100 (vial A dilution)	500
D	0.1	450	50 (vial A dilution)	500
E	0.05	475	25 (vial A dilution)	500
F	0	300	300	300

2.6.3.7 Commercial Ultrafiltration Membranes

Commercial ultrafiltration membranes were obtained from Merck Millipore. The membranes were used as standards to investigate potential draw solutions. The PES-50K membrane was also used as a solid support for composite nanofiltration membranes through in-situ interfacial polymerisation on the surface (see **Chapter 3**).

Table 2.13: Commercial Membrane Materials and MWCO, deionised water (mL/h) at 1 bar.

Composition	MWCO	Deionised water flux (mL/h) at 1 bar pressure
Regenerated Cellulose	10K	180
Polyethersulfone	30K	236
Polyethersulfone	50K	336
Polyethersulfone	100K	2088
Regenerated Cellulose	100K	456

2.7 References

1. G. M. Geise, H.-S. Lee, D. J. Miller, B. D. Freeman, J. E. McGrath, and D. R. Paul, *J. Polym. Sci.*, 2010, **48**, 1685–1718.
2. T. Cath, A. Childress, and M. Elimelech, *J. Membr. Sci.*, 2006, **281**, 70–87.
3. T. S. Chung, X. Li, R. C. Ong, Q. Ge, H. Wang, and G. Han, *Curr. Opin. Chem. Eng.*, 2012, **1**, 246–257.
4. C. B. Herbert and M. N. Blaine, US Pat. 8211 053 B2 (2012) to Equilibrate, LLC.
5. S. G. Rockson, *Am. J. Med.*, 2001, **110**, 288–295.
6. W. L. Olszewski, S. Jamal, B. Lukomska, G. Manokaran, and G. I., *Lymphology*, 1992, **25**, 166–171.
7. V. Kumar, A. K. Abbas, N. Fausto, and J. C. Aster, in *Robbins and Cotran Pathologic Basis of Disease*, Saunders Elsevier, Philadelphia, 7th edn., 2009.
8. H. Yang, Q. Zheng, and R. Cheng, *Colloids Surfaces A Physicochem. Eng. Asp.*, 2012, **407**, 1–8.
9. J. M. Carrillo and A. Dobrynin, *Polymers (Basel)*, 1992, 1897–1913.
10. A. V. Dobrynin and M. Rubinstein, *Prog. Polym. Sci.*, 2005, **30**, 1049–1118.
11. J. L. Barrat, *Adv. Chem. Phys. Polym. Syst.*, 1996, 1–66.
12. G. Maurer, S. Lammertz, and L. Ninni Scafer, *Adv. Polym. Sci.*, 2011, 67–136.
13. R. Chang, Y. Kim, and A. Yethiraj, *Macromolecules*, 2015, **48**, 7370–7377.
14. D. Stigter, *Biophys. J.*, 1995, **69**, 380–388.
15. H. P. Hsu and E. Lee, *Electrochem. commun.*, 2012, **15**, 59–62.
16. R. Schweins and K. Huber, *Eur. Phys. J. E*, 2001, **5**, 117–126.
17. R. R. Netz and D. Andelman, *Phys. Rep.*, 2003, **380**, 1–95.
18. T. Kitano, A. Taguchi, I. Noda, and M. Nagasawa, *Macromolecules*, 1980, **13**, 57–63.
19. R. J. Young and P. A. Lovell, Eds., in *Introduction to Polymers*, Taylor & Francis, 3rd edn., 2011, pp. 237–268.
20. I. Pochard, P. Couchot, C. Geffroy, A. Foissy, and J. Persello, *Rev. L'Institut Fr. Du Pet.*, 1997, **52**, 251–253.
21. K. Huber, *J. Phys. Chem.*, 1993, **97**, 9825–9830.

22. M. J. Stevens and S. J. Plimpton, *Eur. Phys. J. B - Condens. Matter Complex Syst.*, 1998, **2**, 341–345.
23. J. Shao, S. Qin, J. Davidson, W. Li, Y. He, and H. S. Zhou, *J. Hazard. Mater.*, 2013, **244–245**, 472–477.
24. H. Jellinek and M. Luh, *J. Polym. Sci.*, 1969, **7**, 172–177.
25. R. R. Navarro, S. Wada, and K. Tatsumi, *J. Hazard. Mater.*, 2005, **123**, 203–209.
26. P. Atkins, T. Overton, J. Rourke, M. Weller, and F. Armstrong, in *Shriver and Atkins Inorganic Chemistry*, Oxford University Press, 5th edn., 2009, pp. 3–33.
27. Q. Ge, M. Ling, and T.-S. Chung, *J. Membr. Sci.*, 2013, **442**, 225–237.
28. F. C. Andrews, *Science*, 1976, **194**, 567–571.
29. S. Zhao, L. Zou, C. Y. Tang, and D. Mulcahy, *J. Membr. Sci.*, 2012, **396**, 1–21.
30. D. C. Boris and R. H. Colby, *Macromolecules*, 1998, **31**, 5746–5755.
31. H. Schiessel and P. Pincus, *Macromolecules*, 1998, **31**, 7953–7959.
32. A. J. Konop and R. H. Colby, *Macromolecules*, 1999, **32**, 2803–2805.
33. Thermo Scientific Applications Note, Pierce™ BCA Protein Assay Kit Instructions , 2013, 1–7.
34. P. Thevenot, W. Hu, and L. Tnag, *Curr. Top. Med. Chem.*, 2011, **8**, 270–280.
35. P. Roach, D. Farrar, and C. C. Perry, *J. Am. Chem. Soc.*, 2005, **127**, 8168–8173.
36. M. J. Gardener, C. D. Glen, G. R. Richards, P. M. Vanhoutte, G. Edwards, M. Fe, and A. H. Weston, *Br. J. Pharmacol.*, 2001, **133**, 1145–1153.

Chapter 3 – Poly-ylid Membranes by Interfacial Polycondensation

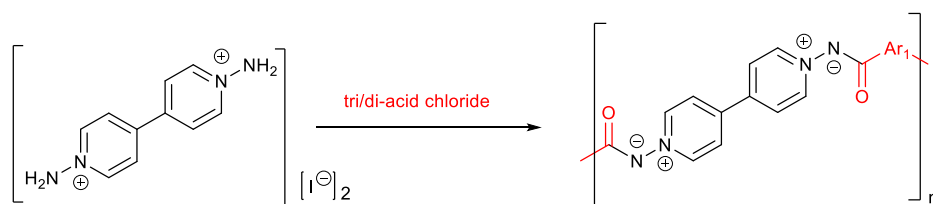
3.1 Abstract

Novel hydrophilic poly-ylids derived from interfacial polycondensation of the 1,1'-diamino-4,4'-bipyridinium ion with aromatic di-sulfonyl chlorides and di-isocyanates were synthesised, characterised and their thin film composite membrane-forming properties analysed. A number of previously reported acid chloride based poly-ylids were also synthesised characterised and used to create thin film composite nanofiltration membranes for comparison. Studies of membrane performance, pH effects and biocompatibility of the new membranes were carried out, as well as more conventional membrane characterisation studies of pure water flux, salt rejection and surface morphology.

3.2 Introduction

Interfacial polycondensation is the most widely used technique to fabricate thin-film composite (TFC) membranes.¹ A highly successful system was developed by Cadotte *et al.*² in 1978 and was based on the interfacial reaction between *m*-phenylenediamine (MPD) and trimesoyl chloride (TMC) and this system is still the most commonly used.³ However, other aromatic diamines have also been explored such as *p*-phenylenediamine as well as some non-aromatic diamines as reviewed by Lau *et al.*^{4,5}

In 1995 a novel heterocyclic diamine was proposed: the 1,1'-diamino-4,4'-bipyridinium cation which was found to produce bright yellow polymers on reaction with aromatic tri and di-substituted acid chlorides.⁶ These hydrophilic polymers had unusual N⁺-N⁻ ylid linkages adjacent to the N-C bonds formed between the amine and the acid chloride (**Scheme 3.1**). Several different diacid chloride monomers were investigated including species with one aromatic ring such as: trimesoyl chloride (1,3,5-benzenetricarbonyl trichloride), isophthaloyl chloride (1,3-benzenedicarbonyl dichloride) and terephthaloyl chloride (1,4-benzenedicarbonyl dichloride) and systems with two aromatic rings: 4,4'-oxydibenzoyl chloride and naphthalene-2,3-dicarbonyl dichloride.



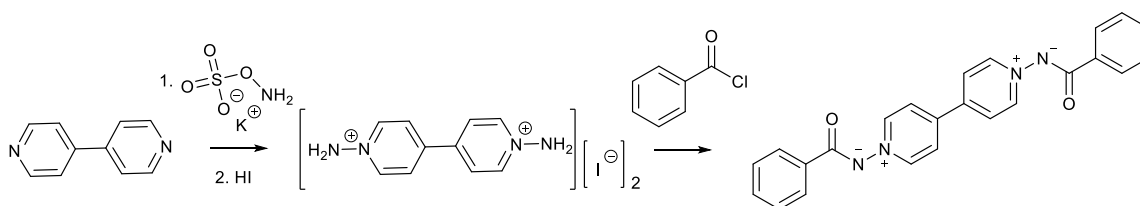
Scheme 3.1: 1,1'-diamino-4,4'-bipyridinium di-iodide salt and poly-ylid formed after polycondensation with tri/di-acid chloride.

Figure 3.1 shows the formation of the poly-ylid shown in **Scheme 3.1** via a stirred interfacial polycondensation reaction between the 1,1'-diamino-4,4'-bipyridinium di-iodide (in aqueous solution) and the trimesoyl chloride (in hexane). The yellow polymer forms at the interface between the two solutions. This acyl poly-ylid was then used to make thin film composite nanofiltration membranes via *in situ* polycondensation on the surface of a polyethersulfone (PES) ultrafiltration membrane. These membranes were found to have reasonable flux and salt rejection properties. Morphological analysis using scanning electron microscopy (SEM) revealed a highly nodular structure.



Figure 3.1: Stirred interfacial polycondensation of TMC in hexane with 1,1'-diamino-4,4'-bipyridinium di-iodide in aqueous solution.

The diamine salt is synthesised following a method reported by Downes where O-hydroxylamine sulfonic acid salt reacts with 4,4'-bipyridine followed by acidification with hydriodic acid (**Scheme 3.2**).⁷ Downes also reported the conversion of the di-iodide salt to an ylid by reaction with benzoyl chloride under Schotten-Baumann conditions.



Scheme 3.2: Synthesis of 1,1'-diamino-4,4'-bipyridinium di-iodide salt and subsequent ylid formation on reaction with benzoyl chloride.

In the present thesis, it was proposed that other monomers could be investigated as alternatives to acid chlorides to create new classes of poly-ylids based on sulfonyl chlorides and isocyanates. Additionally several of the previously reported acid chloride poly-ylids were synthesised for comparative studies (**Figure 3.2**). These include the poly-ylids based on the trimesoyl chloride (**3.1**), isophthaloyl chloride (**3.2**) and terephthaloyl chloride (**3.3**). The membrane forming properties and membrane

characteristics of these poly-ylids were also investigated. Membranes made using poly-ylids from acyl chlorides **3.2** and **3.3** were not previously reported.

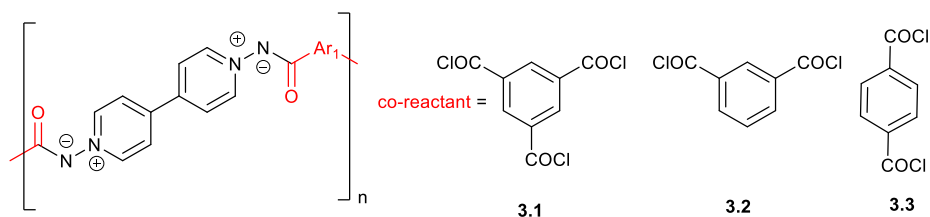


Figure 3.2: Generic structure of acid chloride based poly-ylids (acyl poly-ylids) and investigated monomers **3.1**, **3.2** and **3.3**.

Figure 3.3 shows the novel monomers which included three sulfonyl chlorides: benzene-1,3-disulfonyl dichloride (**3.4**), biphenyl-4,4'-disulfonyl chloride (**3.5**) and 4,4'-oxybis(benzenesulfonyl chloride) (**3.6**) and two isocyanates; methylene diphenyl diisocyanate (**3.7**) and 1,1'-oxybis(4-isocyanatobenzene) (**3.8**).

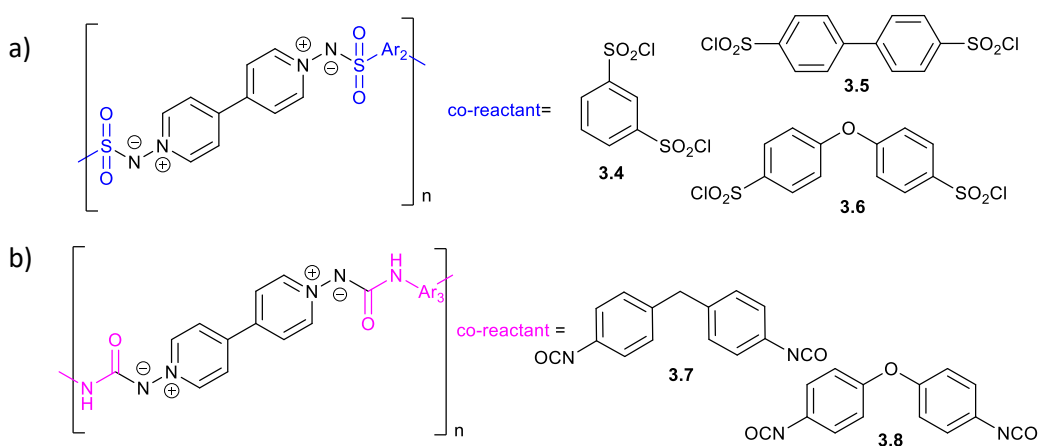


Figure 3.3: Generic structure of a) sulfonyl poly-ylids with co-reactant monomer structures: **3.4**, **3.5** and **3.6** and b) carbamoyl poly-ylids with co-reactant monomer structures: **3.7** and **3.8**.

3.3 Results and Discussion

3.3.1 Synthesis of 1,1'-Diamino-4,4'-bipyridinium di-iodide

The synthesis of 1,1'-diamino-4,4'-bipyridinium di-iodide monomer was carried out using the method reported by Downes (see Section 3.6.3.1).⁷ Analysis of the product by IR spectroscopy confirmed the formation of the diamine di-iodide salt product when compared to the spectrum of the starting material, 4,4'-bipyridine (**Figure 3.4**). Comparing the starting material and product spectra the latter contains a broad NH₂ absorbance at 3300 cm⁻¹ with two bands signifying the presence of a primary amine consistent with the two amine groups present in the diamino-bipyridinium salt product.

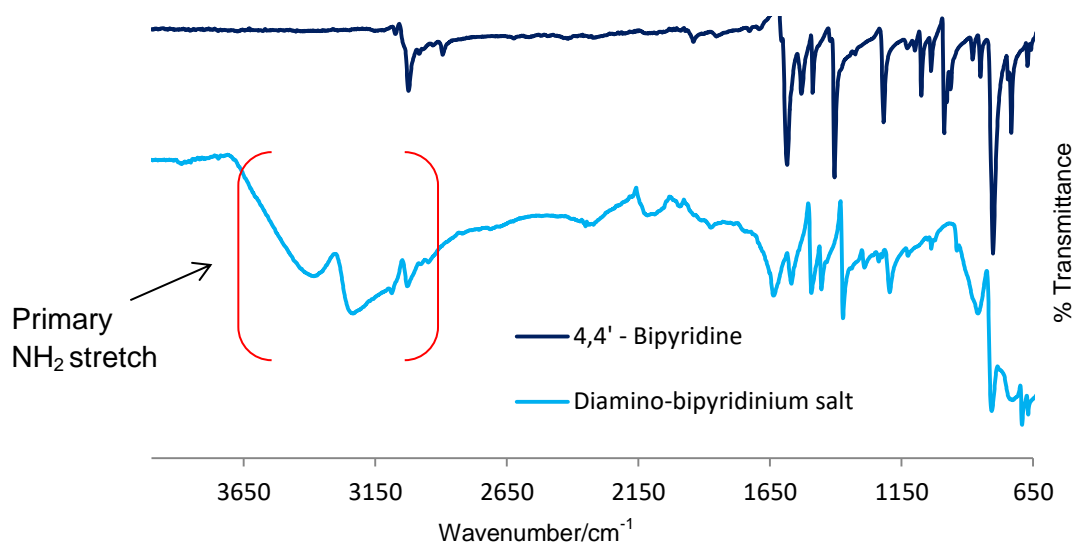


Figure 3.4: IR spectra of 4, 4'-bipyridine starting material and 1, 1'-diamino-4,4'-bipyridinium di-iodide.

Additionally NMR spectroscopy confirmed the formation of the product by providing evidence for the addition of the amine groups to the pyridine nitrogen in the form of a singlet resonance at 8.81 ppm equivalent to the four amino protons which was not evident in the spectrum of 4, 4'-bipyridine. **Figure 3.5** below shows the ^1H NMR spectra of both the starting material and product.

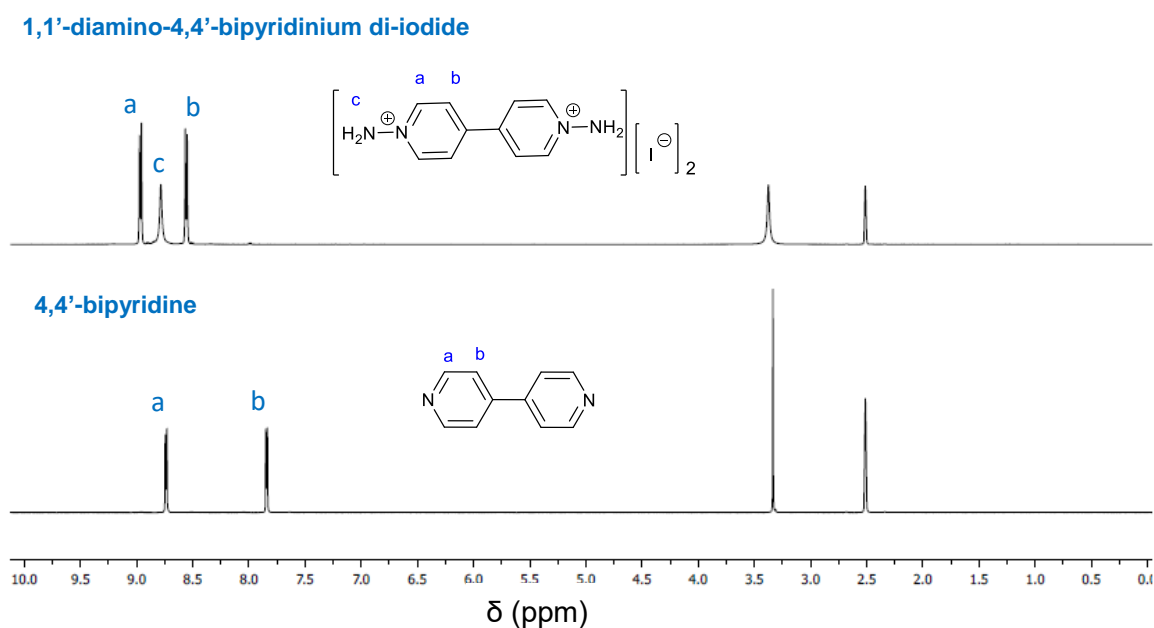


Figure 3.5: ^1H NMR spectra of 4,4'-bipyridine starting material and 1,1'-diamino-4,4'-bipyridinium di-iodide ($\text{DMSO}-d_6$).

3.3.2 Poly-ylid Synthesis

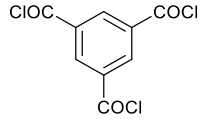
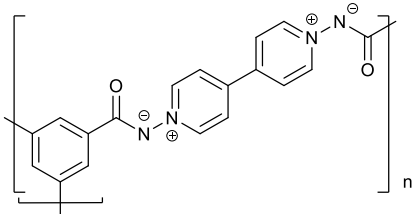
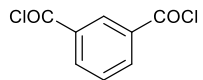
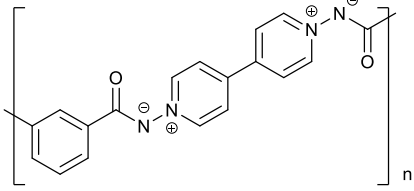
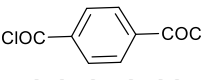
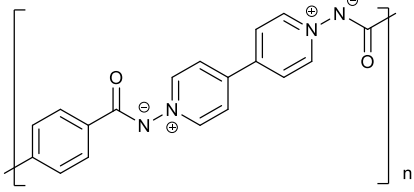
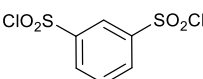
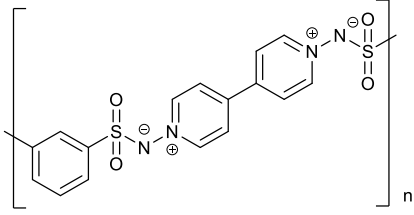
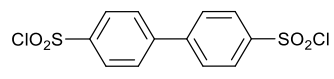
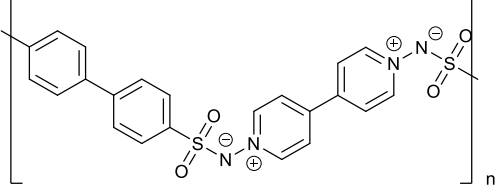
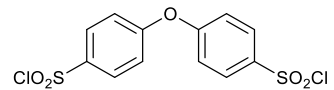
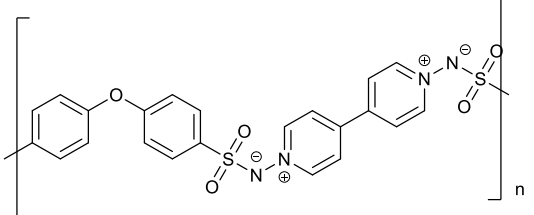
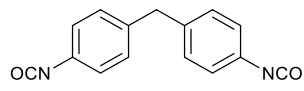
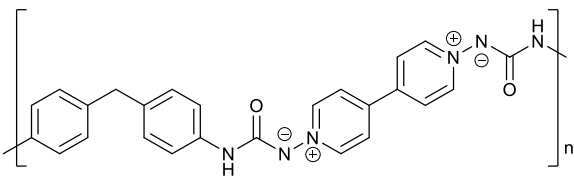
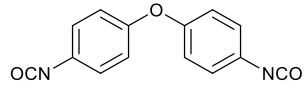
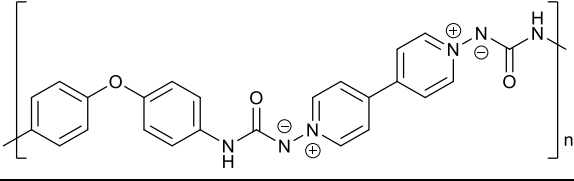
The synthesis of the 1,1'-diamino-4,4'-bipyridinium di-iodide monomer was carried out using the method reported by Downes (see Section 3.6.3.1).⁷ The acid chloride, sulfonyl chloride and isocyanate monomers were used as purchased. The poly-ylids were synthesised by a stirred interfacial polymerisation reaction in which the diamine (1% w/v) in 0.08 M aqueous sodium hydroxide solution was mixed with a 0.1% w/v solution of the acid chloride/sulfonyl chloride/isocyanate in hexane. Exceptions were sulfonyl chlorides **3.5** and **3.6** and isocyanate **3.8**, which proved insoluble in hexane and were instead dissolved in chloroform. The reactant solutions were mixed and stirred rapidly resulting in a polycondensation reaction to produce the polymer product which was then filtered, washed and dried before characterisation. The three different classes of starting material produced polymers of different colours with the acid chlorides producing bright yellow polymers, the sulfonyl chlorides affording yellow-brown polymers and the isocyanates generating red-brown polymers (see **Figure 3.6**).



Figure 3.6: Poly-ylid samples demonstrating the different colours associated with the three different classes of poly-ylid. Acid chloride based polymers **3.1**, **3.2** and **3.3** are yellow while sulfonyl chloride based polymers **3.4**, **3.5** and **3.6** are brown and isocyanate based polymers **3.7** and **3.8** are red.

Table 3.1 shows the structures of the acid chloride/sulfonyl chloride/isocyanate monomers and the poly-ylids produced following stirred interfacial polycondensation with the 1,1'-diamino-4,4'-bipyridinium di-iodide.

Table 3.1: Acid chloride, sulfonyl chloride and isocyanate monomers and their corresponding poly-ylids.

	Monomer	Poly-ylid
3.1	 <p>Trimesoyl chloride</p>	
3.2	 <p>Isophthaloyl chloride</p>	
3.3	 <p>Terephthaloyl chloride</p>	
3.4	 <p>Benzene-1,3-disulfonyl chloride</p>	
3.5	 <p>biphenyl-4,4'-disulfonyl chloride</p>	
3.6	 <p>4,4'-oxybis(benzene sulfonyl chloride)</p>	
3.7	 <p>4,4'-methylenebis(phenylisocyanate)</p>	
3.8	 <p>4,4'-oxybis(phenyl isocyanate)</p>	

3.3.3 Poly-ylid Characterisation

The poly-ylids were characterised using the following analytical techniques; IR, ^1H NMR and ^{13}C NMR spectroscopy, solution viscosity measurements and thermal analysis (TGA and DSC). The results are discussed below.

3.3.3.1 Infrared Spectroscopy

The IR spectra provided evidence for successful formation of the polymers. For example, when investigating the acyl poly-ylids **3.1**, **3.2** and **3.3** the polymer IR spectra (**Figure 3.7**) did not show any evidence of absorbances at 1815-1785 cm^{-1} which are associated with an acid chloride $\nu(\text{C}=\text{O})$ stretch. Instead all three acyl poly-ylids showed a $\nu(\text{C}=\text{O})$ absorbance at a lower wavenumber closer to the expected range for a secondary amide carbonyl stretching absorbances (i.e. 1680-1640 cm^{-1}).

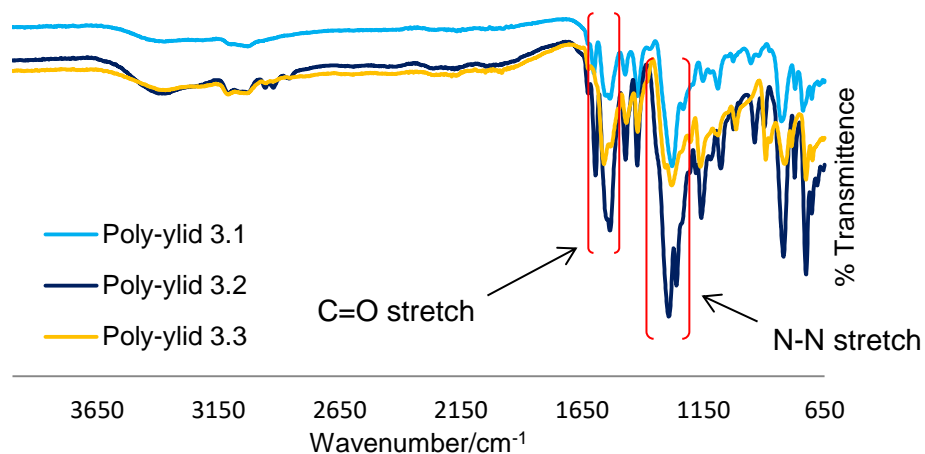


Figure 3.7: IR spectra of the three acyl poly-ylids **3.1**, **3.1** and **3.3**.

Using poly-ylid **3.1** as an example, the $\nu(\text{C}=\text{O})$ absorbance appears at 1602 cm^{-1} , significantly lower than both the acid chloride carbonyl starting material and the expected secondary amide carbonyl absorbance. The shift to a lower wavenumber relative to the starting material acid chloride carbonyl is due to delocalisation of electron density from the adjacent anionic nitrogen (**Figure 3.8**) which lengthens and weakens the $\text{C}=\text{O}$ bond unlike the chloride substituent which is a poor lone pair electron donor due to poor p -orbital overlap (i.e. the $3p$ orbital in chlorine atom is larger than $2p$ orbital in carbon). The acid chloride carbonyl stretching frequencies are instead dominated by inductive effects due to the strongly electron withdrawing electronegative chlorine which results in carbonyl bond shortening and strengthening (i.e. higher wavenumber value).⁸ Additionally, the ylid carbonyl stretching frequencies are even lower than expected because the “amide” nitrogen is deprotonated and therefore negatively charged. Although this negative charge is stabilised by the

adjacent positively charged nitrogen in the aromatic ring the negative charge can also delocalise onto the more electronegative oxygen of the carbonyl bond. Since this second resonance form is more favoured the C=O bond is further weakened when compared to a neutral amide.

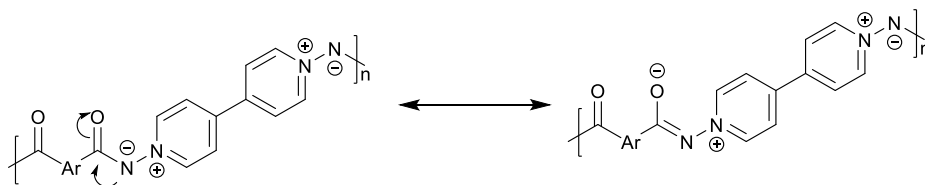


Figure 3.8: Resonance effects on C=O bond arising from conjugation with adjacent amide nitrogen, lengthening and weakening C=O bond resulting in absorbance at a lower frequency.

Furthermore the acyl poly-ylid IR spectra exhibited strong $\nu(\text{N-N})$ stretching absorbances at ca. 1280 cm^{-1} . The remaining acyl poly-ylids absorbances are summarised in **Table 3.2**.

Table 3.2: Acyl poly-ylid IR absorbances

Poly-ylid	$\nu(\text{C=O})/\text{cm}^{-1}$	$\nu(\text{N-N})/\text{cm}^{-1}$
3.1	1602	1279
3.2	1594	1293
3.3	1559	1280

The sulfonyl poly-ylids (**3.4**, **3.5** and **3.6**) showed no evidence of the strong sulfonyl chloride $\nu(\text{S=O})$ stretching absorbances, expected at $1410\text{-}1370\text{ cm}^{-1}$ and $1204\text{-}1177\text{ cm}^{-1}$, in their IR spectra (**Figure 3.9**).

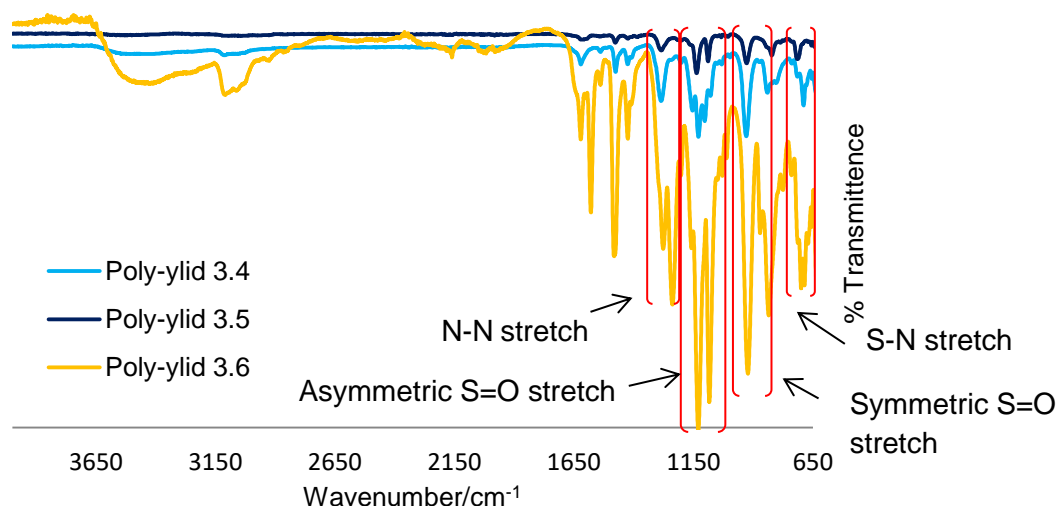


Figure 3.9: IR spectra of the three sulfonyl poly-ylids **3.4**, **3.5** and **3.6**.

Instead the $\nu(\text{S=O})$ absorbance had shifted to a lower wavenumber which is associated with the formation of a sulfonamide bond. Again this shift to a lower

wavenumber is a result of resonance which lengthens and weakens the S=O bond causing it to absorb at a lower frequency (**Figure 3.10**).

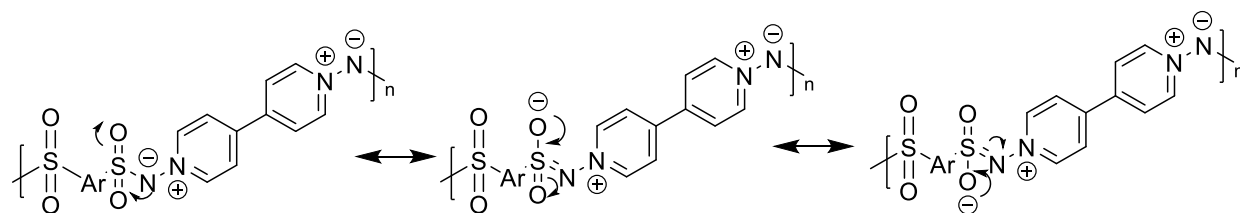


Figure 3.10: Resonance effects on S=O bond arising from conjugation with adjacent nitrogen, lengthening and weakening S=O bond resulting in absorption at a lower frequency.

Sulfonamides typically exhibit multiple S=O stretching frequencies which generally fall between 1225-980 cm^{-1} and often appear as two bands: one for asymmetric S=O stretching between 1420-1300 cm^{-1} and the other corresponding to the symmetric S=O stretch between 1200-1000 cm^{-1} . Using poly-ylid **3.4** as an example, the spectrum of the benzene-1,3-disulfonyl dichloride monomer exhibited characteristic $\nu(\text{S=O})$ sulfonyl chloride absorbances at 1370 cm^{-1} and 1159 cm^{-1} which have shifted to lower wavenumbers in the poly-ylid product spectrum. Poly-ylid **3.4** instead has S=O stretching absorbances at 1131 cm^{-1} and 932 cm^{-1} which are both within the expected range of the sulfonamide $\nu(\text{S=O})$ stretches. The values obtained fall at the lower end of the range due to the negative charge on the sulfonamide nitrogen favouring resonance forms where the charge is delocalised to the more electronegative oxygen. Additionally all three sulfonyl poly-ylids exhibited an $\nu(\text{N-N})$ stretch between 1200-1300 cm^{-1} and an S-N stretch which appears at ca.700 cm^{-1} . These absorbances along with those for the remaining sulfonyl poly-ylids (**3.5** and **3.6**) are summarised in **Table 3.3**.

Table 3.3: Sulfonyl poly-ylid IR absorbances

Poly-ylid	$\nu(\text{N-N})/\text{cm}^{-1}$	Asymmetric $\nu(\text{S=O})/\text{cm}^{-1}$	Symmetric $\nu(\text{S=O})/\text{cm}^{-1}$	$\nu(\text{S-N})/\text{cm}^{-1}$
3.4	1285	1131	932	690
3.5	1284	1140	932	720
3.6	1243	1133	925	701

In the IR spectra of the carbamoyl poly-ylids (**Figure 3.11**), there is no evidence of the isocyanate bonds present in the starting materials, i.e. there is no $\nu(\text{N=C=O})$ absorbance at 2275-2250 cm^{-1} . Instead, evidence for a urea bond can be seen with a $\nu(\text{N-H})$ absorbance present at around 3400 cm^{-1} for both poly-ylids and $\nu(\text{C=O})$ absorbance, within the expected range for a urea carbonyl which is between 1675-1590 cm^{-1} , also present for both poly-ylids (**Table 3.4**).

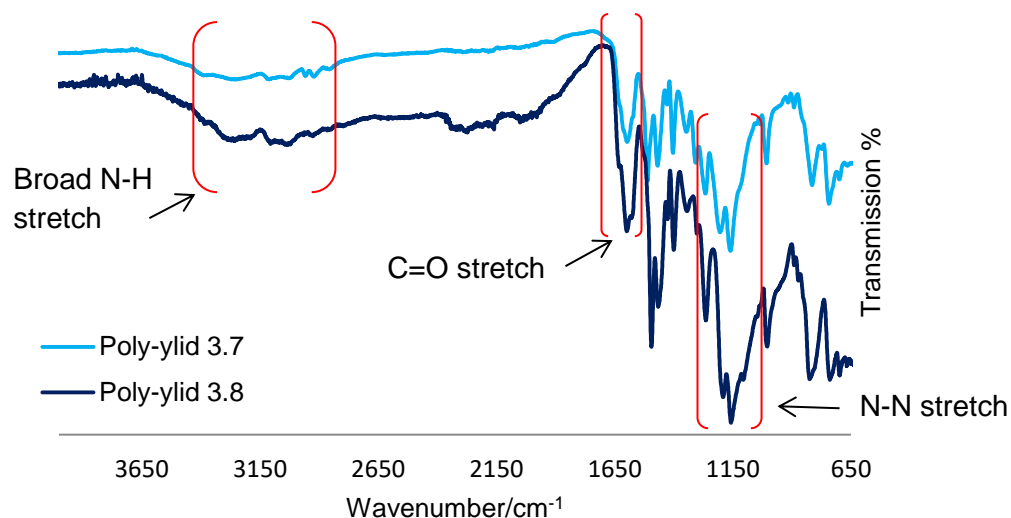


Figure 3.11: IR spectra of the two carbamoyl poly-ylids **3.7** and **3.8**

For both carbamoyl poly-ylids the urea carbonyl absorbance values are slightly lower than might be expected for a neutral urea carbonyl. This is due to delocalisation of the negative charge this time across both the carbonyl oxygen and the second nitrogen again weakening the carbonyl bond (**Figure 3.12**).

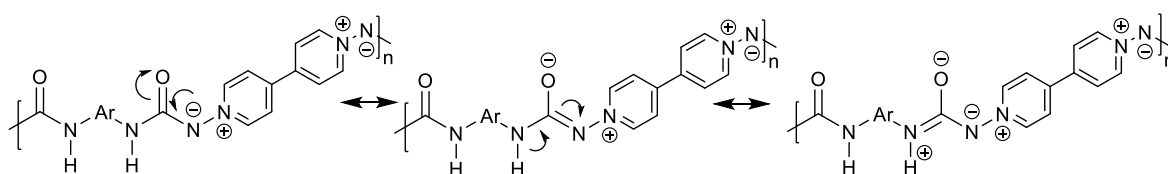


Figure 3.12: Resonance effects on the C=O bond arising from conjugation with adjacent nitrogen atoms, lengthening and weakening the C=O bond, resulting in IR adsorption at a lower frequency.

Additionally both poly-ylids demonstrated the presence of $\nu(\text{N-N})$ stretch at 1159 cm^{-1} and 1162 cm^{-1} for poly-ylids **3.7** and **3.8**, respectively. The remainder of the carbamoyl poly-ylid resonances are summarised in **Table 3.4**.

Table 3.4: Carbamoyl poly-ylid IR absorbances

Poly-ylids	$\nu(\text{N-H})/\text{cm}^{-1}$	$\nu(\text{C=O})/\text{cm}^{-1}$	$\nu(\text{N-N})/\text{cm}^{-1}$
3.7	3390	1596	1159
3.8	3303	1604	1162

In several of the poly-ylid IR spectra broad $\nu(\text{OH})$ absorptions were observed at ca. 3400 cm^{-1} which suggests the presence of solvating water molecules. These broad absorptions may also arise from the additional N-H present in the urea type bond formed in the isocyanate based poly-ylid.

3.3.3.2 ^1H Nuclear Magnetic Resonance Spectroscopy

^1H NMR spectroscopic analysis confirmed formation of the poly-ylids. As each polymer contained the same bipyridinium diamine residue resonances derived from this structure were present in each sample (H_a and H_b , **Figure 3.13**) with additional resonances arising from the acyl, sulfonyl or carbamoyl unit.

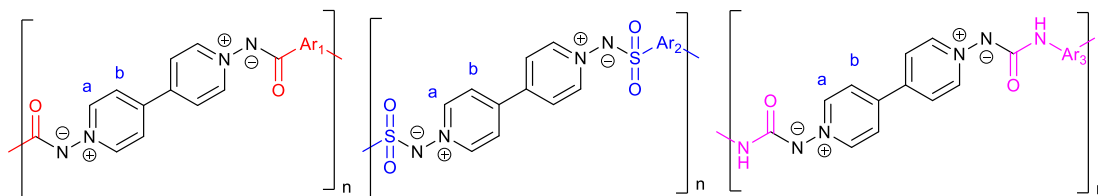


Figure 3.13: Generic structures of poly-ylids containing bipyridine-diamine residue

Comparing the bipyridinium proton resonances in each of the poly-ylids demonstrates some trends as illustrated in **Table 3.5**. The lowest-field resonances were produced by acid chloride based poly-ylid **3.2** at 10.74 ppm for H_a and 9.52 ppm for H_b whilst the other acyl poly-ylid (**3.3**) had bipyridinium proton resonances with a more similar shift to those present in the poly-ylids. The carbamoyl poly-ylids produced slightly higher H_a chemical shifts compared to the sulfonyl poly-ylids whilst the carbamoyl H_b shifts were closer in ppm to the sulfonyl H_b shifts.

Table 3.5: Bipyridinium proton resonances (ppm)

	Poly-ylid	H_a	H_b	
Acyl	3.2	10.74	9.52	
	3.3	9.98	9.44	
Sulfonyl	3.4	9.66	9.21	
	3.5	9.63	9.27	
	3.6	9.64	9.25	
Carbamoyl	3.7	9.77	9.17	
	3.8	9.88	9.29	

Assigning acyl poly-ylid **3.2** (**Figure 3.14**); alongside the two 4H resonances associated with the bipyridinium moiety, labelled H_a and H_b (10.07 ppm and 9.63 ppm, respectively), are the three proton resonances associated with the isophthaloyl chloride residue. The most de-shielded proton resonance on the acid chloride derived ring corresponds to the single proton *ortho* to both carbonyl substituents labelled H_c which is assigned as the 1H singlet at 9.63 ppm. The other single proton resonance at 8.66 ppm therefore must correspond to proton H_e which would be expected to be a triplet, but poor resolution makes this impossible to observe. The remaining two proton resonance at 9.21 ppm therefore corresponds to the H_d protons.

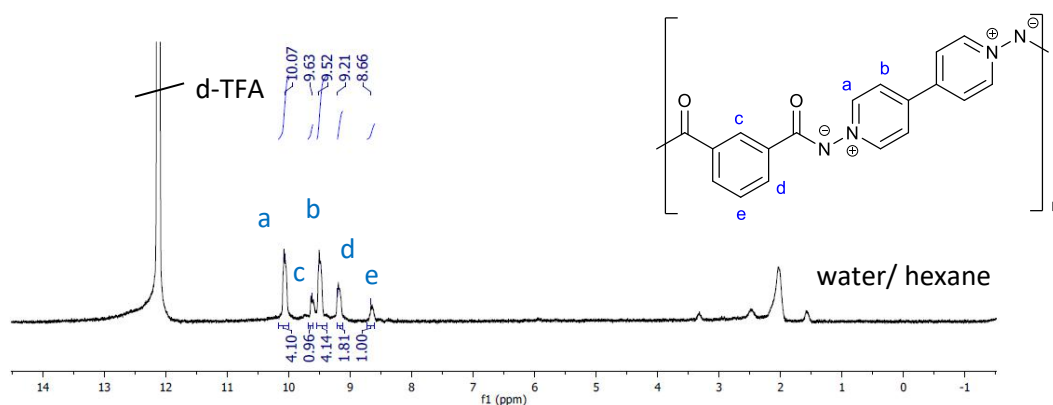


Figure 3.14: ¹H NMR spectra of acyl poly-ylid **3.2** in *d*-TFA.

Assigning the ¹H NMR spectrum of sulfonyl poly-ylid **3.4** (**Figure 3.15**); the two bipyridinium 4H proton resonances are the most deshielded and therefore the furthest down field at 9.66 ppm (H_a) and 9.21 ppm (H_b). Of the remaining three proton resonances, the most deshielded is H_c *ortho* to both sulfonamide substituents (expected to be a singlet), however, this resonance is overlapping with the resonance for the pair of H_d protons (expected to be a doublet) producing a 3H multiplet at ca. 8.94 ppm. The remaining resonance is assigned to H_e the furthest upfield at 8.63 ppm.

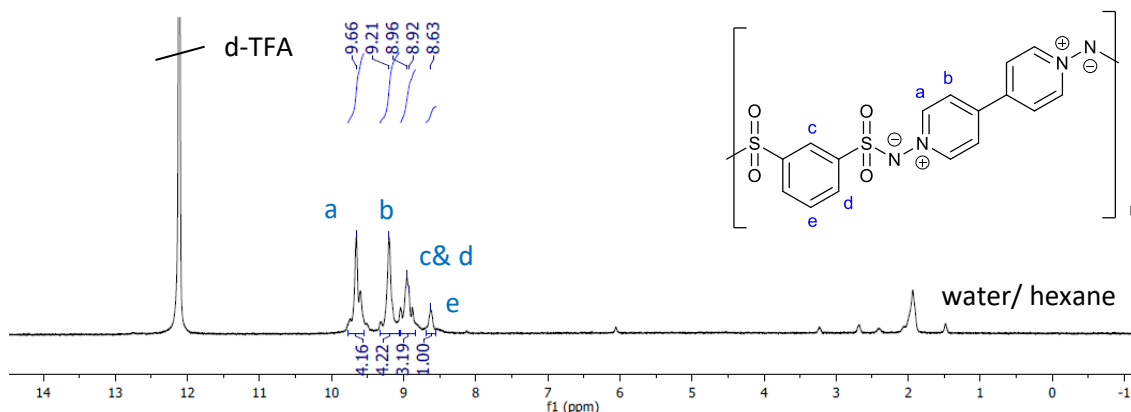


Figure 3.15: ¹H NMR spectra of sulfonyl poly-ylid **3.4** in *d*-TFA.

Assigning the ^1H NMR spectrum of carbamoyl poly-ylid **3.8** (**Figure 3.16**): alongside the bipyridylium resonances at 9.88 ppm and 9.29 ppm there are resonances at 8.07 ppm and 7.76 ppm assigned to the aromatic protons on the oxybis(phenyl isocyanate) moiety (H_c and H_d). The urea amide proton (H_e) is not observed due as a result of proton-deuterium exchange with the deuterated TFA solvent. This occurs because d -TFA is a strong acid (pK_a 0.23) favouring dissociation therefore facilitating proton exchange with the urea (pK_a is ca. 26.9). This effect also occurs for poly-ylid **3.7** with no amide proton observed in the ^1H NMR spectrum.

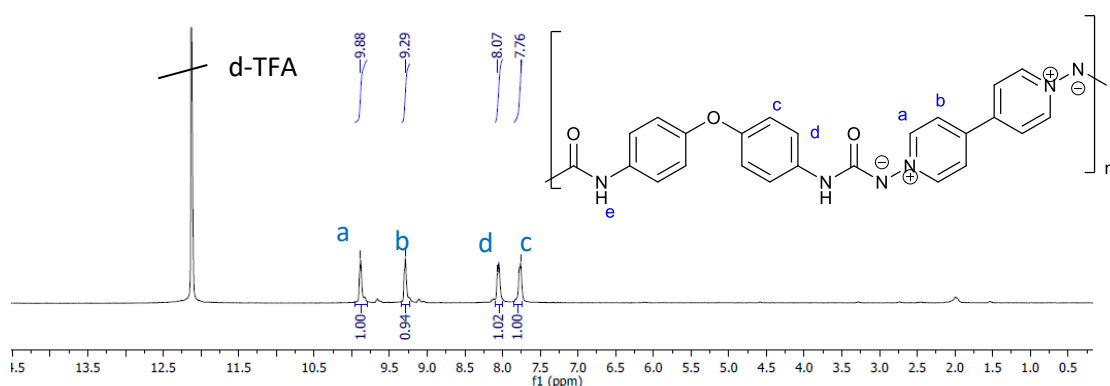


Figure 3.16: ^1H NMR spectra of isocyanate based poly-ylid **3.8** in d -TFA

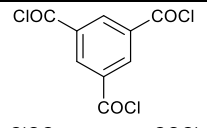
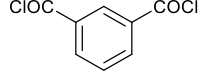
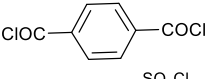
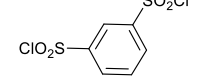
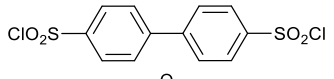
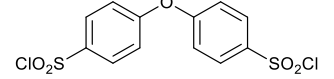
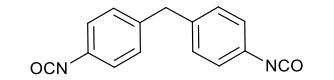
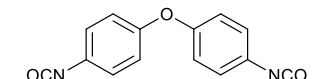
3.3.3.3 Inherent Viscosity

The poly-ylid inherent viscosities were determined by measuring the relative viscosity (η_{inh}) of a 0.1% w/v solution in formic acid alongside a formic acid solvent blank at 25 °C and calculating the η_{inh} using **Equation 1**.

$$\eta_{inh} = \left(\frac{\ln \frac{t_2}{t_1}}{c} \right) \quad (1)$$

Where η_{inh} is the inherent viscosity (dL g^{-1}), t_1 and t_2 are the average absolute viscosities ($\text{mm}^2 \text{s}^{-1}$) of the solvent and polymer solution(s) respectively and c is the concentration of the polymer solution (g dL^{-1}). The inherent viscosity provides information on the relative molecular weights of polymers of similar types, though not absolute molecular weights. As a general rule the higher the molecular weight of the polymer the higher the viscosity. Whilst none of the poly-ylids have exceptionally high inherent viscosities the highest values obtained were for the two acid chloride based poly-ylids **3.2** and **3.3** at 1.53 and 1.68 dL/g respectively (**Table 3.6**). All other poly-ylids had an inherent viscosity of less than 1 dL/g , indicating these polymers are of significantly lower molecular weight.

Table 3.6: Inherent viscosity characterisation data for the poly-ylids.

	Monomer	Polymer inherent viscosity^a (dL/g)
3.1		Cross-linked
3.2		1.53
3.3		1.68
3.4		0.42
3.5		0.15
3.6		0.74
3.7		0.69
3.8		insoluble

^a Inherent viscosity measured for a 0.1% solution in formic acid at 25°C

3.3.3.4 Thermogravimetric analysis

Thermogravimetric analysis (TGA) was used to determine poly-ylid degradation temperatures (T_{deg}). Samples were heated at 15°C/min in an inert atmosphere and the thermogram was analysed to determine the T_{deg} . This was defined as the temperature at which 10% weight loss was observed after weight equilibration to allow for evaporation of any residual solvent.

For each class of poly-ylid, similarities between the thermogram profiles could be observed. For example, in the acyl poly-ylids, both **3.2** and **3.3** exhibit similar degradation temperatures of 261 °C and 265 °C, respectively (**Figure 3.17**). This may be attributed to the similarity in their structures with the only difference being *meta* or *para* substitution of the second arene-dicarbonyl residue. Acyl poly-ylid **3.1** however had an unexpectedly low T_{deg} of 233 °C particularly considering its cross-linked structure.

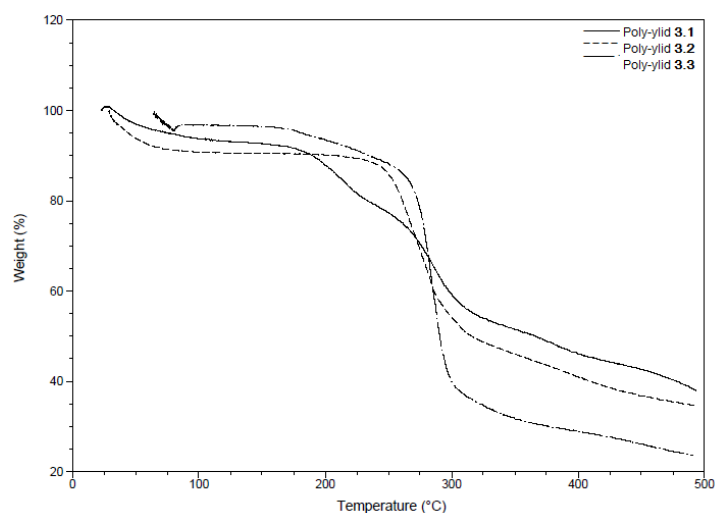


Figure 3.17: TGA thermograms of the acyl poly-yliids **3.1**, **3.2** and **3.3**.

Figure 3.18 a) shows the TGA thermograms of the three sulfonyl poly-yliids. Whilst two of the poly-yliids have a very similar T_{deg} at 312 °C for poly-ylid **3.4** and 317 °C for poly-ylid **3.5**, the third sulfonyl poly-ylid (**3.6**) exhibited a significantly lower T_{deg} of 261 °C. The low T_{deg} for poly-ylid **3.6** is unexpected since the sulfonyl chloride monomer exhibits a structural similarity to monomer **3.5** differing only in the presence of an ether linker between the aromatic rings rather than a methylene group. **Figure 3.18 b)** demonstrates that both of the carbamoyl poly-yliids had similar degradation temperatures; 252 °C for poly-ylid **3.6** and 255 °C for poly-ylid **3.7**.

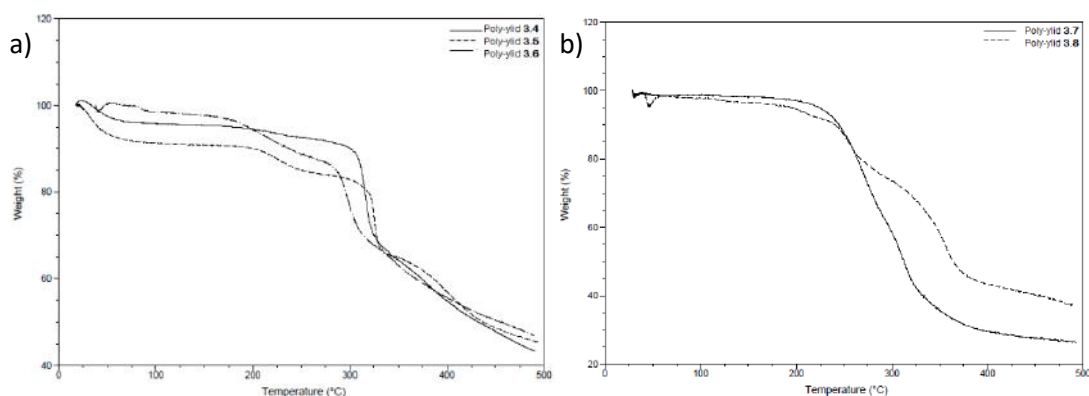


Figure 3.18: a) TGA thermograms of the sulfonyl poly-yliids **3.4**, **3.5** and **3.6** and b) TGA thermograms of the carbamoyl poly-yliids **3.7** and **3.8**.

The sulfonyl poly-yliids demonstrated the highest degradation temperatures which may be attributed to extensive delocalisation of the negative charge on the ylid nitrogen onto the very strongly electron-withdrawing sulfone group. The acyl and carbamoyl poly-yliids had more similar degradation temperatures about 60-80 °C less than the sulfonyl chlorides, averaging at 253 °C.

3.3.3.5 Differential Scanning Calorimetry

Differential Scanning Calorimetry (DSC) was used to analyse the thermal properties of the poly-ylids. The poly-ylid samples were heated to 200 °C at a ramp rate of 10 °C/min for one cycle before undergoing a second cycle heating to 350 °C, again at a ramp rate of 10°C/min. The first cycle ensured all solvent was removed as the hydrophilicity of the poly-ylids resulted in water adsorption and therefore it was the second cycle that was analysed. The second cycle heated the polymers beyond their degradation points as determined by TGA analysis (see Section 3.3.3.4).

Typically three types of thermal transitions can be observed using DSC: the glass transition temperature (T_g), the crystallisation temperature (T_c) and the melt temperature (T_m). None of the poly-ylids demonstrated any characteristic crystallisation or melt thermal transitions within this temperature range at this ramp rate (see **Figures 3.19, 3.20 and 3.21**). The lack of a crystallisation peak is consistent with materials which are already highly crystalline and therefore cannot easily undergo further crystallisation during heating, although 100% crystallinity is unusual and most crystalline polymers will contain amorphous regions.⁹ Crystallinity is determined by polymer structure and intermolecular forces.¹⁰ All of the poly-ylids (apart from poly-ylid **3.1** which is cross-linked) are linear polymers with no possibility of branching due to the substitution of the monomers. Additionally the high degree of aromaticity within the poly-ylids increases polymer rigidity both of which suggest a highly ordered structure.

The high aromatic character of the poly-ylids also contributes to potential intermolecular bonding arising from π - π stacking. Additionally for some of the poly-ylids there is also the potential for hydrogen bonding. Within the carbamoyl poly-ylids the urea bond contains both a hydrogen-bond donor (urea nitrogen atom) and a hydrogen-bond acceptor (urea carbonyl oxygen atom) facilitating intermolecular hydrogen bonding. In the case of the acyl poly-ylids the amide nitrogen is assumed to be deprotonated since it is also part of the adjoining N-N ylid bond. Thus the bond only provides the hydrogen-bond accepting portion of a hydrogen bond although if the ylid nitrogen was protonated both components of a hydrogen bond would be present. This additional intermolecular bonding contributes to increased polymer ordering and therefore potentially to polymer crystallinity. Crystalline materials show a melting peak when the melt temperature is achieved due to a phase transition from solid to liquid involving a structural reordering of crystalline regions from ordered solid to disordered

liquid.¹¹ The lack of a melting peak in the poly-ylid DSC thermograms was attributed to the poly-ylids undergoing degradation before melt temperature can be attained.

The third thermal transition which can usually be observed in DSC analysis is the glass transition (T_g) which is associated with thermal transitions within amorphous polymers or amorphous regions within semi-crystalline polymers and involves the reversible transition from a glassy state to a rubbery state due to changes in polymer chain mobility as the sample is heated.¹² As previously stated it is uncommon for polymers to exist in a purely crystalline state, and so some amorphous regions will exist which are capable of undergoing a glass transition upon heating to appropriate temperature. However the T_g was undetectable in all of the poly-ylids studied in the present work.

Figure 3.19 shows the second cycle thermograms of the three acid chloride poly-ylids and highlights the lack of a characteristic crystallisation exotherm (positive peak) or melting endotherm (negative peak). Additionally a T_g transition was not observed although each acyl poly-ylid undergoes degradation demonstrated by the degradation exotherm peaks above 200 °C. The degradation peaks are fairly broad and in the case of **3.1** and **3.2** occur between 200-300 °C additionally these degradation peaks have two maxima suggesting a two stage degradation process. Poly-ylid **3.3** has a sharper degradation peak between 250-300 °C.

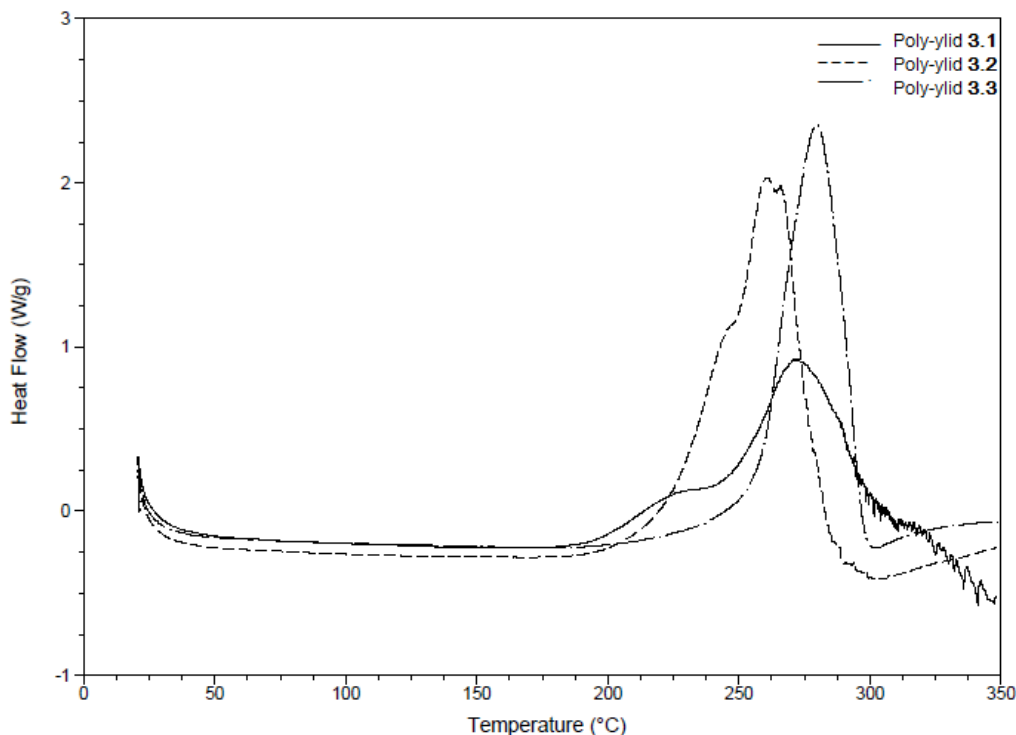


Figure 3.19: DSC thermograms of poly-ylids **3.1**, **3.2** and **3.3**.

Figure 3.20 shows the second cycle thermograms of the three sulfonyl poly-ylids **3.4**, **3.5** and **3.6**. As for the acyl poly-ylids no characteristic crystallisation or melt peaks were detectable and the T_g transition is similarly indiscernible. However, degradation is observed this time occurring over a higher temperature range 275-325 °C. The degradation peaks are also much narrower suggesting the degradation occurs over a smaller temperature range. For example poly-ylid **3.4** begins to degrade at 275 °C and by 300 °C, an increase of only 25 °C the polymer is degraded.

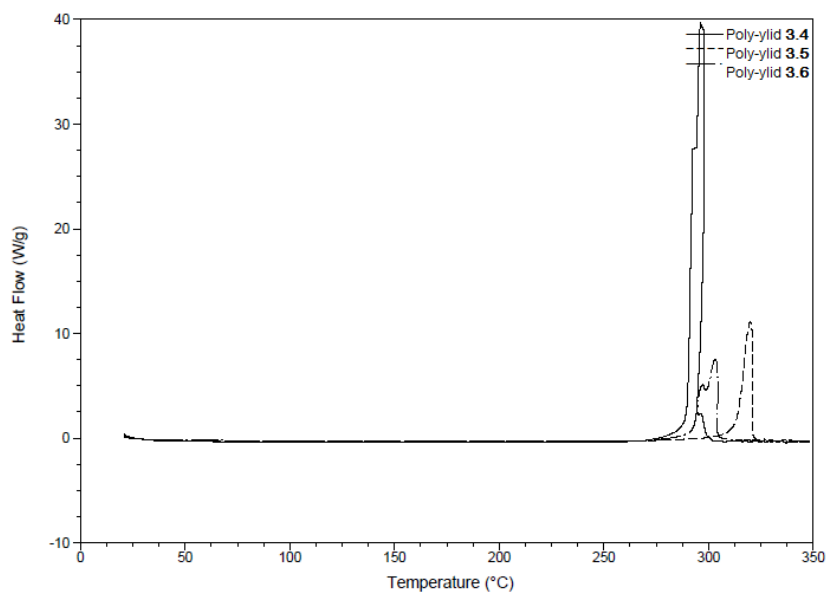


Figure 3.20: DSC thermograms of sulfonyl poly-ylids **3.4**, **3.5** and **3.6**.

Figure 3.21 shows the second cycle thermogram of the carbamoyl poly-ylids **3.7** and **3.8**. The degradation peaks are broader than the sulfonyl poly-ylid degradation peaks and occur over a lower temperature range of 200-250 °C.

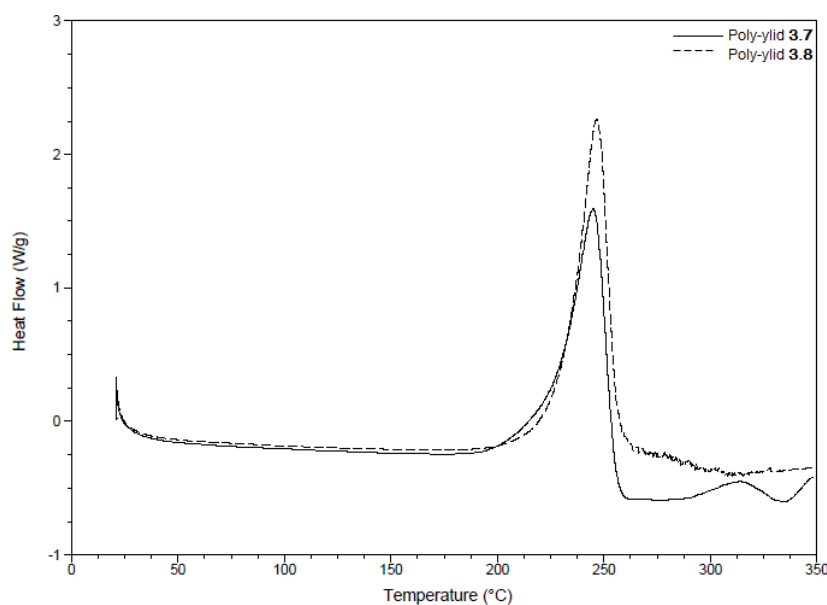


Figure 3.21: DSC thermograms of carbamoyl poly-ylids **3.7** and **3.8**.

3.3.4 Membrane Fabrication

The UF support-membrane was soaked in a 0.1% (w/v) solution of the bipyridinium salt in aqueous 0.08M sodium hydroxide for 15 minutes. The membrane was then removed from the aqueous solution and allowed to stand briefly to drain excess diamine solution before the surface was contacted for 30 seconds with a 0.01% solution of the relevant monomer in hexane (**Figure 3.22**). Monomers **3.5**, **3.6** and **3.8** could not be used to produce interfacial PES based membranes as they were insoluble in hexane. The composite membrane was then rinsed with, and stored in, deionised water before being characterised. Both commercially available and laboratory-fabricated PES UF membranes were evaluated as support-membranes.

To fabricate support-membranes, membrane casting solutions were first prepared by adding PES polymer granules to a mixture of dimethylformamide (DMF) and diglyme and stirring in a sealed vessel until fully dissolved. To cast the support-membranes, Awa 10 non-woven polyester backing paper was taped to a glass plate which was then clipped onto a casting block. The membrane casting solution was pipetted onto the backing paper and a casting blade set to the desired membrane thickness (typically 300 μ m) was used to create a thin film of polymer solution which was then immersed in tap water. The resulting membrane was rinsed for one hour under running water before cutting into disks and storing in deionised water.

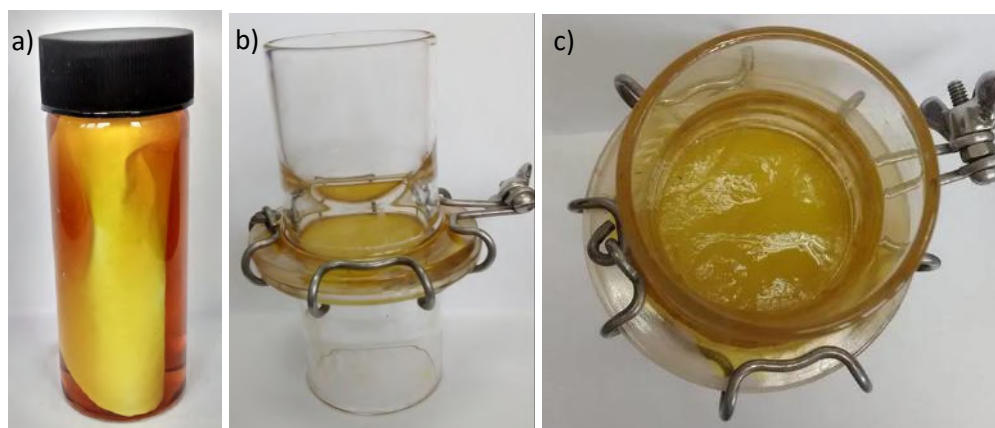


Figure 3.22: *In-situ* interfacial polymerisation of diamino-bipyridinium salt with trimesoyl chloride on a PES ultrafiltration membrane solid support a) membrane soaking in diamine, b) membrane clamped and surface contacted with acid chloride c) membrane surface following interfacial polymerisation.

3.3.5 Membrane Characterisation

Thin film composite membranes for nanofiltration and reverse osmosis are typically analysed for their pure water flux and salt rejection properties. Both these parameters

can be determined by crossflow-filtration of an appropriate feed solution under high pressure and monitoring the permeate volume and in the case of salt rejection, conductivity, over time. In the present work, this was achieved using a custom built crossflow rig capable of pumping fluid across a membrane surface (membrane area = 52.27 cm²) at 5 bar pressure (**Figure 3.23**).

Additionally, due to the ylid linkage present in all of the poly-ylids, which can potentially undergo reversible protonation and deprotonation of the nitrogen depending on the conditions, studies into the effect of pH on membrane filtration were also carried out.

Membrane surface morphology was analysed using electron microscopy. Initial biocompatibility tests were performed to investigate whether the hydrophilicity of the poly-ylid coatings affected protein adhesion in comparison to uncoated PES support membranes.

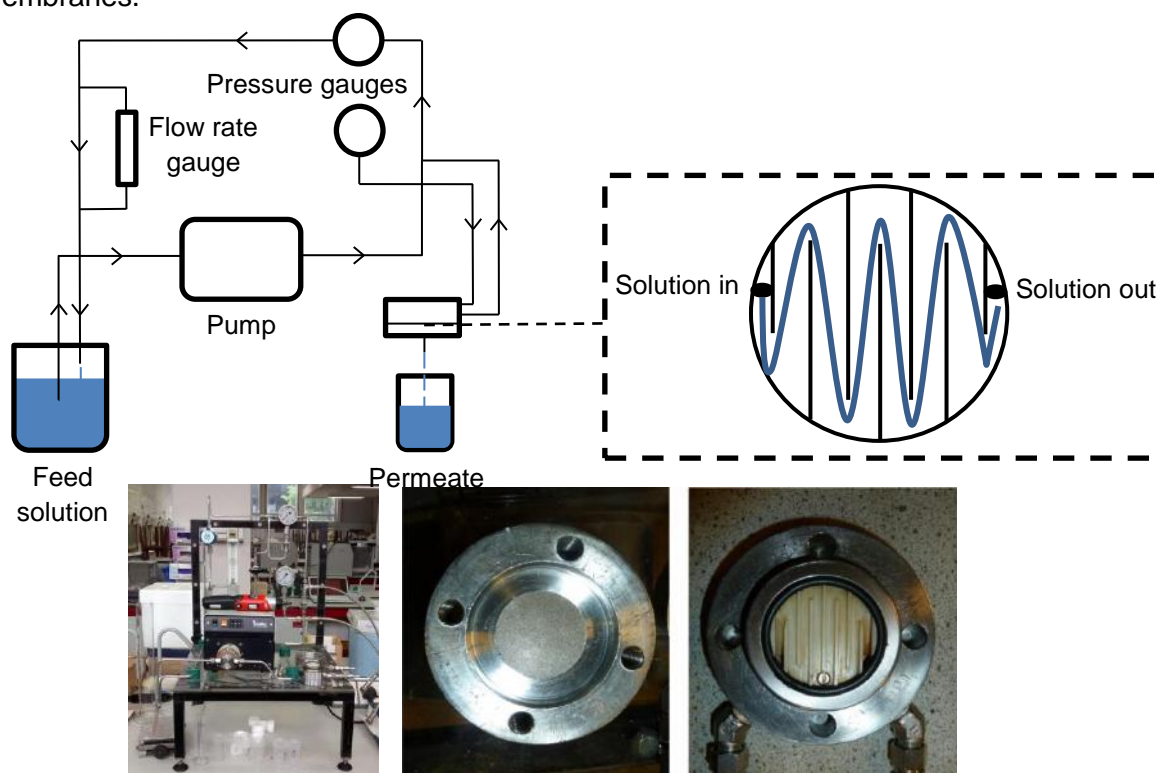


Figure 3.23: Schematic and images of custom built cross-flow rig and membrane holder.

3.3.5.1 Membrane Permeability

In a cross-flow filtration rig running at 5 bar transmembrane pressure, with a membrane area of 52.27 cm² and a deionised water feed, the volume of aqueous permeate was measured every hour to determine the average water flux as a volume (mL) per hour (**Figure 3.24**) which can be converted to the standard units of membrane flux, L m⁻² h.

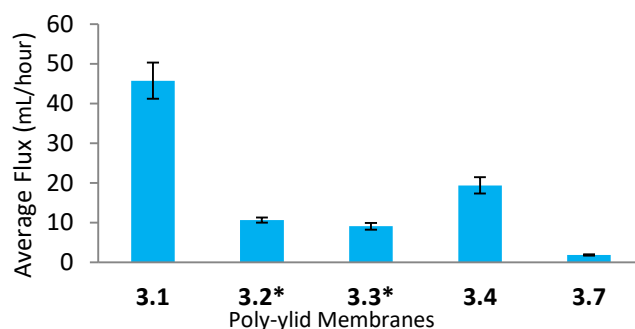


Figure 3.24: Average deionised water flux (mL/hour) for composite membranes **3.1-3.4** & **3.7** at 5 bar pressure (* Membranes **3.2** & **3.3** made using lab-fabricated PES UF membranes as microporous supports).

The trimesoyl composite acyl ylid membrane **3.1** had the highest water permeability with an average flow rate of 45.75 mL/hour. The carbamoyl ylid membrane **3.7** had a very low flow rate of only 1.88 mL/hour despite a reduced interfacial polymerisation time (15 seconds contact time for isocyanate solution) to reduce the poly-ylid coating thickness. The other membranes had similar average flow rates of approximately 10 mL/hour the exception being the sulfonyl ylid **3.4** coated membrane which had an average flux of 19.4 mL/hour.

Converting these results to standard membrane flux units ($L m^{-2} h^{-1}$) gives the results shown in **Table 3.7** below. The active membrane area within the cross flow rig was $5.03 \times 10^{-3} m^2$. The average flux for an RO membrane in a domestic module, using the example of the membrane used in **Chapter 2** (RO membrane information taken from accompanying data sheet, experiments performed at 4.13 bar), is $0.38 m^3/d$ with a membrane area of $0.46 m^2$. This is equivalent to 15.83 L/h or taking into consideration the membrane area; $34.4 L m^{-2} h^{-1}$. Membrane **3.1** has the highest flux at $9.12 L m^{-2} h^{-1}$ which is still significantly less than the commercial membrane flux at approximately a third of the value.

Table 3.7: Average deionised water flux ($L h^{-1}$ and $L m^{-2} h^{-1}$) for composite membranes **3.1-3.4** & **3.7** at 5 bar pressure (* Membranes **3.2** & **3.3** made using lab-fabricated PES UF membranes as microporous supports).

Membrane	Deionised water Flux (L/h)	Deiniosed water Flux ($L m^{-2} h^{-1}$)
3.1	0.04575	9.10
3.2	0.01066	2.12
3.3	0.0091	1.81
3.4	0.0194	3.86
3.7	0.0019	0.32

3.3.5.2 Salt Rejection

Salt rejection properties of the membranes for both monovalent and divalent salts were measured (**Figure 3.25**). All membranes exhibited a higher percentage rejection for the divalent salt MgSO_4 than for the monovalent NaCl , which is attributed to the larger radii of hydration for divalent anions and cations making these species less able to permeate through a membrane. The sulfonyl ylid coated membrane **3.4** however, showed an unusually high rejection for the monovalent salt (70%), very close to the rejection value for the divalent species (73%).

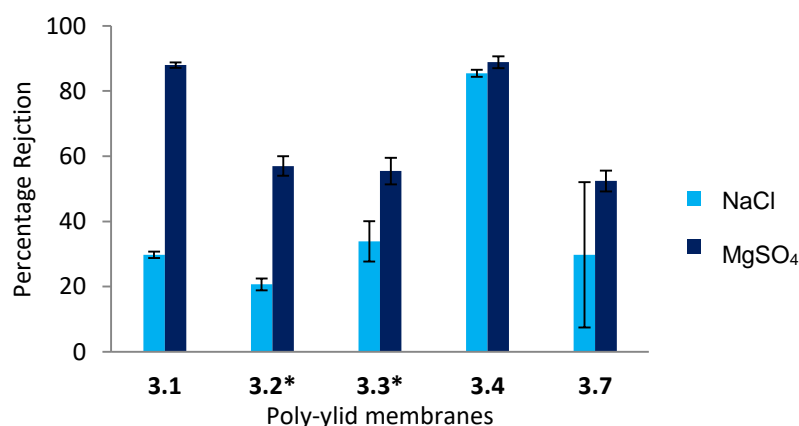


Figure 3.25: Percentage salt rejection of NaCl and MgSO_4 solutions (both 500 ppm) for composite membranes **3.1-3.4** and **3.7** at 5 bar pressure. (* Membranes **3.2** and **3.3** were made using lab-fabricated PES UF membranes as microporous supports).

In **Figure 3.26** the percentage salt rejection, of both NaCl and MgSO_4 , is plotted against flux for the PES TFC poly-ylid membranes. For magnesium sulfate, the higher the flux the higher the rejection with the highest flux and rejection coinciding at 19.6 mL/hour, 87% rejection – a trend that is not typically observed since generally the reverse is observed: high flux = low rejection. For sodium chloride it would appear the higher rejections are generally associated with a lower flux with the highest rejection 70% associated with a more modest flux of 10 mL/hour.

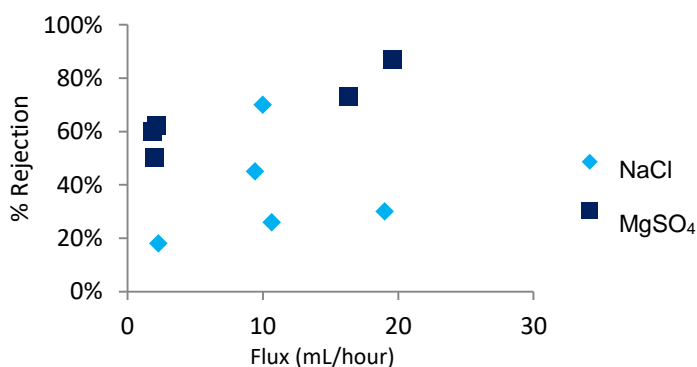


Figure 3.26: Flux vs. rejection for NaCl and MgSO_4 of the PES-bipyridinium -acyl/sulfonyl /carbamoyl TFC membranes (500ppm salt solutions, 5 bar pressure).

3.3.5.3 pH Effects on permeability

Each of the poly-ylids contains an unusual N-N ylid bond adjacent to the bond formed during the polymerisation step (an amide, sulfonamide or urea depending on the monomer) see **Figure 3.27**.

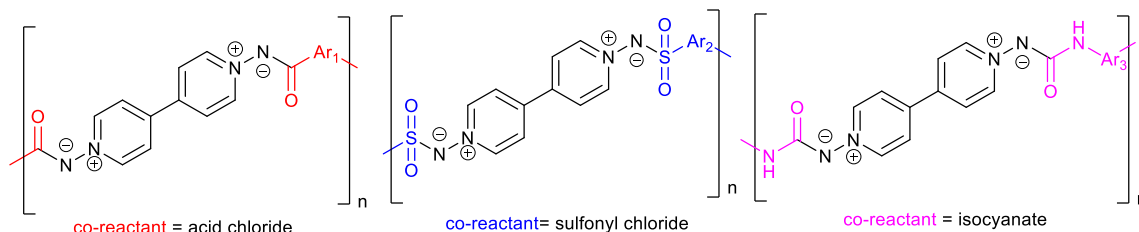


Figure 3.27: Ylid bond adjacent to bond formed in polymerisation reaction between 1,1'-diamino-4,4'-bipyridinium di-iodide and either an acid chloride, sulfonyl chloride or isocyanate.

In neutral conditions the ylid is relatively stable as a result of delocalisation of the positive charge around the aromatic ring system whilst the negative charge is stabilised by resonance with the amide carbonyl or sulfonamide sulfur-oxygen bonds or urea carbonyl group. The negatively charged ylid nitrogen is, however, still susceptible to protonation. This results in a colour change which can be clearly observed when a membrane sample is placed in acidic and basic solutions. Using membranes coated with poly-ylid **3.1**, **3.4** and **3.7** as examples, which are yellow in neutral conditions, when placed in acid, the bright yellow colour is diminished to a very much paler version whilst subsequently in base the yellow colour re-intensifies (**Figure 3.28**).

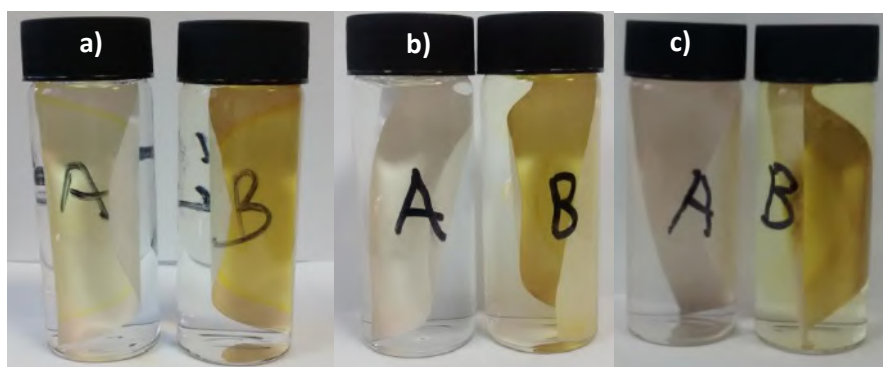


Figure 3.28: a) Acyl poly-ylid **3.1**, b) Sulfonyl poly-ylid **3.4** and c) Carbamoyl poly-ylid **3.7** composite membranes in acidic conditions (A) and basic conditions (B).

In acidic conditions, the ylid nitrogen is protonated, which decreases the polarity of the N-N bond and therefore decreasing the hydrophilicity of this linkage. Comparing fluxes obtained with feed solutions of differing pH shows that this phenomenon significantly affects the membrane filtration properties. Three different membranes were

investigated, with an example from each type of poly-ylid i.e. membrane **3.1** (acyl poly-ylid), **3.4** (sulfonyl poly-ylid) and **3.7** (carbamoyl poly-ylid).

Figure 3.29 shows that when these membranes are used to process feed solutions at two different pH's; pH 4 and pH 10, there is a pH dependent change in flux. Generally lower fluxes are observed under the acidic conditions. This is thought to be caused by the reduced hydrophilicity caused by ylid protonation producing a polymer which can form strong hydrogen bonds between the chains rather than with approaching water molecules reducing the membrane permeability to water. In basic conditions, the ylid nitrogen is deprotonated resulting in a more hydrophilic bond and therefore a more permeable membrane: hence then the increased fluxes in basic conditions. When compared to pure deionised water generally both the acidic and basic feed solutions have a lower flux relative to pure water, an exception being membrane **3.4** which gave higher flux at pH 10.

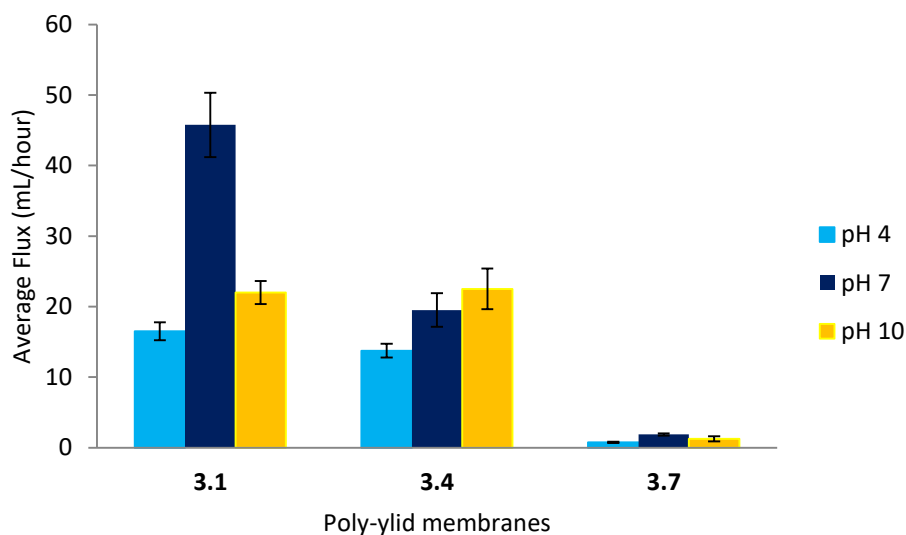


Figure 3.29: Average flux (mL/hour) for buffered solutions at pH 4, 7 and 10 at 5 bar pressure.

3.3.5.4 Surface Morphology

Environmental scanning electron microscopy (ESEM) was used to image the membrane surfaces to investigate their morphology. The majority of the membranes had a smooth featureless surface, with no evidence of any fine structure (see **Figure 3.30**).

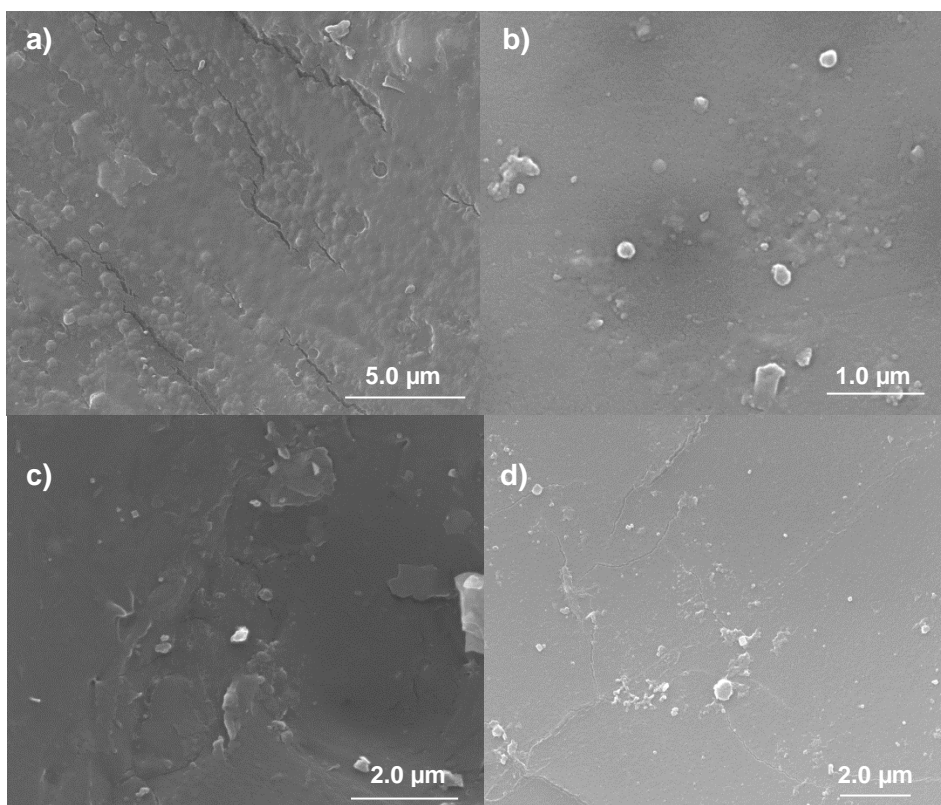


Figure 3.30: Environmental scanning electron micrographs of gold coated poly-ylid membranes a) **3.2** magnification x14,000, b) **3.3** magnification x 54,000, c) **3.4** magnification x 29,000 and d) **3.7** magnification x 20,000.

The coating obtained from the polymer based on monomer **3.1** has an unusual nodular structure creating an increased surface area (**Figure 3.31**). These features are absent in the other composite membranes suggesting that this structure could be related to the cross-linked nature of the polymer resulting from the tri-substituted monomer. For comparison the surface of a membrane coated with the standard polyamide used in commercial RO membranes is shown. This polyamide is made via a polycondensation reaction between *m*-phenylenediamine and trimesoyl chloride and also results in a polyamide with a highly structured surface morphology.

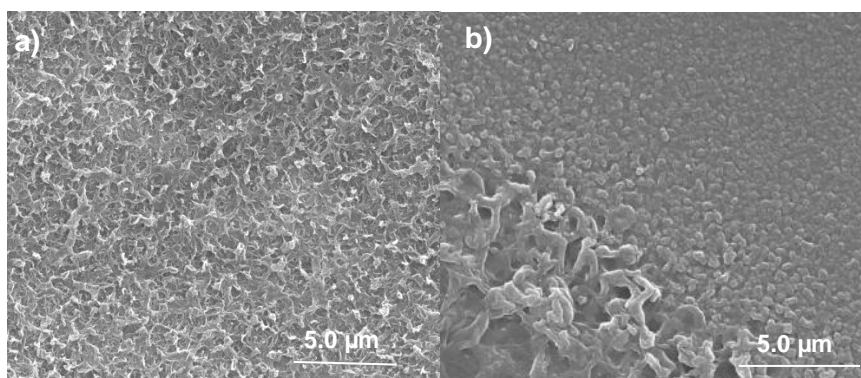


Figure 3.31: Environmental scanning electron micrographs of gold-coated TFM membranes a) *m*-phenylenediamine-trimesoyl chloride, magnification x 10,000 b) trimesoyl- 1,1'-diamino-4,4'-bipyridinium , magnification x 12,000.

Blends of monomers **3.1** and **3.4** gave rise to an intermediate structure with nodules present surrounded by flat featureless surfaces suggesting that perhaps combinations of monomers could be used to fine tune membrane surface properties as required.

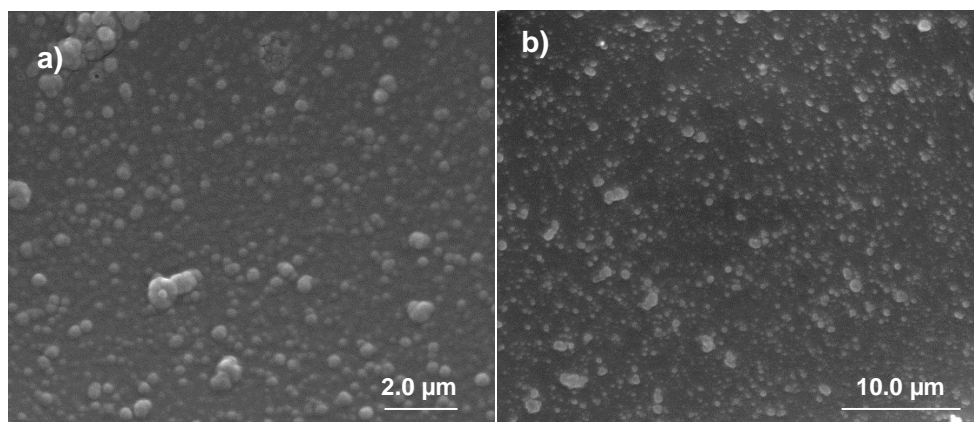


Figure 3.32: Environmental scanning electron micrograph of gold-coated blend composite membrane (from monomers **3.1** and **3.4**, a) 1:1, magnification x 20,000 and b) 2:1, magnification x 6,600.

3.3.5.5 Biocompatibility testing

In order to evaluate the biocompatibility of the poly-ylid coatings, protein adhesion studies were carried out. Two different plasma proteins were investigated; bovine serum albumin (BSA) and fibrinogen (FIB). Serum albumin usually makes up approximately 55% of the blood plasma protein content in humans whilst fibrinogen represents around 7%.¹⁵

To perform the study, coated and uncoated membrane samples were incubated at 37 °C in a 10 mg/mL protein (BSA or fibrinogen) in phosphate buffered (PBS) solution for 24 hours. Following this the membranes were rinsed to remove any non-adhering protein and the samples were then heated in sodium dodecyl sulfate (SDS)-hydroxide to desorb the attached proteins. The resulting supernatant was analysed using the BCA assay (bicinchoninic acid assay, described in **Chapter 2**) to determine the protein concentration present in each sample which was then extrapolated to estimate the protein concentration per unit membrane area. Control samples in protein-free solutions (PBS only) were also incubated and assayed. Calculated concentrations resulting in a 'negative concentration' signify zero absorption and therefore zero protein present.

Figure 3.33 shows the calculated protein concentration (mg/mL) present in 25 μ L of supernatant from the protein denaturation step following 24hrs incubation in a 10 mg/mL BSA solution (69 kDa). The uncoated PES support membrane gave an average

concentration of 2.01 mg/mL. Membranes coated with poly-ylids **3.1** and **3.4** gave similar protein concentrations suggesting that the increased hydrophilicity of the poly-ylid coating did little to prevent protein adhesion (1.96 mg/mL and 2.19 mg/mL). However, the sample coated with poly-ylid **3.7** did show a 31% reduction in protein concentration from 2.01 mg/mL in the uncoated sample to 1.39 mg/mL in the coated sample.

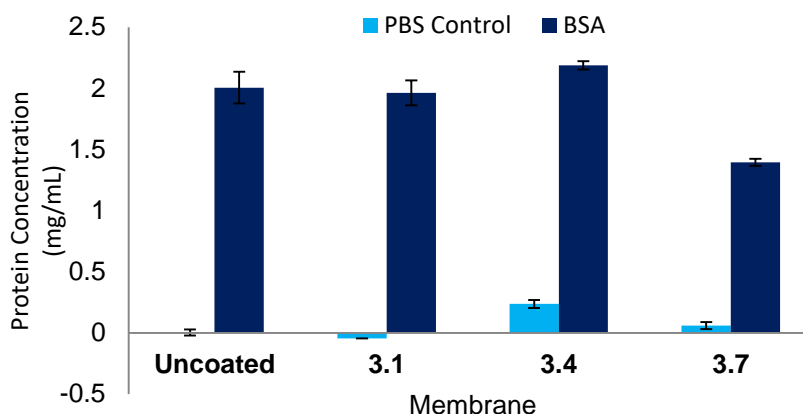


Figure 3.33: Calculated average BSA protein concentration mg/mL in 25 μ L samples from SDS-OH supernatant.

The data collected from the assay were used to estimate the protein concentration per membrane area see **Table 3.8** below. All four membranes were found to have reasonably similar protein concentrations. Membrane **3.1** had a protein concentration of 0.40 mg/cm² which was more or less the same as the uncoated membrane (0.41 mg/cm²) and membrane **3.4** had slightly more protein than the uncoated membrane (0.45 mg/cm²). However, membrane **3.7** had significantly less adsorbed protein than the uncoated membrane, at only 0.28 mg/cm². This suggests that the increased hydrophilicity of the membrane surface provided by poly-ylid **G** may increase the biocompatibility of hydrophobic PES membranes and so reduce levels of protein adhesion.

Table 3.8: Calculated BSA protein concentration per unit membrane area.

Membrane	Protein concentration per unit membrane area (mg/cm ²)
Uncoated	0.41
3.1	0.40
3.4	0.45
3.7	0.28

The study was repeated using fibrinogen – a larger protein at 340 kDa but results suggested that the uncoated membrane performed better than the TFC poly-ylid membranes, with zero adhered protein detected (**Figure 3.34**).

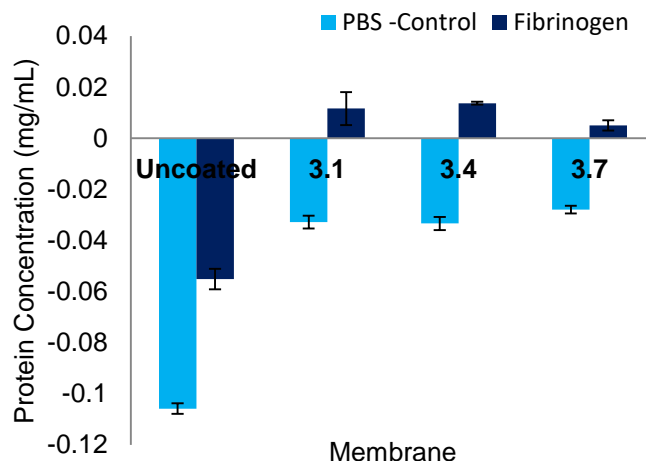


Figure 3.34: Calculated average fibrinogen protein concentration mg/mL in 25 μ L samples from SDS-OH supernatant.

The amount of protein adhering to the coated membranes however was significantly smaller (by a factor of 10) than for the BSA studies with an average protein concentration of 0.056 mg/cm² present on the coated membranes in the fibrinogen study compared with an average of 0.5133 mg/cm² for the BSA study (**Tables 3.8 and 3.9**).

Table 3.9: Calculated fibrinogen protein concentration per unit membrane area.

Membrane	Protein concentration per unit membrane area (mg/cm ²)
Uncoated	0
3.1	0.0581
3.4	0.0687
3.7	0.0249

A final study involved the use of porcine plasma which contains a number of different plasma proteins (**Figure 3.35**). The same protocol was used exchanging 10 mg/mL protein incubation for the plasma both neat and diluted tenfold with PBS. Again a protein free control was also incubated and assayed. Only one type of poly-ylid membrane was analysed; poly-ylid **3.1** coated compared with an uncoated control. When incubated in neat plasma little difference was observed between the uncoated and coated membranes which gave concentrations of 1.36 mg/mL and 1.28 mg/mL, respectively, equivalent to a 6% decrease. When the plasma was diluted the coated membrane showed again a decrease in protein concentration this time by approximately 26%.

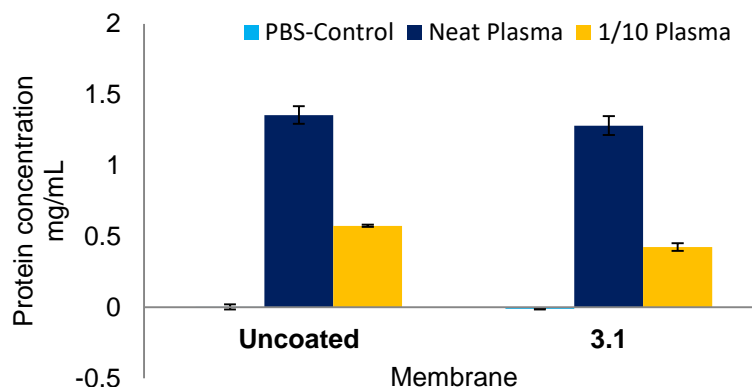


Figure 3.35: Calculated average protein concentration mg/mL in 25 μ L samples from SDS-OH supernatant.

Overall it appears that the increased hydrophilicity provided by the poly-ylid coatings does not generally reduce the amount of protein that adheres relative to an uncoated membrane with an exception being poly-ylid **3.7** which was able to reduce BSA protein adhesion significantly relative to an uncoated membrane.

3.4 Conclusions

Five novel poly-ylids based on sulfonyl chloride and isocyanate monomers (and three previously reported acid chloride poly-ylids) were successfully synthesised and fully characterised using a variety of techniques including; infrared and proton NMR spectroscopy, inherent viscosity measurements and thermal analysis (Thermogravimetric Analysis and Differential Scanning Calorimetry).

Two of the novel poly-ylids along with three previously reported acid chloride-derived poly-ylids were then used to fabricate thin-film composite nanofiltration membranes via *in situ* polycondensation reactions on the surface of a polyethersulfone ultrafiltration support membrane. Both commercially available and lab-fabricated PES UF membranes were investigated. The resulting thin film composite membranes were then characterised by analysing their pure water flux and salt rejection properties (for both mono- and di-valent salts). It was found that the highest pure water fluxes were achieved with the membrane coated with the previously reported acyl poly-ylid **3.1**. This is attributed to the tri-substituted monomer producing an unusual nodular surface (see Section 3.3.5.4) therefore increasing the membrane surface area and hence increasing the water flux. Despite this the average flux could not compete with a commercial RO membrane which had a flux of 34.4 L m⁻² h⁻¹ compared to membrane **3.1** which had an average flux of 9.10 L m⁻² h⁻¹.

As for the salt rejection studies, when comparing mono and divalent salt rejection, in all cases the divalent salt showed a higher percentage rejection although membranes coated with poly-ylid **3.4** showed an unusually high monovalent salt rejection of 70% relative to the divalent salt rejection at 73%. The highest overall rejection was again achieved with the poly-ylid **3.1** coating; 88% rejection of the divalent magnesium sulfate. Novel poly-ylid **3.7** achieved comparable sodium chloride rejection (52%) to poly-ylids **3.2** (56%) and **3.3** (55%).

Additionally, due to the presence of a novel ylid linker which contains a negatively charged nitrogen atom susceptible to reversible protonation and deprotonation, further flux studies under different pH's were performed to examine the effect of pH on membrane permeation. It was found that changing the pH of the feed did affect the flux with all three membranes examined (**3.1**, **3.4** and **3.7**) achieving higher fluxes in basic conditions than under acidic conditions. It is proposed that this is a result of the reduced hydrophilicity caused by ylid protonation in acid conditions which produces a polymer which can form strong hydrogen bonds between the chains rather than forming hydrogen bonds with approaching water molecules. This then reduces the membrane permeability to water. In basic and neutral conditions, the ylid nitrogen is deprotonated resulting in a more hydrophilic bond and therefore a more permeable membrane, hence then increased fluxes in basic conditions.

Scanning electron microscopy was used to analyse the membrane surface morphology. It was found that only the tri-substituted crosslinking monomer trimesoyl chloride was able to produce any morphological effects creating a characteristic nodular surface. All other poly-ylids produced flat featureless membrane surfaces although bends of the trimesoyl chloride monomer and a di-substituted sulfonyl chloride monomer (benzene-1,3-disulfonyl chloride) were able to produce an intermediate surface structure with both flat and nodular regions.

Initial biocompatibility studies were carried out to examine the effect of the increased hydrophilicity of the TFC membranes as a result of coating with the highly polar poly-ylids. Protein adhesion was studied with two different proteins (BSA and fibrinogen) and porcine plasma containing a mixture of plasma proteins. It was found that the increased hydrophilicity of the membrane surfaces did not generally decrease the protein adhesion relative to uncoated control membranes except in one study: poly-ylid **3.7** with BSA.

3.5 Future Work

A continuation of the work presented in this chapter should include investigation into the structure of the novel sulfonyl and carbamoyl poly-ylids by synthesising model oligomer compounds for single-crystal X-ray diffraction analysis. Additionally alternative sulfonyl chloride and isocyanate monomers could be synthesised to expand the library of 1,1'-diamino-4,4'-bipyridylium poly-ylids. Following characterisation of any novel poly-ylids their membrane forming abilities' should be assessed.

The existing TFC membranes should be further analysed by investigating their rejection of different salts or mixtures of salt solutions. Furthermore the effect of changing pH on flux suggests that the pH of the feed could also affect salt rejection properties, so analysing the membrane salt rejection at different pH values would also be worthy of investigation. Additional SEM analysis could be performed to image the membrane cross-sections for further information on the membrane morphology. The blended coatings incorporating both trimesoyl chloride and a di-substituted sulfonyl chloride in different ratios could be analysed in terms of their flux and salt rejection properties and to quantify the impact of the changing ratio of monomers. Finally, other biocompatibility experiments could be performed i.e. investigating bacterial adhesion onto coated vs. uncoated membranes.

3.6 Experimental

3.6.1 Materials

The following materials were sourced from Fisher Scientific UK Ltd (Leicestershire, UK); Pierce™ BCA Protein assay kit (containing; Reagent A - bicinchoninic acid, Reagent B - 4% (w/v) copper sulfate, 2mg/mL albumin standard ampules), 96-well flat-bottomed micro-plates and the micrometre feeler gauge. The 50K MWCO polyethersulfone UF disks were purchased from Merck Millipore (Massachusetts, USA). The "Awa 10" backing paper used to fabricate UF membranes was obtained from Awa Paper Ltd (Japan) and the membrane casting blade was sourced from Mitutoyo (Japan). The Victrex® 5200 High MW aromatic polyethersulfone also used in UF membrane fabrication was ex ICI plc. All remaining materials including; acetic acid, acetone, benzene-1,3-disulfonyl chloride, bovine serum albumin, biphenyl-4,4'-disulfonyl chloride, 4,4'-bipyridyl dihydrate, deuterated dimethyl sulfonic acid, deuterated trifluoroacetic acid, diglyme, dimethylformamide, fibrinogen, hexane, hydriodic acid, hydrochloric acid, hydroxylamine-O-sulfonic acid, isophthaloyl chloride, magnesium sulphate, methanol, 4,4'-methylenebis(phenylisocyanate), oxybis(benzene

sulfonyl chloride), oxybis(phenyl isocyanate), phosphate buffered saline, potassium carbonate, potassium hydroxide, sodium chloride, sodium dodeceyl sulfate, sodium hydrogen carbonate, sodium hydroxide, terephthaloyl chloride, trimesoyl chloride were purchased from Sigma Aldrich (Dorset, UK)

3.6.2 Equipment

The following items of equipment were sourced from Fisher Scientific UK Ltd (Leicestershire, UK); conductivity meter, disposable glass test tubes, Eppendorf tubes (0.5, 1.5 and 2mL), micropipettes (1000 μ L and 200 μ L) and tips and NMR vials with polyethylene lids.

IR spectra were recorded using a Perkin Elmer Spectrum FT-IR spectrometer equipped with a universal attenuated total reflectance accessory. Both monomer and polymer samples were analysed in powder form.

^1H and ^{13}C NMR spectra were obtained on a Bruker Nanobay 400 or 100 MHz spectrometer and were referenced to residual solvent resonances. Samples were dissolved in appropriate solvents at room temperature. When assigning ^1H and ^{13}C NMR spectra all values representing chemical shifts (δ) are in units of parts per million (ppm).

The absolute viscosities of the poly-ylids were measured at 25 °C for 0.1% (w/v) polymer solutions in $\geq 96\%$ formic acid with a Schott-Geräte CT-52 auto-viscometer using glass capillary No. II. Samples were stirred overnight to ensure complete dissolution. Following this inherent viscosity was calculated using **Equation 1** relative to the flow time of the solvent.

$$\eta_{inh} = \left(\frac{\left\{ \ln \frac{t_2}{t_1} \right\}}{c} \right) \quad (1)$$

Where η_{inh} is the inherent viscosity (dL g^{-1}), t_1 and t_2 are the average absolute viscosities ($\text{mm}^2 \text{s}^{-1}$) of the solvent and polymer solution(s) respectively and c is the concentration of the polymer solution (g dL^{-1}). The t values are an average of 5 measurements per sample. In some cases the absolute viscosities were used for comparison rather than calculating the inherent viscosity.

Thermogravimetric Analysis employed a TA Instruments TGA Q50 attached to a TGA heat exchanger, platinum crucible and an aluminium TA-Tzero pan (ramp rate of 15 °C/min up to 500 °C).

Differential scanning calorimetry analysis employed a TA DSC Q2000 with TA Refrigerated Cooling System 90 (aluminium TA-Tzero pans and lids) with a ramp rate of 10 °C/ min: first cycle to 200 °C and second cycle to 350 °C).

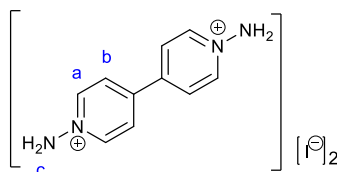
Nanofiltration experiments were carried out using a custom built cross-flow rig. Conductivity measurements were made using a calibrated conductivity meter

Electron micrographs were obtained using an FEI Quanta FEG 600 Environmental Scanning Electron Microscope (ESEM). Samples were sputter coated with gold before imaging with high vacuum ESEM.

Absorbance data was collected using a FLUOstar Omega Microplate Reader. Samples and standards were transferred to a clear flat-bottomed 96-well microplate before the absorbance was read at 562 nm. In both cases the samples and standards underwent an assay before the absorbance was read (described in Section 3.6.3.7).

3.6.3 Methods

3.6.3.1 Synthesis of 1,1'-diamino-4,4'-bipyridinium di-iodide⁷

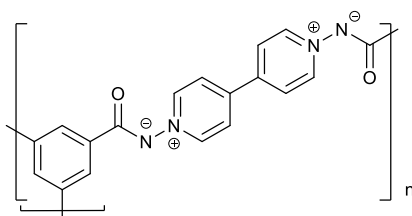


Hydroxylamine-O-sulfonic acid (11.3 g, 100mmol) in water (20 mL) was cooled to -5 °C and neutralised with potassium hydroxide (5M, 20 mL). The solution was added to a suspension of 4,4'-bipyridyl dihydrate (9.6 g, 62mmol) in water (30 mL) at 30 °C. The suspension was stirred on a steam-bath until the solid dissolved, and then stirred for a further 2 hours. The cooled solution was treated with a saturated aqueous solution of potassium carbonate (6.9 g, 50mmol in 60mL). The resulting yellow solution was diluted with methanol until no further solid separated, and the potassium sulfate filtered off. The filtrate was made acid with concentrated hydriodic acid and cooled to 0 °C. The solid which separated was filtered off, washed with acetone and recrystallised from water, affording the diamino-bipyridinium di-iodide salt as yellow/orange crystals, (7.9 g, 42mmol, 68%), IR (ATR)/cm⁻¹ 3440, 3251, 3033, 1641, 1495, 1373, 1198, ¹H NMR (400 MHz, DMSO-d₆) 8.95 (appt. d, 4H, H_a), 8.81 (s,4H, H_c), 8.51 (appt. d, 4H, H_b) ppm, ¹³C NMR (100 MHz, DMSO-d₆) 143.1, 137.9, 126.4 ppm. T_{deg} 203 °C.

3.6.3.2 Stirred Interfacial Polycondensation

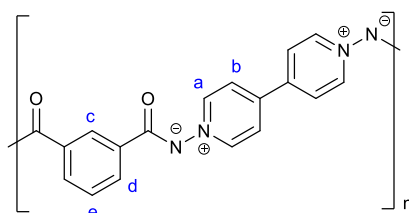
The synthesis of the 1,1'-diamino-4,4'-bipyridinium di-iodide monomer (above) was carried out using the method reported by Downes.⁷ Acid chloride, sulfonyl chloride and isocyanate monomers were used as purchased. The poly-ylids were synthesised in bulk by a stirred interfacial polymerisation reaction in which the diamine (0.9% w/v) in 0.08 M aqueous sodium hydroxide solution was mixed with a 0.6% w/v solution of the acid chloride/sulfonyl chloride/isocyanate in hexane. Exceptions were sulfonyl chlorides **3.5** and **3.6** and isocyanate **3.8**, which proved insoluble in hexane and were instead dissolved in chloroform. The reactant solutions were mixed and stirred rapidly, with the poly-ylid forming instantly at the interface of the two solutions. The solid was filtered off, washed and then dried in a vacuum oven (80 °C, 4 hours) before characterisation.

Acyl Poly-ylid 3.1;



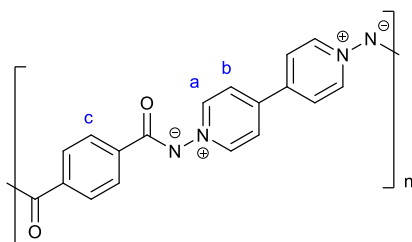
as yellow flakes, (0.2891g, 73%), IR (ATR)/cm⁻¹ 3500, 3029, 1602, 1534 1472, 1422, 1279, 1091, 954, 828, 772, 739; (cross-linked, insoluble); T_{deg} 232 °C.

Acyl Poly-ylid 3.2;



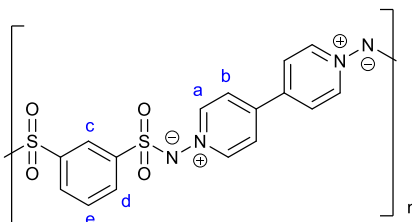
as yellow flakes, (0.2237g, 55%), IR (ATR)/cm⁻¹ 3370, 3108, 1595, 1535, 1471, 1423, 1293, 1261, 1159, 1079, 1026, 939, 899, 819, 774, 726, 703; ¹H NMR (100 MHz, *d*-TFA) 10.07 (m, 4H, H_a) 9.63 (s, 1H, H_c), 9.52 (m, 4H, H_b) 9.21 (m, 2H, H_d), 8.66 (m, 1H, H_e); Inherent viscosity (25 °C, formic acid) 1.53 dL/g; T_{deg} 260 °C.

Acyl Poly-ylid 3.3;



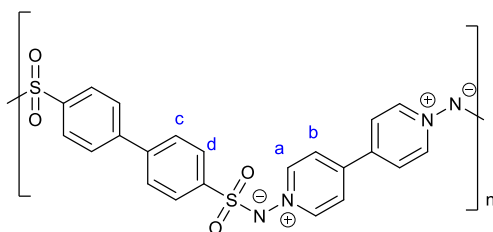
as yellow flakes, (0.1876, 47%), IR (ATR)/cm⁻¹ 3500, 3111, 1560, 1467, 1421, 1281, 1162, 1015, 893, 817, 786, 727, 700; ¹H NMR (100 MHz, *d*-TFA) 9.98 (m, 4H, H_a), 9.44 (m, 4H, H_b) 8.96 (m, 4H, H_c); Inherent viscosity (25 °C, formic acid) 1.68 dL/g; T_{deg} 265 °C.

Sulfonyl Poly-ylid 3.4;



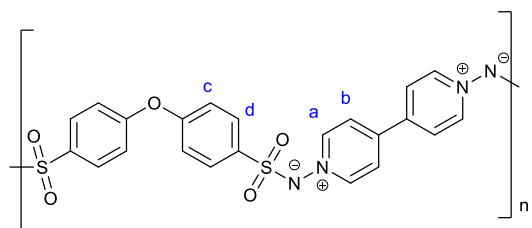
as brown powder, (0.2495g, 56%), IR (ATR)/cm⁻¹ 3531, 3115, 1621, 1476, 1425, 1285, 1154, 1129, 1103, 929, 840, 689, 636, 568; ¹H NMR (100 MHz, *d*-TFA) 9.66 (m, 4H, H_a), 9.21 (m, 4H, H_b), 8.96 (t, 1H, H_c), 8.92 (m, 2H, H_d), 8.63 (s, 1H, H_e); Inherent viscosity (25 °C, formic acid) 0.42 dL/g; T_{deg} 312 °C.

Sulfonyl Poly-ylid 3.5;



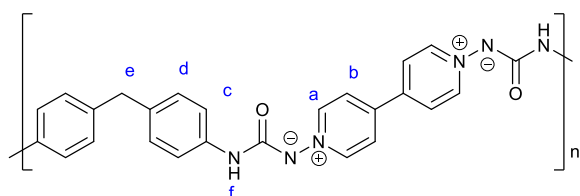
as a brown powder, (0.2007g, 47%), IR (ATR)/cm⁻¹ 3540, 3118, 1624, 1477, 1284, 1136, 1088, 927, 822, 714, 587; ¹H NMR (100 MHz, *d*-TFA) 9.63 (m, 4H, H_a), 9.27 (m, 4H, H_b), 8.57 (m, 4H, H_d), 8.57 (m, 4H, H_c); Inherent viscosity (25 °C, formic acid) 0.15 dL/g; T_{deg} 317 °C.

Sulfonyl Poly-ylid 3.6;



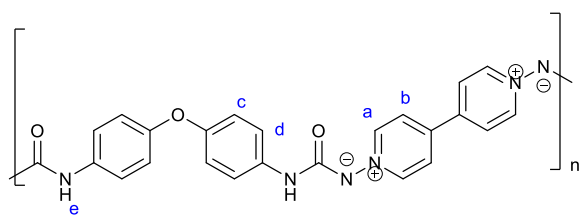
as a brown powder, (0.04007g, 11%), IR (ATR)/cm⁻¹ 3124, 1581, 1484, 1243, 1133, 1124, 925, 838, 701; ¹H NMR (100 MHz, *d*-TFA) 9.64 (m, 4H, H_a), 9.25 (m, 4H, H_b), 8.58 (m, 4H, H_d), 7.94 (m, 4H, H_c); Inherent viscosity (25 °C, formic acid) 0.74 dL/g; T_{deg} 261 °C.

Carbamoyl Poly-ylid 3.7;



as red-brown flakes, (0.0878, 18%), IR (ATR)/cm⁻¹ 3390, 3255, 3112, 2036, 2963, 2923, 1596, 1509, 1467, 1403, 1346, 1265, 1203, 1160, 1007, 814, 743; ¹H NMR (100 MHz, *d*-TFA) 9.79 (m, 4H, H_a), 9.19 (m, 4H, H_b), 7.96 (m, 4H, H_d), 7.84 (m, 4H, H_c), 4.60 (s, 2H, H_e); Inherent viscosity (25 °C, formic acid) 0.69 dL/g; T_{deg} 251 °C.

Carbamoyl Poly-ylid 3.8;



as red-brown flakes, (0.3407g, 73%), IR(ATR)/cm⁻¹ 3303, 3000, 1604, 1496, 1268, 1162, 831; ¹H NMR (100 MHz, *d*-TFA) 9.88(m, 4H, H_a), 9.29 (m, 4H, H_b), 8.07 (m, 4H, H_d), 7.76 (m, 1H, H_c); T_{deg} 255 °C.

3.6.3.3 Thin-film Composite Membrane Fabrication

The UF support-membrane was soaked in a 1% (w/v) solution of the bipyridinium salt in aqueous 0.08M sodium hydroxide for 15 minutes. The membrane was then removed from the aqueous solution and was drained in the vertical position and then allowed to stand horizontally before the surface was contacted for 30 seconds with a 0.1%

solution of the relevant monomer in hexane. Monomers **3.5**, **3.6** and **3.8** could not be used to produce interfacial membranes as they were insoluble in hexane. The composite membrane was then rinsed with, and stored in, deionised water before being characterised. Both commercially available and laboratory-fabricated PES UF membranes were used as support-membranes.

To fabricate PES support-membranes in the laboratory, membrane casting solutions were first prepared. PES polymer granules (20.2 wt%) were gradually added to the solvent [DMF (73.3 wt%) + diglyme (6.5 wt%)] and were then stirred in a sealed vessel until fully dissolved. To cast the support-membranes, Awa 10 non-woven polyester backing paper was taped to a glass plate which was then clipped onto a casting block. Approximately 25mL of membrane casting solution was poured onto the backing paper and a casting blade set to the desired membrane thickness (typically 300 μ m) was used to create a thin film of polymer solution, and the glass plate with the backing paper and polymer film was then immersed in water. The resulting membrane was rinsed for one hour under running water before cutting into disks and storing in deionised water.

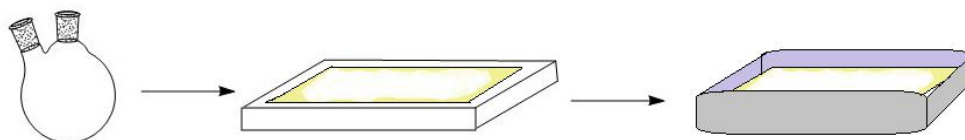


Figure 3.36: Schematic demonstrating membrane casting process 1) casting solution prepared, 2) solution cast into thin film on backing paper taped to casting block, 3) casting block, backing paper and film submerged in non-solvent precipitation bath.

3.6.3.4 Membrane Flux Determination

Nanofiltration membrane water flux was determined using the cross-flow rig with 500 mL of deionised water at a pressure of 5 bar and a cross-flow velocity across the membrane surface of 1 m s⁻¹. The volume of water which permeated through the membrane every hour was recorded. This was used to calculate the average permeate volume per hour (mL/h) which was then converted to units of flux (L m⁻² h).

3.6.3.5 Membrane Salt Rejection Determination

Nanofiltration membrane salt rejection was carried out using the cross-flow rig with 500 mL solutions of 500 ppm sodium chloride and magnesium sulfate at a pressure of 5 bar and a cross-flow velocity across the membrane surface of 1 m s⁻¹. The conductivity of the feed solution was compared with the conductivity of the permeate to determine the percentage salt rejection, R, using **Equation 2**:

$$R = \left(1 - \frac{C_p}{C_f}\right) \times 100\% \quad (2)$$

Where C_p is the conductivity of the permeate and C_f is the conductivity of the feed.

3.6.3.6 pH Effects on Permeability

Buffer solutions of differing pH values were prepared and filtered through the membrane at a pressure of 5 bar using the cross-flow rig. The volume of the permeate was measured every hour.

Table 3.10: Buffer solution compositions

pH 4	pH 10
423.5 mL 0.1 M acetic acid	500 mL 0.05 M sodium hydrogen carbonate
76.5 mL 0.1 M sodium acetate	21.4 mL 0.1 M sodium hydroxide

3.6.3.7 Biocompatibility Testing

The membrane-protein adhesion studies involved three steps;

- 1) A 'protein challenge' where samples and controls were incubated in protein solution
- 2) A sample preparation step to isolate adhered proteins in solution for analysis
- 3) An assay to determine protein concentration in samples relative to a standard curve of standards of known concentration

Protein Challenge

Membrane samples were incubated for 24 hours at 37 °C in either PBS buffer alone (control) or in a 10 mg/mL protein solution in PBS (either BSA or fibrinogen).

Sample Preparation

Following the protein challenge the membranes were rinsed to remove any non-adhering protein and the samples were then heated to 95 °C for 20 minutes in a known volume of SDS-hydroxide (1% (w/v) SDS solution in 0.2M NaOH) to desorb the attached proteins.

Bicinchoninic Acid Assay

The resulting supernatant was analysed using the BCA assay (bicinchoninic acid assay) to determine the protein concentration present in each sample with respect to a

standard curve of BSA solutions of known concentrations. The calculated concentration of the unknown samples was then extrapolated to estimate the protein concentration per unit membrane area.

A standard curve was prepared using a 2 mg/mL stock solution of BSA with dilutions ranging from 2000-25 µg/mL. The diluent was the SDS-NaOH solution.

Table 3.11: Preparation of standard BSA solutions for standard curve

Solution	Final BSA Concentration (µg/mL)	Volume of Diluent (µL)	Volume and source of BSA (µL)	Final Volume (µL)
A	2000	0	300 (stock)	300
B	1500	125	375 (stock)	325
C	1000	325	325 (stock)	325
D	750	175	175 (vial B dilution)	350
E	500	325	325 (vial C dilution)	325
F	250	325	325 (vial E dilution)	325
G	125	325	325 (vial F dilution)	550
H	25	400	100 (vial G dilution)	500
I	0	400	0	400

The BCA standard working reagent was prepared by combining the BCA reagent (component A) with 4% (w/v) CuSO₄ (component B) in a ratio of 50:1.

Standards and samples were vortex-mixed before 25 µL of each was added to a clear, flat-bottomed 96-well microplate in triplicate. Following this, 200 µL of the BCA standard working reagent was added in a randomised pattern to each well containing a sample or standard. The microplate was incubated for 37 °C for 30 minutes before measuring the absorbance at 562 nm in a FLUOstar Omega Microplate Reader.

3.7 References

1. K. C. Khulbe, C. Y. Feng, and T. Matsuura, in *Synthetic Polymeric Membranes Characterisation by Atomic Force Microscopy*, Springer-Verlag, Berlin, 2008, pp. 5–14.
2. J. E. Cadotte, *US Patent 4,277,344* (1981), to FilmTec Corporation.

3. B. S. Lalia, V. Kochkodan, R. Hashaikeh, and N. Hilal, *Desalination*, 2013, **326**, 77–95.
4. S. Veríssimo, K. V. Peinemann, and J. Bordado, *J. Membr. Sci.*, 2006, **279**, 266–275.
5. W. J. Lau, A. F. Ismail, N. Misdan, and M. A. Kassim, *Desalination*, 2012, **287**, 190–199.
6. H. M. Colquhoun, A. L. Lewis, C. A. Mahoney, and D. J. Williams, *Polymer*, 1995, **36**, 443–446.
7. J. E. Downes, *J. Chem. Soc. (C)*, 1967, 1963–1964.
8. J. Clayden, N. Greeves, S. Warren, and P. Wothers, in *Organic Chemistry*, Oxford University Press, Oxford, 2012, pp. 43–79.
9. J. M. G. Cowie, in *Polymers: Chemistry and Physics of Modern Materials*, Nelson Thornes Ltd, Cheltenham, 2002, pp. 247–271.
10. J. D. Roberts and M. C. Caserio, *Basic Principles of Organic Chemistry*, 1977, pp. 1419–1459.
11. J. He, W. Liu, and Y.-X. Huang, *PLoS One*, 2016, **11**, 1–12.
12. Mettler Toledo, Applications Note, *Thermal Analysis of Polymers - Selected Applications*, 2008, pp. 1–40.
13. S. Sivakova, D. A. Bohnsack, M. E. Mackay, P. Suwanmala, and S. J. Rowan, *J. Am. Chem. Soc.*, 2005, **127**, 18202–18211.
14. B. D. Kaushiva, S. R. McCartney, G. R. Rossmly, and G. L. Wilkes, *Polymer*, 2000, **41**, 285–310.
15. N. L. Anderson, *Mol. Cell. Proteomics*, 2002, **1**, 845–867.

Chapter 4 – Membranes based on Polyetherketone (PEK)

4.1 Abstract

Novel hydrophilic poly-ylids derived from interfacial polycondensation of the 1,1'-diamino-4,4'-bipyridylium ion with aromatic di-sulfonyl chlorides and di-isocyanates as described in **Chapter 3** were here synthesised on the surfaces of lab-fabricated polyetherketone (PEK) support membranes to produce thin film composite nanofiltration membranes with the potential to carry out organic separations, owing to the crystalline, solvent resistant character of PEK. This strategy also allows the use of monomers that are not soluble in apolar solvents, such as hexane, which are the only type of solvents compatible with traditional polysulfone membranes. The latter are non-crystalline and are therefore readily attacked by many solvents.

4.2 Introduction

Thin film composite (TFC) membranes are traditionally made by coating a polysulfone support (an ultrafiltration membrane) with a thin polyamide film via interfacial polycondensation. In the previous chapter (**Chapter 3**) a novel class of polymer coatings was explored as a route to new TFC membranes based on polycondensation between 1,1'-diamino-4,4'-bipyridylium di-iodide and a variety of di and tri-substituted aromatic monomers to create poly-ylids. Although five novel poly-ylids were synthesised and characterised (see **Figure 4.1**) only two of them were suitable for use in TFC membrane fabrication (**3.4** and **3.7**). This is due to limitations arising from the chemical stability of the polysulfone support membrane which is degraded by most organic solvents. Since the membrane coating process involves an *in situ* polycondensation on the membrane surface where the chosen monomer is in an organic solvent, the chosen solvent must be compatible with the support membrane. To overcome this limitation, it was decided that alternative support membranes could be investigated, not only widening the scope of potential monomers but also creating a completely novel solvent resistant TFC membrane which could have new applications in organic separations.

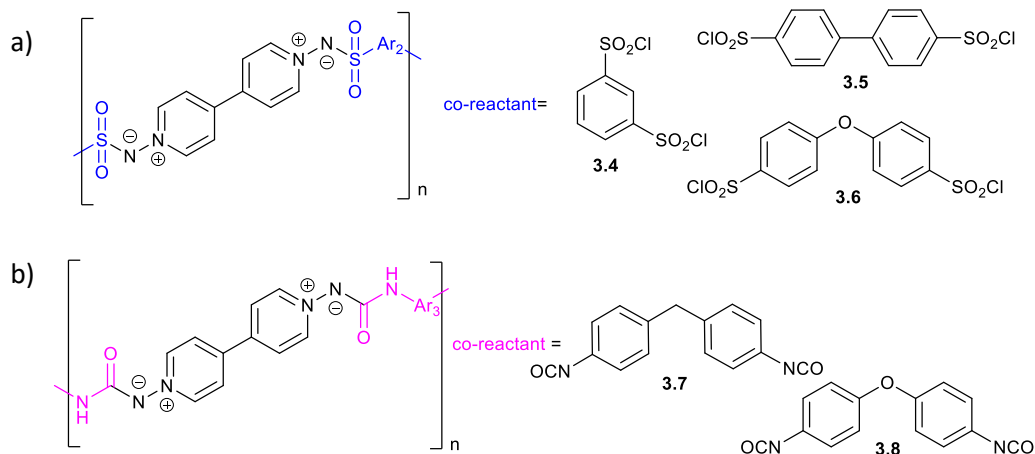


Figure 4.1: Generic structure of a) sulfonyl poly-ylids and sulfonyl chloride monomers **3.4**, **3.5** and **3.6** and b) carbamoyl poly-ylids with isocyanate monomers **3.7** and **3.8**.

Polyaryletherketones (PAEK) are a type of high-performance industrial thermoplastic characterised by their stability at high temperatures. When compared with amorphous polyarylethersulfones (PAESs), see **Figure 4.2**, PAEKs are crystalline as a result of better chain packing which in PAESs is disrupted by conformational effects and steric hindrance arising from the bulky sulfone group.¹ This increased crystallinity makes PAEKs resistant to all organic solvents at room temperature. In this study, it was proposed that this solvent resistance may allow access to previously unexplored monomers in TFC membrane fabrication via use of a PEK solid support.

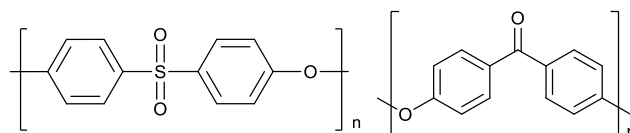


Figure 4.2: Polyethersulfone vs. polyetherketone

Modifying the supporting polymer membrane had implications for other the components of the TFC membrane. Whilst polysulfones are soluble in solvents such as dimethylformamide or *N*-methylpyrrolidone, the high crystallinity of PEK means it will only dissolve in solvents which interact chemically with the carbonyl group. One such suitable solvent is concentrated sulfuric acid. However, it was suspected that this solvent would degrade the non-woven polyester AWA backing paper used for polysulfone membranes therefore requiring that an alternative substrate be found.

Preliminary work into hollow-fibre and flat-sheet PEK membranes was reported in a patent by Colquhoun and co-workers who found the optimum PEK concentration to be between 7-15 wt%.² The group also found that the films cast from concentrated sulfuric

acid produced membranes with low crystallinity (~15%) and therefore a post-treatment was developed to increase crystallinity. However, this process also reduces flux and molecular weight cut-off (MWCO) of the membranes corresponding to a reduction in pore size.³ Initial experiments into alternative support substrates found that polyphenylenesulfide (PPS) paper produced promising results. Gelation in strong acids is known to produce membranes with low porosity and additional work by the group found that adding polyvinylpyrrolidone (PVP) could improve membrane porosity, by acting as a pore forming agent.⁴

In this study, the monomers chosen for exploration as components of novel PEK based TFC membranes were biphenyl-4,4'-disulfonyl chloride, 4,4'-oxybis(benzene sulfonyl chloride) and 4,4'-oxybis(phenyl isocyanate), shown in **Figure 4.3**.

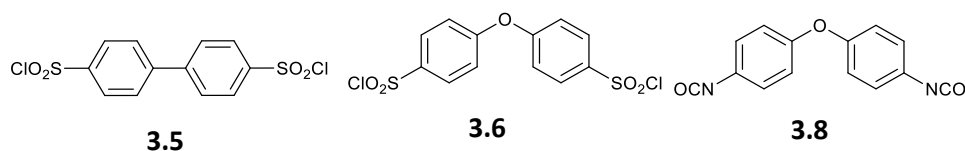


Figure 4.3: sulfonyl chloride (3.5, 3.6) and isocyanate (3.8) monomers.

4.3 Results and Discussion

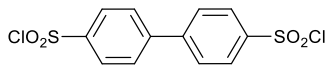
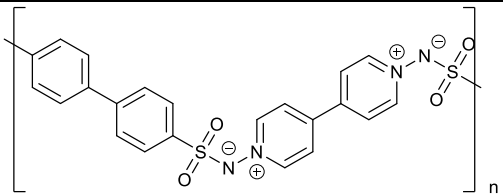
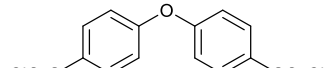
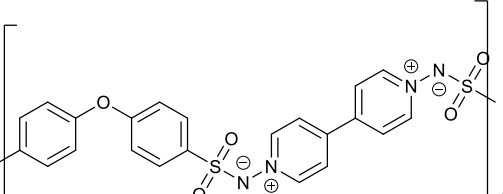
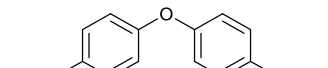
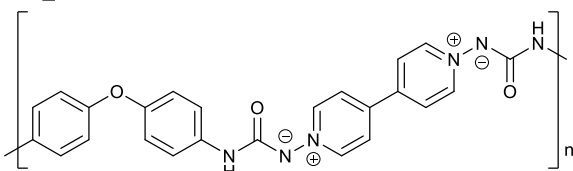
4.3.1 PEK TFC Membrane Fabrication

PEK support UF membranes were fabricated in the laboratory. A casting solution was prepared by dissolving 9% (w/v) PEK with a 2% (w/v) 44K polyvinylpyrrolidone additive in 98% sulfuric acid and stirring until fully dissolved. This solution was then cast as a thin film using a casting blade set to the desired membrane thickness (typically 300µm) onto a variety of substrates. A novel potential substrate Tyvek® (a non-woven polyethylene paper) was investigated (*Section 4.3.3*) although the best results were obtained when the solution was cast directly onto the glass plate. Following membrane casting the film was immersed in tap water and rinsed for one hour under running water before cutting into disks and storing in deionised water until use.

To convert the PEK support membranes into TFC membranes an *in situ* interfacial polymerisation on the membrane surface was performed. The UF support-membrane was soaked in a 0.1% (w/v) solution of the bipyridylium salt in aqueous 0.08M sodium hydroxide for 15 minutes. The membrane was then removed from the aqueous solution and excess solution was drained from the surface before it was contacted for 30 seconds with a 0.01% solution of the relevant monomer in chloroform. The composite

membrane was then rinsed with, and stored in, deionised water before being characterised.

Table 4.1: Sulfonyl chloride and isocyanate monomers and their corresponding poly-ylids

	Monomer	Poly-ylid
3.5	 <p>biphenyl-4,4'-disulfonyl chloride</p>	
3.6	 <p>4,4'-oxybis(benzene sulfonyl chloride)</p>	
3.8	 <p>4,4'-oxybis(phenyl isocyanate)</p>	

4.3.2 Membrane Characterisation

The novel PEK based TFC membranes* were analysed for their pure water flux and salt rejection properties in the same way as the PES based membranes described in **Chapter 3**. Both of these parameters can be determined by filtration of an appropriate feed solution under high pressure and monitoring the permeate volume and in the case of salt rejection, conductivity, over time. This was achieved using the previously described cross flow rig capable of pumping fluid at 1 m s^{-1} crossflow velocity across a membrane surface (membrane area = 52.27 cm^2) at a pressure of 5 bar. In addition, as a result of ylid linkage present in all of the poly-ylids (which can potentially undergo reversible protonation and deprotonation of the nitrogen depending on the conditions) studies into the effect of pH on membrane filtration were also performed. Furthermore membrane morphology was analysed using electron microscopy and initial biocompatibility tests were performed to investigate whether the hydrophilicity of the poly-ylid coatings affected protein adhesion in comparison to uncoated PEK support membranes.

*All TFC PEK membranes discussed in *Section 4.3.2* were made using laboratory-fabricated PEK support membranes cast directly onto glass.

4.3.2.1 Membrane Permeability

Figure 4.4 demonstrates the PEK membrane permeability which was determined by measuring the average deionised water flux. Using the cross-flow filtration rig (running at 5 bar transmembrane pressure, with a membrane area of 52.27cm² and a deionised water feed) the volume of deionised water permeate was measured every hour to determine the average water flux as a volume (mL) per hour. This figure was then converted to the standard units of membrane flux: L m⁻² h⁻¹.

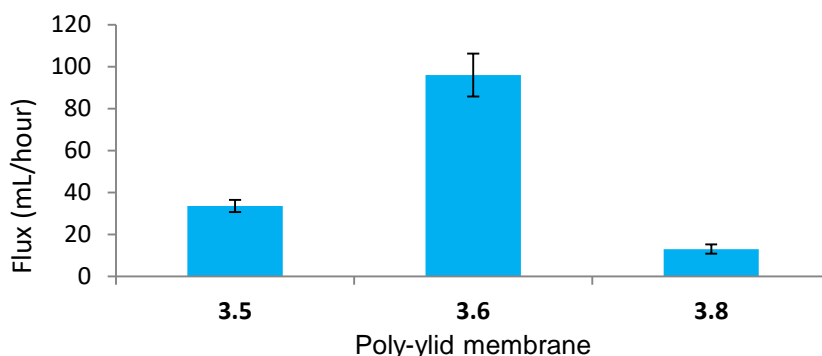


Figure 4.4: Average DI water flux (mL/hour) for composite membranes 3.5, 3.6 and 3.8 at 5 bar pressure.

Membranes **3.5** and **3.8** had low average flux rates, 33.6 mL/hour and 13 mL/hour respectively relative to membrane **3.6** which had a very high average flux rate of 96 mL/hour. Although poly-ylids **3.5** and **3.8** differ only in the bond linking the monomers i.e. a sulfonamide bond for **3.5** and a urea bond for **3.8** there is a significant difference in the flux properties of membranes coated by these polymers. As discussed in the introduction, the difference between a carbonyl and sulfonyl group can affect the properties of the support membranes used in TFC when exchanging PEK for PES which is traditionally used. Therefore it is unsurprising that what would appear to be a small difference in structure can have large effects on the poly-ylid membrane properties. Whilst the carbon and sulfur atoms have similar Pauling electronegativities (2.55 and 2.58, respectively), in poly-ylids **3.5** and **3.8** these atoms are in different oxidation states. The sulfonyl sulfur is in an oxidation state of 6+ as a result of the presence of the two oxygen atoms bonded to it whereas the carbonyl carbon atom is in an oxidation state of 4+. This means the sulfur is much more strongly electron withdrawing than the carbon therefore resulting in a more polar and more hydrophilic bond increasing membrane hydrophilicity and therefore enhancing water flux. Converting these results to standard membrane flux units (L m⁻² h⁻¹) gives the results shown in **Table 4.2** below. The active membrane area within the crossflow rig was 5.03 x 10⁻³ m². The average flux for an RO membrane in a domestic module, using the example of the RO membrane used in **Chapter 2** (information taken from

accompanying data sheet, experiments performed at 4.13 bar), is 0.38m³/d with a membrane area of 0.46m². This is equivalent to 15.83 L/hour or taking into consideration the membrane area: 34.4 L m⁻² h⁻¹. The flux data for Membrane **3.6** is comparable to the commercial membrane which has a flux value of 19.10 L m⁻² h⁻¹.

Table 4.2: Average deionised water fluxes (L h⁻¹ and L m⁻² h⁻¹) for composite membranes **3.5**, **3.6** and **3.8** at 5 bar pressure.

Membrane	Deionised water	
	Flux (L/h)	Flux (L m ⁻² h ⁻¹)
3.5	0.0336	0.40
3.6	0.096	19.10
3.8	0.013	2.59

4.3.2.2 Salt Rejection

The salt rejection properties of the membranes for both monovalent and divalent salts were measured using the protocols described for the PES membranes (see Section 3.6.3.5). All of the membranes exhibited a higher percentage rejection for the divalent salt magnesium sulfate than for the monovalent sodium chloride, which again is attributed to the larger radii of hydration for divalent anions and cations making these species less able to permeate through a membrane. For all three membranes (**3.5**, **3.6** and **3.8**) the percentage rejection was low even for the divalent salt solutions. The average percentage rejection (for all three membranes) for sodium chloride was 24% whilst for magnesium sulfate it was 46%.

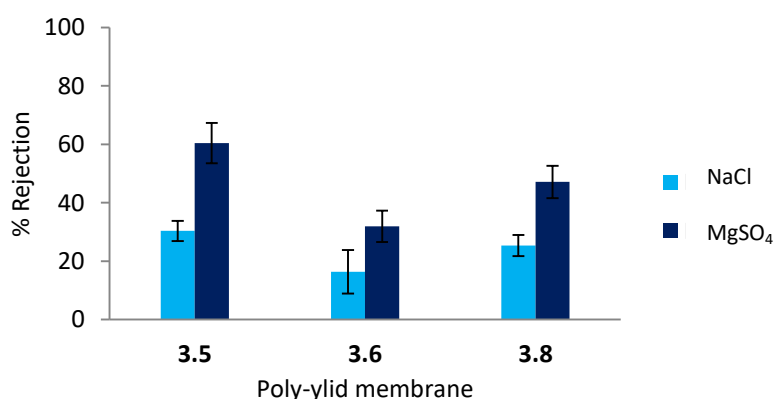


Figure 4.5: Percentage salt rejection of 500ppm NaCl and MgSO₄ solutions for composite membranes **3.5**, **3.6** and **3.8** at 5 bar pressure.

Although the rejection for both salts was generally much lower than those recorded for the PES based membranes, the difference between mono and divalent salt rejection was much less than the difference observed with the PES based membranes. For the PES membranes, excluding membrane **3.4** which had an unusually high NaCl rejection the average difference between NaCl and MgSO₄ rejection was 35% whereas for the PEK membranes this dropped to 12%.

4.3.2.3 pH Effects on Permeability

As previously discussed each of the poly-ylids contains an ylid bond adjacent to the bond formed during the polymerisation step (either sulfonamide or urea depending on the monomer) see **Figure 4.6**.

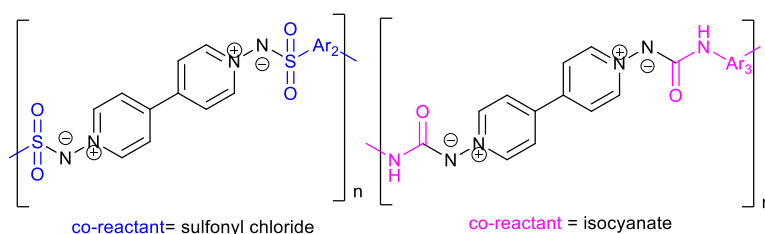


Figure 4.6: Ylid bond adjacent to bond formed in polymerisation reaction between 1,1'-diamino-4,4'-bipyridinium di-iodide and either a sulfonyl chloride or isocyanate

In neutral conditions the ylid is quite stable as a result of delocalisation of the positive charge around the aromatic ring system whilst the negative charge is stabilised by resonance with the amide carbonyl or sulfonamide sulfur-oxygen bonds or urea carbonyl group. The negatively charged ylid nitrogen is, however, susceptible to protonation in the correct conditions. For example at an acidic pH, the ylid nitrogen would be protonated, decreasing the polarity of the N-N bond. This, in turn, decreases the hydrophilicity of the ylid linkage which will reduce the membranes permeability to water. Comparison of the flux measurements performed with feed solutions of differing pH indicates that this phenomenon may affect the membrane filtration properties. All three of the PEK TFC membranes were investigated (**3.5**, **3.6** and **3.8**) at different pH values.

Figure 4.7 shows that when these membranes are used to process feed solutions at two different pH's values (4 and 10, respectively), there is a pH dependent change in flux. For membranes **3.5** and **3.6** lower flux rates were observed in acidic conditions. This is attributed to the reduced hydrophilicity caused by protonation of the ylid as discussed in **Chapter 3**. In basic conditions, the ylid nitrogen is deprotonated resulting in a more hydrophilic bond and therefore a more permeable membrane, leading to

increased flux rates in basic conditions. Membrane **3.8** showed little difference between flux rates in acidic and basic conditions. For the majority of the PEK membranes, deionised water flux was higher than for the buffered solution with the exception of membrane **3.6** which produced a higher flux with pH 10 buffered solution.

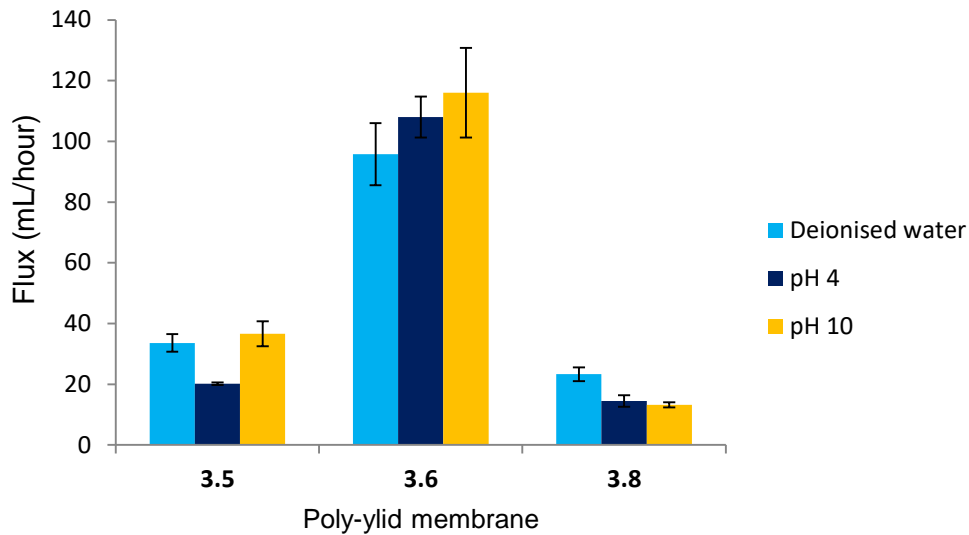


Figure 4.7: Average flux (mL/hour) for deionised water and buffered solutions at pH 4 and 10 at 5 bar pressure.

4.3.2.4 Surface Morphology

ESEM was used to image the membrane surfaces to investigate their morphology. Additionally the uncoated PEK membrane was imaged for comparison before and after coating. The uncoated surface (**Figure 4.8**) was flat and featureless and, as in the case of the other non-cross-linked poly-ylid membranes imaged in **Chapter 3**, the poly-ylid coated membranes were also flat and featureless (**Figure 4.9**).

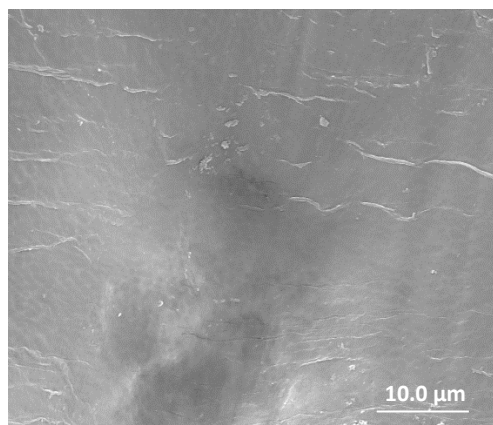


Figure 4.8: Uncoated PEK lab fabricated UF membrane (magnification x 5,000)

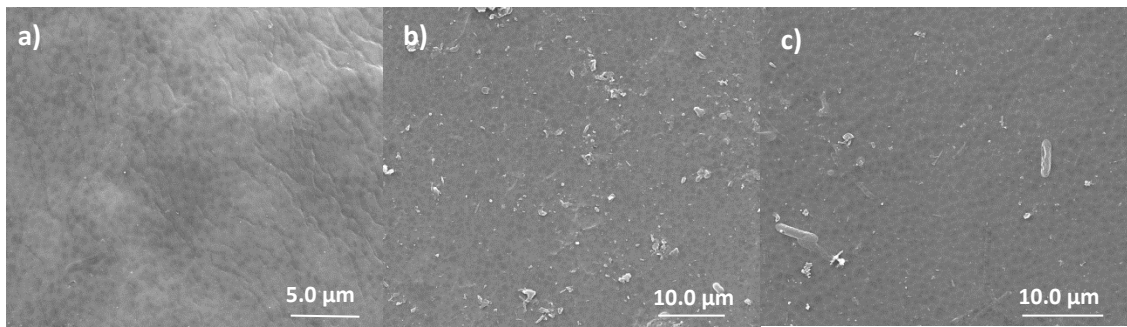


Figure 4.9: Environmental scanning electron micrograph of gold coated poly-ylid TFC PEK membranes a) **3.5** magnification x 10,000), b) **3.6** magnification x 5,000 and c) **3.8** magnification x 6,000.

4.3.2.5 Biocompatibility Testing

Initial biocompatibility studies were performed to analyse the effects of the increased hydrophilicity produced by the poly-ylid coatings relative to uncoated PEK. To analyse this, protein adhesion studies were carried out. One plasma protein was investigated: bovine serum albumin (BSA). Serum albumin is the most abundant plasma protein in humans and usually makes up approximately 55% of the plasma protein content.⁵ It is also present in oedema fluids in varying amounts depending on the mechanism of oedema formation (see *Section 1.5.7 Fluid Composition*).

As previously described coated and uncoated membrane samples were incubated at 37 °C in a 10 mg/mL protein (BSA) in phosphate buffered (PBS) solution for 24 hours. The membranes were then rinsed to remove any non-adhering protein and the samples were then heated in SDS-hydroxide to desorb the attached proteins. The resulting supernatant was analysed using the BCA assay (see **Chapter 2**) to determine the protein concentration present in each sample which was then extrapolated to estimate the protein concentration per membrane area. Control samples in protein free solutions (PBS only) were also incubated and assayed. As stated previously, calculated negative concentration values are taken to be equivalent to zero absorbance which therefore signifies zero protein present.

Figure 4.10 shows the calculated protein concentration (mg/mL) present in 25 μ L of supernatant from the protein desorption step following 24 hours incubation in a 10 mg/mL BSA solution. The uncoated PEK support membrane has an average concentration of 1.06 mg/mL. All three coated membranes showed a decrease in protein concentration relative to the uncoated membrane. Poly-ylid **3.5** gave the largest decrease in protein concentration with an average of 0.53 mg/mL which was equivalent to a 50% decrease relative to the uncoated PEK membrane. Poly-ylid **3.8** produced a decrease of 39% whilst poly-ylid **3.6** produced a decrease of 30%.

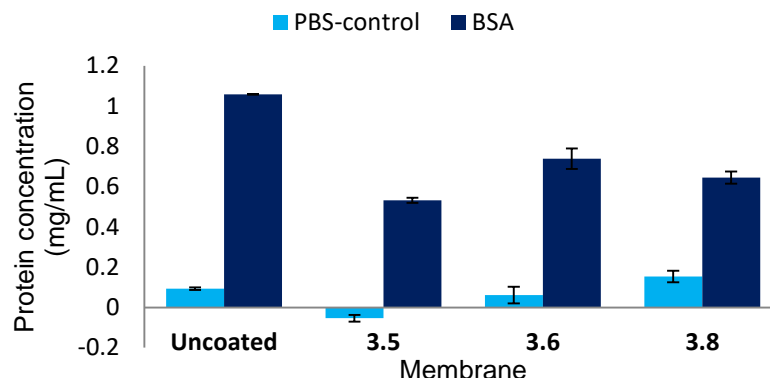


Figure 4.10: Calculated average BSA protein concentration mg/mL in 25 μ L samples from SDS-OH supernatant.

The data collected from the assay was used to estimate the protein concentration per membrane area (see **Table 4.4**). The uncoated membranes had the highest protein concentration per membrane area at 0.54 mg/cm² so that all three PEK TFC poly-ylid membranes were able to reduce protein adhesion relative to an uncoated control. Membrane **3.5** reduced the protein adhesion the most with a reduction in concentration of 50%. Membranes **3.6** and **3.8** produced smaller reductions in protein concentration of 30% and 39%, respectively.

Table 4.4: Calculated BSA protein concentration per membrane area

Membrane	Protein concentration per membrane area (mg/cm ²)
Uncoated	0.54
3.5	0.27
3.6	0.37
3.8	0.32

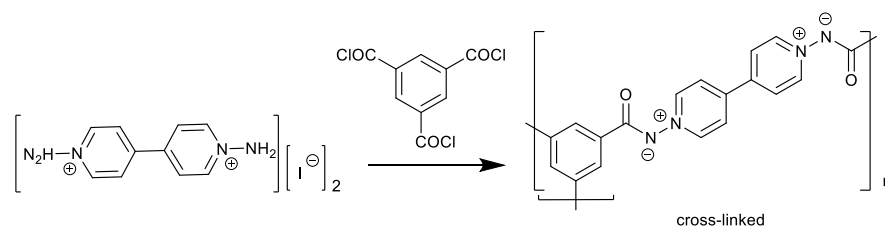
4.3.3 PEK Support Membrane Optimisation

In addition to examining a novel backing paper support (Tyvek®) a post-membrane casting treatment known to increase membrane crystallinity was explored in an attempt to optimise PEK membrane performance.

4.3.3.1 Backing Paper Exploration

Whilst casting PEK directly onto glass created more reproducible membranes, a true thin-film composite nanofiltration membrane requires a solid support layer to enable it to withstand the high pressures of the nanofiltration process. The polyethylene based material Tyvek® was explored as a potential backing paper as a result of its resistance to the concentrated sulfuric acid require to cast the PEK films. The Tyvek® backed

PEK membranes were coated with Poly-ylid **3.1** (**Scheme 4.1**, see **Chapter 3**) via an *in situ* polycondensation reaction between the bipyridylium salt and trimesoyl chloride to create thin film composite nanofiltration membranes.



Scheme 4.1: *In situ* polycondensation between bipyridylium salt (in aqueous solution, soaked into membrane) and trimesoyl chloride (in organic solution, contacted with membrane surface for 30 seconds) to produce poly-ylid **3.1**.

As previously described these composite membranes were then analysed for water flux and salt rejection properties. The glass-cast TFC membrane had a higher average flux than the membrane cast onto Tyvek® - 82 mL/hour and 42.5 mL/hour, respectively (**Figure 4.11**).

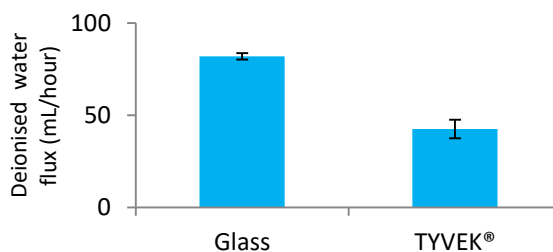


Figure 4.11: Deionised water flux (mL/min) for composite membranes using poly-ylid **3.1** on glass and Tyvek® at 5 bar pressure.

In salt rejection studies the Tyvek® membranes performed slightly better than the glass-cast producing higher percentage rejections for both sodium chloride and magnesium sulphate (**Figure 4.12**) with a NaCl rejection of 33% and an $MgSO_4$ rejection of 46% when compared to 28% (NaCl) and 32% ($MgSO_4$) for the glass-cast membrane.

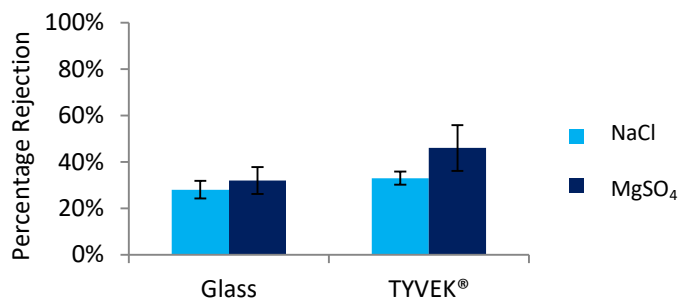


Figure 4.12: Percentage salt rejection of 500 ppm NaCl and $MgSO_4$ solutions for composite membranes using poly-ylid **3.1** on glass and Tyvek® at 5 bar pressure.

4.3.3.2 PEK Crystallisation

PEK membranes cast onto TYVEK® backing paper (see *Section 4.3.1*) were heated in deionised water for 1 hour at 60 °C to remove residual PVP. Following the procedure developed by Colquhoun³ the membrane was then heated in a mixture of acetone, methanol and glycerol (70:20:10) and stirred under reflux at 56 °C for 30 minutes. Following this the membranes were removed and allowed to dry in air overnight, leaving the membrane pores coated with glycerol to promote subsequent re-wetting.

Samples of both crystallised and non-crystallised PEK were removed from the backing paper, extracted with water to remove the glycerol, dried and analysed by differential scanning calorimetry (DSC, **Figure 4.13**). In the non-crystallised sample a crystallisation peak (exothermic) occurs at around 175 °C, and additionally there is evidence of a glass transition (T_g) just before crystallisation at around 150 °C. The T_g in the crystallised sample occurs at a slightly higher temperature of around 160 °C. Both samples demonstrate a strong crystal melting peak (endothermic) at ca. 360 °C.

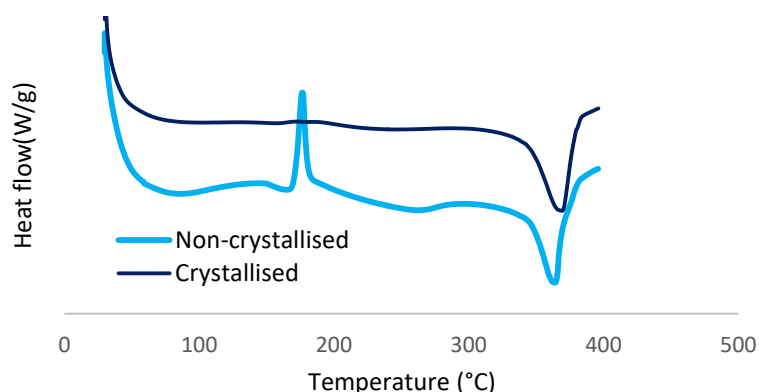


Figure 4.13: DSC thermograms of crystallised and non-crystallised PEK UF membrane.

4.3.3.3 Characterisation of Crystallised PEK Membranes

As for the PEK thin film composite membranes PEK support membrane, permeability was determined by measuring the average deionised water flux. Since the PEK support is essentially an ultrafiltration membrane, lower pressures are required than for the nanofiltration thin film composite membranes. Using the stirred cell (running at 1 bar transmembrane pressure, with a membrane area of 31.66 cm² and a deionised water feed) the volume of permeate was measured every hour to determine the average water flux as a volume (mL) per hour and this value was then converted to the standard units of membrane flux; L m⁻² h⁻¹. The crystallisation process reduced the flux by a half from 0.25 L/h to 0.12 L/h suggesting a reduction in pore size as observed in previous work.³

Table 4.5: Average deionised water flux ($L h^{-1}$ and $L m^{-2} h^{-1}$) for non-crystallised and crystallised PEK UF membranes at 1 bar pressure.

Membrane	Deionised water Flux (L/h)	Deionised water Flux ($L m^{-2} h^{-1}$)
Non-crystallised	0.25	7.93
Crystallised	0.12	3.89

Additionally membrane molecular weight cut-off (MWCO) was investigated via filtration of polyethylene glycol (PEG) standards of known molecular weight. The permeate collected was analysed by GPC and the chromatogram produced was compared with that of the unfiltered PEG standard to determine whether the crystallisation process affected the pore size therefore affecting what permeates through. MWCO is defined as the lowest molecular weight solute of which 90% is retained by the membrane (conventionally in units of Daltons).⁶

For both a 6K and 35K PEG standard the amount of PEG present in the permeate following filtration with the crystallised membrane was significantly less than in the permeate obtained from filtration with the non-crystallised membrane (**Figure 4.15**) again suggesting a reduction in membrane pore size as a result of crystallisation.

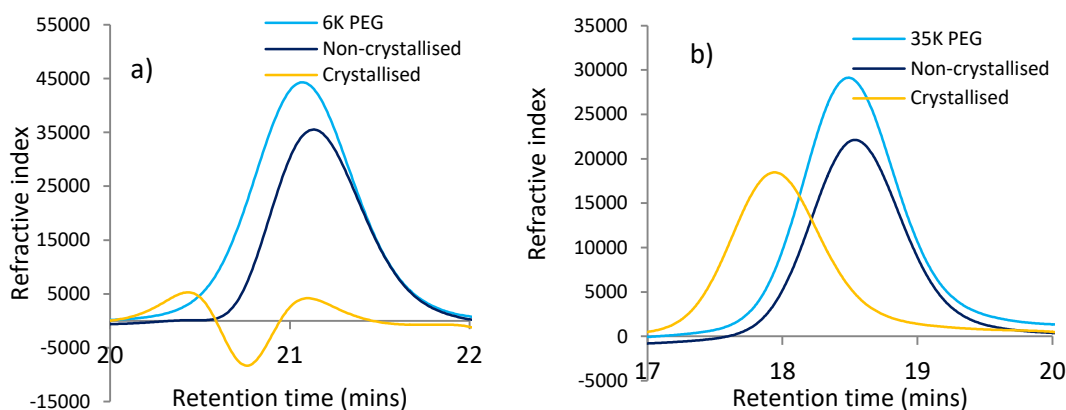


Figure 4.14: GPC chromatograms of a) unfiltered 6K PEG standard and filtrate from both non-crystallised and crystallised PEK membranes b) unfiltered 35K PEG standard and filtrate from both non-crystallised and crystallised PEK membranes.

Calculating the percentage retention of both the non-crystallised and crystallised PEK membranes and comparing the percentage retention with a commercial membrane with a known MWCO gave an indication of the fabricated membranes approximate MWCO (**Figure 4.15**). The commercial membrane with a known MWCO of 10K retained 100% of the 100K PEG, as did both PEK membranes. The 10K membrane

also retained 89% of the 35K PEG and 46% of the 6K PEG. The lab fabricated PEK membranes, however, retained less of the lower MW PEG samples suggesting they have a higher MWCO than 10K and lower than 100K. Comparing the percentage retention for the 35K PEG, the crystallised membrane retains a higher percentage (38%) with respect to the non-crystallised membrane (31%) again suggesting the crystallisation process reduces the membrane pore-size.

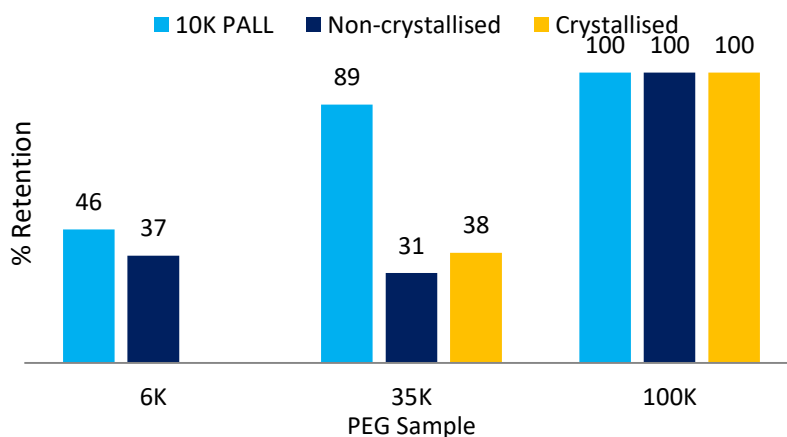


Figure 4.15: Percentage retention of different molecular weight PEG samples by a 10K commercial membrane and two lab fabricated PEK membranes (non-crystallised and crystallised). Note: % retention not calculated for crystallised PEK, 6K PEG as a result of negative peak interference (see **Figure 4.14**).

4.3.3.4 Interfacial Polycondensation on a Crystallised PEK Membrane

Both non-crystallised and crystallised PEK membranes were coated using the procedure described in *Section 4.3.1*. However the bipyridylum salt was replaced by *m*-phenylenediamine which is traditionally used in combination with trimesoyl chloride to form polyamide coated TFC nanofiltration and reverse osmosis membranes. Additionally a commercial 10K MWCO PES membrane was coated for comparison. Following the standard procedure the commercial UF membrane produced TFC membranes with low salt rejection (26% for sodium chloride) so the coating method was modified to increase the amine solution concentration to 2%. Additionally the membrane was pre-treated with a 10% ethanol solution to improve amine wetting and following coating the membrane was oven dried for 5 minutes at 50 °C which improved the sodium chloride rejection to 95%. Attempts to repeat this modified procedure with the PEK membranes proved unsuccessful and the polyamide coatings produced were shown to be severely defected by SEM. An alternative pre-treatment to improved PEK membrane wetting was investigated; soaking the membranes in 10% aqueous acetone which when applied to a crystallised PEK membrane which then was coated following the modified procedure (involving an increased diamine concentration and oven drying step) produced a membrane with 26% sodium chloride rejection.

Initial attempts to optimise the PEK membranes have shown that small modifications to the membrane fabrication procedure can have significant effects on membrane performance and further work is required in order to develop solvent resistant membranes with properties which rival existing membrane systems.

4.4 Conclusions

Three novel poly-ylids synthesised in **Chapter 3** were used to create solvent resistant thin film composite nanofiltration membranes based on a lab-fabricated polyetherketone support. The TFC membranes were characterised in terms of their deionised water flux and salt rejection properties and were found to perform reasonably well. Additionally the effect of feed solution pH was investigated and it was found that (as for the PES based TFC poly-ylid membranes in **Chapter 3**) the flux could be affected by pH, with generally lower fluxes in acidic conditions which is attributed to the reduced hydrophilicity or increased internal hydrogen-bonding as discussed earlier, caused by ylid protonation which in turn would reduce the membrane permeability to water. In basic conditions, the ylid nitrogen is deprotonated resulting in a more hydrophilic bond and therefore a more permeable membrane, hence then increased flux rates in basic conditions. Furthermore membrane surface morphology was investigated by scanning electron microscopy and it was found that the poly-ylid coating formed a flat and featureless film on the PEK surface. Initial biocompatibility testing found that all three PEK TFC poly-ylid membranes were able to reduce protein adhesion relative to an uncoated PEK support membrane.

Initial studies into PEK membrane optimisation found that adding a support layer to the PEK membrane to strengthen it could also improve its salt rejection properties when compared with a PEK film cast directly onto glass. The additional layer does reduce the average flux.

Some preliminary work into PEK crystallisation to improve solvent resistance properties demonstrated that the previously reported crystallisation process can be used to increase PEK membrane crystallinity and will also reduce the membrane pore size therefore reducing flux and lowering the MWCO as explored by PEG filtration coupled with GPC analysis.

Attempts to coat the non-crystallised and crystallised PEK membranes with a polyamide layer to form thin film composite membranes have shown that a modified procedure is required when working with these novel PEK support membranes but it

has also been demonstrated that small modifications in the membrane fabrication procedure can have significant effects on membrane performance.

4.5 Future Work

Further research into the work carried out in this chapter could include further optimisation of the PEK support membranes including developing a protocol for reproducible membrane fabrication using the additional backing paper support which was omitted for the TFC membranes analysed in the first sections of the chapter. This would strengthen the membranes and allow them to better withstand the high pressures used in nanofiltration. Additionally the protocol for coating onto these supported PEK membranes requires optimisation again to ensure reproducible results. Finally, since these membranes have been designed to be solvent resistant; filtration studies examining flux and rejection in organic solvents could also be performed to test membrane performance in conditions which standard nanofiltration membranes would fail.

4.6 Experimental

4.6.1 Materials

The following materials were sourced from Fisher Scientific UK Ltd (Leicestershire, UK); Pierce™ BCA Protein assay kit (containing; Reagent A - bicinchoninic acid, Reagent B - 4% (w/v) copper sulfate, 2mg/mL albumin standard ampules), 96-well flat-bottomed microplates and micrometre feeler gauges. The membrane casting blade was obtained from Mitutoyo (Japan). The PEK was grade 220P (ex ICI plc.). And the Tyvek® paper was purchased from Spenic Ltd (Gloucestershire, UK). The remaining materials; acetic acid, bovine serum albumin, chloroform, hydrochloric acid, magnesium sulphate, phosphate buffered saline, sodium chloride, sodium dodecyl sulfate, sodium hydrogen carbonate, sodium hydroxide, and concentrated sulfuric acid were obtained from Sigma Aldrich (Dorset, UK) .

4.6.2 Equipment

The following equipment was sourced from Fisher Scientific UK Ltd (Leicestershire, UK); conductivity meter, disposable glass test tubes, Eppendorf tubes (0.5, 1.5 and 2 mL), micropipettes (1000 µL and 200 µL) and tips, NMR vials with polyethylene lids.

Nanofiltration experiments were carried out using a custom built cross-flow rig. Conductivity measurements were made using a calibrated conductivity meter

Electron micrographs were obtained using an FEI Quanta FEG 600 Environmental Scanning Electron Microscope (ESEM). Samples were sputter coated with gold before imaging with high vacuum ESEM.

Absorbance data was collected using a FLUOstar Omega Microplate Reader. Samples and standards were transferred to a clear flat-bottomed 96-well microplate before the absorbance was read at 562 nm. In both cases the samples and standards underwent an assay before the absorbance was read (described in Section 3.6.3.7).

4.6.3 Methods

4.6.3.1 PEK Thin-film composite membrane fabrication

Two steps were required to prepare PEK-TFC membranes; 1) To create PEK support membranes a casting solution was prepared by adding PEK polymer beads (9 wt%) to the solvent [conc. sulfuric acid (89 wt%) + 44K PVP (2 wt%)] which was then stirred in a sealed vessel until fully dissolved. Following this, thin films were cast from the polymer solution either directly onto glass or onto the backing paper (Tyvek®) which was taped to the glass plate. Approximately 25 mL of membrane casting solution was poured onto the glass/backing paper and a casting blade set to the desired membrane thickness (300 µm as standard) was used to create a thin film of polymer solution, following this the glass plate (with the backing paper if being used) and polymer film was then immersed in water. The resulting membrane was rinsed for one hour under running water before cutting into disks and storing in DI water.

2) The second step involved coating the PEK support membrane with a thin film of poly-ylid. The PEK support-membrane was soaked in a 1% (w/v) solution of *m*-phenylenediamine in aqueous 0.08M sodium hydroxide for 15 min. The membrane was then removed from the aqueous solution, drained and allowed to stand briefly in air before the surface was contacted for 30 s with a 0.1% solution of the relevant monomer in chloroform. The composite membrane was then rinsed with, and stored in, DI water before being characterised. Modifications to this second step included 1) Pre-treating the membranes by soaking in 10% aqueous acetone solution before interfacial polymerisation, 2) increasing the amine concentration to 2% and 3) oven drying the membranes for 5mins at 50°C following interfacial polymerisation.

4.6.3.2 Membrane Flux Determination

See **Chapter 3**

4.6.3.3 Membrane Salt Rejection Determination

See **Chapter 3**

4.6.3.4 pH Effects on Permeability

See **Chapter 3**

4.6.3.5 Biocompatibility Testing

See **Chapter 3**

4.6.3.6 PEK Crystallisation

Lab-cast PEK membranes were heated in deionised water for 1 hour at 60 °C to remove any remaining PVP additive, after which they were crystallised using a procedure described by Colquhoun.³ The membranes were added to a mixture of acetone, methanol and glycerol (7:1:2) and this solution was heated under reflux at 56 °C for 30 minutes, after which the membranes were removed from the solution and allowed to air dry overnight.

4.6.3.7 PEK Crystallinity Investigation via DSC Analysis

Samples of both crystallised and non-crystallised PEK were separated from the backing paper, compressed into pellets and placed into pre-weighed DSC pans. The pan lids were sealed and the samples were loaded into the DSC instrument. The samples were heated from 30-400 °C at a ramp rate of 10 °C per minute under a nitrogen atmosphere.

4.6.3.8 MWCO Analysis

Gel permeation chromatography (GPC) was used to estimate the MWCO of the PEK membranes before and after the crystallisation process. Stock standard solutions of known MW PEG's (6K, 35K and 100K) were prepared using the GPC mobile phase (0.1% w/v) and stirred overnight to ensure complete dissolution. A fraction of each standard solution was retained for GPC analysis as a control whilst the remainder of each PEG solution was filtered through the membrane being analysed (i.e. non-crystallised or crystallised PEK) using the stirred cell under 1 bar pressure. The first

few mL of permeate were discarded for each PEG solution and the membrane was rinsed with GPC mobile phase between PEG solutions.

Following this a sample of each individual standard or sample solution was manually injected into the GPC and run through the column (a PL-Aquagel column fitted with a 5 μ m guard column) at a rate of 1 mL/min after first being filtered through a 1.5 μ m nylon syringe filter. All runs were conducted at 40 °C and the samples were detected by and refractive index detector. Data capture and subsequent analysis were carried out using Agilent GPC software.

4.7 References

1. P. T. Mcgrail and P. T. Mcgrail, *Polym. Int.*, 1996, **41**, 103–121.
2. H. M. Colquhoun, K. Roberts, A. Simpson, and T. Taylor, in *Effective Membrane Processes - New Perspectives*, Mechanical Engineering Publications Ltd, 1993, pp. 371–380.
3. H. Colquhoun, UK Pat. 2285261, 1995, to Northwest Water PLC.
4. H. M. Colquhoun, A. F. Simpson, and V. Rogers, WO Pat. 95/15809, 1995, to Northwest Water PLC.
5. N. L. Anderson, *Mol. Cell. Proteomics*, 2002, **1**, 845–867.
6. A. Idris, N. Mat Zain, and M. Y. Noordin, *Desalination*, 2007, **207**, 324–339.

Chapter 5 – Device Prototype Design, Fabrication and Testing

5.1 Abstract

Several prototypes were designed, fabricated and tested to obtain proof-of-concept for the medical device proposed, but not exemplified, by US Patent 8, 211, 053 B2 (interosmolar fluid removal)¹. This was achieved with the assistance of fundamental research into draw solutions, membranes and using forward osmosis to transport both fluid and macromolecules carried out in **Chapters 2-4**. Following the design and fabrication of the prototypes they were tested in both an *in vitro* and *ex vivo* oedema model. For the latter, a porcine perfused-limb system was developed to simulate the condition of oedema. Additionally plans for future design optimisation and manufacture of a biomedical device based on the present work were developed, requiring consultation with a design house and manufacturer, both specialising in medical devices.

5.2 Introduction

The research motivation for this project was to develop an implantable medical device to treat oedema and lymphoedema. After researching membrane materials, draw solutions and the transport of fluid and proteins through membranes, as described in **Chapters 2-4**, device design and testing were investigated. Several prototypes were designed and fabricated for testing within a perfused limb oedema model developed specifically for this project.

As outlined in **Chapter 1**, the device concept was based on a US patent licenced to BioInteractions Ltd for interosmolar fluid removal.¹ This patent proposed, but did not exemplify, the idea of an implantable medical device based on a semipermeable membrane compartment containing trapped osmotic solutes which can act as a draw solution. The described device would function by removing abnormally accumulated fluid in the tissues surrounding the medical device, allowing them to be drained from the body via a tube in communication with an external reservoir (**Figure 1.1**). Current treatments for such oedemic conditions rely on complex manual therapies involving massage, bandaging and exercise in an attempt to direct accumulated fluid towards an area in the body where drainage is not comprised. In extreme cases, when the affected tissue is damage beyond repair, surgery is required. Additionally pharmaceutical interventions are often required such as the use of diuretics in an attempt to reduce fluid accumulation. The main advantage of the proposed osmotic approach is that the fluid is removed directly and does not require harsh suction or pumping which may

exacerbate the condition, thereby offering an alternative option for a currently unmet clinical need.

In the present project, device design was investigated by the development of simple prototypes to obtain proof-of-concept through testing with in both *in vitro* and *ex vivo* models. Whilst the patent proposed possible device configuration and components, practical factors were not considered. These included:

- The method of implantation and subsequent removal of the device as required. Ideally both processes being as minimally invasive as possible;
- the necessity of replenishing the draw solution once saturated.

The prototypes also had to be reproducible, both in fabrication and mode of action and simple to make whilst also providing as large a membrane surface as possible area for efficient fluid transport. Two generations of prototypes were made. The 1st generation prototype was based on a simple membrane pouch and the 2nd generation was based on a sealed membrane cylinder with a double lumen outlet/inlet tube (**Figure 5.1**).

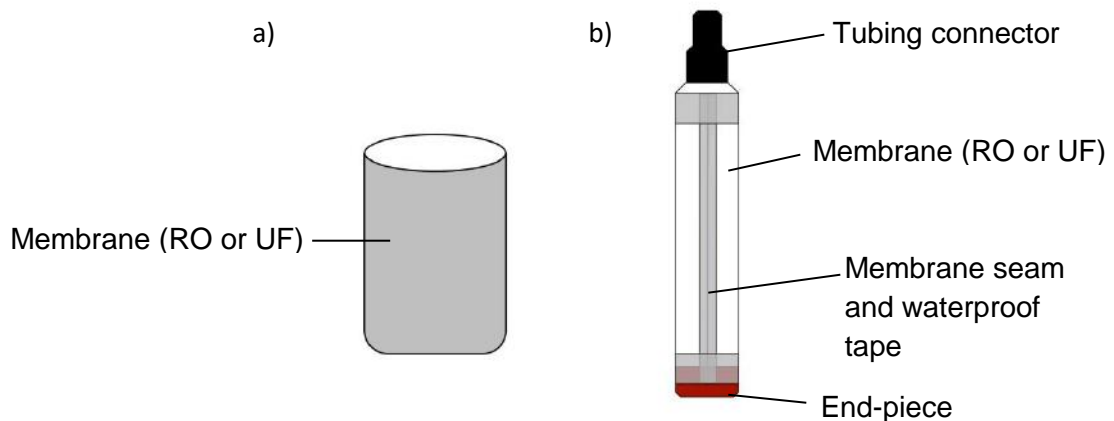


Figure 5.1: a) 1st Generation prototype, b) 2nd Generation prototype.

Alongside designing and fabricating the prototypes, *in vitro* and *ex vivo* models were then developed. The *in vitro* model was based on an extremely simplified system. This involved suspending the prototype in a beaker containing the chosen feed solution and monitoring the feed and draw solution volumes. The *ex vivo* model was significantly more complex involving inducing oedema in a porcine hind limb, from a freshly-slaughtered animal, via perfusion of a physiological salt solution through the femoral artery which creates fluid accumulation in the surrounding tissues. This occurs as a result of the oncotic pressure difference between the perfused salt solution within the circulatory system which, although isotonic, contains no proteins, and the surrounding tissues which contain proteins (*Section 1.5.2*). The oncotic pressure difference causes

large volumes of fluid to move from the blood vessels into the surrounding tissues where it accumulates. Matheis *et al.* have shown that rat hind limb perfusion using a solution without colloid osmotic pressure (i.e. not containing macromolecules) produces severe limb oedema and that including macromolecules with a molecular weight similar to albumin should prevent oedema occurring.² Similarly Fisher *et al.* have shown that perfusion of isolated ventilated rat lungs with a Krebs physiological salt solution results in alveolar oedema within 40-85 minutes, however the addition of bovine serum albumin can prevent oedema formation for up to 5 hours.³ Whilst, to the author's knowledge, no *ex vivo* model exists to simulate oedema, however porcine perfused limbs have been used for transdermal adsorption studies⁴ and for pharmacokinetic studies.⁵

In the *ex vivo* perfused limb model developed during the project a peristaltic pump was used to perfuse a porcine limb with a physiological salt solution (Krebs solution) to create the oedema (as a result of the oncotic pressure difference, described previously). Following which an incision was made to create a cavity to accommodate the device. After implantation the opening was sealed using a cyanoacrylate adhesive. **Figure 5.2** shows schematics of both the *in vitro* and *ex vivo* models and demonstrates the movement of fluid into the prototype devices as a result of the encapsulated osmotic agents.

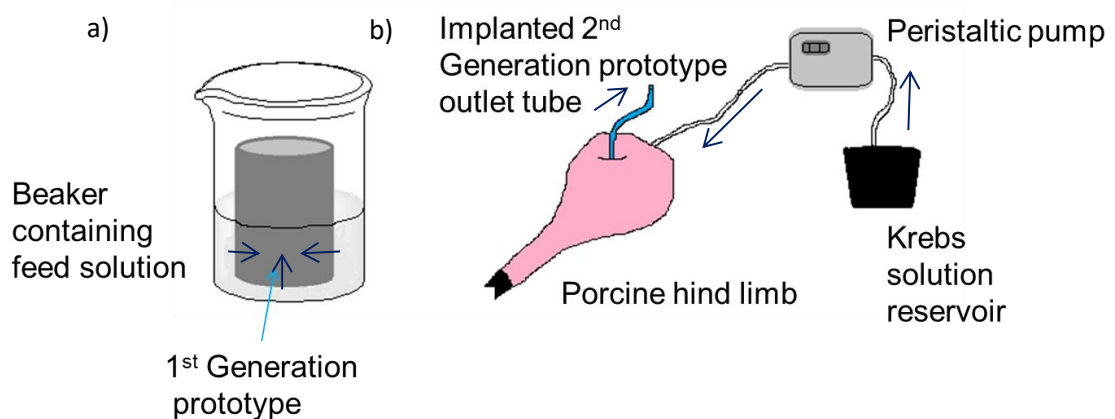


Figure 5.2: a) *In vitro* model testing of 1st Generation prototype, b) *ex vivo* model testing of 2nd Generation prototype, dark blue arrows show direction of fluid flow.

5.3 Results and Discussion

5.3.1 Prototype Design

The basic design of the system encompasses two main parts, an implanted device and an external reservoir. The implanted device consists of a semipermeable membrane containing trapped osmotic solutes which act as a draw solution for accumulated fluid in tissue surrounding the implant (see **Figure 5.3**). The implanted portion of the device is in communication with the external portion, a fluid reservoir, via a tube connected to a transdermal port allowing for fluid collected within the implanted device to be drained and removed.

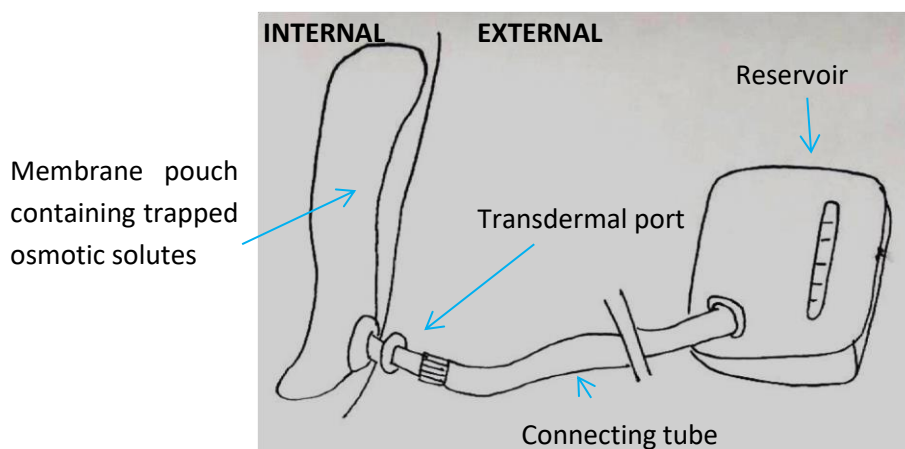


Figure 5.3: Schematic representation of the components of the proposed implantable membrane device (and external reservoir) for the treatment of oedema.

Several different designs were proposed based around the general device concept depicted in **Figure 5.3**. A key consideration was the implantable pouch portion which was required to fulfil several design considerations including:

- **Material limitations** - the majority of the pouch must be made from membrane and additionally must be made from biocompatible materials and suitable for sterilization;
- **Collapsible design** - to aid minimally invasive implantation procedure without compromising large surface area required for rapid fluid exchange across the membrane;
- **Connected to exterior** - through transdermal port;
- **Maximum possible membrane area** - to ensure efficient exchange of fluids across the membrane surface.

Figure 5.4 below illustrates some of the proposed designs which were used to discuss the prototype with a design house, Hunt Developments Ltd.

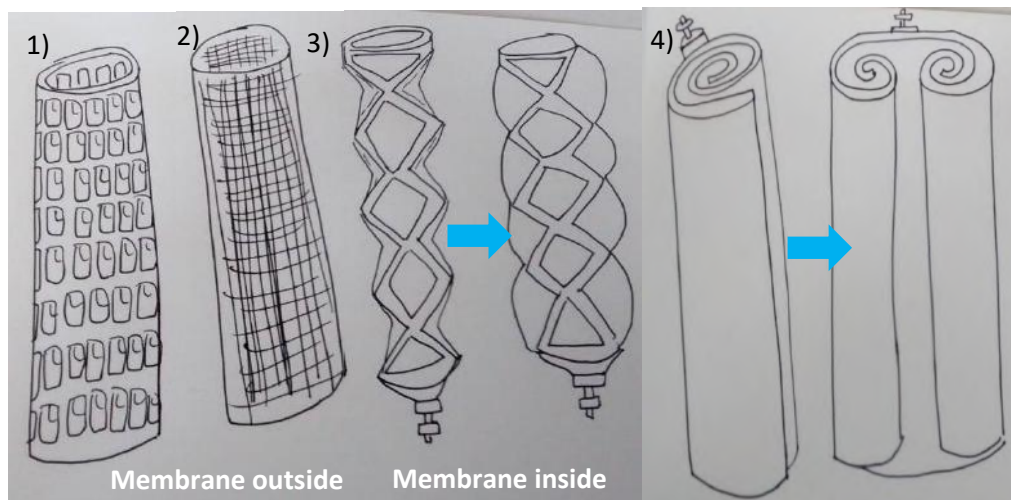


Figure 5.4: Sketches showing potential device designs 1) Silicone/thermoplastic polyurethane solid support 2) Stainless steel mesh, rigid solid support 3) Membrane pouch within silicone/thermoplastic polyurethane rigid solid support 4) Membrane pouch without a solid support inserted in a spiral-wound form.

5.3.2 Prototype Fabrication

In order to explore the device capability first a simplified prototype was made based on the implanted pouch component of the device. Two different membrane materials were investigated and a number of different adhesive options were also explored. After *in vitro* tests with this system a more sophisticated second generation prototype was made with a connecting tube – suitable for implantation within the perfused limb model.

5.3.2.1 1st Generation Prototype

The 1st Generation prototypes were based on simple square pouches of membrane which were filled with a known volume of draw solution and suspended in a beaker of either deionised water (control) or Krebs physiological salt solution (Section 5.6.3.2). The membrane pouches were made by adhesive bonding of two rectangles of membrane along three sides, with the membrane active layer facing out (**Figure 5.5**).

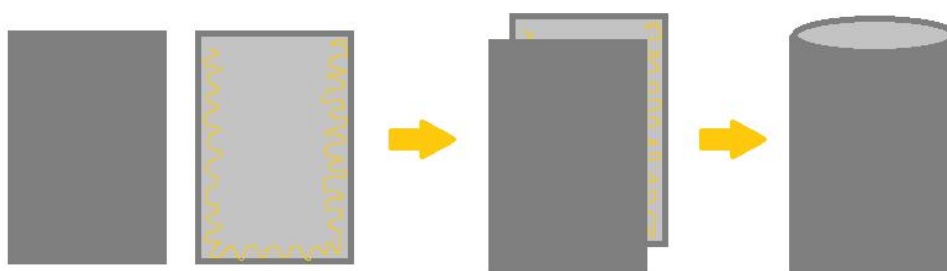


Figure 5.5: Schematic of Membrane pouch fabrication.

A number of different membrane materials, adhesives and draw solutions were investigated in the fabrication of the 1st generation prototypes. Both ultrafiltration membranes (lab-cast polyethersulfone, PES) and a reverse osmosis membrane (thin film composite membrane consisting of polysulfone coated with ultrathin layer of polyaramid) were explored. The different materials used dictated the draw solutions which could be used and also affected what could be transported. For example, using a non-porous RO membrane would only allow transport of water across the membrane and could be used in combination with a traditional salt based draw solution whilst using a porous UF membrane enabled solutes within the feed solution to be transported along with the fluid as demonstrated in **Chapter 2** where high molecular weight polyethylene glycols and proteins were transported by osmosis through porous UF membranes. As a consequence of the porosity of the membrane a salt based draw solution was no longer suitable due to backflow of the salt into the feed. An alternative approach explored in **Chapter 2** was the use of high molecular weight polyelectrolyte draw solutions (5% 225K sodium polyacrylate). The final component in membrane pouch fabrication was the adhesive. A good seal was essential to allow the prototype to function effectively. Both hot-melt, epoxy and cyanoacrylate adhesives were explored. The hot-melt material was found to damage the membrane and the epoxy was difficult to work with therefore the cyanoacrylate adhesive was chosen for the 2nd generation prototypes.

5.3.2.2 2nd Generation Prototype

A more sophisticated prototype suitable for implantation within the perfused limb was developed consisting of a sealed 'membrane tube' connected to silicone tubing with a double lumen, allowing for both draw solution injection (following device implantation) and fluid withdrawal by forward osmosis. The tube was created by cutting a sheet of membrane to size (either RO or UF) and placing it around a cylindrical former before sealing with waterproof tape. The tape seams were further reinforced through additional sealing using cyanoacrylate adhesive. After sealing and removing the former the membrane tube ends were closed; one with a plastic end-piece and the other with a plastic tubing connector which were both also taped and glued into place. The prototypes were allowed to cure overnight before being tested for leaks by filling with DI water, after which a double lumen silicone tube (i.e. two tubes one inside the other) was connected to the device. **Figure 5.6** shows both a schematic and an image of the completed 2nd generation prototype.

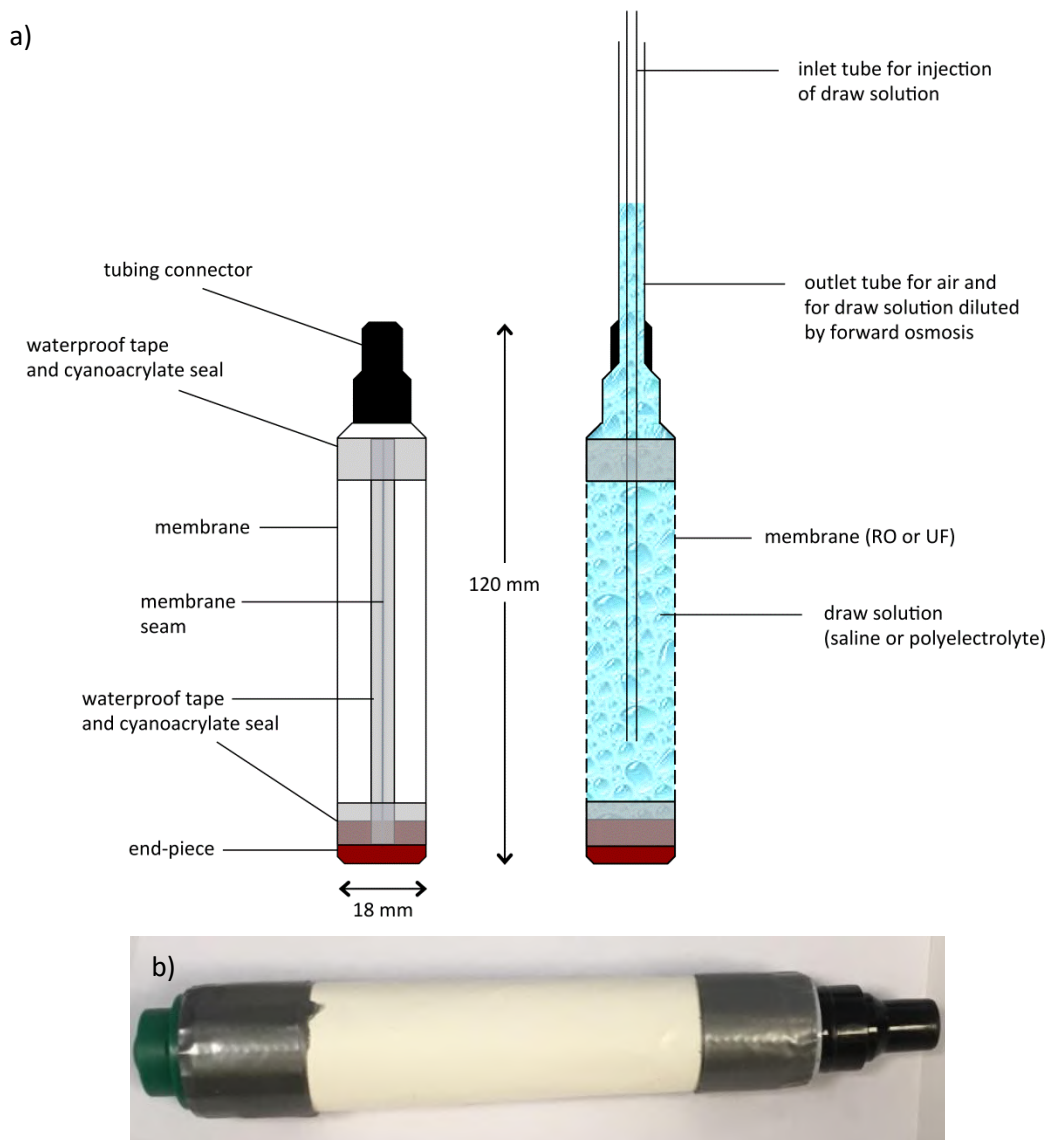


Figure 5.6: a) 2nd generation prototype device schematic b) 2nd generation prototype device (RO, membrane) based on sealed membrane tube capped at each end with end-piece and connector for double lumen tubing, active membrane area approximately 14 cm².

Fluid monitoring was achieved through over-filling the device so that the meniscus of the draw solution was visible in the tubing; this level was marked and was designated the starting point. Once the device was submerged into a reservoir containing the feed solution, any fluid moving into the device across the membrane increased the fluid level resulting in the meniscus rising (**Figure 5.7**).



Figure 5.7: 2nd Generation prototype device (RO membrane, saline draw).

Two versions of the second generation prototype were constructed: 1) using a commercial RO membrane (taken from a domestic RO module) and tested with a range of sodium chloride draw solutions of different concentrations and 2) using a 10K MWCO PES UF membrane with a 5% 225K sodium polyacrylate draw solution.

5.3.3 Prototype Testing

Two methods of prototype testing were developed. The first involved a simple 'bench-top' *in vitro* system, as outlined above, and the second a significantly more complex perfused limb model designed to simulate the condition of oedema.

5.3.3.1 *In vitro* testing

For the basic bench-top tests a beaker was filled with the chosen feed solution: either deionised water as a control or the physiological Krebs solution. The prototype device was suspended within the beaker and filled with the chosen draw solution. The subsequent change in draw volume was measured every hour either by direct measurement for the 1st generation membrane pouches (i.e. pouring into a measuring cylinder) or by measuring the change in fluid height within the tubing for the second generation prototypes.

1st Generation Prototype *In vitro* Testing

The 1st generation prototypes were based on an extremely simplified design consisting of a square or rectangular pouch sealed on three sides, but left open along the top edge. A draw solution of a known concentration and volume was added through this opening and the pouch was suspended in the chosen feed solution (**Figure 5.8**). The

volumes of both the feed and draw solution were monitored over time. Many problems were encountered when testing these simple prototypes due to issues with obtaining a watertight seal and many experiments were terminated when the pouches were found to have failed. However, these preliminary studies provided important information when considering the design and fabrication of the 2nd Generation prototypes. Additionally it was clear that although the simple square design could provide the large surface area necessary for efficient membrane exchange the shape was wholly unsuited to testing in the perfused limb model and also was difficult to seal efficiently. Furthermore the shape produced other problems related to the internal volume of the pouch which was vastly reduced following the application of the adhesive due to the subsequent 'seam' formation. Attempts to create this necessary internal volume capable of accommodating both draw and permeating feed by adhering membrane sheets around a shaped 'former' also failed due to the inflexibility of the membrane material which could not be shaped without creasing damaging the membrane surface and creating folds which were then difficult to seal.

Studies focused on testing the optimal polyelectrolyte draw solution 5% 225K NaPA determined by experiments discussed in **Chapter 2**. Two membrane materials were compared; commercial RO membrane and lab-cast PES ultrafiltration membrane. In both experiments flux was observed despite the system being unstirred, unlike the procedure described in **Chapter 2**. This key result was necessary for proof of device concept as the implanted system would necessarily be static.



Figure 5.8: Membrane pouch containing draw solution suspended in beaker of DI water, from above and side view.

Comparing the lab-cast PES UF membrane with the commercial RO membrane (**Table 5.1**) the latter produced a higher flux rate (almost tenfold) despite being non-porous whilst the lab-cast PES membrane contains large pores due to the phase inversion

process. This unexpected result confirmed it was worthwhile investigating both RO and UF membrane devices in the 2nd generation prototypes.

Table 5.1: 1st Generation prototype *in vitro* testing average flux results.

Pouch Material	Sealant	Draw solution	Average Flux (mL/hour/cm ²)
Lab-cast PES	Hot melt adhesive	5% 225K NaPA	0.055
RO membrane	Epoxy resin	5% 225K NaPA	0.31

2nd Generation Prototype *In vitro* Testing

Since the RO membrane produced the higher flux in the 1st generation prototypes and was also available in larger quantities with high reproducibility (as a commercial product) when compared to the lab-fabricated UF membranes, 2nd generation *in vitro* studies focused on the RO prototypes. Additionally, the decision was made to investigate traditional salt based draw solutions which are compatible with a non-porous RO membrane system and are known to generate higher flux rates due to their higher osmotic pressure (**Chapter 2**).

The 2nd generation RO membrane prototype was tested in an *in vitro* system with both a deionised water feed and a Krebs physiological salt feed solution. Additionally different concentration salt feed solutions were investigated. As observed in previous studies that varied the salt draw solution concentration (**Chapter 2**), increasing salt concentration results in an increase in ‘average flux’ which in this case is taken as the change in fluid meniscus height per hour which is directly proportional to the fluid volume change. For this ‘flux value’ the units are mm/hour since it is the meniscus height that is being monitored. This would be expected due to the increasing osmotic pressure resulting from the increasing draw solution concentration. Additionally, as previously observed changing the feed solution from pure deionised water to Krebs physiological salt solution containing multiple cations/anions drastically decreases the flux.

Figure 5.9 demonstrates the average ‘fluxes’ generated by different concentration saline draw solutions during the *in vitro* experiments with both a deionised water and Krebs feed. The average change in flux obtained from changing the feed solution from deionised water to Krebs solution was a decrease of 5.5 mm/h. Doubling the saline draw concentration from 5% to 10% appeared to have little effect on the flux for both the DI water experiments and the Krebs solution experiments the former changing from 8.3 mm/h to 9.1 mm/h and for the latter 2.6 mm/h to 2.9 mm/h. However, comparing the 2% saline draw solution to the saturated 26% saline draw solution a large change

in flux was observed going from 5.5 mm/h to 11.9 mm/h in the deionised water experiments, an increase of 6.4 mm/hour. In the Krebs solution feed experiments changing the saline draw concentration from 2% to 26% produced an increase of 5.1 mm/h going from 1.1 mm/h to 6.3 mm/h.

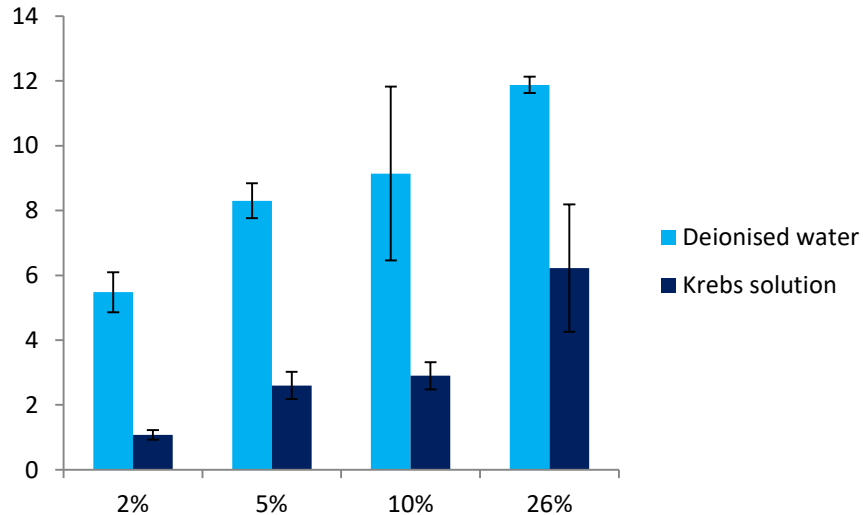


Figure 5.9: Average rate of increase in fluid height (mm/hour) testing 2nd Generation Prototype Device (RO membrane) in deionised water and Krebs solution with differing concentration sodium chloride draw solutions.

5.3.3.2 Perfused Limb Model

A porcine perfused limb model was developed to simulate the condition of oedema in order to test the prototype device. The basic concept involved the perfusion of a porcine limb from a freshly-slaughtered pig transported from a nearby abattoir, with a physiological salt solution. Without the usual protein content to balance the osmotic pressure gradient between the fluid within the blood vessels and the fluid in the surrounding tissues, perfusion quickly resulted in massive oedema of the interstitial tissues neighbouring the perfused blood vessels (see **Figure 5.10**). An hour long perfusion generated sufficient oedemic-type swelling of the limb to test the prototype devices. Several attempted limb perfusion studies were required to develop a reproducible protocol; each attempt required a round-trip to the abattoir to source limbs from a freshly slaughtered animal and the preparation of 10L of Krebs solution.



Figure 5.10: Perfused limb after 1 hour of perfusion (right hand side) compared to non-perfused limb (left hand side).

In order to implant the prototypes an incision was made in the tissue connecting the skin and muscle to access a naturally occurring cavity between these two layers. After implantation the incision was sealed using cyanoacrylate adhesive and the device was filled with the draw solution. The draw solution was allowed to reach a level that meant the outlet tube was also filled and the starting point was marked using a cable tie. The limb was perfused throughout the device testing to simulate a real-life disease state. The fluid height within the outlet device was monitored over a set period of time.

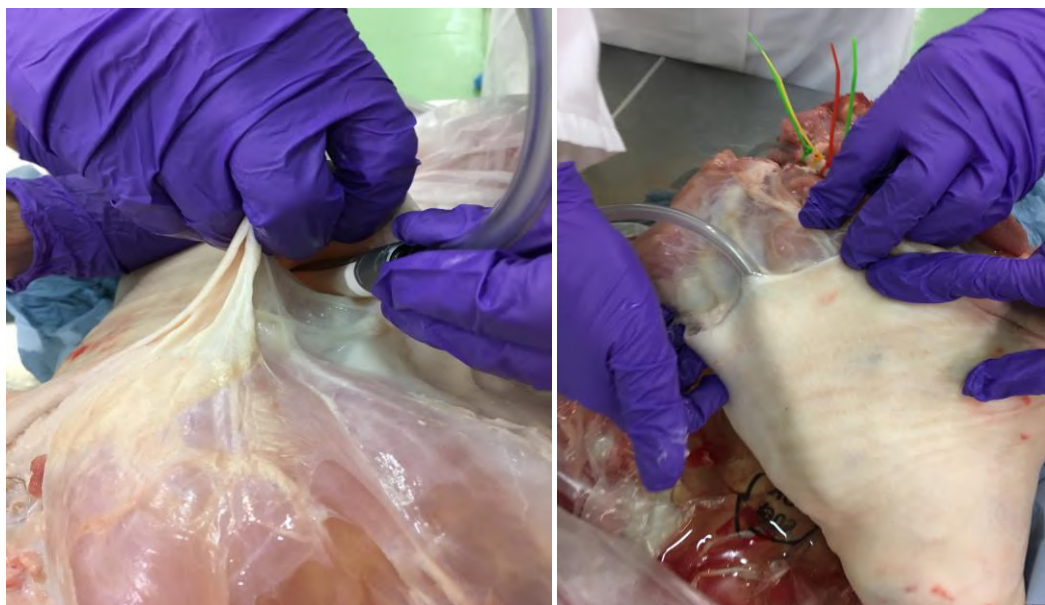


Figure 5.11: Device implantation into porcine limb model with simulated oedema.

Both the UF and RO membrane 2nd generation prototypes were tested. In this case a sample of commercial 10K MWCO PES UF membrane was used to create the prototype. The UF membrane device was filled with a 5% 225K NaPA draw solution

and it was observed that the higher viscosity of the polyelectrolyte draw solution relative to a traditional saline draw solution (as used in the RO device) created problems during injection. Additionally the high viscosity complicated fluid level measurement in the outlet tube as it was difficult to establish a level starting point free of air bubbles. With the UF device, no change in fluid height was detectable even after an hour.

The RO device was filled with a saturated saline draw solution. After implantation an increase in fluid height was easily detected within minutes of starting the measurement. A marker (cable tie) was placed at the fluid height every 10 minutes for 30 minutes. The change in height was an increase by 1 cm in 10 minutes on average which using the tube dimensions was calculated to be equivalent to 2.6 mL/10mins which equates to 15.6 mL/hour. The porcine limb weighed 7.3 kg before perfusion and 8.2 kg after an hour of perfusion at which point the device was implanted. Taking the limb weight in the oedematous state the device fluid removal rate is equivalent to 1.9 mL/hour per kg of tissue. The human lymphatic system removes 0.1 mL/min of fluid per kg of tissue which is equivalent to 6 mL hour per kg of tissue.⁶ The prototype device was able to remove fluid at a rate equivalent to approximately a third of the rate the entire human lymphatic system. This demonstrates that the prototype device was able to remove fluid from the oedema limb model at a physiologically significant rate, therefore providing proof of concept.

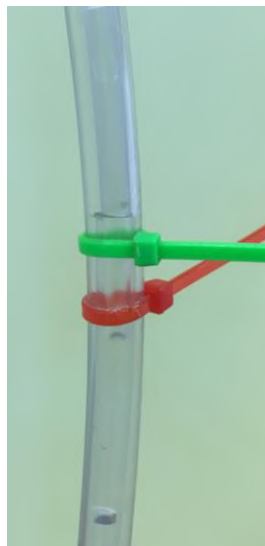


Figure 5.12: Fluid movement after device implantation, cable ties mark fluid height every 10 minutes.

5.4 Conclusions

Following fundamental research into using forward osmosis to transport fluids in **Chapter 2** along with consultation with researchers and clinicians in the field, combined with discussions with a design house specialising in medical device design, several potential prototypes were constructed taking into account key design considerations and limitations. These included:

- Materials used which not only had to be biocompatible and also sterilisable but also were limited to the materials from which membranes can be fabricated;
- a minimally invasive implantation procedure without compromising the large membrane area necessary for effective transport of oedemic fluids;
- the ability to load and replace the draw solution as necessary.

Additionally, for the purposes of this project, the design had to be simple enough to be fabricated in the lab without requiring over-specialised equipment. Subsequently two classes of prototypes were made: the 1st Generation based on extremely simple pouch design and the 2nd Generation of prototypes involved a more sophisticated design involving a sealed implantable membrane tube with concentric inlet and outlet tubing. Again both a UF membrane based device (with a polyelectrolyte draw) and an RO membrane based device with a (saline draw) were tested.

The 1st generation prototypes were tested using a simple *in vitro* model and demonstrated that forward osmosis could be used to remove water from a deionised water feed solution using a novel polyelectrolyte draw solution (explored in **Chapter 2**) despite the system being unstirred. Flux was observed using both UF and RO membranes although the RO membrane performed better.

The 2nd generation prototypes were designed to be suitable for implantation into an *ex vivo* perfused limb oedema model specially developed for the project. Both a UF membrane and and RO membrane prototype were tested, the UF prototype with a polyelectrolyte draw solution and the RO with a traditional salt-based draw solution. The RO membrane system was additionally tested using the simple *in vitro* model.

In vitro experiments with the second generation RO membrane prototype showed that a flux of 6.22 mL/hour could be achieved with a physiological salt feed solution. Lymph nodes remove around 0.1 mL/min of fluid per kg of tissue in a human under normal physiological conditions⁶ which is equivalent to 6 mL/hour. Therefore the RO prototype device was able to produce an *in vitro* flux at a physiologically significant rate.

Testing both the UF and RO 2nd generation prototypes with the *ex vivo* perfused limb produced mixed results. No fluid removal was observed with the UF device and loading the polyacrylate draw solution via the silicone tube was difficult due to the high viscosity of the solution. In contrast, a significant level of fluid removal was observed when using the RO membrane device equivalent to 15.6 mL/hour offering proof of device concept.

5.5 Future Work

As a continuation of the work carried out in this chapter, more sophisticated next generation prototypes will need to be fabricated for testing with the perfused limb oedema model. During the course of the project a design house specialising in medical devices was consulted for prototype future designs. Additionally a manufacturer was also consulted for advice on device construction. Future work would necessarily involve collaboration with such experts in the field. Furthermore the existing prototypes could be used to provide further evidence for proof-of-concept i.e. via the repetition of *in vitro* studies using a feed solution containing proteins. Samples of the draw solution could then be analysed for protein content using the BCA assay as done in **Chapter 2** for the FO studies using proteins. Additionally the second generation UF membrane/polyacrylate draw device could be re-tested in the *ex vivo* perfused limb model.

5.6 Experimental

5.6.1 Materials

The following supplies were sourced from Fisher Scientific (Leicestershire, UK); cable ties, disposable scalpels, Masterflex™ Tygon internal diameter 1.6mm peristaltic pump tubing, waterproof tape, epoxy adhesive, cyanoacrylate adhesive. The porcine hind limbs were collected as a pair within a few hours of slaughter from Newman's Abattoir (Farnborough). The 225,000 MW Poly(acrylic acid) sodium salt (20% aqueous solution) was purchased from Polysciences, Inc. The Pall 10 K MWCO PES UF membrane was acquired from Pall Corporation (Portsmouth, UK) and the commercial RO membrane was obtained from a Vontron® Residential Membrane Element (Vontron®, China). All other materials were including; calcium chloride, glucose, magnesium sulphate, potassium chloride, potassium phosphate monobasic, sodium chloride, sodium hydrocarbonate and sodium hydroxide were purchased from Sigma Aldrich (Dorset, UK).

5.6.2 Equipment

The peristaltic pump was purchased from VWR International (Leicestershire, UK) and the model type was the FASTLoad Manual Control peristaltic pump.

5.6.3 Methods

5.6.3.1 Prototype Fabrication

1st Generation

Two rectangles of the same size (7 cm x 15 cm) were cut from a membrane sheet. One rectangle was placed active side down on a clean surface and adhesive was applied around three edges of the sheet in a continuous line to avoid gaps. The second sheet was placed on top of the first, solid support layer facing down, to create a membrane pouch (**Figure 5.6**). The sheets were clamped and allowed to dry for the appropriate time based on the type of adhesive used. Before testing, the pouches were examined for defects and were filled with water to check for leaks before use with desired draw solution which was poured in through the opening in the membrane pouch.

2nd Generation

The chosen membrane was cut to size (rectangle; 9.5 cm long, 6 cm wide) and a tubular former (cylinder; 12 cm long, diameter of 1.8 cm) was employed to create a membrane cylinder with the active surface facing outwards. The seam was sealed with a strip of waterproof tape which was further reinforced by a coat of cyanoacrylate adhesive which was allowed to dry before the following steps. Both ends of the membrane tube were capped again using both waterproof tape and the cyanoacrylate to fix the caps; one end with a closed plastic seal, the other with a tube connector. Again the prototype was allowed to cure before testing for leaks, after which a 7 mm silicone tube containing a 4 mm silicone tube (producing a double lumen) was attached to the tube connector. When tested, the chosen draw solution was injected through the inner lumen using a syringe. The device was filled until excess fluid entered the outer tube and upon reaching a suitable level and removing any air bubbles the draw solution starting point was marked upon the tube before measurements began.

The active membrane area was approximately 14 cm².

5.6.3.2 Prototype Testing

Prototypes were tested using both an *in vitro* and an *ex vivo* model. In both cases the model feed solution was either deionised water or Krebs physiological salt solution (**Table 5.2**)

Table 5.2: Krebs Solution composition⁷

Component	Concentration (mM)	Mass (g) in 1L
NaCl	118	6.9
KCl	3.4	0.25
CaCl ₂	2.5	1.3 mL
KH ₂ PO ₄	1.2	0.16
MgSO ₄	1.2	0.14
NaHCO ₃	2.5	2.10
Glucose	11.1	2.00

***In Vitro* Testing**

The 'bench-top' *in vitro* testing involved suspending the prototype in a beaker containing a known volume of feed solution; either deionised water control or Krebs solution. The draw solution was introduced into the prototype and the volumes of both the feed and draw solutions were measured every hour.

***Ex vivo* Perfused Limb Model Testing**

The porcine limbs were collected within hours of slaughter and if still joined together were separated using a saw. The femoral artery was identified and a section cleaned of connective tissue and fat to allow visualization of the area the cannula would be inserted. Additionally it was ensured there were no side branches that would mean the perfusion solution would leak rather than perfuse tissue. Next the femoral artery was cannulated with a silicone tube (bore size 3mm, 0.75mm wall thickness) and secured with cable ties. The cannula was then connected to the peristaltic pump tubing (1.6cm diameter, which was pre-loaded with Krebs solution. The Krebs solution was then slowly introduced into the limb using the peristaltic pump to check for leaks, blockages and check the security of the cannula. Flow was then steadily increased to maximal rate of approximately 40 mL/min in order to prevent backflow and de-cannulation. The system was perfused for 1 hour and was observed for evidence of oedema. When perfusion was successful the swelling was detectable by eye, and generally an hour's perfusion produced sufficient swelling to simulate an oedemic state. An incision was

made through the skin and the device was introduced before the opening was sealed using cyanoacrylate adhesive. The draw solution was injected into the prototype device and the fluid level was noted before starting the experiment. The limb was perfused throughout the measurement.

5.7 References

1. C. B. Herbert and M. N. Blaine, US Pat. 8 211 053 B2 (2012), to Equilibrate LLC.
2. G. Matheis, F. Beyersdorf, A. Hanselmann, A. Unger, A. Wildhirt, S. Kruger, G. Zimmer, and P. Satter, *Cardiovasc. Surg.*, 1994, **2**, 725–736.
3. A. B. Fisher, C. Dodia, and J. Linask, *Exp. Lung Res.*, 1980, **1**, 13–21.
4. S. Wagner, A. Nogueira, M. Paul, D. Heydeck, S. Klug, and B. Christ, *J. Artif. Organs*, 2003, **6**, 183–191.
5. M. Friebe, J. Stahl, and M. Kietzmann, *J. Veterinary Pharmacol. Ther.*, 2001, **36**, 292–297.
6. G. Pockock, C. D. Richards, and D. Richards, in *Human Physiology*, Oxford University Press, Oxford, 2013, pp. 359–443.
7. M. J. Gardener, C. D. Glen, G. R. Richards, P. M. Vanhoutte, G. Edwards, M. Fe, and A. H. Weston, *Br. J. Pharmacol.*, 2001, **133**, 1145–1153.